NIST-GCR-96-687

SPARSE WATER SPRAYS IN FIRE PROTECTION

Marino di Marzo

Department of Mechanical Engineering
University of Maryland
College Park, MD 20817

December 1995
Issued June 1996

U.S. Department of Commerce
Michael Kantor, *Secretary*
Technology Administration
Mary L. Good, *Under Secretary for Technology*
National Institute of Standards and Technology
Arati Prabhakar, *Director*

Notice

This report was prepared for the Building and Fire Research Laboratory of the National Institute of Standards and Technology under grant number 60NANB5D0136. The statement and conclusions contained in this report are those of the authors and do not necessarily reflect the views of the National Institute of Standards and Technology or the Building and Fire Research Laboratory.

SPARSE WATER SPRAYS IN FIRE PROTECTION

Marino di Marzo

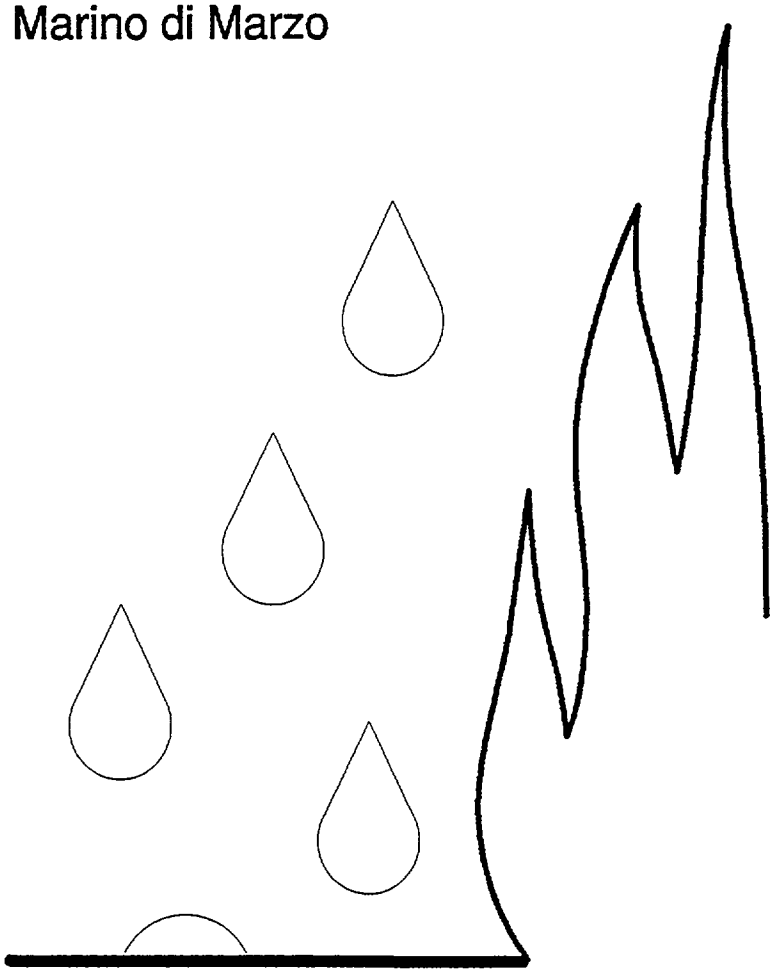

SPARSE WATER SPRAYS IN FIRE PROTECTION

Marino di Marzo

prepared for the
Building and Fire Research Laboratory
National Institute of Standards and Technology
Gaithersburg, MD 20899

December 1995

Mechanical Engineering Department
University of Maryland at College Park

FOREWORD

This is a collection of seventeen manuscripts over the period January 1985 - January 1996 which outline the development of the models which enables to predict the cooling effect of sparse sprays on solid surfaces exposed to fire. The manuscripts are organized by topic in four parts and three appendices:

Part 1: The cooling effect of a single water droplet deposited on a high thermal conductivity semi-infinite solid heated by conduction from below.

Part 2: The cooling effect of a single water droplet deposited on any semi-infinite solid heated by conduction from below.

Part 3: The cooling effect of a single water droplet deposited on any semi-infinite solid subjected to radiant heat input from above.

Part 4: The cooling effect of a sparse water spray on any semi-infinite solid subjected to radiant heat input from above.

Appendix A: Effect of surfactants in the water
Appendix B: Effect of dissolved gasses in the water
Appendix C: Criteria for liquid flooding of the solid surface.

The first paper is provided in the way of an executive summary.

ACKNOWLEDGMENTS

This research was made possible by the guidance and support of Dr. D.D. Evans (BFRL-NIST). The contribution of Dr. H. Baum (BFRL-NIST) was essential to the formulation of most of the theoretical analyses. Dr. S. Chandra and Mr. Y.M. Qiao (University of Toronto, Canada) provided the experimental data for the study of the effect of surfactants in the water (Appendix A). Dr. P. Tartarini (University of Bologna, Italy) contributed significantly to the research program over a period of several years.

The experimental and analytical work was performed by:

Mr. A. Trehan	Mr. J. Ham	Dr. P. Tartarini
Dr. W. Meng	Mr. C. Kidder	Dr. Y. Liao
Dr. M. Klassen	Ms. M. Lederer	Mr. G. White
Mr. F. Kavoosi	Mr. R. Mahajan	Ms. S. Tinker

TABLE OF CONTENTS

Part Four:

Appendix A:

Appendix B:

Appendix C:

EXECUTIVE SUMMARY

M. di Marzo, Dropwise evaporative cooling, Heat and Technology (1996) in press

PAPER # 1

DROPWISE EVAPORATIVE COOLING

Marino di Marzo

Mechanical Engineering Department - University of Maryland
College Park, MD 20817, USA

ABSTRACT

A comprehensive review of the findings that punctuated ten years of research on dropwise evaporative cooling is presented. The first studies consider a single droplet evaporating on a high thermal conductivity solid surface. The solid-liquid coupling is addressed when considering the case of a low thermal conductivity solid. A powerful, non-intrusive, infrared thermographic technique is instrumental in describing the thermal behavior of the solid surface. The applications relevant to fire suppression suggest the input of radiant heat from above the surface instead of heat conducted through the solid. Once the single droplet behavior is fully documented experimentally and accurately modelled, the study of sparse water sprays is undertaken. A superposition model is formulated which well represents the experimental data.

1. INTRODUCTION

Evaporative cooling induced by droplets deposited on hot surfaces is of interest in a number of applications such as metal quenching, turbine blades cooling, and fire protection. The vaporization process depends on the degree of superheat of the solid surface. At high surface temperatures, the droplets float over thin vapor layers [1]. As the surface temperature is lowered, wetting occurs. The transition from the levitated state to the wetting state is known as the Leidenfrost transition. Since it was Leidenfrost who described the phenomenon in the first known two-phase heat transfer investigation which dates 1756 [2]. As the droplets wet the surface, nucleate boiling is observed. For lower surface temperatures, the bubble nucleation, at the liquid-solid interface, subsides and the vaporization occurs at the liquid-vapor interface. This process known as evaporation is the topic addressed here. As the surface temperature is further dropped, the vaporization rate is insufficient to remove the incoming water flux and the solid surface floods with liquid [3].

Extensive observations of a single droplet evaporation are available in the literature [4,5,6]. Modelling efforts available to date are based on a variety of simplifying assumptions and few address the behavior of sparse water sprays [7,8,9,10]. Most predictions are based on adjustments of constants fitted to the experimental data. The research presented here systematically progresses from the single droplet to the sparse spray. The heat input is at first by conduction from below the surface. Later, the heat is generated by radiant panels above the surface to simulate and environment closer to the typical fire protection applications. This paper parallels the experimental and the theoretical aspects and attempts to sinergize the experimental observations with the insights provided by the theoretical results.

2. SINGLE DROPLET ON A SOLID HEATED BY CONDUCTION

2.1 High thermal conductivity solids

A spherical droplet impacting on a solid surface spreads on it. The final configuration of the liquid varies a great deal and depends on a multitude of parameters [11]. For the case of water gently deposited on a surface at near-saturation temperature, the shape can be regarded as a segment of a sphere [12]. The parameter β, defined as the ratio of the radius of the wetted region over the radius of the sphere of equivalent liquid volume [8] is sufficient to characterize the shape of deposited droplets of 10 to 50 μl. For gently deposited water droplets on aluminum, β ranges between 1.2 and 1.5 as the surface temperature increases from 75 to 105 °C. For this experimental range, the radius of the wetted area remains constant throughout most (i.e. 90 percent) of the droplet evaporation time.

A simple model, based on one-dimensional conduction in the liquid, is proposed [13]. The temperature at the solid-liquid interface is assumed constant and uniform. Its value is estimated considering the contact temperature between two semi-infinite solids brought in sudden contact [14]. The temperature at the liquid-vapor interface is obtained from a heat and mass transfer energy balance for the steam-air mixture [15]. A spherical cap, based on the fixed radius of the wetted region and on the residual liquid inventory, describes well the transient droplet shape and defines the thickness of the liquid layer at each radial location from the center of the droplet.

The model is validated by comparing the calculated and measured evaporation times. These values agree within 10 percent. Further validation is achieved via photographic techniques. Figure 1 demonstrates the excellent agreement between the data and the computations. The model can provide insight into the flux distribution at the liquid-solid interface. Figure 2 shows the radial heat flux at various times during the transient. At first, the evaporation is taking place in the outer region of the droplet near its edge. Later in the process the whole surface contributes. This effect is clearly due to the variation in the thickness of the liquid layer which is associated with the decreasing curvature of the droplet liquid-vapor interface.

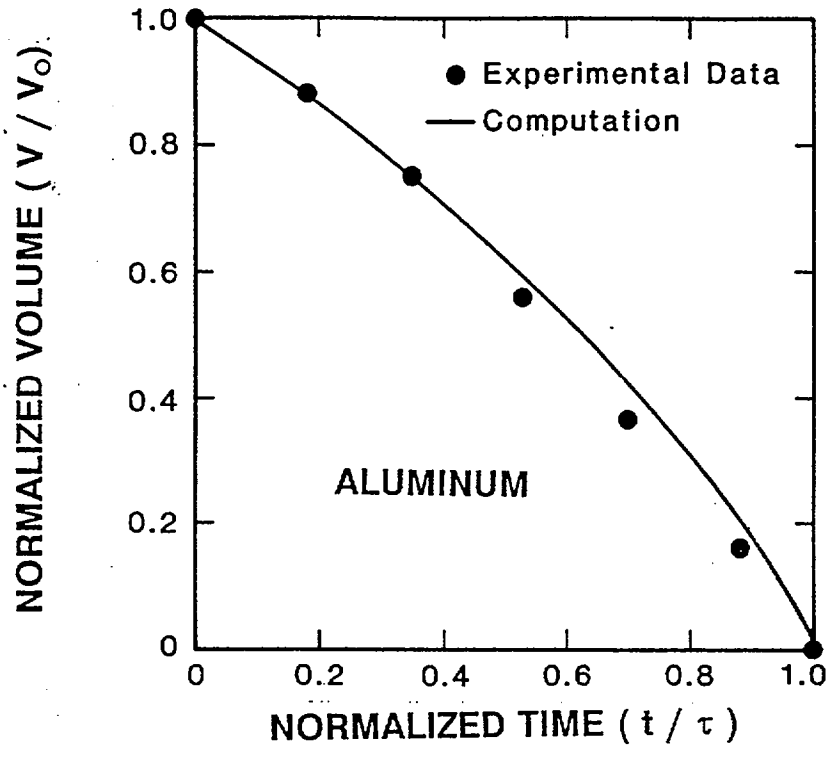

Figure 1 Liquid water inventory versus time (V_o = 30 μl; T_o = 98 °C).

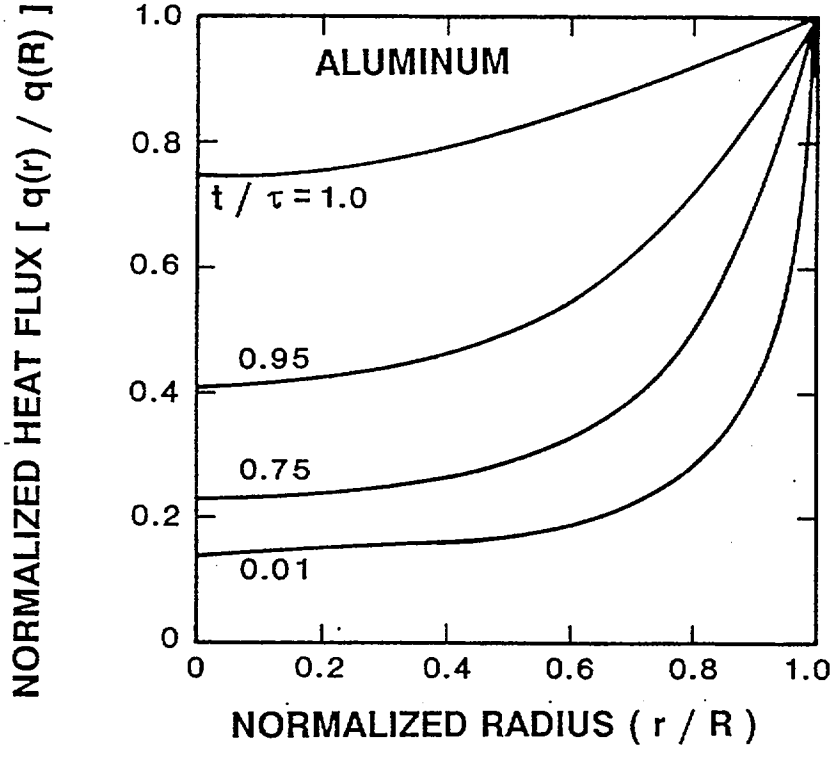

Figure 2 . Temporal and spatial heat flux behavior (V_o = 30 μl; T_o = 98 °C).

The cooling effect on the solid surface is quantified by considering the heat flux distribution, due to the droplet evaporation, as a boundary condition in solving the semi-infinite solid transient conduction equation [16]. These studies demonstrate the adequacy of a simple conduction heat transfer model for the liquid layer. The hypothesis of negligible convective heat transfer is also supported by direct observation of the droplet with tracers and by studies of surface-tension-induced circulation [17]. Another important result is the validation of the liquid-vapor interfacial boundary condition casted in terms of a combined heat and mass transfer energy balance.

2.2 Generalization to low thermal conductivity solids

The previous work is extended to include solids with low thermal conductivity. The initial solid surface temperature is ranged from 90 to 180 °C with droplets of 10 to 50 μl. The solid used for the experiments is Macor, a glass-like material. This solid has high emissivity which allows the use of infrared thermography to gather information on the transient thermal behavior of the solid surface [18]. An Inframetrics (Model 525) camera is used to capture the thermographic emission from the solid surface. The typical distance of the camera from the solid surface is of about 0.5 meters with a field of view of about 0.02 meters. The video signal from the camera is digitized by a PC-based frame grabber which converts the video image to a matrix of numbers representing gray levels. The gray levels identified by this equipment are 64 where 0 is black and 63 is white.

The image has infrared intensities on the vertical axis and radial positions, from the droplet center, on the horizontal axis. The digitized image is further processed by tresholding. This eliminates noise which is constituted by pixels of the digitized image with gray levels of less than 10. Additionally, an erosion technique is applied to verify the consistency of the data by checking if at least other six data points exist in the proximity of a given data point. To identify a reference temperature scale, the surface temperature is measured with an Omega surface probe (Series 68000) which is placed in the field of view. By comparing the temperatures read by the probe and the actual infrared images, immediately after the probe removal, the infrared intensity scale is associated with the temperature scale. Figure 3 illustrates a typical transient obtained with this procedure.

The extension of the model to the low thermal conductivity solids requires the introduction of the implicit coupling of the liquid and the solid whereas in the high thermal conductivity case (i.e. metal solids) the two could be treated separately. As observed in Fig. 2, the heat fluxes are significant at the droplet edge. This implies that the thermal gradients in the solid in the proximity of the droplet edge are very large. This fact precludes the application of a finite difference technique to integrate the solid transient conduction governing equation.

A different solution scheme is formulated for the solid region which is based on Boundary Element Methods (BEM)[19]. The BEM formally requires that all past information must contribute to the present solution. The advantage of the time

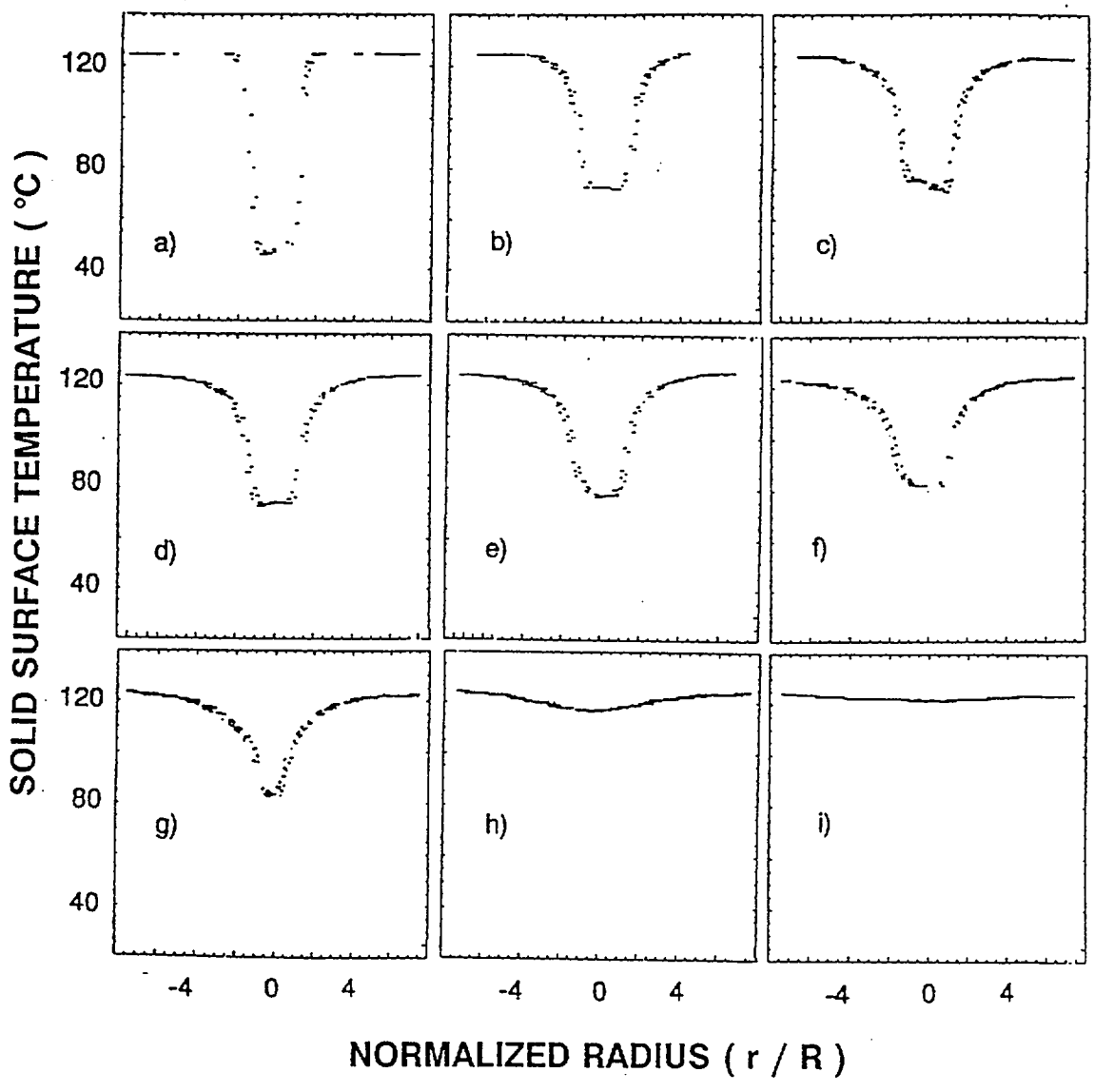

Figure 3 Evaporative cooling transient: a) at 1s; b) at 10 s; c) at 30 s; d) at 50 s; e) at 70 s; f) at 90 s; g) at 100 s; h) at 110 s; i) at 130 s (V_o = 30 μl; T_o = 124 °C; Macor).

discretization scheme used here, is that only a limited amount of past information must be collected in order to obtain the solution. The complex geometry of the liquid droplet suggests that a Control Volume Method (CVM) be used for the integration of the transient conduction equation in the liquid region. A simple nodalization scheme is used and the governing equation is discretized for each elementary control volume [20,21].

Figure 4 provides a comparison of the typical results of the model with the experimental data. Insights from the calculations are obtained for the temperature distribution at the solid-liquid interface. Figure 5 illustrate the dramatic difference between the behavior of high and low thermal conductivity materials. As it can be seen in this figure, the assumptions of the simple model for metallic solids finds clear supporting evidence in these results. For the low thermal conductivity case, it is clear that the temperature at the liquid-solid interface is not uniform nor constant. It is also important to point out that the transition to nucleate boiling occurs when the solid-liquid interfacial temperature exceeds saturation. Note that as soon as the droplet is deposited, the interfacial temperature drops significantly lower than the initial solid surface temperature. Therefore, while nucleate boiling on aluminum is observed for an initial solid surface temperature of 103 °C, it is necessary to reach about 164 °C to obtain nucleate boiling on Macor. The temperature distribution in the water layer is examined to assess the adequacy of a one-dimensional heat conduction model for the liquid region. Figure 6 compares the axial and radial components of the heat flux. Only at a few locations near the edge of the droplet for limited times, the radial flux is comparable to ten percent of the axial flux. Therefore, the assumption of one-dimensionality which is used in the model for high thermal conductivity solids holds and it is retained in the following.

3. SINGLE DROPLET ON A SOLID HEATED BY RADIATION

3.1 Phenomenology

In order to better approximate an actual fire environment, heat input by conduction from below the solid is substituted by radiant heat input from above the solid surface. The radiant heat input is provided by two conical shaped heaters positioned symmetrically with respect the solid surface [22]. The phenomena associated with the vaporization of a water droplet under these conditions is quite different from the previous case. Two major differences must be noted: a) the vaporization process is due to the direct heat input at the liquid-vapor interface in addition to the heat conducted from the solid surface through the liquid; b) the solid temperature distribution is the opposite of the previous case because the temperature decreases in the depth of the solid whereas before it was increasing. The temperature decrease in the depth of the solid is due to the radiant heat input from above the solid surface and to the use of a chilled plate at the lower surface of the solid to provide a constant temperature boundary condition. The effects of these two differences on the vaporization process are outlined in the following.

Figure 4

Model validation: solid surface temperatures for water on Macor at $t/\tau = 0.9$ with:

a) $V_o = 30\ \mu l$, $T_o = 160\ °C$;
b) $V_o = 30\ \mu l$, $T_o = 101\ °C$;
c) $V_o = 10\ \mu l$, $T_o = 143\ °C$; and
d) $V_o = 30\ \mu l$, $T_o = 143\ °C$.

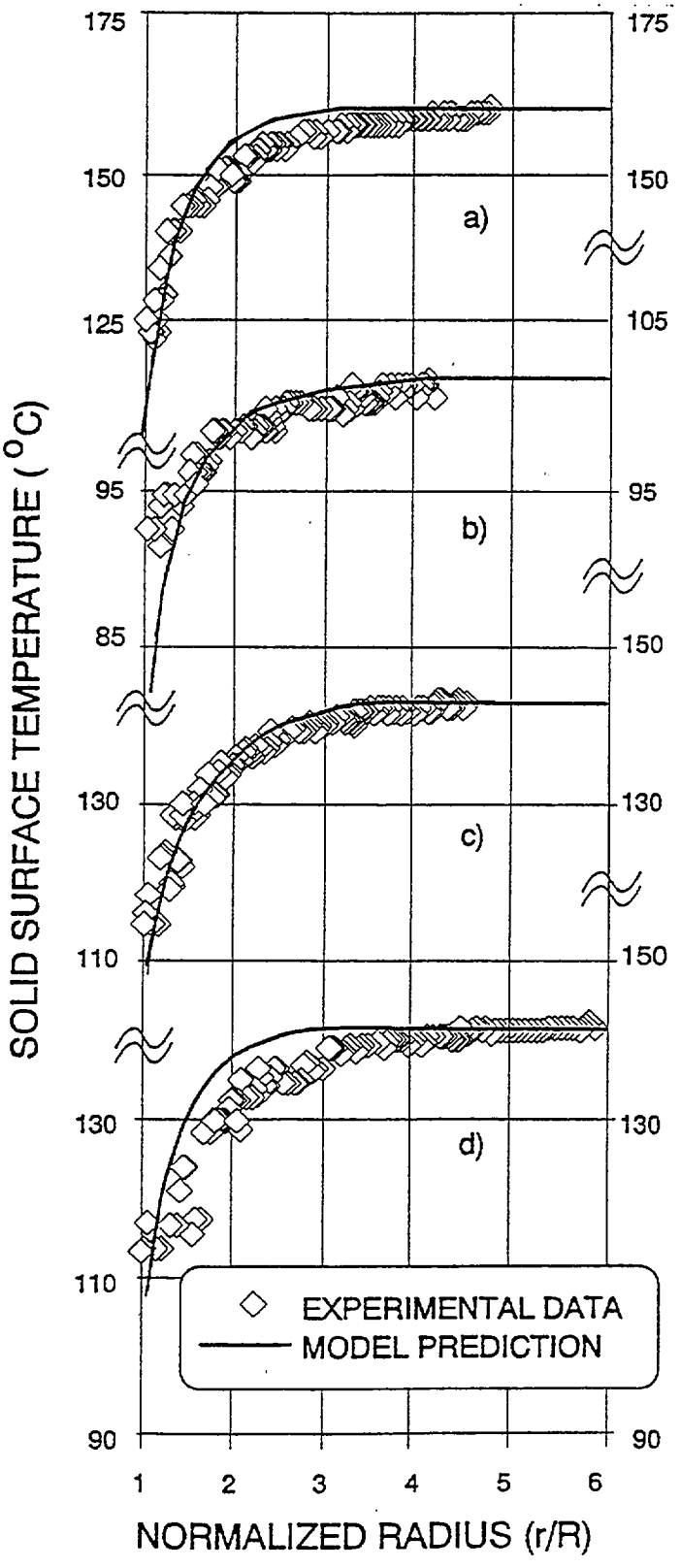

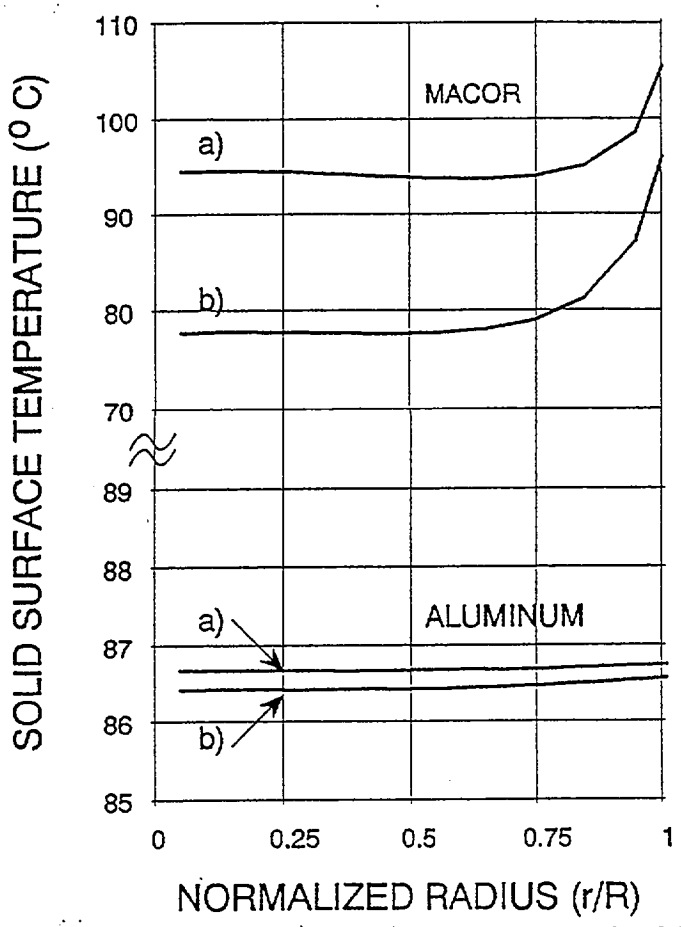

Figure 5 Typical liquid-solid interfacial temperatures for Macor and aluminum with initial contact temperature [14] of 82 °C for water droplets with V_o = 30 μl at a) t/τ = 0.3 and b) t/τ = 0.9 (model computations).

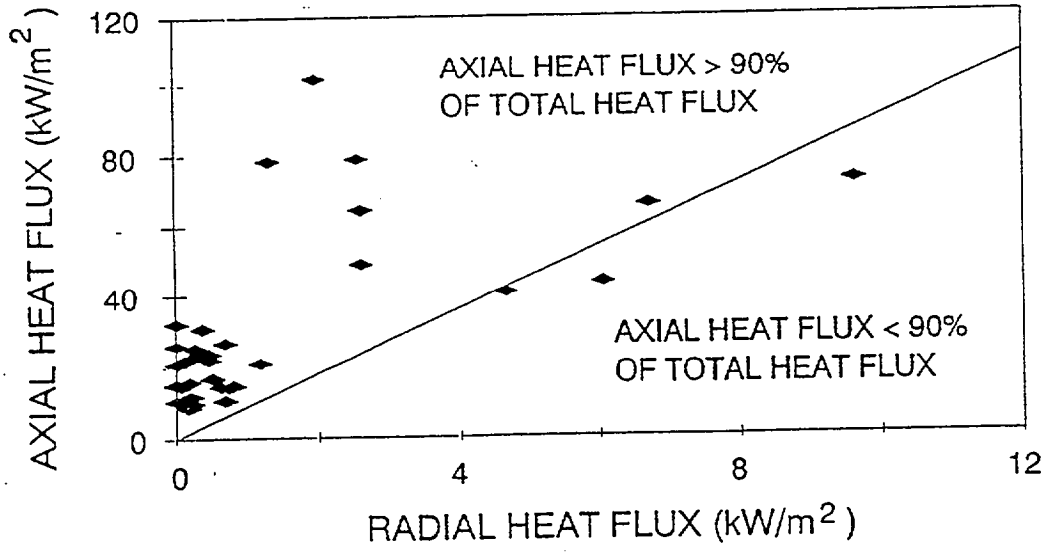

Figure 6 Calculated axial and radial heat flux components.

Figure 7 illustrates the behavior of the shape factor β as a function of the initial solid surface temperature. Note that the same material (i.e. Macor) exhibits values of β between 1.2 and 1.5 over the same range of temperatures for the case of heat input by conduction. The pronounced difference observed in these data is due to the effect of the direct radiant heat absorption at the liquid-vapor interface which increases the interfacial temperature and decreases the surface tension. The decrease in surface tension leads to a more pronounced initial spreading of the droplet on the solid surface. Note also that, as the nucleate boiling transition is approached (i.e. for temperatures of about 160 °C), the measurement scatter also increases. The increased spreading of the liquid on the solid surface implies that the liquid layer is thinner and, therefore, the resistance due to the heat conduction through the liquid layer is lessened. Another effect of the reduced thickness of the liquid layer at deposition is that the contact angle at the droplet edge is less than in the conduction case. As the droplet evaporates, the contact angle decreases from its initial value. There is a limiting value which is identified as the receding angle [23,24]. In this case the receding angle is between 7 and 10°. When this value of the contact angle is reached, the surface under the droplet starts shrinking and the liquid retains its aspect ratio while continuing to evaporate. Figure 8 clearly depict this occurrence. It is clear that as the initial value of the shape factor increases, the receding angle is reached sooner during the evaporative process, as it can be seen in the figure.

The other important difference has to do with the temperature distribution in the solid depth in relation to the cooling due to the droplet deposited on the solid surface. For the conduction case, the heat flux lines are converging from the hot depth of the solid toward the droplet. In the radiant case, the opposite is true since now the depth of the solid is cold. Therefore, as the surface cools, at the location of the deposited droplet, the heat flux lines diverge away from that region. The result of this opposite behavior is that the conduction heat input contribution to the vaporization process is far less than in the pure conduction case. The thinning of the liquid layer mitigate this effect and the vaporization by direct radiant heat input at the liquid-vapor interface compensate for the reduced heat input by conduction. The net result is a similar overall vaporization time which nonetheless is achieved by a substantially different mechanism.

3.2 Theoretical modelling

The first concern associated with the modelling of these complex phenomena relates to the estimate of the direct radiant heat input at the liquid-vapor interface. This estimate is based on the following description of the volumetric heat absorption in the depth z of a liquid layer of thickness δ [25]:

$$H = 2\int_0^{\infty} E_\lambda \kappa_\lambda \int_0^{\pi/2} \frac{1}{\mu} A_\phi \cos\phi \sin\phi \,(1 - \rho_\phi)\, e^{-\frac{\kappa_\lambda(\delta - z)}{\mu}}\, d\phi\, d\lambda \qquad (1)$$

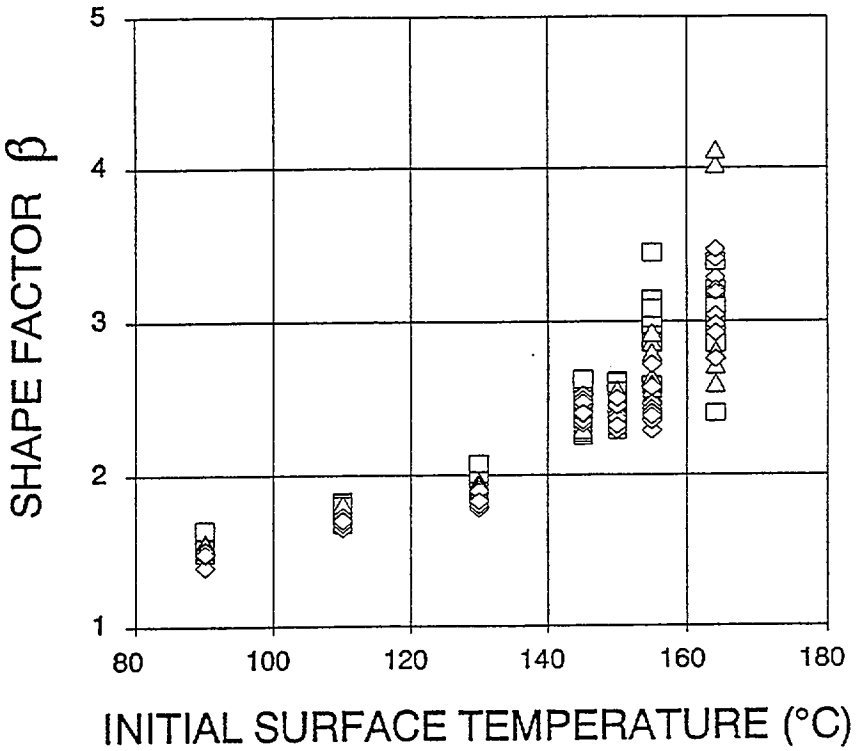

Figure 7 Shape factor: ◊) 50 μl; ▵) 30 μl; □) 10 μl.

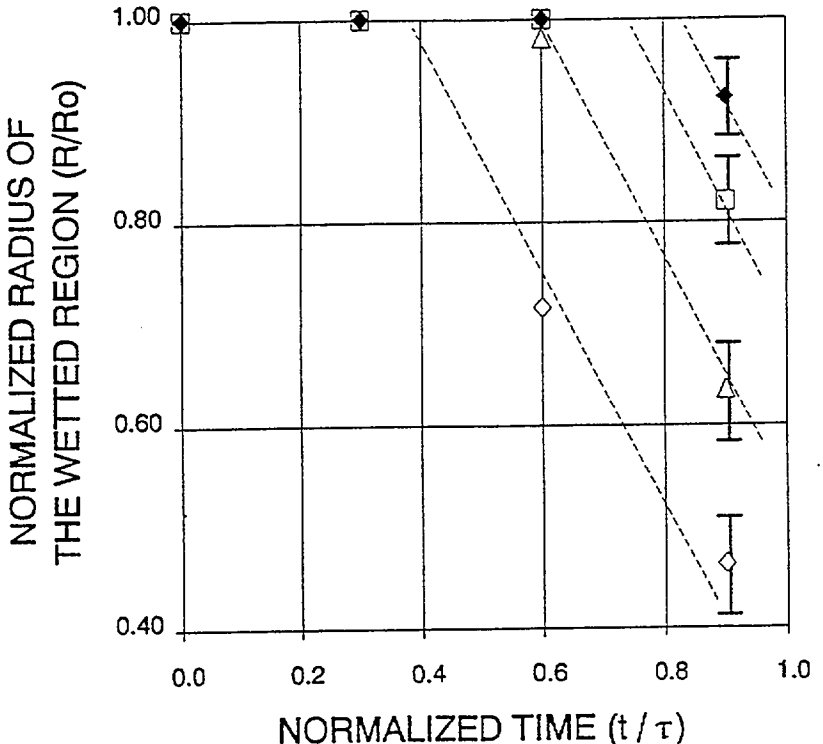

Figure 8 Normalized radius of the wetted region: ◆) T_o = 130 °C; □) T_o = 155 °C; ▵) T_o = 164 °C; ◊) T_o = 180 °C.

Here, the geometry of the radiant heat source is identified in terms of the fractional surface area coverage occupied by the source, A_ϕ, at various azimuthal angles, ϕ, above the solid surface. The following assumptions are made: a) the radiant heat sources behave as black bodies; b) the radiation scattering within the water droplet is negligible; c) the liquid-vapor interface is horizontal and flat; and d) the radiation reaching the liquid-solid interface is completely absorbed by the solid. The absorption coefficient, κ_λ, is a very strong function of the wave length, λ, the direction cosine, μ, is given by the Snell's law and the reflectivity, ρ_ϕ, is less than 0.1 for ϕ less than 65° and it is given by the electromagnetic theory.

Figure 9 shows that the volumetric heat absorption is high in a thin layer near the liquid-vapor interface (consider a layer thickness of about 0.05 mm). This is true over a broad range of the radiant surface temperatures. Therefore, one can split the direct radiation in three parts: a) an interfacial flux term (which is the integral of H over the thickness of a thin liquid layer); b) a volumetric heat absorption term which can be considered a constant, uniformly distributed heat source throughout the liquid layer; and c) a residual term which accounts for the incoming radiation at the solid-liquid interface. This last term is evaluated from an energy balance by deducting from the incoming radiant flux at the liquid-vapor interface the two previous terms. Careful consideration must be given to the fact that the liquid-vapor interface is not flat. The flat surface assumption is useful to obtain simple results as shown in Fig. 9. However, some error can be introduced in the evaluation of the total incoming radiation when significant radiant surfaces are present at large polar angles ($\phi > 60°$). To rectify this problem, a multiplier must be introduced which accounts for the liquid-vapor interface orientation given the transient geometrical configuration of the droplet.

The modelling of the droplet shape is a modification of the model based on a representation of the liquid layer as a segment of a sphere. The actual configuration is more flattened [11]. Two parameters are used to characterize the droplet shape at deposition: a) the contact angle, θ; and b) the shape parameter, β. The shape of the droplet, when the contact angle reaches its receding value, is assumed to be a segment of a sphere. This assumption is based on the minimization of the liquid-vapor interface which is consistent with the subsequent surface-tension-induced shrinkage of the droplet. Figure 10 illustrates the effect of the initial value of the contact angle. It is clearly shown that the receding angle is reached at about the same time during the transient. This means that the effect of the initial value of the contact angle has little or no effect on the overall phenomena. There is a compensatory effect in the droplet shape: a flattened shape has a uniform conduction heat input contribution while the spherical cap has very high heat transfer at the edge an far less heat transfer in the central region. The results shown here demonstrate that the overall effect is quite similar. Therefore, the simple model, based on the spherical cap configuration with the proper consideration for the receding angle, is adequate to represent the phenomena. The more complex two-parameters model is not used because there is no payoff from its increase complexity.

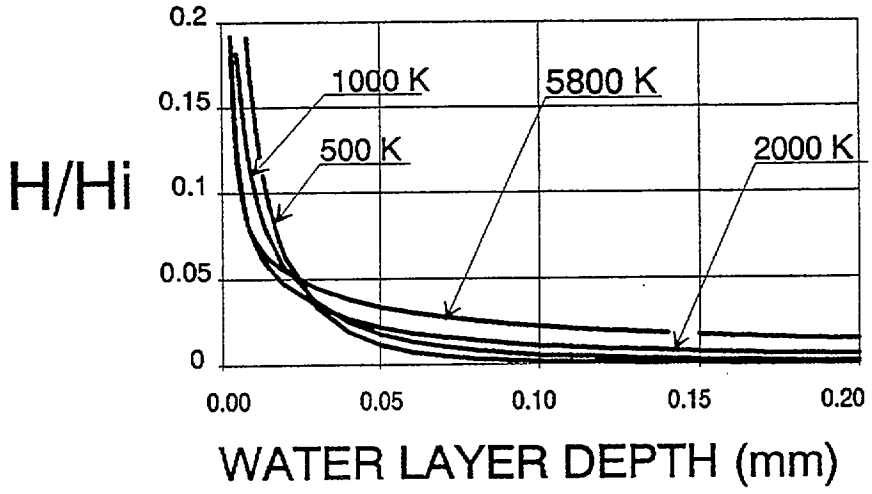

Figure 9 Normalized heat absorption in the liquid due to direct radiation.

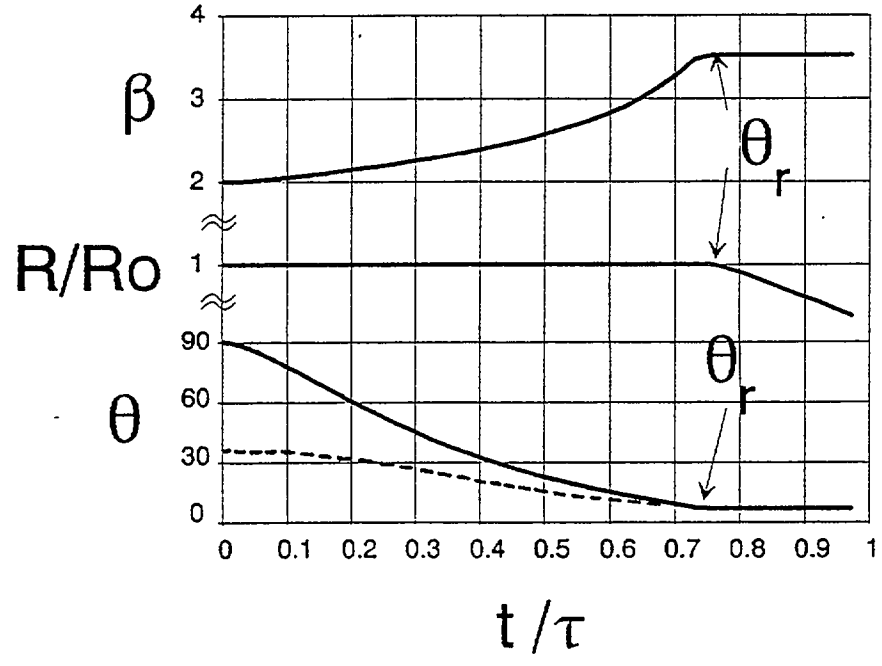

Figure 10 Transient behavior of the parameters governing the droplet shape (T_o = 130 °C; V_o = 10 μl); — : θ_o maximum - - - : θ_o minimum.

The model for the direct radiant heat input and the new model for the transient droplet shape, which now includes the wetted surface shrinkage (as the receding angle is reached), are incorporated in the previous code for the coupled solid-liquid. Two independent versions of the same code are obtained. One of the codes is developed at the University of Bologna [26] and the other at the University of Maryland [27]. The code developed at the University of Bologna retains a full two-dimensional description of the liquid layer while the code developed at the University of Maryland uses a one-dimensional representation of the liquid layer transient conduction, as suggested by the results of the model for the conduction heat input case which were discussed previously. Both codes compared very well with the data. Figure 11 demonstrates the agreement between the infrared data and the calculated predictions.

4. SPARSE SPRAY ON A SOLID HEATED BY RADIATION

4.1 Experimental studies

A sparse spray is applied to a hot solid surface and the transient thermal response is monitored [28]. Figure 12 depicts the major components of the experimental apparatus. The solid surface is heated by three radiant panels. Two are positioned opposite to each other and the third is a low-aspect-ratio panel that surrounds the periphery of the solid surface. The infrared thermography is obtained with the same equipment previously described. Note that the camera observes the surface through a long chilled pipe to eliminate stray radiation and to avoid the direct reflection of the panels on the solid surface. The solid is chilled at its lower surface to achieve a controlled boundary condition. The sparse spray is obtained using a droplet dispenser capable of generating constant size droplets (the droplets volume is of about 10 μl) with a constant frequency which is set in the range from 1 to 0.1 Hz. The dispenser moves within a positioning plate which controls the droplet distribution.

Figure 13 shows a typical droplet distribution as measured via video-camera. The dispenser is positioned by three bumpers that periodically move in and out on the position plate. These bumpers randomly hit the dispenser which is suspended by four wires. The droplet distribution is characterized by a polynomial which is subjected to the following conditions in terms of the spray normalized radius, n:

- at $n = 0$; $f = 0$ and $df/dn = 2$ which ensure that the distribution is proportional to the surface are (i.e. $f \propto n^2$)
- at $n = 0.56$; $df/dn = 0$ which sets a maximum value of the distribution at the radius bounding the region of free random motion of the droplet dispenser which is unconstrained by the bumpers motion (i.e. $n = 0.56$)
- at $n = 1$; $f = 0$ which insures that the outer maximum radial position is never reached
- the distribution f is normalized so that its integral over the whole spray region is set to unity

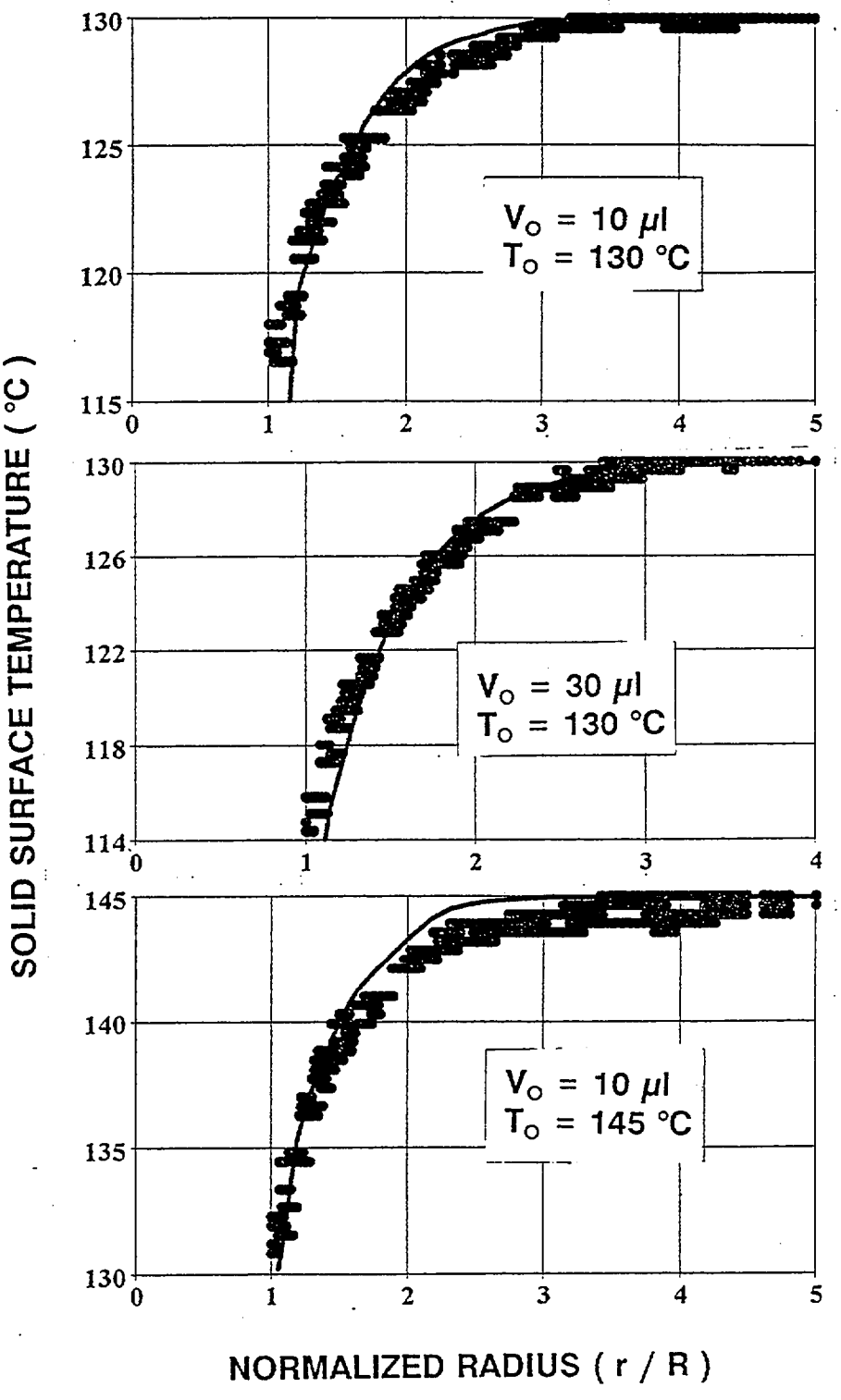

Figure 11 Model validation: solid surface temperatures for water on Macor at $t = 0.3\ \tau$ (— : numerical simulation; ■ : experimental data).

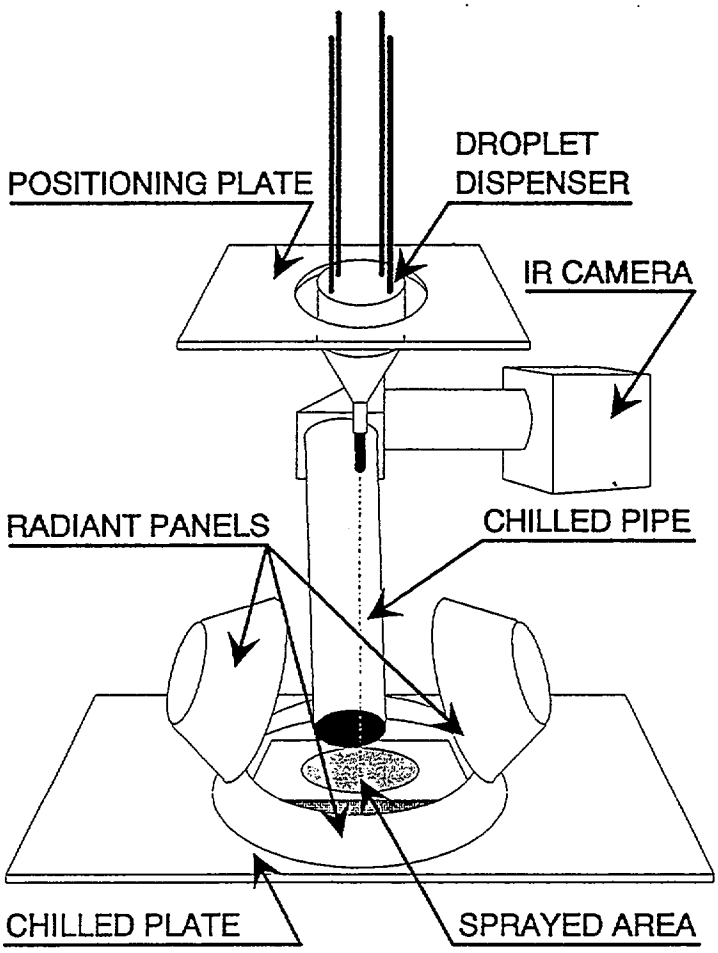

Figure 12 Experimental apparatus.

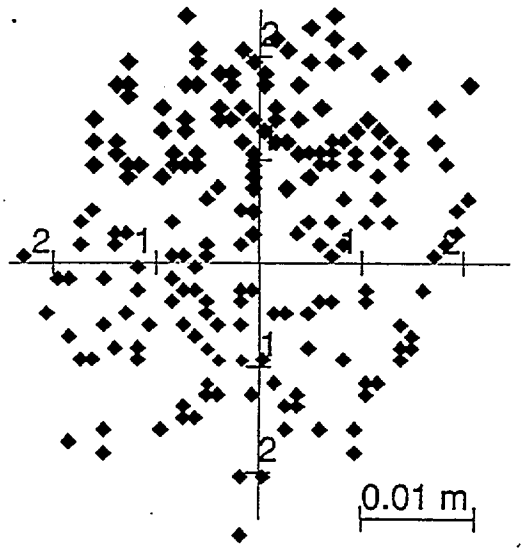

Figure 13 Typical droplet distribution.

With these conditions, the function f, describing the droplet distribution is given as:

$$f = 9.15\ n^4 - 22.64\ n^3 + 11.49\ n^2 + 2.00\ n \qquad (2)$$

The integral of this distribution function is checked against the cumulative droplet distribution obtained from the figure and shows excellent agreement.

The infrared data is processed by a video digitizing system composed of a Matrox MVP-AT frame-grabber board installed in an IBM PC-AT. Once digitized, each frame is analyzed pixel-by-pixel using Image-AT software linked with a user-written source code. Figure 14 shows the typical data collected from an individual frame which is taken every 30 seconds during the transient. The overall experiments lasts about 15 minutes for a total of 30 frames. There are 130 shades of gray associated with the infrared intensity levels. Since the temperature range is of 100 °C, the temperature resolution is 0.77 °C/gray-value. A spatial resolution of 70 microns could be achieved. The data storage requirements limit the spatial resolution to about 0.5 mm. The gray value of every fifth pixel is used over an image covering a region 0.046 m x 0.034 m. For each frame, the temperature is averaged and a single data point is obtained. Figure 15 shows the typical transient behavior of the average surface temperature. The deviation of the data points from a smooth decay occurs due to the nature of the data acquisition. Since only a portion of the sprayed area is viewed and averaged, at any instant, the number of droplets that are in the field of view may be different than at other instants thus resulting in oscillations of the average temperature of the sampled surface. An exponential fit is used to curve-fit the data representing the transient behavior of the average solid surface temperature.

4.2 Theoretical Model

The theoretical model for a sparse spray is based on the super position of the cooling effect of individual droplets [29]. Therefore, the temperature at a given point on the solid surface is the result of the combined effect of the cooling due to all the droplets previously deposited. In order to determine, in a compact form, the single droplet cooling effect, the droplets are subdivided in two groups depending on their proximity to the point of concern. The droplets outside a circular region of radius equal to five deposited droplet radii are considered in the far-field and their effect is reduced to that of instantaneous point sinks [30]. The droplets inside the previously defined circular region are considered in the near-field. Note that the size of the circular region is dependent on the cooling agent (i.e. water) and on the solid thermal properties (i.e. Macor). To seek a simple formulation of the cooling effect of a single droplet, one must study the effect of the solid-liquid interfacial boundary condition under the droplet [31]. Figure 16 shows the solid liquid transient boundary conditions calculated by the coupled code described previously in comparison with the closed form solution for the case of uniform and constant heat flux and for the for the case of uniform and constant contact temperature. The solution for uniform and constant temperature is discarded since it does not conserve energy. The solution for the case

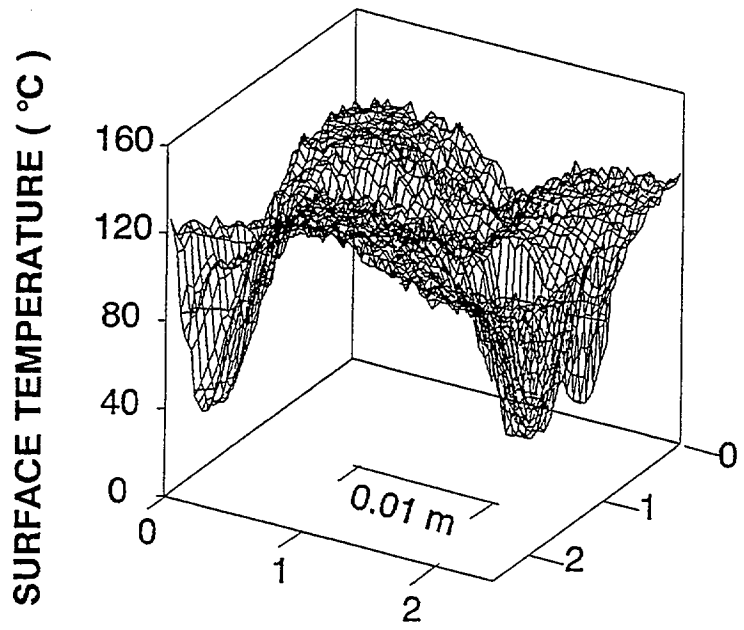

Figure 14 Typical surface temperature distribution for water on Macor (after 60 s; T_o = 140 °C; V_o = 10 μl; G = 1.50 g/m²s).

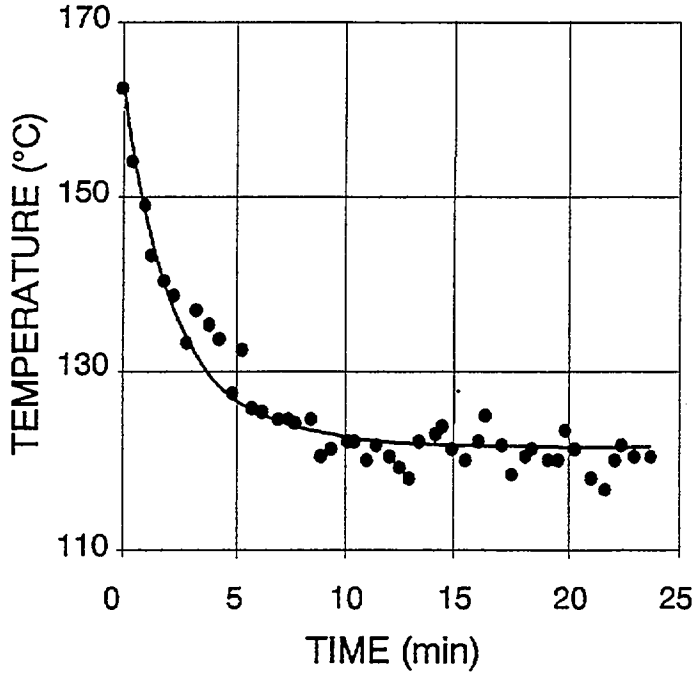

Figure 15 Transient average surface temperature (T_o = 162 °C; G = 0.97 g/m²s).

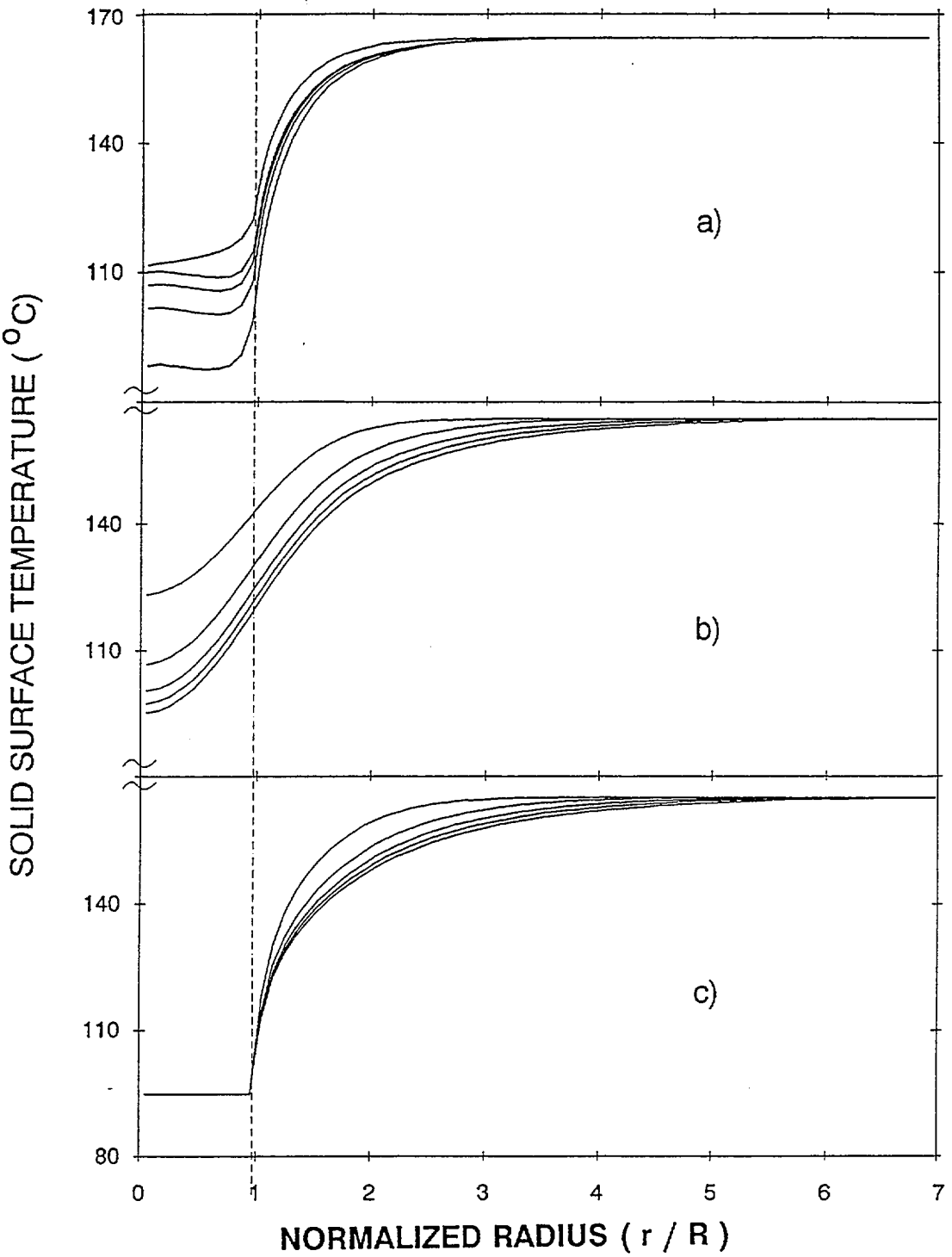

Figure 16 Typical solid surface temperature profiles for a 10 μl water droplet on Macor with T_o = 165 °C at t/τ = 0.1, 0.3, 0.5, 0.7 and 0.9: a) coupled code; b) code with constant and uniform heat flux; and c) code with constant and uniform interfacial temperature.

of uniform and constant heat flux is modified to include the recovery transient after the droplet evaporation is complete. The result can be written as:

$$T_o - T = \frac{q_o z}{k} + \zeta \frac{(q_c - q_o)\, R}{k} \times \int_0^\infty J_o\left(\frac{\lambda r}{R}\right) J_1(\lambda) \left[erf\left(\frac{\lambda \sqrt{\alpha t}}{R}\right) - erf\left(\frac{\lambda \sqrt{\alpha (t-\tau)}}{R}\right)\right] \frac{d\lambda}{\lambda} \quad (3)$$

The constant ζ encompasses: a) the adjustment due to the shrinking of the wetted region; and b) the adjustment associated with the effect of the droplet curvature on the radiant heat input. This constant is set at 0.9 for the case of droplets of initial volume of 10 μl over the range of initial solid surface temperatures from 70 to 164 °C which are bounding the experimental range under consideration. Note that the temperatures upper bound corresponds to the onset of nucleate boiling of water on Macor.

There are two inputs into the closed form solution which must be obtained from the single droplet code previously described. The fraction of vaporization heat input due to conduction from the solid (which is the heat flux q_c) and the droplet evaporation time τ. Both these quantities are function of the solid surface temperature at droplet deposition. With the near-field and the far-field solutions defined, the super-position of the cooling effects of all the droplets is evaluated for the point of concern. Note that the solid surface temperature at the location of deposition of each droplet must be known at the deposition time.

Figure 17 provides a comparison of the measured and calculated solid surface temperature distribution at two different times during the transient. Great care is taken to identify an identical portion of the spray area both in the model and in the computations. This is very important since just a portion of the spray area is seen and, therefore, the averaged surface temperature varies depending whether a central or peripheral field of view is considered. At the early stages (t = 50s), the individual droplets are clearly defined by deep temperature drops at the deposition sites. This is evident for the experiment in the lower right end corner of the frame and for the mid-left region of the frame in the calculation. For both, the temperature excursion is between 80 and 140 °C. As the time progresses, the interactions of multiple droplet cooling effects become evident. Multi-droplet clusters are evident at 600 s in both the calculation and the data. Note the position of the isothermal at about 130 °C in both frames.

Figure 18 shows a comparison of data and calculations for a variety of cases in terms of the average solid surface temperature which has been normalized with respect to the initial solid surface temperature prior to the spray application and with respect to the final long-term steady state temperature evaluated by the model. There are

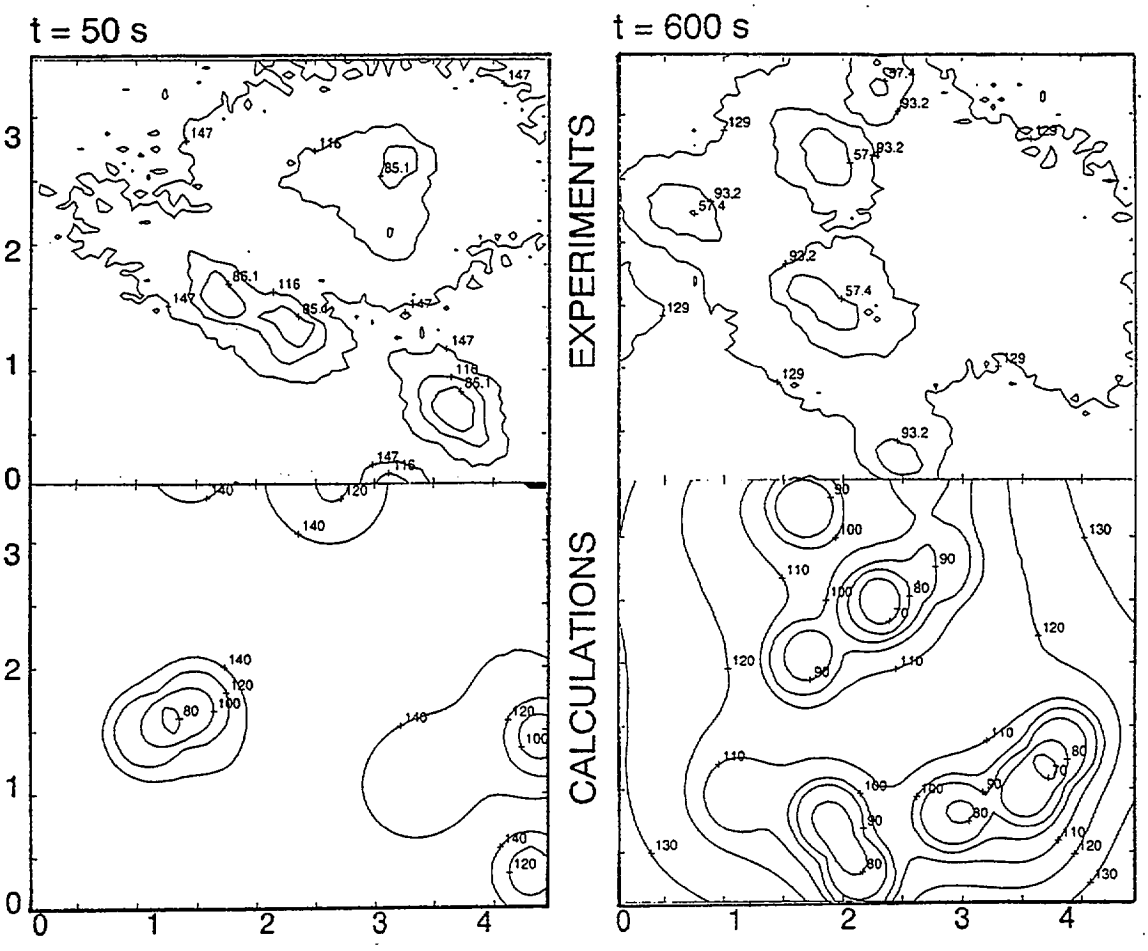

Figure 17 Typical transient surface temperature distributions (G = 0.96 g/m²s; T_o = 151 °C; distances on both axes in centimeters).

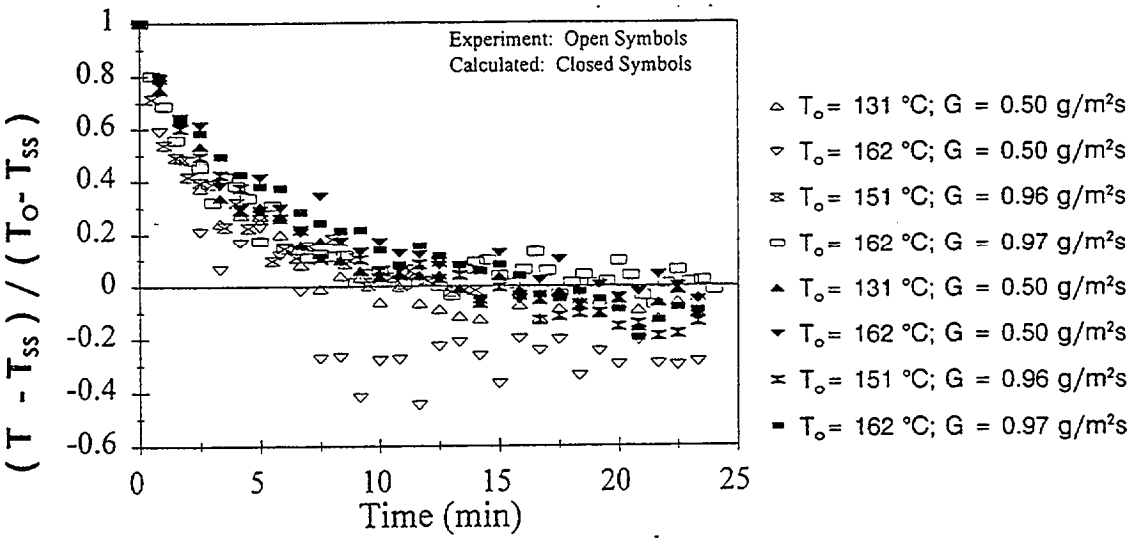

Figure 18 Summary of results: calculations versus experiments.

discrepancies between the calculations and the data for the set at 162 °C and G = 0.5 g/m^{2}s. This is due to the occurrence of nucleate boiling in the early portion of the transient in the data. The model is limited to evaporative cooling and, therefore, it predicts a far less intense cooling. Note that, as the temperature of the surface drops, the data show a return to full evaporative cooling. However, the intense initial cooling due to nucleate boiling has deeply depleted the heat stored in the solid. It will take almost one hour for the system to recover the predicted steady state value in the experiment due to its large time constant. With this notable exception, the data and the computations agree very well. The independence of the surface cooling with respect to the water mass flux is evident. The substrate properties, that is the thermal properties of the solid, play a far more significant role. A cursory examination of the time constant and of the solid thermal diffusivity provides a value of the thermal penetration depth of the order of the droplet radius of influence on the solid surface. This quantitative correspondence can be use to estimate the overall response of solid surfaces subjected to spray cooling.

7. CONCLUSIONS

An overview of the research on dropwise evaporative cooling leading to the prediction of sparse spray cooling of hot solid surfaces has been presented. Early work on single droplets deposited on high thermal conductivity solids is used to validate the liquid-vapor boundary conditions and the assumption of negligible convective heat transfer in the liquid layer. The coupling of the liquid and the solid transient conduction equations allows the solution of the single droplet evaporating over low thermal conductivity solids and provides insight into the solid-liquid boundary conditions. The assumption of one-dimensionality of the conduction heat transfer in the liquid layer is also justified. Extension to the radiant heat input case is implemented by carefully evaluating the effect of direct vaporization of the liquid due to the radiant heat input absorption in the water layer. The differences between the conduction and radiant heat inputs are studied to gain in-depth understanding of the governing phenomena. With these models for the single droplet, the cooling effect of a sparse spray of uniform-size droplets is successfully evaluated. The average spray cooling is linked to the substrate properties (i.e. the solid thermal properties).

ACKNOWLEDGEMENTS

The research was conducted at the Building and Fire Research Laboratory of the National Institute of Standards and Technology (BFRL-NIST). The guidance and support of Drs. Evans and Baum (BFRL-NIST) were essential to the performance of this work. The experiments and the analyses were performed by: Ham, Liao, Kavoosi, Kidder, Klassen, Mahajan, Meng, Tinker, Trehan, and White. The author wishes to thank Dr. Tartarini (University of Bologna) for his invaluable contribution over the last five years of this research.

NOMENCLATURE

A_ϕ	fractional area coverage
E_λ	monochromatic emissive power
f	droplet distribution function
G	water spray mass flux
H	volumetric heat absorption
H_i	limiting value of H for $z \to 0$
J_o, J_1	Bessel functions
k	thermal conductivity
n	spray normalized radius
q	heat flux
q_c	conduction heat flux
r	radial coordinate
R	radius of the wetted region
T	solid surface temperature
T_{ss}	steady state surface temperature
V	droplet volume
x, y, z	cartesian coordinates

Greek

α	thermal diffusivity
β	shape factor
δ	liquid layer thickness
ζ	constant; see Eq. (3)
η	integration variable
θ	contact angle
θ_r	receding angle
κ	absorption coefficient
μ	direction cosine
ρ	reflectivity
τ	droplet evaporation time
ϕ	azimuthal angle

Subscripts

o	identifies initial conditions

REFERENCES

1. K.J. Choi and S.C. Yao, Mechanism of film boiling heat transfer of normal impacting spray, *Int. J. Heat Mass Transfer*, **13**, 311-318 (1987).
2. J.G. Leidenfrost, *De aquaea communis nonnullis qualitatibus tractatus*, (1756).
3. W.M. Grissom and F.A. Wierum, Liquid spray cooling of a heated surface, *Int. J. Heat Mass Transfer*, **24**, 261-271 (1981).
4. S. Inada, Y. Miyasaka and K. Nishida, Transient heat transfer for a water droplet impinging on a heated surface, *Bull. JSME*, **28**, 2675-2681 (1985).
5. C.O. Pedersen, An experimental study of the behavior and heat transfer characteristics of a water droplet impinging upon a heated surface, *Int. J. Heat Mass Transfer*, **13**, 369-381 (1970).
6. K. Makino and I. Michiyoshi, Discussion of transient heat transfer to a water droplet on heated surfaces under atmospheric pressure, *Int. J. Heat Mass Transfer*, **30**, 1895-1905 (1987).
7. S. Toda, A study of mist cooling. first report: Investigation of mist cooling, *Heat Transfer Jap. Res.* **1**, 39-50 (1972).
8. C. Bonacina, S. Del Giudice and G. Comini, Dropwise evaporation, *J. Heat Transfer*, **101**, 441-446 (1979).
9. J.J. Rizza, A numerical solution to dropwise evaporation, *J. Heat Transfer*, **103**, 501-507 (1981).
10. K.K. Tio and S.S. Sadhal, Thermal analysis of droplet spray evaporation from a heated solid surface, *J. Heat Transfer*, **114**, 220-233 (1992).
11. S. Chandra and C.T. Avedisian, On the collision of a droplet with a solid surface,

Proc. Royal Soc., **432**, 13-41 (1991).
12. N. Zhang and W.J. Wang, Natural convection in evaporating minute drops, *J. Heat Transfer*, **104**, 656-662 (1982).
13. M. diMarzo and D.D. Evans, Evaporation of a water droplet deposited on a hot high thermal conductivity surface, *J. Heat Transfer*, **111**, 210-213 (1989).
14. M. Seki, H. Kawamura and K. Sanokawa, Transient temperature profile of a hot wall due to an impinging liquid droplet, *J. Heat Transfer*, **100**, 167-169 (1978).
15. T.H. Chilton and A.P. Colburn, Mass transfer (adsorption) coefficients prediction data on heat transfer fluid motion, *Ind. Eng. Chem.*, **26**, 1183-1187 (1934).
16. M. diMarzo and D.D. Evans, Dropwise evaporative cooling of high thermal conductivity materials. *Heat and Technology*, **5**, 126-136 (1987).
17. S. Ostrach and A. Pradhan, Surface-tension induced convection at reduced gravity, *AIAA J.*, **16**, 419-424 (1978).
18. M. Klassen, M. diMarzo and J. Sirkis, Infrared thermography of dropwise evaporative cooling. *Exp. Thermal Fluid Sci.*, **5** 136-141 (1992).
19. L.C. Wrobel and C.A. Brebbia, A formulation of the boundary element method for axisymmetric transient heat transfer conduction, *Int. J. Heat Mass Transfer*, **24**, 843-850 (1981).
20. M. diMarzo, Y. Liao P. Tartarini, D.D. Evans and H. Baum, Dropwise evaporative cooling of a low thermal conductivity solid. *Fire Safety Science - Proc. of the 3rd Int. Symp.*, ed. G. Cox & B. Longford 987-996 (1991)
21. M. diMarzo, P. Tartarini, Y. Liao, D.D. Evans and H. Baum, Evaporative cooling due to a gently deposited droplet. *Int. J. Heat Mass Transfer*, **36** 4133-4139 (1993)
22. M. diMarzo, C.H. Kidder and P. Tartarini, Infrared thermography of dropwise evaporative cooling of a semiinfinite solid subjected to radiant heat input, *Exp. Heat Transfer*, **5** 101-114 (1992).
23. S.S. Sadhal and M.S. Plesset, Effect of solid properties on contact angle in dropwise condensation and evaporation, *J. Heat Transfer*, **101**, 48-54 (1979).
24. F.F. Simon and Y.Y. Hsu, Wetting dynamics of evaporating drops on various surfaces, *NASA Tech. Memo.* NASA TM X-67913 (1971).
25. R. Siegel and J.R. Howell, *Thermal Radiation Heat Transfer*, Hemisphere Publishing Co., New York (1981).
26. P. Tartarini and M. diMarzo, Dropwise evaporative cooling in a radiant heat field. *Proc. of the 10th Int. Heat Transfer Conf.*, ed. G.F. Hewitt, **6** 277-282 (1994).
27. G. White, S. Tinker and M. diMarzo, Modelling of dropwise evaporative cooling on a semi-infinite solid subjected to radiant heat input, *Fire Safety Science - Proc. of the 4th Int. Symp.*, ed. T. Kashiwagi 217-228 (1994).
28. H.F. Dawson and M. diMarzo, Multi-droplet evaporative cooling: experimental results. *AIChE Symp. Ser.*, **89** 26-35 (1993).
29. S. Tinker and M. diMarzo, Multi-droplet evaporative cooling. *Annual Conference on Fire Research*, NISTIR 5499 69-70 (1994).
30. H.S. Carslaw and J.C. Jaeger, *Conduction of Heat in Solids*, Clarendon Press, Oxford (1959).
31. P. Tartarini and M. diMarzo, The solid-liquid interfacial conditions for dropwise evaporative cooling. *Heat and Technology*, **10** 130-144 (1992).

PART ONE

The cooling effect of a single water droplet deposited on a high thermal conductivity semi-infinite solid, heated by conduction from below, is the simplest possible configuration that can be investigated. The key findings of these first studies are:

1. The boundary condition at the liquid-vapor interface can be expressed by a combined mass transfer and heat transfer conservation statement.
2. The convective heat transfer inside the deposited droplet during the evaporative transient is negligible.
3. The droplet shape can be characterized as a segment of a sphere and the area of the solid-liquid interface remains constant for most of the transient.

M. diMarzo & D.D. Evans, Evaporation of a water droplet deposited on a hot high thermal conductivity surface, Journal of Heat Transfer 111 (1989) 210-213.
M. diMarzo & D.D. Evans, Dropwise evaporative cooling of high thermal conductivity materials, Heat and Technology 5 (1987) 126-136.

PAPER # 2

Evaporation of a Water Droplet Deposited on a Hot High Thermal Conductivity Surface

M. di Marzo[1] and D. D. Evans[2]

Nomenclature

c = specific heat
D = mass diffusivity
h = overall heat transfer coefficient
h_c = convective heat transfer coefficient
h_m = mass transfer coefficient
k = thermal conductivity
M = molecular weight
q = heat flux
r = radial coordinate tangent to the solid surface orginating at the center of the wetted area
R = radius of the wetted area
s = nondimensional thickness of the droplet $= y_i/R$
t = time
T = temperature
V = droplet volume
W = vapor molar flux
x = vapor molar fraction
y = coordinate normal to the solid surface originating at the center of the wetted area
z = nondimensional radius $= r/R$
α = thermal diffusivity
β = wetting parameter
γ = shape parameter $= s$ (at $r=0$)
Λ = latent heat of vaporization
ρ = density

Subscripts

a = air
i = interface
o = initial value (at $t=0$)
s = solid or solid surface
w = water

Introduction

Many studies have been performed to quantify the vaporization process for both single droplets and multiple-droplet arrays impacting on hot surfaces. For the studies found in the published literature, the full span of the droplet vaporization processes is usually reported. These would include evaporation, nucleate boiling, film boiling, and Leidenfrost transition. The present investigation is limited in the span of vaporization processes studied, being only concerned with the evaporation of a droplet on a hot surface. The study does report very detailed results for spatial and temporal variation of the heat flux at the exposed surface of the droplet, and for temporal variation of the droplet volume. Limiting the study to evaporation implies that conditions are maintained under which nucleate boiling is fully suppressed.

[1]Mechanical Engineering Department, University of Maryland, College Park, MD 20742.
[2]Center for Fire Research, National Bureau of Standards, Gaithersburg, MD 20899.

Contributed by the Heat Transfer Division for publication in the JOURNAL OF HEAT TRANSFER. Manuscript received by the Heat Transfer Division November 18, 1986. Keywords: Evaporation, Sprays/Droplets, Transient and Unsteady Heat Transfer.

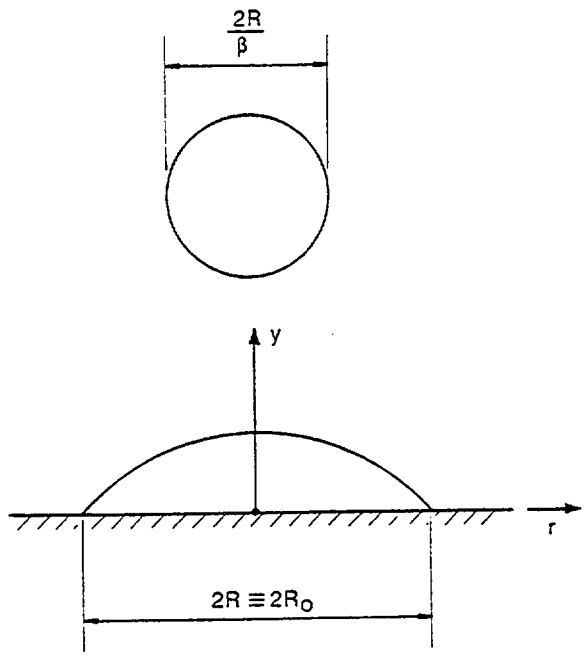

Fig. 1 Parameter β and coordinate system

Phenomenology

A spherical droplet impacting on a solid surface spreads on it. The final configuration of the liquid varies a great deal and depends on a multitude of parameters. For the case of water impinging on a surface at near-saturation temperature, the shape can be regarded as a segment of a sphere (Zhang and Yang, 1982). Note that, in this study, the droplet is considered to be homogeneous in the liquid phase at all times, and *evaporation* at the liquid-vapor interface is the only mean of generating the vapor phase.

The radius of the wetted area is a very important parameter, as recognized by Bonacina et al. (1979) and other investigators. In the literature, the radius of the wetted area is nondimensionalized with the radius of the sphere with equivalent initial liquid volume. This ratio is the parameter β_o. For droplets "softly" deposited on the surface (droplet released from height less than 1 cm), a value of β_o in the range 1.2 to 1.5 is observed. However, for sprayed water, several investigators have reported values of β_o up to 4.5 (Bonacina et al., 1979; Rizza, 1981). In this study the emphasis is on "softly" deposited droplets. It is crucial to note that these values of β_o are referred to the initial condition at deposition before evaporation begins ($t=0$). Values for the more general parameter β based on the liquid volume at any time during the evaporation process can be calculated using as a reference the radius of the wetted area and normalizing it with the radius of the spherical droplet having volume equal to the instantaneous volume of the water present. *Note that the radius of the wetted area is constant throughout most (90 to 95 percent) of the total evaporation time* as illustrated in Fig. 1. Wayner (1973) proposed a model to evaluate the liquid-solid contact angle during the evaporative process of a droplet wetting surface of constant radius.

The importance of the parameter β is that it accounts for the effects of a number of variables that characterize the surface conditions (wettability, roughness, etc.), the fluid (surface tension, wetting ability, etc.), and the droplet deposition process. All the present experimental data were obtained for pure, degassed and de-ionized water droplets deposited on an aluminum block that was coated with a very thin (≈ 0.06 μm) chromium layer. The chromium was vapor deposited on the aluminum to obtain a polished, smooth (roughness of 0.1-0.15 μm), and scratch-resistant surface. Prior to each droplet deposition, the surface was cleaned with ethyl alcohol to remove particles and grease. In spite of this careful procedure, some scatter in the experimental data was observed. This scatter is due mainly to the deposition technique, in which there was some uncertainty in positioning the hypodermic needle used to dispense the water above the surface. For each temperature considered (seven values between 75 and 100°C) and for each volume considered (five between 10 and 50×10^{-9} m^3) ten values of β_o were measured for a total of 350 data points. No systematic variation with volume was found because, in the limited range of droplet volume of interest, the values of β_o obtained for the various volumes were not clearly distinguishable. The temperature dependence of β_o was more evident; most of the data especially in the low-temperature range lie in the 5 percent band about the linear regression of the average values, which is given by

$$\beta_o = 0.009\, T_{so} + 0.6 \tag{1}$$

An analytical formulation defining the surface of a spherical segment representing the droplet on the surface in cylindrical coordinates is given by equating the volume of the spherical segment to the volume of the spherical droplet (and by assuming that at the droplet outer edge its thickness is zero). By introducing nondimensional coordinates, the equation for the droplet shape can be written as

$$s = \left[\frac{(1/\gamma+\gamma)^2}{4} - z^2\right]^{1/2} - \frac{(1/\gamma-\gamma)}{2} \tag{2}$$

where s is y/R, z is r/R, and γ is found to be

$$\gamma = [4/\beta^3 + (1+16/\beta^6)^{1/2}]^{1/3} + [4/\beta^3 - (1+16/\beta^6)^{1/2}]^{1/3} \tag{3}$$

Theoretical Evaporation Time

The high thermal conductivity of the metal solid suggests that the temperature of the solid surface under the droplet can be assumed constant during the evaporative process. This assumption implicitly uncouples the solid substrate properties from the evaporation process. For the case of a low-conductivity material it is anticipated that such uncoupling will not be possible.

In order to evaluate the liquid-vapor interfacial molar fraction, mass transfer as well as heat transfer must be considered. The heat balance at the interface can be written as

$$q = W\Lambda M_w + h(T_i - T_a) \tag{4}$$

where W is the molar flux of the vapor at the water-air interface. The temperature profile in the liquid can be assumed to be linear (Bonacina et al., 1979), and the heat transfer contribution by convection and radiation can be neglected; this yields

$$\frac{k_w(T_s - T_i)}{Rs} = \left[\frac{x_i - x_a}{1 - x_i}\right]\rho_a h_m \Lambda \left[\frac{M_w}{M_a}\right] \tag{5}$$

where T_s is the surface temperature defined by Seki et al. (1978). By noting that the water-air molecular weight ratio is 0.624 and referring to Chilton and Colburn (1934), one obtains

$$\frac{k_w}{Rh_{cs}}(T_s - T_i) = 0.624\left[\frac{D}{\alpha_a}\right]^{2/3}\left[\frac{\Lambda}{c_a}\right]\left[\frac{x_i - x_a}{1 - x_i}\right] \tag{6}$$

Note that the only unknown x_i is a single-valued function of T_s. The left-hand side of this equation is finite at $r=R$ if the temperature at the droplet exposed surface coincides with the solid surface temperature. This condition seems reasonable

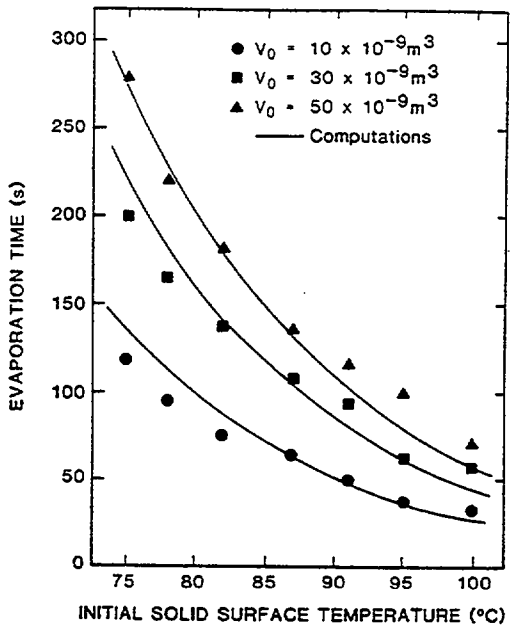

Fig. 2 Evaporation time as a function of initial solid surface temperature for various droplet volumes

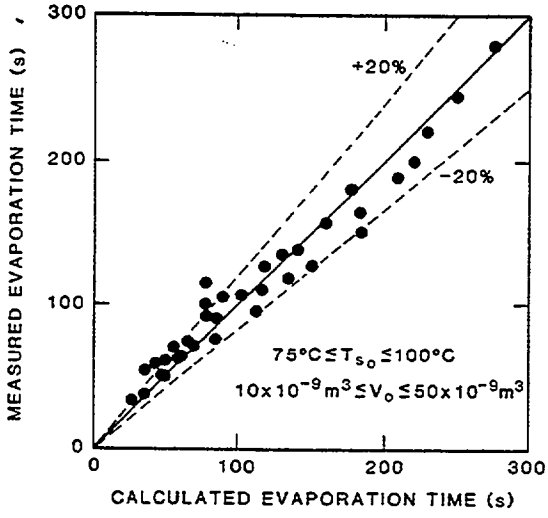

Fig. 3 Evaporation time: theory versus experiments

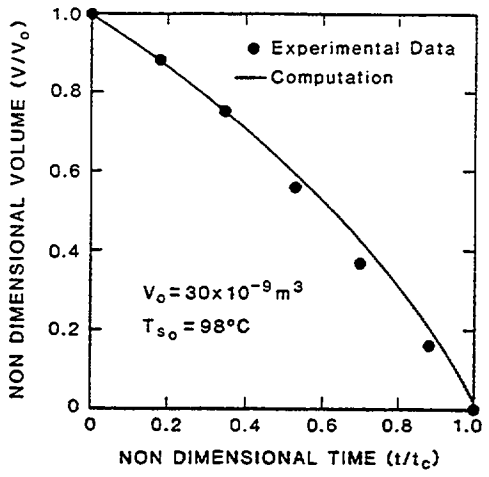

Fig. 4 Liquid water inventory versus time

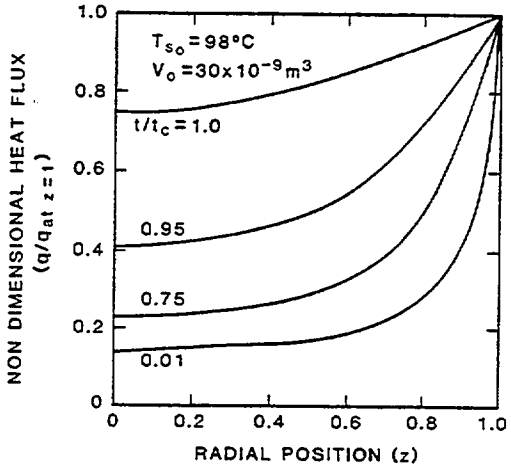

Fig. 5 Temporal and spatial heat flux behavior

and it is used to determine the vapor molar fraction in the air at the outer edge of the droplet.

By considering the energy balance on the liquid droplet, the instantaneous rate of evaporation is then deduced as

$$-\frac{dV}{dt}=\frac{2\pi R^2(0.624)h_c}{\rho_w c_a}\left[\frac{D}{\alpha_a}\right]^{2/3}\int_0^1\left[\frac{x_i-x_a}{1-x_i}\right]z\,dz \qquad (7)$$

and the local heat flux at the liquid-vapor interface is given by

$$q=0.624h_c\left[\frac{\Lambda}{c_a}\right]\left[\frac{D}{\alpha_a}\right]^{2/3}\left[\frac{x_i-x_a}{1-x_i}\right] \qquad (8)$$

When the initial volume is known, a numerical technique allows one to determine the total evaporation time from equation (7). Note that at each time step the evaporative mass flux is obtained by computing the integral in the right-hand side of the equation.

Model Validation

The details of the experimental setup and a complete description of the data acquistion, in particular concerning the overall and convective heat transfer coefficients, are given by diMarzo and Trehan (1986). Figure 2 illustrates the comparison of results between the computations of the model developed in this study and experiments. Good agreement is observed. Figure 3 shows a comparison of the total evaporation time measured and calculated for a large number of experiments conducted in this study. In all these experiments, the droplet volume ranges between 10 and 50×10^{-9} ms, and the initial surface temperature is in the range of 75 to 100°C. To validate the model further, the normalized liquid volume is plotted versus the time, nondimensionalized with respect to the total evaporation time, in Fig. 4. Very good agreement is found for the data, which were obtained from measurements of the volumes observed in photographic sequences of the droplet evaporation.

It is interesting to deduce information concerning the temporal and spatial distribution of the heat flux on the droplet-to-air interface from the model calculations. Figure 5 shows model predictions of the spatial heat flux distribution. The high heat flux at the droplet outer edge is evident. This finding is in agreement with the trends illustrated by the computations of Cook et al. (1981) based on measured local liquid mass flow rates at the liquid-solid contact line. Note that for three quarters of the total evaporation time the central portion of the droplet liquid-vapor interface does not contribute much to the process; in the last quarter, the dramatic flux increase is produced by the contribution of most of the droplet surface

because the reduced thickness of the droplet enhances the heat transfer across the liquid layer.

Michiyoshi and Makino (1978) observed that the temperatures at the solid surface and at a fixed point above it (in the liquid) are constant during the evaporation process. This fact implies that the heat flux is also constant. The results just shown confirm that during most of the evaporation process, in the region close to the droplet symmetry axis, the heat flux does not vary significantly.

These results show that the heat flux at the droplet edge can be as high as three times the spatial average heat flux at the beginning of the evaporation process. As the phenomenom progresses, the spatial average heat flux increases but the flux distribution in the radial direction becomes more uniform. Note that the droplet under consideration has a radius of about 3×10^{-3} m and that a gradient of 1°C across that distance produces a heat flux of more than 40,000 W/m^{-2} in the aluminum. It follows that the hypothesis of uniform temperature distribution under the droplet seems reasonable since the temporal and spatial average heat flux for this case is about 50,000 W/m^{-2}. The application of this simple boundary condition to the case of low thermal conductivity solid materials is not possible and a significant temperature distribution in the radial direction under the droplet is expected. To solve this problem, the droplet energy equation must be coupled with the solid energy equation at the liquid-solid interface in order to obtain a solution that accounts for the temperature distribution under the droplet.

Conclusions

A model based on the assumption of uniform solid surface temperature is formulated for applications to droplets deposited on solids with large thermal conductivity. The droplet shape is successfully characterized using a spherical segment. The energy equation written for the droplet and at the liquid-vapor interface allows the determination of the evaporation time in reasonable agreement with experimental data. Further validation of the model is presented to describe the spatial and temporal behavior of the evaporative heat flux.

Acknowledgments

This research was supported by a grant of the Center for Fire Research of the National Bureau of Standards. The authors are deeply indebted to Professor Michiyoshi for his prompt and courteous comments on the experimental data reported in his paper. The Computer Science Center of the University of Maryland provided funding for the numerical computation.

References

Bonacina, C., Del Giudice, S., and Comini, G., 1979, "Dropwise Evaporation," ASME JOURNAL OF HEAT TRANSFER, Vol. 101, pp. 441–446.

Chilton, T. H., and Colburn, A. P., 1934, "Mass Transfer (Absorption) Coefficients—Prediction Data on Heat Transfer Fluid Motion," *Industrial Engineering Chemistry*, Vol. 26, pp. 1183–1187.

Cook, R., Tung, C. Y., and Wayner, P. C., 1981, "Use of Scanning Microphotometer to Determine the Evaporative Heat Transfer Characteristics of the Contact Line Region," ASME JOURNAL OF HEAT TRANSFER, Vol. 103, pp. 325–330.

diMarzo, M., and Trehan, A. K., 1986, "Transient Cooling of a Hot Surface by Droplets Evaporation," Technical Report, NBS-GCR-86-516, National Bureau of Standards, Gaithersburg, MD.

Michiyoshi, I., and Makino, K., 1978, "Heat Transfer Characteristics of Evaporation of a Liquid Droplet on Heated Surfaces," *International Journal of Heat and Mass Transfer*, Vol. 21, pp. 605–613.

Rizza, J. J., 1981, "A Numerical Solution to Dropwise Evaporation," ASME JOURNAL OF HEAT TRANSFER, Vol. 103, pp. 501–507.

Seki, M., Kawamura, H., and Sanokawa, K., 1978, "Transient Temperature Profile of a Hot Wall Due to an Impinging Liquid Droplet," ASME JOURNAL OF HEAT TRANSFER, Vol. 100, pp. 167–169.

Wayner, P. C., 1973, "Fluid Flow in the Interline Region of an Evaporating Non-zero Contact Angle Meniscus," *International Journal of Heat and Mass Transfer*, Vol. 16, pp. 1777–1783.

Zhang, N., and Yang, W. J., 1982, "Natural Convection in Evaporating Minute Drops," ASME JOURNAL OF HEAT TRANSFER, Vol. 104, pp. 656–662.

PAPER # 3

HEAT and TECHNOLOGY
CALORE e TECNOLOGIA
Vol. 5 • No. 1-2 • 1987

DROPWISE EVAPORATIVE COOLING OF HIGH THERMAL CONDUCTIVITY MATERIALS

Marino di Marzo (*), David D. Evans (**)

ABSTRACT

Transient cooling of solid surfaces by water droplet evaporation has been investigated through controlled experiments using a large heated aluminum cylinder. Quantitative prediction of droplet evaporation time and in-depth transient temperature distribution in the solid have been made. In the case studied, a single droplet is deposited on a horizontal non-porous surface with initial temperatures in the range of 75°C to 100°C. The liquid-vapor interfacial temperature and the water vapor molar fraction in the air at the exposed surface of the water droplet are deduced from the coupled heat and mass transfer energy balance at the interface. Spatial and temporal integration of the overall droplet energy equation is used to predict the instantaneous evaporation rate and the droplet evaporation time. The boundary conditions for the wetted region proposed by Seki are used to obtain the transient temperature distribution for a semi-infinite solid. The region of the body affected by the droplet cooling is identified and its volume (normalized with the volume of the droplet) is plotted against the evaporation time. All data, regardless of the droplet volume or of the initial body surface temperature, lie within a narrow band about a straight line. This finding is the first important step to obtain a simple model for spray cooling based on local accurate description of the droplet-solid interactions. Modeling of spray cooling phenomena is the foundation for the construction of a thermal model for solid fuel fire extinguishment.

(*) Mechanical Engineering Department, University of Maryland, College Park, MD 20742.
(**) Center for Fire Research, National Bureau of Standards, Gaithersburg, MD 20899.

NOMENCLATURE

A, B, C, A', B', C'	constants
c	specific heat
D	mass diffusivity (steam-air)
f	generic function
h	convective heat transfer coefficient
k	thermal conductivity
L	latent heat of vaporization (water)
q	heat flux
r	radial coordinate tangent to the solid surface originating at the center of the wetted region
R	wetted region radius
t	time
T	temperature
T_o	initial solid surface temperature prior to the droplet deposition
V	droplet volume
V_i	volume of influence
x	molar fraction of steam in air
y	coordinate normal to the solid surface originating at the center of the wetted region upward oriented (in the droplet region)
z	coordinate normal to the solid surface originating at the center of the wetted region downward oriented (in the solid region)
α	thermal diffusivity
β	ratio of the wetted region radius to the radius of the spherical droplet of equivalent liquid volume
γ	square root of the product of specific heat, density and thermal conductivity
δ	shape parameter
ρ	density

Subscripts

a	air property
c	cumulative or total
i	at the droplet exposed surface
o	initial value
s	solid property or at the exposed solid surface
u	at the solid surface under the droplet
w	liquid water property

INTRODUCTION

The thermal behavior of a semi-infinite solid subjected to local surface cooling induced by a single evaporating droplet has been described in detail by Seki [1]. Numerous theoretical and experimental studies are found in the literature concerning the mechanism of evaporation of droplets impinging on a hot surface. A simple model is derived by Bonacina [2] which identifies an important geometrical parameter for the droplet-surface interaction. Grissom [3] investigated the cooling effect of a spray on a heated surface. The evaporation of single droplets are the objective of the work of Michiyoshi and Makino [4,5] which give a detailed insight into the thermal features of the evaporation process. Sadhal [6] provides an interesting analysis of the droplet-solid interactions for evaporation and condensation. The optical studies of the droplet configuration on a solid surface reported by Zhang [7] allow one to conclude that a spherical segment is a good geometrical representation of the actual droplet shape. In a previous paper di Marzo and Evans [8] derived a rigorous analytical model to predict the evaporation time, the evaporation rate and the local heat flux distribution at the droplet exposed surface during its evaporation.

In many of these studies, the full range of vaporization processes (including evaporation, nucleate boiling, film boiling, and transition boiling) are reported. This detailed study of the water droplet vaporization is intended to form the basis for a thermal model of solid fuel fire extinguishment, so this study is limited to investigations of the evaporation phenomena only.

The objective of this paper is to show that a simple relationship exists between the evaporation time and the volume of the portion of the solid affected by the cooling process induced by the droplet evaporation. In order to illustrate this finding, the basic heat transfer governing equation for the semi-infinite solid will be derived and merged with the previously developed model for the prediction of the evaporation time [8] to determine the cooling effect in the solid.

The high thermal conductivity of the heated aluminum block used in this study allows one to assume that the temperature, T_u, at the solid surface, under the droplet is constant. This hypothesis was successfully tested by Seki [1] against experimental data. The experimental findings by Michiyoshi [4] infer that the temperature of the solid surface under the

droplet is also constant during the evaporation process. This information coupled with the one reported by Seki [1] provides a simple boundary condition for the wetted region of the solid surface.

MODEL FORMULATION

A spherical droplet upon impacting a solid surface spreads on it. The final configuration of the liquid varies a great deal and depends on a multitude of parameters. For the case of liquid water impinging a surface at near water saturation temperature, the shape can be regarded as a spherical segment [7,8].

In Fig. 1, a typical sequence of photographs of an evaporating droplet is presented. It is important to note that the wetted region of the semi-infinite solid surface remains constant in size throughout most of the evaporative process.

The ratio of the wetted area radius to the radius of an equivalent liquid volume spherical droplet is identified by the parameter β [2]. This parameter is the only experimental input used in the analysis. The complexity of the parameters influencing the initial droplet shape (surface tension, surface wettability, etc.) is such that this semi-empirical approach was selected to formulate a reasonable simple analysis. The effect of the droplet kinetic energy (before impact) on the parameter β is negligible for droplet release height of less than 1.7 centimeters. This study is concerned only with droplet released at less than 1.7 centimeters from the solid surface. These droplets are referred to as "softly" deposited droplets [2,3].

The cooling effect induced by the droplet evaporation is complex to model analytically. The boundary conditions of the energy equation written for the droplet should match the boundary conditions of the energy equation written for the solid. Namely, the heat flux and the temperature should be set equal at each location and at each time at the liquid-solid boundary.

The model proposed by Seki [1] is based on a simplifying assumption. He considers the solid-liquid boundary to be at uniform constant temperature. This assumption finds its justification in the large values of the thermal conductivity of the metals. The heat flux required for the droplet evaporation is induced by small temperature gradients in the solid. Since Michiyoshi [4,5] confirmed experimentally that the solid-liquid interfacial temperature does not change appreciably in time, one can conclude that a uniform, constant temperature, T_u, under the droplet is a reasonable boundary condition. The advantages of such hypothesis is that now the energy equation for the solid can be integrated independently from the droplet behavior and only the overall evaporation time is required to obtain information on the solid cooling.

The solid thermal behavior is described by the energy equation and its boundary conditions, as previously derived by Seki [1]. In summary, for the system configuration depicted in Fig. 2, one can write

$$\frac{\partial T}{\partial t} = \alpha_s \left(\frac{\partial^2 T}{\partial z^2} + \frac{1}{r} \frac{\partial T}{\partial r} + \frac{\partial^2 T}{\partial r^2} \right) \qquad (1)$$

with the following boundary conditions:

$$r = 0 \qquad \partial T/\partial r = 0 \tag{2}$$

$$r \to \infty \qquad \partial T/\partial r = 0 \tag{3}$$

$$z \to \infty \qquad q = - k_s \partial T/\partial z \tag{4}$$

$$z = 0 \text{ and } r > R \qquad h_a(T_s - T_a) = - k_s \partial T/\partial z \tag{5}$$

$$z = 0 \text{ and } r \leq R \text{ for } t \leq 0 \text{ and } t > t_c$$

$$h_a(T_s - T_a) = - k_s \partial T/\partial z \tag{6}$$

$$z = 0 \text{ and } r \leq R \text{ for } 0 < t \leq t_c \qquad T = T_u \tag{7}$$

The evaporation time, t_c, is obtained from the model predictions as will be shown in the following section. Equation (1) is numerically integrated and the temperature distribution in the solid is obtained at each instant of time during the evaporation process and thereafter in the thermal recovery transient.

The spatial and temporal temperature distribution information generated by this process is overwhelming. In order to compact this information and to deduce useful correlations between the magnitude of the cooling effect and the droplet evaporation phenomena, a new quantity is introduced, namely the volume of influence. The volume of influence is the volume of the region where the temperature variation with respect to the steady state conduction temperature distribution prior to the droplet deposition exceeds a given value. The maximum possible temperature variation occurring in the solid is the difference between the solid surface temperature prior to the droplet deposition and the contact temperature (between the water and the solid) given by Seki [1] as

$$T_u = \frac{T_w \gamma_w + T_s \gamma_s}{\gamma_w + \gamma_s} \tag{8}$$

The volume of influence will be defined as the volume where the temperature variation exceeds ten percent of the maximum possible temperature difference. The results of the computations will be shown in terms of volume of influence and in particular in terms of the maximum volume of influence which is observed at the end of the evaporation process.

EVAPORATION TIME PREDICTION

In an earlier paper, di Marzo and Evans [8] showed that the droplet geometrical configuration is given by

$$y = \left[\frac{(1/\delta + \delta)^2}{4} - r^2\right]^{1/2} - \frac{(1/\delta - \delta)}{2} \tag{9}$$

where δ is

$$\delta = R \left\{\left[4/\beta^3 + \left(1 + 16/\beta^6\right)^{1/2}\right]^{1/3} + \left[4/\beta^3 - \left(1 + 16/\beta^6\right)^{1/2}\right]^{1/3}\right\} \tag{10}$$

and β is defined as the ratio of the radius of the wetted area to the radius of an equivalent liquid volume spherical droplet. The droplet configuration can be approximated to a spherical segment throughout all the evaporative process. It must be noted, however, that in the last portion of the process ($t > 0.95\ t_c$) the liquid film becomes very thin and the wetted surface suddenly receeds. The temperature at the exposed surface of the liquid droplet can be evaluated by a heat balance at the liquid vapor interface. By considering that the heat conducted through the liquid layer to the interface is equal to the energy required to evaporate the liquid droplet plus the small amount of energy convected away, one can write

$$\frac{k_w (T_u - T_i)}{y} = 0.624\ h_a \left(\frac{D}{\alpha_a}\right)^{2/3} \left(\frac{L}{c_a}\right)\left(\frac{x_i - x_a}{1 - x_i}\right) + h_a (T_i - T_a) \quad (11)$$

where the mass transfer coefficient is evaluated by making use of the Chilton-Colburn analogy [9]. Note that the only unknown is x_i since the interfacial temperature, T_i, is the saturation temperature of steam at the pressure corresponding to its molar fraction.

The overall heat balance on the droplet allows one to calculate the instantaneous evaporation rate as

$$-\frac{dV}{dt} = \frac{2\pi\ (0.624)\ h_a}{\rho_w c_a}\left(\frac{D}{\alpha_a}\right)^{2/3} \int_o^R \frac{x_i - x_a}{1 - x_i}\ r\,dr \quad (12)$$

where x_i is function both of y and t.

By integrating this equation over the droplet exposed surface at each instant of time and by reassessing the liquid inventory (and subsequently the shape of the droplet) at each time step, the overall evaporation time can be determined. Figure 3 illustrates the results obtained with the model in comparison with experimental data for water droplets evaporating on an aluminum cylindrical block. For a more complete description of the experimental apparatus and procedures, refer to Trehan [10]. A complete derivation of the evaporation time model is given by di Marzo in the aforementioned reference [8]. Comparison of the model results with experimental data obtained by Michiyohsi and Makino [4,5] show that the solid material does not influence the results provided that its thermal conductivity is such that uniform temperature at the solid surface under the droplet can be regarded as a reasonable assumption. In Fig. 4, various experimental data for different materials are compared with the theoretical calculations. Note that the evaporative heat flux is directly related to the evaporation time.

This droplet evaporation model provides detailed information on the local heat fluxes at the solid liquid-boundary during the evaporation. Therefore, a coupled solution of Eq. (11) and Eq. (1) could yield the desired results without imposing the constant temperature condition at the liquid-solid interface. The drawback of this approach is that an iterative computation scheme needs to be set up to solve both the solid and droplet energy equations simultaneously.

By making use of a closed form analytical solution described by Carslaw and Jaeger [11], it was determined that the temperature disuniformities in the liquid solid interfacial region amount to about 1°C. This result was obtained imposing, as a boundary condition of the

solid energy equation, heat fluxes of the order of those required for the droplet evaporation.

In conclusion, one can argue that, with respect to the heat and mass transfer phenomena, three resistances in series can be envisioned where the first resistance in the solid is negligible with respect to the other two. The heat transfer resistance in the droplet is comparable to the mass transfer resistance in the air-vapor region. For the case of low conductivity solids, these three resistances are all of the same order of magnitude; therefore, the full coupled problem must be solved.

To elaborate further on these results, it is interesting to note that the evaporation time has an exponential behavior with respect to the initial solid surface temperature. This means that

$$\ln t_c = - A' T_o + f(V_o) \tag{13}$$

Furthermore, in order to find the intercept, $f(V_o)$, one can observe that

$$f(V_o) = B' \ln(V_o) + C' \tag{14}$$

By combining these two equations, the following result is obtained

$$t_c = A V_o^B e - C T_o \tag{15}$$

The numerical values for the constant A, B, C were found to be respectively 880, 0.7 and 0.05 for water droplets on heated aluminum surfaces. The scatter of the experimental data about the model predictions is in the order of 15 percent.

SOLID THERMAL BEHAVIOR

The results of the numerical integration of Eq. (1) are illustrated in Fig. 5 through 7. The effectiveness of the volume of influence in compacting the cooling effect information is evident if one compares Fig. 5 and Figs. 6 and 7.

The volume of influence as a function of the initial solid surface temperature for various droplet volumes is depicted in Fig. 8. Again, an exponential pattern is observed both for the volume of influence curves as well as for the various droplet volumes. Consider, therefore, the plot of the volume of influence versus the evaporation time for the same droplet volume and initial solid surface temperature, as shown in Fig. 9. The uncertainties of the various parameters determining the evaporation time and the volume of influence are such that the points can be considered to lie in close proximity to the linear regression of the point values (for more details on the order of approximation, see di Marzo [8]).

The expression for the linear fit is given by

$$V_i = V_o(0.021 t_c + 3) \tag{16}$$

By combining Eq. (15) and (16), one obtains

$$V_i = 18 V_o^{1.7} e - 0.05 T_o + 3 V_o \tag{17}$$

This closed form, simple, analytical result illustrates the power of the analysis. Note that the specific numerical constants are for aluminum. The same governing equations and boundary conditions are common for high thermal conductivity materials. Therefore, similar trends in the volume of influence are expected, thus leading to a linear dependence of the non-dimensional volume of influence with the evaporation time. The temperature spatial and temporal uniformity under the droplet is the condition that allows the uncoupling of the droplet evaporation process from the solid thermal behavior. In order to obtain this result the thermal conductivity of the solid must be larger than the thermal conductivity of the liquid water. The volume of influence is the basic information that allows one to predict the cooling effect in a semi-infinite body subjected droplets evaporation. Further research based on these results will provide information on the cooling effect of an array of droplets impinging a surface, thus leading to a comprehensive model to predict spray cooling.

CONCLUSIONS

The energy equation, written in cylindrical coordinates for the semi-infinite metal body, provides information on the spatial and temporal temperature distribution in the body. A more compact information is given in terms of the volume of influence. The boundary conditions for the energy equation are formulated by using the liquid-solid contact temperature suggested by Seki [1] coupled with the evaporation time calculated by di Marzo [8]. This analytical model to predict the evaporation time requires that the wetting parameter β must be determined by experiments.

The volume of influence is found to correlate linearly with the evaporation time and to be independent from the droplet volume and the initial solid surface temperature. A consequence of this finding is that a simple, closed form expression for the volume of influence can be obtained. This information is the first step towards the analysis of multi-droplet cooling effect thus leading to the modelling of spray cooling processes.

ACKNOWLEDGMENTS

This research is supported by a grant of the Center for Fire Research of the National Bureau of Standards. The Computer Center of the University of Maryland provided partial funding for the numerical computations.

REFERENCES

[1] M. Seki, H. Kawamura, K. Sanokawa, "Transient Temperature Profile of a Hot Wall Due to an Impinging Liquid Droplet", Transaction of the ASME, Journal of Heat Transfer, Vol. 100, pp. 176, 1978.

[2] C. Bonacina, G. Comini, "Dropwise Evaporation", Transaction of ASME, Journal of Heat Transfer, Vol. 101, pp. 441-446, 1979.

[3] W.M. Grissom, F.A. Wierum, "Liquidspray Cooling of a Heated Surface", International Journal of Heat and Mass Transfer, Vol. 24, pp. 261-271, 1981.

[4] I. Michiyoshi, K. Makino, "Heat Transfer Characteristics of Evaporation of a Liquid Droplet on Heated Surfaces", International Journal of Heat and Mass Transfer, Vol. 21, pp. 605, 1978.

[5] K. Makino, I. Mikiyoshi, "Effect of Initial Size of Water Droplet on Its Evaporation on Heated Surfaces", International Journal of Heat and Mass Transfer, Vol. 22, pp. 979, 1979.

[6] S.S. Sadhal, M.S. Plesset, "Effect of Solid Properties and Contact Angle in Dropwise Condensation and Evaporation", Transaction of ASME, Journal of Heat Transfer Vol. 101, pp. 48-54, 1979.

[7] N. Zhang, W.J. Yang, "Natural Convection in Evaporating Minute Drops", Transaction of the ASME, Journal of Heat Transfer, Vol. 104, pp. 656, 1982.

[8] M. di Marzo, D.D. Evans, "Evaporation of a Water Droplet on a Hot High Thermal Conductivity Solid Surface", NBSIR 86-3384, 1986.

[9] T.H. Chilton, A.P. Colburn, "Mass Transfer (Absorption) Coefficients Prediction Data on Heat Transfer Fluid Motion", Industrial Engineering Chemistry, Vol. 26, pp. 1183, 1934.

[10] A.K. Trehan, M. di Marzo, D.D. Evans, "Transient Cooling of a Hot Surface by Droplet Evaporation", Proceedings of the Eastern Session of the Combustion Institute, Fall Technical Meeting, pp. 61-1, 1985.

[11] H.S. Carslaw, J.C. Jaeger, Conduction in Solids, Oxford University Press, Oxford, England, 1946.

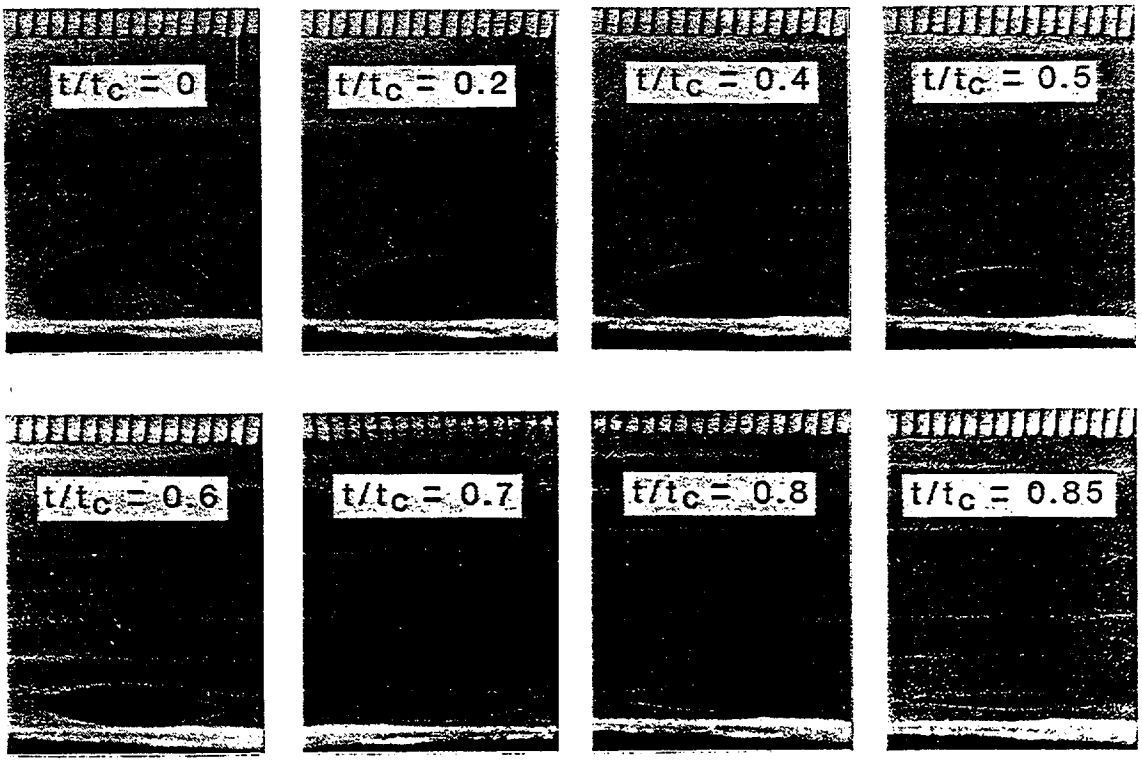

FIGURE ONE - Typical droplet evaporation phenomenology

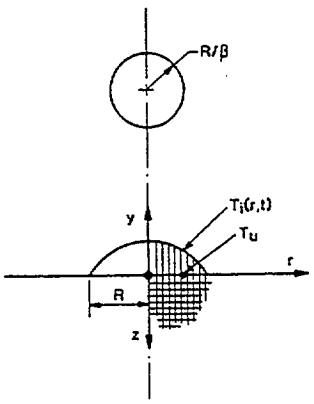

FIGURE TWO - Model and coordinate system

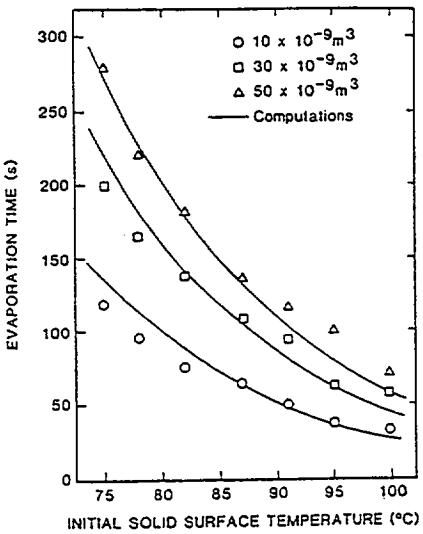

FIGURE THREE - Predicted and measured evaporation time versus initial solid surface temperature for various droplet volumes

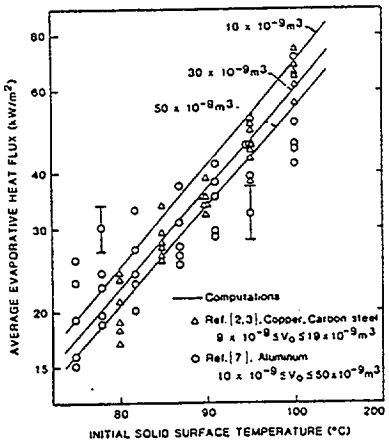

FIGURE FOUR - Average evaporative heat flux versus initial solid surface temperature for various solid materials and droplet volumes

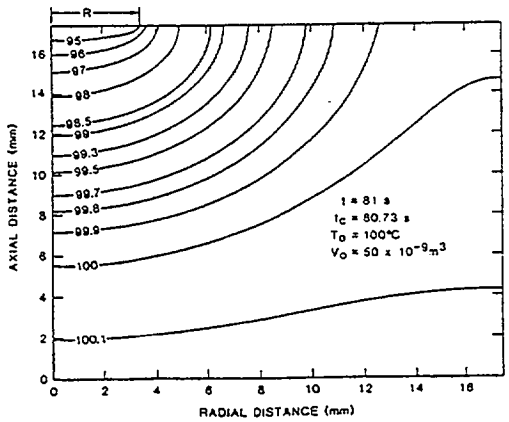

FIGURE FIVE - Spacial temperature distribution in the semi-infinite solid at time $t = t_c$

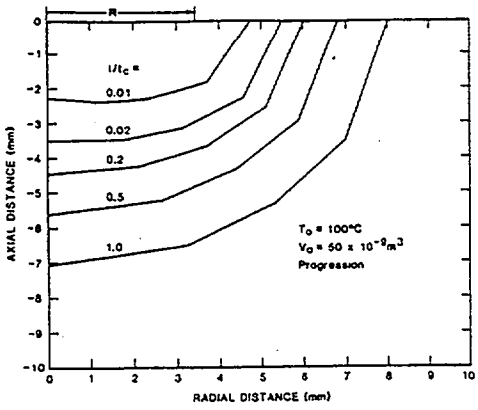

FIGURE SIX - Volume of influence at various times (progression)

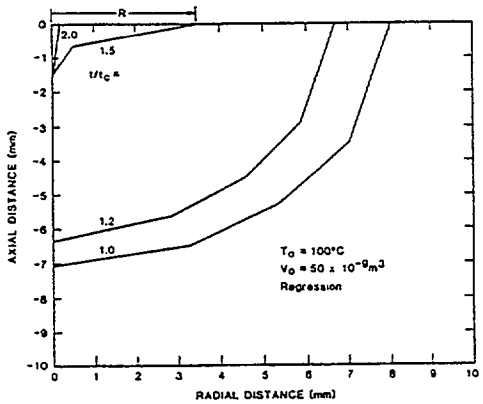

FIGURE SEVEN - Volume of influence at various times (regression)

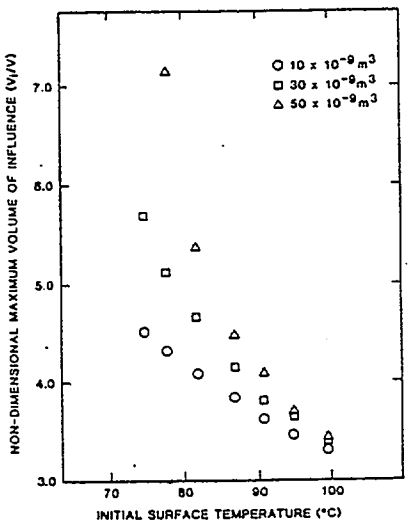

FIGURE EIGHT - Maximum non-dimensional volume of influence versus initial solid surface temperature for various droplet volumes

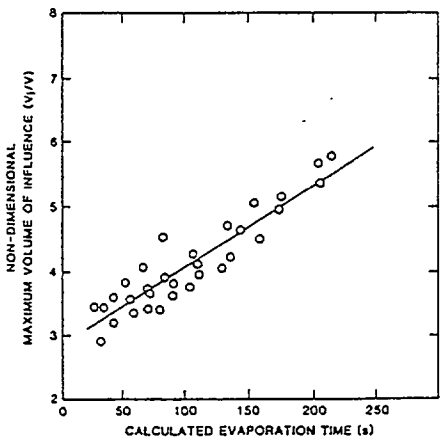

FIGURE NINE - Non-dimensional volume of influence versus predicted evaporative time

PART TWO

The previous results are extended to the case of low thermal conductivity solids. The temperature distribution at the liquid solid-interface is not uniform nor constant. However, for high thermal conductivity solids, the temperature variation is small. Therefore, it is possible to assume a constant and uniform temperature under the droplet. This assumption enables one to the decouple the solution for the liquid and solid domains. For low thermal conductivity solids, the coupled solution of the solid and the liquid domains is necessary. The major findings in this portion of the research program are:

1. It is possible to monitor the transient temperature distribution over the solid surface via infrared thermography.
2. The coupled solution for the liquid and the solid domains cannot be obtained with finite difference methods because the temperature gradients in the solid at the droplet edge are very large. Therefore, the solution for the solid domain is obtained with a boundary element method.
3. The closed-form solution based on constant and uniform heat flux over a circular disk on a semi-infinite solid surface provides a reasonable fit of the couple model results.

M. Klassen & M. diMarzo, Infrared thermography of dropwise evaporative cooling, Experimental Thermal and Fluid Science 5 (1992) 136-141.
M. diMarzo, Y. Liao, P. Tartarini, D. Evans & H. Baum, Dropwise evaporative cooling of a low thermal conductivity solid, in Fire Safety Science, IAFSS (1991) 987-996.
P. Tartarini & M. diMarzo, The solid-liquid interfacial conditions for dropwise evaporative cooling, Heat and Technology 10 (1992) 130-144.
M. diMarzo, P. Tartarini, Y. Liao, D. Evans & H. Baum, Evaporative cooling due to a gently deposited droplet, International Journal of Heat and Mass Transfer 36 (1993) 4133-4139.
P. Tartarini & M. diMarzo, Mixed numerical scheme solution for dropwise evaporative cooling, in Advanced Computational Methods in Heat Transfer III (1994) 473-480.

PAPER # 4

Infrared Thermography of Dropwise Evaporative Cooling*

Michael Klassen

Marino di Marzo

James Sirkis

Mechanical Engineering Department, University of Maryland, College Park, Maryland

■ An infrared thermographic technique is developed to obtain the transient solid surface temperature distribution in the neighborhood of an evaporating droplet. This technique is nonintrusive and is not affected by the time response of the measuring device (i.e., thermocouple). The entire surface is monitored at any instant of time, and information on the area influenced by the evaporative cooling process is easily derived. A detailed description of the image processing based data reduction is provided. A water droplet in the range of 10–50 μL is deposited on an opaque glasslike material (Macor) that has an initial surface temperature between 100 and 165°C. The evaporative cooling process is fully documented, and these new findings are contrasted with the published literature to gain a better understanding of the phenomena involved.

Keywords: *infrared thermography, evaporative cooling, droplet flow, image processing*

INTRODUCTION

The evaporative cooling induced by droplets impinging on hot surfaces has been the subject of numerous investigations. Thermal quenching, spray cooling, and fire extinguishment are a few of the processes inspiring the study of solid thermal behavior induced by droplet evaporative cooling. Early works considered the overall process [1, 2]. The models proposed by these investigators are simply posed and rely on arbitrary empirical parameters to fit the experimental data. More detailed studies (numerical and experimental) by Rizza [3], Seki et al [4], and di Marzo and Evans [5] are based on numerical integration of the transient conduction equation in the solid. Uniform constant-temperature boundary conditions at the solid–liquid interface under the droplet are used. These theoretical studies model the thermal behavior of high thermal conductivity solids.

Transient temperature measurements of the solid are given by several investigators. These measurements show the extent of evaporative cooling within the sold. The complete span of vaporization processes is documented in great detail by Michiyoshi and Makino [6]. More recently, Abu-Zaid and Atreya [7] provided temperature traces at several locations in both porous and nonporous solids.

The investigation reported here illustrates the use of a nonintrusive infrared thermographic technique to monitor the superficial temperature distribution during the evaporation of a single droplet on a glasslike opaque material of low thermal conductivity (Macor). Two major advantages of this technique are the monitoring of the complete temperature distribution over the surface as opposed to the local temperature–time traces obtained with thermocouples and the immediate time-response of the measurements, which is not possible with finite-size thermocouples.

EXPERIMENTAL APPARATUS

Figure 1 is a diagram of the experimental setup. The droplet is placed on a solid block of Macor ceramic. Macor was selected for this study because it is a solid with low thermal conductivity and high emissivity, and it can withstand large thermal stresses. the Macor block is cylindrical, and its sides are insulated with ceramic fiber insulation to ensure uniform radial temperature distribution. The solid is heated from below by an electric heater (not depicted in Fig. 1) that is controlled by a voltage regulator. Thermocouples are embedded in a high thermal conductivity paste between the heater surface and the Macor block. On the upper surface there are three thermocouples that monitor the surface temperature at the edges of the block. These thermocouples, mounted on the solid on both the top and bottom surfaces, are used to obtain heat flux data and to ensure that the solid has achieved a radially uniform temperature distribution. The size (7.62 cm depth by 10.16 cm diameter) of the solid is large enough for it to be considered semiinfinite with respect to the droplet. The droplet size and evaporation are monitored by a video camera with a high-magnification lens. The droplet evapora-

Address correspondence to Dr. Marino di Marzo, Mechanical Engineering Department, University of Maryland, College Park, MD 20742.

Experimental Thermal and Fluid Science 1992; 5:136–141

0894-1777/92/$3.50

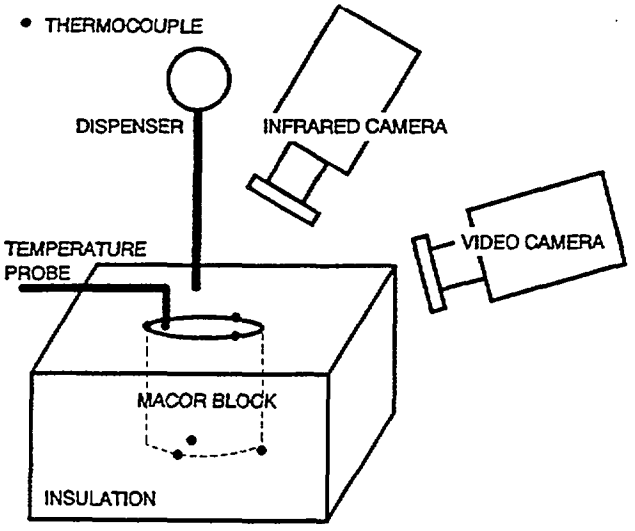

Figure 1. Schematic of the experimental setup.

tion time is measured with a stopwatch and is also monitored on the video and by infrared camera recording [5].

The droplet deposition apparatus used is designed to strictly control the droplet release height and the position of the microdispenser with respect to the surface. This degree of accuracy is necessary because these factors affect the final configuration (shape) of the droplet, which is a governing parameter controlling the droplet evaporative behavior [8].

The initial shape of the droplet on the surface and thus the droplet behavior is influenced by the surface properties and conditions. As every effort is made to produce a droplet of consistent diameter and shape, the surface of the solid must be uniform in every respect. To achieve this repeatability, the surface is cleaned with 98% ethyl alcohol to remove grease and then rinsed with deionized water. This provides a clean surface and establishes a water microlayer prior to droplet deposition.

Previous work [9] provides the total evaporation time of droplets of various volumes on Macor by repeating the measurement 10 or more times for each droplet volume and surface temperature and accepting values that are within 5% of each other. Infrared data are accepted only if the total evaporation time matches (within 5%) the evaporation time previously attained.

A droplet is "gently" placed on the surface of the solid by the dispenser. A release height of up to 1.5 cm from the surface provides identical droplets. The dispenser is motor-driven, and the release height is set at 1.2–1.4 droplet diameters (this is the diameter of the droplet in its spherical configuration). The final droplet configuration on the surface is extremely repeatable. Deionized water is completely degassed through repeated freezing/boiling cycles under vacuum. The water treatment is necessary to remove all mineral impurities and dissolved gases from the droplet. The presence of minerals and gases causes variations in the heat transfer characteristics of the droplet. Mineral impurities within the water tend to deposit on the solid's surface, causing a degradation of the surface finish. Dissolved gases in the water form bubbles within the deposited droplet, thus altering the droplet formation (size and shape) and changing its heat transfer characteristics.

DATA PROCESSING

The infrared equipment (Inframetrics Model 525 infrared thermal imaging system) used is able to capture the thermographic data from a distance of about 0.5 m in a small region of the solid within approximately five diameters of the wetted region ($\approx$ 0.02 m). A one-dimensional temperature profile of the solid surrounding the droplet is found by using the line-scan function of the system, which provides the temperature profile along a line arbitrarily placed on the screen image. In this case the line is positioned through the center of the liquid–solid contact region, and the transient temperature distribution is obtained for the solid during the entire evaporation process. Note that only the data relative to the exposed solid surface are meaningful. The signal relative to the infrared radiation in the solid region covered by the droplet cannot be translated into a reliable temperature reading. All the information is recorded onto video tape for later retrieval. The thermographic system supplies the line-scan temperature distribution as an X–Y plot on the video monitor (and video tape).

To extract the temperature data from the video signal (standard RS-330), the desired video image is digitized by a PC-based frame grabber (width × height = 641 × 201 pixels), then processed with appropriate algorithms. The frame grabber (two-dimensional A/D converter) converts the video image to a matrix of numbers (gray levels). Each position in the matrix (representing a pixel) has a gray level that is proportional to the intensity of the corresponding point in the original video signal. The six bit frame grabber used here assigns gray levels ranging from 0 (black) to 63 (white).

The datum received from the infrared equipment is not temperature, but a difference in the radiance level between a reference surface of known emissivity and temperature and the unknown target surface about which information is desired. The reference surface is taken as the solid surfce at a distance far removed from the droplet perimeter and area of influence. The general radiometric equation is given by

$$\Delta I = \left[\epsilon_t f(T_t) + (1 - \epsilon_t) f(T_b)\right] - \left[\epsilon_r f(T_r) + (1 - \epsilon_r) f(T_b)\right] \quad (1)$$

where $f(T)$ represents the overall spectral response of the infrared system at the temperatures of the various surfaces.

This system transfer function is unique to each type of infrared system. In the present application, Eq. (1) is reduced further, because the emissivity of the target and of the reference are the same, to become

$$\Delta I = \epsilon_t \left[f(T_t) - f(T_r)\right] \quad (2)$$

The background radiance is thus eliminated from the parameters affecting the apparent radiance temperature difference. The accuracy of the radiance reading given by the infrared equipment is further improved when both the target and reference surfaces have the same shape or contour and the same orientation to the background radiance level. This is true for the present application because the reference and target points are taken from the same solid surface. Thus, with the elimination of these variables, fairly precise and

accurate temperature measurements (within 1-2°C) can be obtained with this equipment and test setup.

Image processing involves the editing and highlighting of features from a digital image in order to enhance the quality of the image to extract useful information [10]. The image received from the infrared thermographer contains the temperature of both the solid and the droplet and an isotherm scale. Figure 2 is a 641 × 201 digital representation of the captured image. The only portion of this image that is needed is the temperature of the solid. The isotherm scale is represented by pixels that must be distinguished from the temperature pixels. Once the temperature pixels are isolated, they can be fitted with an appropriate curve in the image space. Finally, when scaled to the position-temperature space, this curve represents the actual temperature data.

To identify a reference temperature (or a temperature scale) in the position-temperature space, the following procedure is used.

1. The temperature is measured with a surface probe (Omega surface probe Series 68000) at a given location.
2. The surface probe is removed, ad simultaneously a reading from the infrared camera is recorded.
3. Steps 1 and 2 are repeated at various heater powers to obtain a temperature scale.
4. The surface temperature detected by the three thermocouples at the edge of the Macor block is compared with the calibrated reading from the infrared camera.

It turns out that the two values are in very good agreement (within 1-2°C). The infrared measurements are extremely repeatable and reliable because each data point is the result of at least 10 independent measures, which concur to the same results.

The accuracy is within 1-2°C because the thermographic image shows the temperature on a line (see Fig. 3) passing through the center of the wetted area. The vertical dimension in the picture is the temperature scale. Usually the temperature span top to bottom is on the order of 100°C. There are 201 pixels in the vertical direction. The thickness of the thermographic trace is two pixels, and double traces are often present. Therefore, a double trace is four pixels thick, which corresponds to about 2°C. The spatial resolution (in the horizontal direction) depends on the field of view selected. The pixel dimension in the horizontal direction ranges between 0.05 and 0.1 mm. The time resolution of the image is 1/30 s as one should expect from the usual VCR frame per second recording standard.

Image processing begins with the image captured by the video digitizer from a paused video tap. To extract the necessary information, various C language image processing procedures are applied to the data file received from the frame grabber. The pixels representing the actual temperature data typically take on gray-level values ranging from 0 to 10 (where 0 is black and 63 is white). Much of the image noise has higher gray levels. Typical noise is given by the speckles that appear on a VCR frozen image. Therefore, gray-level thresholding can be used to discard much of the unwanted information. One first chooses a gray-level threshold. The image is then raster-scanned, and each pixel is compared to the threshold. If the gray level is above the threshold, then that pixel is considered white and is assigned a new gray level of 63. If the gray level is equal to or below the threshold,

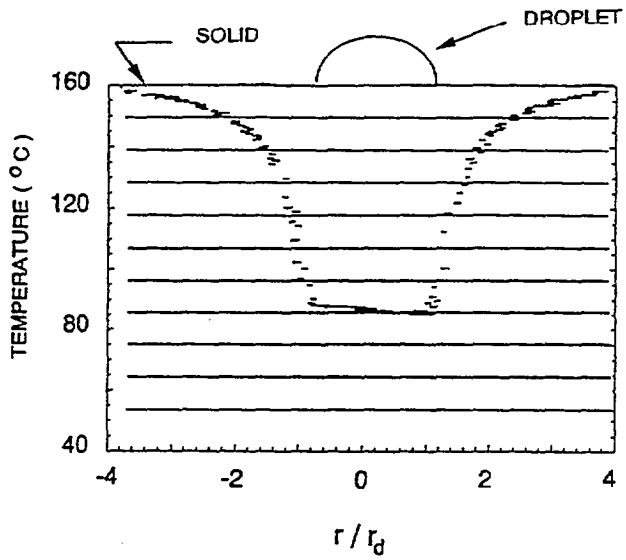

Figure 2. Captured thermographic image of (50 μL droplet 40 s after deposition on Macor at 160°C).

then the pixel is considered black and is assigned a new gray level of 0. This technique binarizes the image and generally removes all background portions of the image, leaving the temperature distribution data, any "noise" left in the image, and the isotherm scale. The gray-level threshold is set at 10 by trial and error. It was found that if one lowers the threshold, data will be lost, and if one raises the threshold, more noise will be associated with the data.

Erosion is employed to filter out isolated groupings of noise. The idea behind erosion is that a black pixel with many black neighbors is most likely part of the temperature distribution. On the other hand, a black pixel with very few black neighbors is isolated and is most likely noise. This algorithm requires an erosion threshold to be defined. This threshold designates the minimum number of black pixels to differentiate between noise and the temperature information. For this study, a value of six black pixels is representative of

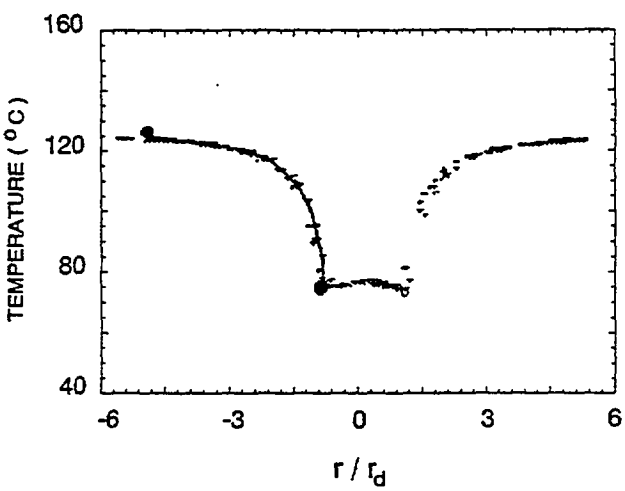

Figure 3. Data processing sample (30 μL droplet 60 s after deposition on Macor at 124°C).

the threshold used in a 121-pixel neighborhood. The erosion threshold is set after the image has been binarized; isolated "black" (0) pixels are considered noise if less than six adjacent pixels are "black." If more than six pixels (out of the 121 adjacent pixels considered) are black, then the black pixel is data. This value is obtained by trial and error. If the threshold is higher than 6, noise will appear in the processed image. If the threshold is less than 6, data will be lost.

The isotherm scale is eliminated from the digitized picture by determining the position of each line of the scale and removing those pixels. Adjacent isotherm lines are an equal distance apart; thus, once the top line position is obtained, the remaining lines are easily eliminated.

With all extraneous information removed from the image, the temperature distribution of the solid surface is now fitted with a curve using a general least squares fitting routine as illustrated in Fig. 3. Several types of curves are fitted, but it is found that an exponential fitting is generally the most accurate and appropriate. The temperature distribution best fit is obtained with an exponential of the form

$$T_s = Ae^{-B/r} \tag{3}$$

where A and B are constants determined by the fitting routine. The goodness of fit is determined by the chi-squared test [11].

Recall that the data received from the infrared thermographer are in terms of the apparent radiance temperature difference (ΔI) and must be converted from this state to actual temperature. ΔI versus temperature curves were generated and curve-fitted for each surface temperature. These curves are provided by the supplier of the infrared equipment and validated with the procedure previously described. The scale of apparent radiance temperature can be considered linear with the temperature scale in the range of temperatures of concern. With this information, the temperature distribution is curve-fitted in terms of its screen coordinates, then converted to isothermal units, and finally converted to temperature.

EXPERIMENTAL RESULTS

The transient thermal behavior of the solid surface subjected to the droplet evaporative cooling is described in great detail. Typical results are illustrated in Figs. 4*a*–4*i*. The first interesting feature is the deep temperature drop following the droplet deposition. The assumption that the solid–liquid interfacial temperature would be reasonably modeled by the two semiinfinite bodies in sudden contact [12] fails. This assumption is adequate for high thermal conductivity solids [8] where heat is drawn quickly from the solid in the vicinity of the droplet. The deep temperature drop at deposition is an

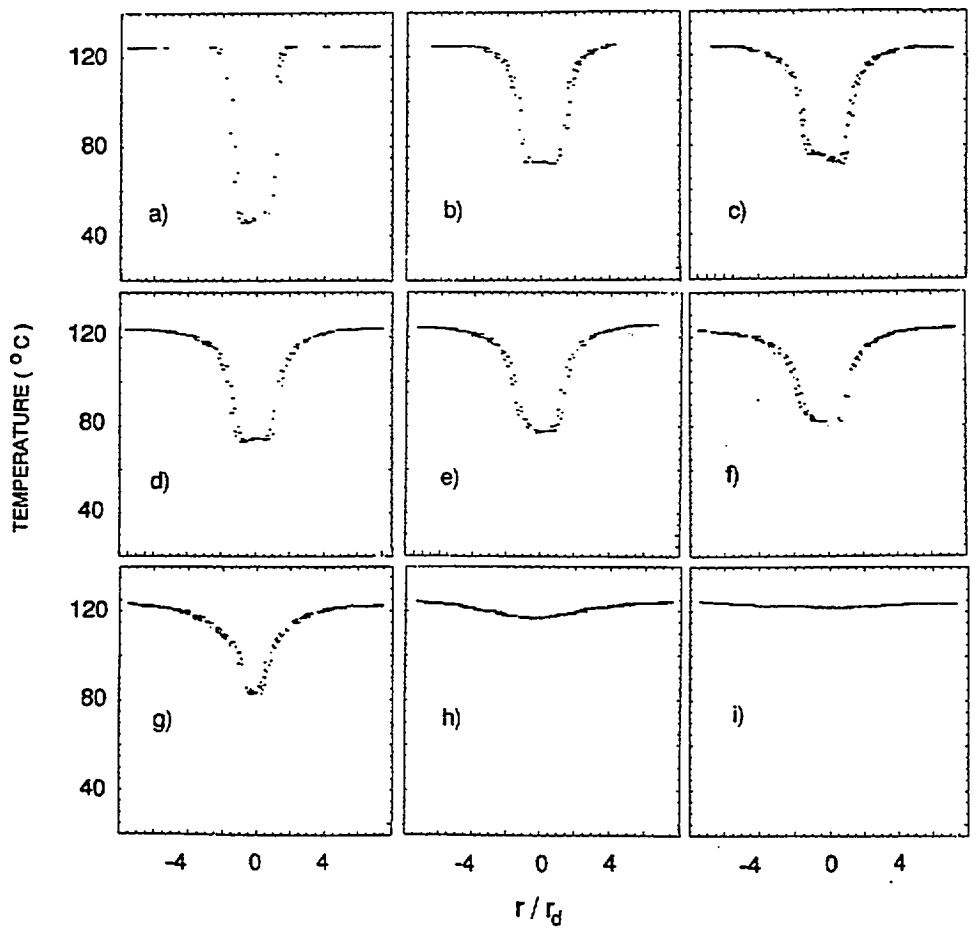

Figure 4. Evaporative cooling transient. (a) At 1 s; (b) at 10 s; (c) at 30 s; (d) at 50 s; (e) at 70 s; (f) at 90 s; (g) at 100 s; (h) at 110 s; (i) at 130 s. (30 μL droplet deposited on Macor at 124°C.)

important consideration in all applications where thermally induced stresses can cause structural failure in the solid.

Results concerning the area of the solid influenced by the evaporative cooling are also unexpected. Figure 5 shows the radius of influence as a function of time. Note that the radius of influence (r_i) is defined here as the radial distance where the temperature drop (with respect to the initial solid temperature) is 10% of the difference between the initial solid surface temperature and the calculated contact temperature. The radius of influence is normalized with respect to the initial value of the wetted solid surface region (r_d), which remains constant throughout most of the evaporation process. The sudden increase in the radius of influence toward the end of evaporation is remarkable. The reason for this increase becomes clear if one considers that the heat flux through the droplet increases as the droplet thickness decreases. Since the radius of the wetted region is constant throughout most of the droplet evaporation, it follows that an almost exponential rise in the heat flux can be expected. This is predicted by di Marzo and Evans [8] and explains well the dramatic increase in the radius of influence. However, all the previous numerical computations of solid thermal behavior are based on uniform, constant temperature at the liquid–solid interface [3–5] and not on more appropriate variable flux boundary conditions. Therefore, all these numerical predictions fail to describe the behavior of the radius of influence in the latter portion of the evaporation transient.

The temporal behavior of the radius of influence, as seen in Fig. 5, is plotted for various droplet sizes and initial solid surface temperatures. Each plot yields an average value of the normalized radius of influence (r_i / r_d), which is then plotted versus the evaporation time of the droplet under consideration. Figure 6 summarizes the behavior of the time-averaged radius of influence (r_i) for various droplet sizes and initial solid surface temperatures. In the evaporative range it is found that radii of influence for various droplet sizes and initial solid surface temperatures are about equal to four times the radius of the wetted region (r_d) on the Macor solid. In order to identify each of the data points depicted in Fig. 6, Table 1 provides the total evaporation times as a function of droplet size and initial solid surface temperature.

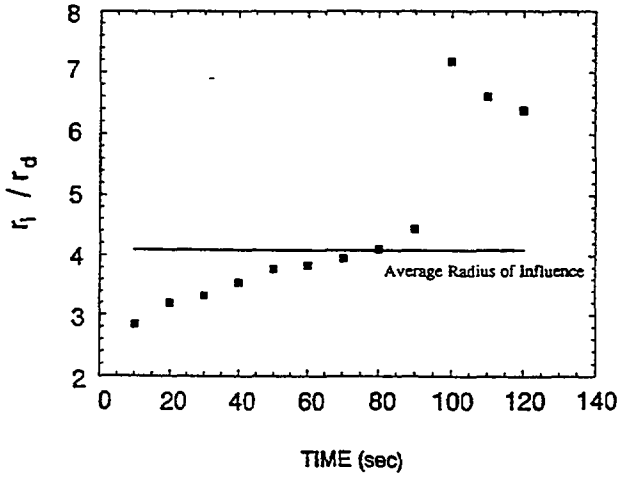

Figure 5. Radius of influence as a function of time (30 μL droplet deposited on Macor at 124°C).

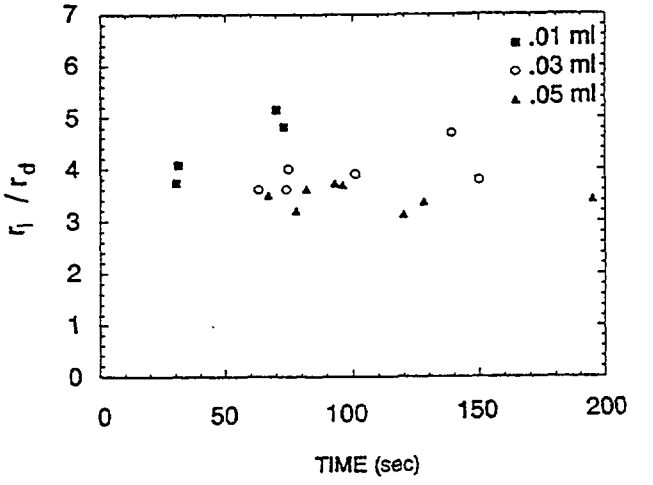

Figure 6. Average normalized radius of influence versus evaporation time for various droplet volumes and initial solid surface temperatures.

PRACTICAL SIGNIFICANCE / USEFULNESS

Insight into the droplet evaporative process is obtained with a nonintrusive thermographic technique. In particular, the sharp temperature drop in the initial portion of the evaporative transient is relevant to quenching applications where induced thermal stresses can affect material characteristics or integrity.

The behavior of the radius of influence shows increased flux at the end of the evaporative transient. This insight is relevant to applications where intense cooling is sought (i.e., extinguishment or cooling of surfaces exposed to fire).

CONCLUSIONS

This thermographic technique provides novel insight into the dropwise evaporative cooling phenomenon. It clearly identifies a severe temperature drop following deposition. Other investigators [6, 7] have reported this phenomenon to a lesser extent due to the time response associated with their measuring devices. This technique also allows one to study temporal behavior of the radius of influence and provides interesting observations concerning the modeling of solid thermal behavior. Finally, the data also provide the basis for validation of a more complex model describing the coupled evaporative cooling and droplet evaporative process for low thermal conductivity solids.

Table 1. Total Evaporation Time (s) for Various Droplet Sizes and Initial Solid Surface Temperatures

Initial Solid Surface Temperature (°C)	*Droplet Size (μL)*		
	50	*30*	*10*
101	191	146	73
124	124	99	46
143	94	75	36
152	82	62	30
160	70	50	28

This research has been supported by a grant from the Building and Fire Research Laboratory of the National Institute for Standards and Technology.

NOMENCLATURE

A constant in temperature distribution fit, K
B constant in temperature distribution fit, m
$f(\cdot)$ generic function, W/m^2
r radial surface coordinate, m
r_d radius of the wetted area, m
r_i radius of influence, m
T temperature °C

Greek Symbols

ΔI radiance level difference between target and reference surfaces, W/m^2
ϵ emissivity, dimensionless

Subscripts

b background
r reference
s surface
t target

REFERENCES

1. Toda, S., A Study of Mist Cooling, 1st Report: Investigation of Mist Cooling, *Heat Transfer Jpn. Res.*, **1**, 39-50, 1972.
2. Bonacina, C., Del Giudice, S., and Comini, G., Dropwise Evaporation, *J. Heat Transfer, Trans. ASME*, **101**, 441-446, 1979.
3. Rizza, J. J., A Numerical Solution to Dropwise Evaporation, *J. Heat Transfer, Trans. ASME*, **103**, 501-507, 1981.
4. Seki, M., Kawamura, H., and Sanokawa, K., Transient Temperature Profile of a Hot Wall Due to an Impinging Liquid Droplet, *J. Heat Transfer, Trans. ASME*, **100**, 167-169, 1978.
5. di Marzo, M., and Evans, D. D., Dropwise Evaporative Cooling of High Thermal Conductivity Materials, *Heat Technol.*, 5(1/2), 126-136, 1987.
6. Michiyoshi, M., and Makino, K., Heat Transfer Characteristics of Evaporation of a Liquid Droplet on Heated Surfaces, *Int. J. Heat Mass Transfer*, **21**, 605-613, 1978.
7. Abu-Zaid, M., and Atreya, A., Effect of Water on Piloted Ignition of Cellulosic Materials, Natl. Inst. Standards and Technology Rep. NIST-GCR-89-561, 1989.
8. di Marzo, M., and Evans, D. D., Evaporation of a Water Droplet Deposited on a Hot High Conductivity Solid Surface, *J. Heat Transfer, Trans. ASME*, **111**, 210-213, 1989.
9. di Marzo, M., Wang, Z., and Meng, W. H., Transient Cooling of a Hot Surface by Droplets Evaporation, Natl. Bureau of Standards Rep. NBS-GCR-87-534, 1987.
10. Dawson, B. M., Introduction to Image Processing Algorithms, *BYTE*, **12**(3), 169-186, 1987.
11. Press, W. H., Flannery, B. P., Teukolsky, S. A., and Vetterling, W. T., *Numerical Recipes in C: The Art of Scientific Computing*, pp. 528-539, Cambridge Univ. Press, New York, 1988.
12. Carslaw, H. S, and Jaeger, J. C., *Conduction of Heat in Solids*, 2nd ed., p. 88, Oxford Univ. Press, Oxford, 1959.

Received January 28, 1991; revised September 19, 1991.

PAPER # 5

Dropwise Evaporative Cooling of a Low Thermal Conductivity Solid

M. DI MARZO, Y. LIAO and P. TARTARINI
Mechanical Engineering Department
University of Maryland
College Park, Maryland 20742, USA

D. EVANS and H. BAUM
Building and Fire Research Laboratory
National Institute of Standards and Technology
Gaithersburg, Maryland 20899, USA

ABSTRACT

Insight on extinguishment of a solid fuel fire by sprinkler generated droplets is obtained by detailed modelling of a single droplet evaporative cooling on a hot low thermal conductivity solid. The assumption of constant and uniform temperature at the solid-liquid interface, which decouples the solid and the liquid modelling, cannot be applied to this case because strong local cooling of the solid requires the solutions of both regions (liquid and solid) to be coupled. The large thermal gradients observed at the edge of the droplet preclude the application of finite difference techniques for the integration of the transient conduction governing equation. A mixed technique that uses a control volume method for the liquid and a boundary element formulation for the solid is proposed. Both methods are briefly outlined and the computed predictions are validated with experimental measurements which encompass high resolution thermography of the solid surface subjected to evaporative cooling. Insight on the temperature distribution at the solid-liquid interface is obtained deduced from the model and the deviation from the constant and uniform temperature at the liquid-solid interface is assessed. The radial versus axial conduction in the liquid droplet is also quantified.

KEYWORDS: evaporation, cooling, drops

INTRODUCTION

Local cooling induced by an evaporating droplet deposited on a hot solid surface is investigated. The long term objective of this study is the construction of a model for the prediction and optimization of sprinkler based extinguishment systems performance. In particular, the prediction of evaporative phenomena is considered here, which implies that nucleate boiling at the solid-liquid interface under the droplet is fully suppressed. Note that the evaporative phenomena occur at surface temperatures lower than the one

obtained by direct exposure to flame radiation. However, evaporation is observed on compartment surfaces exposed to fire (walls, ceiling, furniture, etc.). For the case of high thermal conductivity solids, a simple model [1,2] was based on the assumption that the temperature at the solid-liquid interface is constant and uniform during the evaporation process as suggested by Michiyoshi and Makino [3] and Seki [4].

Fire safety applications are mostly involved with low conductivity materials. For this case the liquid and solid solutions must be coupled since the thermal conditions under the droplet are non-uniform and vary during the evaporation process. The thermal gradients in the proximity of the droplet edge are very large in the initial portion of the transient. This fact precludes the application of finite difference techniques to integrate the transient conduction governing equation. Pronounced numerical instabilities were observed at the edge of the droplet in the solid region. These numerical instabilities could be controlled by reducing the temporal step size. However, the round-off error consequent to the small temporal increments made the solution unacceptable.

A different solution scheme is formulated for the solid region which is based on Boundary Element Methods (BEM). BEM are applied to a number of conduction problems by Carslaw and Jaeger [5]. More recently a review by Pina and Fernandez [6] specifically described BEM applications to transient heat conduction. A very important contribution by Wrobel and Brebbia [7] focuses on the axisymmetric geometry which is the case of this study. Their formulation is different from the one proposed here because it employs a series expansion in time as opposed to the temporal discretization used in this paper. The BEM formally requires that all past information must contribute to the present solution. The advantage of the time discretization scheme presented here, is that only a limited amount of past information must be collected in order to obtain the solution. In the limit it can be shown that the method reduces to an explicit scheme and all the past contributions become negligible.

The complex geometry of the liquid droplet and the future plan to incorporate radiative fluxes into the liquid solution suggest that a Control Volume Method (CVM) be used for the integration of the transient conduction governing equation in the liquid region. A simple nodalization scheme is presented and the governing equation is discretized for each elementary control volume.

MODEL FORMULATION

The transient conduction equation is applied to the solid region and to the liquid which is considered motionless. In general, the governing equation is written for both the liquid and the solid (with the appropriate thermal diffusivity) as:

$$\frac{\partial T}{\partial t} = \alpha \nabla^2 T \tag{1}$$

The boundary conditions can be summarized as (see Fig 1):

at $z = 0; r \leq R$

$$k_s \nabla T_s \cdot \hat{n} = k_l \nabla T_l \cdot \hat{n} \tag{2}$$

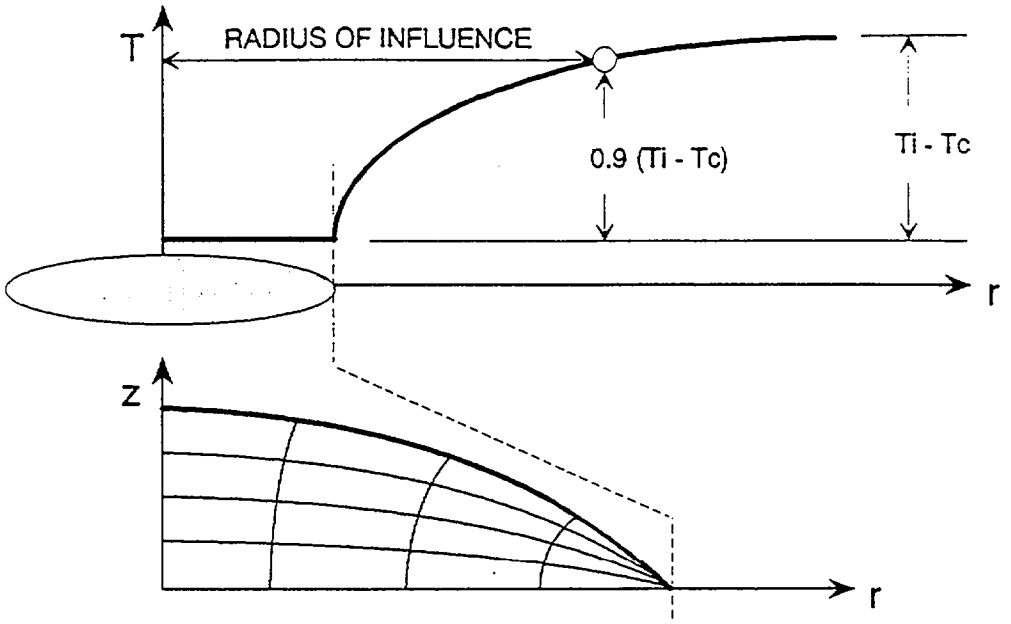

FIGURE 1 - Coordinate system, radius of influence and nodalization

$$T_s = T_l \tag{3}$$

at $z = 0; r > R$

$$-k_s \nabla T_s = h_a (T_s - T_a) + \sigma \varepsilon (T_s^4 - T_a^4) \tag{4}$$

at $z = f(r)$ liquid-vapor interface

$$-k_l \nabla T_l \cdot \hat{n} + h_a (T_a - T_l) = 0.624\, h_a\, Le\, \frac{h_{fg}}{c_{pa}}\, \frac{x_i - x_a}{1 - x_i} \tag{5}$$

Here x_i and x_a are molar fractions (see the nomenclature for definitions) the radiant heat transfer component and the density variations in the air-vapor mixture at the liquid-vapor interface are neglected. The function $f(r)$ which describes the liquid-vapor interface is a segment of a sphere and is provided in detail in reference [2]. The overall and convective heat transfer coefficients are derived from experimental measures [1,2]. The axisymmetric nature of the problem requires that the radial gradient of T is zero on the vertical axis through the origin of the coordinate system. The initial condition will be either a linear one-dimensional temperature distribution in the solid and uniform temperature in the liquid or uniform temperatures in both liquid and solid. Note that the initial contact temperature at the liquid-solid interface is set to the contact temperature T_c defined by Seki [4]. This contact temperature depends on the water and solid properties and on their respective initial temperatures; therefore, it is a constant reference value. Initially, the water is considered at the ambient temperature (T_a).

The use of a BEM is desirable because the solution at a given point is obtained by superimposing all the heat flux contributions from the neighboring points; hence the localized, drastic thermal changes of this cooling process are smoothed out. When a finite difference technique is used the sharp gradients are locally amplified thus causing the observed instabilities in the solution unless an extremely fine nodalization is used. Furthermore, the computation is limited to the surface points and allows a more precise definition of the noding in the region of concern (e.g., at the droplet outer edge).

To obtain the desired formulation, it is necessary to introduce an adjoint equation to Eq. (1) in terms of the Green's function $G(\vec{v},\vec{v}_o,t,t_o)$; that is

$$\frac{\partial G}{\partial t} = -\alpha \nabla^2 G \tag{6}$$

where the vector position $\vec{v}$ is in terms of any specified coordinate system. Note that G depends on the point $\vec{v}$ which is the point of interest and on the point $\vec{v}_o$ which is the generic point identified by the integration coordinates. Similarly, a backward time scale t_o must be introduced. The origin of this time scale is at the present time t and the time t_o increases in the negative direction of actual time. In what follows, t_o is identified as the recollection time. The need for this dual time scale is required by the definition of the adjoint equation which carries a negative sign on the right hand side. By multiplying Eq. (1) by G and Eq. (6) by T, respectively, and integrating over the domain with Gauss' theorem, one obtains:

$$\int_t \int_v \frac{\partial (T G)}{\partial t} \, dv_0 \, dt_0 = \alpha \int_t \oint_s (T \nabla G - G \nabla T) \cdot \hat{n} \, ds_0 \, dt_0 \tag{7}$$

At this point the left-hand-side is expanded into two volume integrals at the present time and at initial time, respectively. One of the properties of the function G is that as the recollection time goes to zero ($t_o \rightarrow 0$), G becomes the Dirac function. Therefore, the volume integral at the present time reduces to T. Further, one can introduce a new variable u in lieu of the solid temperature T such that it is zero in all the volume at the initial time. For instance, for the solid region subjected to constant heat flux in the axial direction, one can define u as:

$$u = T - T_i + \frac{q z}{k_l} \tag{8}$$

With these two modifications and by selecting a function G such that ∇G is zero at $z = 0$, the final result is achieved in the form:

$$u = \alpha \int_t \int_s G \nabla u \cdot \hat{n} \, ds_0 \, dt_0 \tag{9}$$

This integral is performed over a closed surface. However, the surface bounding the solid region below the plane $z = 0$ is far ahead of the advancing thermal wave. Therefore, the contribution of the points on the surface bounding the domain in the far

field is negligible. With the implementation of the cylindrical coordinate system, the equation is further simplified since the angular integration can be expressed in terms of a Bessel function. The final form results in a double integral in time and along the radius r which can be cast in the following form:

$$u(r,t) = \frac{1}{\sqrt{4\pi\alpha}} \int_0^t \int_0^\infty \nabla u(r_0, t-t_0)\, r_0\, t_0^{-\frac{3}{2}}\, L_0\left(\frac{2rr_0}{4\alpha t_0}\right) e^{-\frac{(r^2-r_0^2)}{4\alpha t_0}}\, dr_0\, dt_0 \qquad (10)$$

In order to simplify the task of handling these complex surface integrals, a decomposition in two portions is proposed: the value of the forcing function or of the unknown function (∇u) is assumed to be constant in the small intervals dr_o and dt_o. This introduces formal errors of the order $(dr_o/R)^2$, and $(dt_o/t)^2$ into the analysis. The various surface integrals can be recast in the form:

$$u = \sum_{i=1}^{n} W_i \cdot \vec{f}_i + W_0 \cdot \vec{f}_0 \qquad (11)$$

where W is a weight matrix and $\vec{f}$ is the vector of the forcing and unknown functions. The summation term is known since it involves previously calculated parameters. The second term on the right-hand-side of Eq. (11) contains unknown functions or the specified boundary conditions.

The effect of the forcing function at the point of concern and the singular behavior of points at the origin of the spacial and temporal coordinates must be considered. The first particular case of interest is when the point of concern coincides with the source point. This corresponds to the maximum influence of a source point because the distance between the two points is minimal. In terms of weight this yields:

$$W(r \equiv r_0, t_0) = r\, t_0^{-1}\, L_0\left(\frac{2r^2}{4\alpha t_0}\right) erf\left(\frac{\Delta r_0}{\sqrt{16\alpha t_0}}\right) \Delta t_0 \qquad (12)$$

Note that the term Δt_o is consistent with the formulation of Eq. (12) where the forcing function f is multiplied by the weight W. By comparing Eq. (12) with the general formulations for u [Eq. (10)] it is clear that a temporal and spacial integration must be performed on the weighing function. The integration in this case is performed analytically in space and numerically in time. The units of the weight W are those of length as expected.

The singularities at the origin of the spacial and temporal coordinates are addressed by staggering the discretization of the domain. The region neighboring the axis of symmetry is handled by locating the node nearest the symmetry axis at $\Delta r_o/2$. Similarly, the time discretization is not carried to the recollection time origin (i.e. the present time or $t_o = 0$).

As far as the liquid region is concerned a Control Volume Method (CVM) is used to discretize the governing equation and its boundary conditions. The droplet

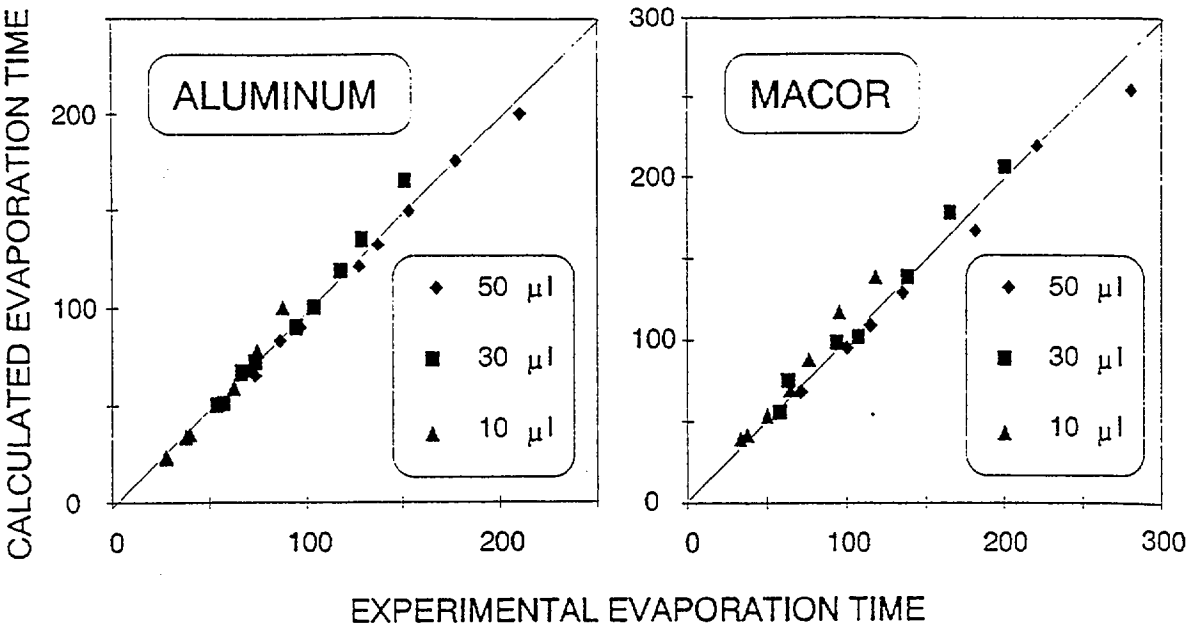

FIGURE 2 - Evaporation time: computations versus measurements

shape is described as a segment of a sphere [1]. The nodalization scheme consists of two sets of curves: a) arcs of circumference passing through the outer edge of the droplet (at z = 0) and centered on the *z* axis and b) arcs of circumference centered on z = 0 with radii inversely proportional to the distance between the origin and the intercept of each arc with the *r* axis (see Fig. 1).

The governing equation integrated over each elementary control volume reduces to a transient energy balance where each incoming flux is evaluated with respect to its component normal to the surface bounding the elementary volume. The nodalization of the outer edge of the droplet is carried out by locating the nodes at $\Delta r/2$ from the droplet edge. Particular care is taken in the integration of the heat and mass transfer fluxes at the droplet edge to account for the sharp changes in temperature in that region.

MODEL VALIDATION

The predictions of the coupled solid-liquid model are compared with experimental data for aluminum and Macor. Macor is a glass-like material which is able to withstand strong local thermal stress. The properties of these two materials are listed in TABLE 1.

TABLE 1 - Solid Properties

	Aluminum [8]	Macor [9]
Specific Heat (J/Kg°C)	962	835
Thermal Conductivity (W/m°C)	180	1.29
Thermal Diffusivity (m^2/s)	4.55×10^{-5}	6.19×10^{-7}
Total Emittance	0.08	0.94

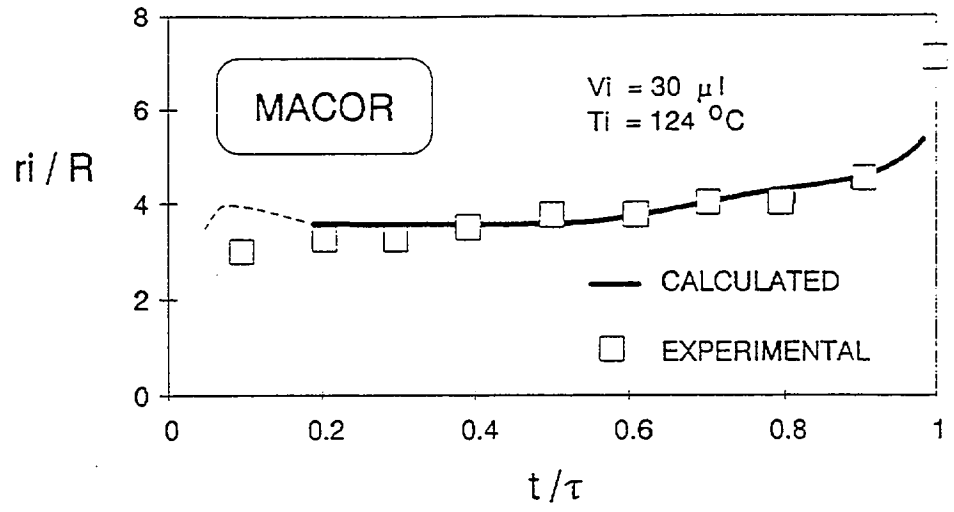

FIGURE 3 - Radius of influence versus time: computations versus measurements

Consider the difference of two orders of magnitude in the thermal properties and note that the model is able to predict the evaporation time for both cases with reasonable agreement with the experimental data as shown in Fig.2.

Some discrepancies are observed for high evaporation time, that is for the low temperature cases. Such discrepancies are within the fifteen per cent band. This error band is to be expected in light of the uncertainties involved in the determination of the mass transfer coefficient and the materials thermal properties. The droplet size range is one order of magnitude larger than the average sprinkler droplet size. However, the smaller sprinkler generated droplets might not be able to reach the solid surface due to up-drafts and/or evaporation, hence the droplet size distribution is skewed towards the higher sizes.

To further validate the model, the radius of influence during the evaporation of a water droplet on Macor is calculated and compared with the radius of influence behavior deduced from the infrared thermography of the solid surface. Note that this comparison involves temperature profiles on the solid surface at various times during the transient. Figure 3 demonstrates the model capabilities. In the initial portion of the transient, the sudden contact of solid and liquid with large temperature differences causes a substantial dip in the solid temperature in the experiments and an overshoot of the radius of influence in the model (as can be seen in the dashed line portion of the curve). Further refining of the model is needed to reconcile these discrepancies. However, the contribution of the initial portion of the transient does not affect significantly the overall results.

RESULTS AND CONCLUSIONS

The detailed model presented here provides an understanding of the limitations associated with the simplified model for high thermal conductivity solid described in earlier works [1,2]. This simplified model is based on the assumption of uniform and constant temperature at the liquid-solid interface and on the dominance of the axial component of the flux over its radial component in the liquid droplet heat transfer.

Figure 4 shows typical temperature profiles on the solid surface. Note that for aluminum all the variations in temperature span less than one degree centigrade, while

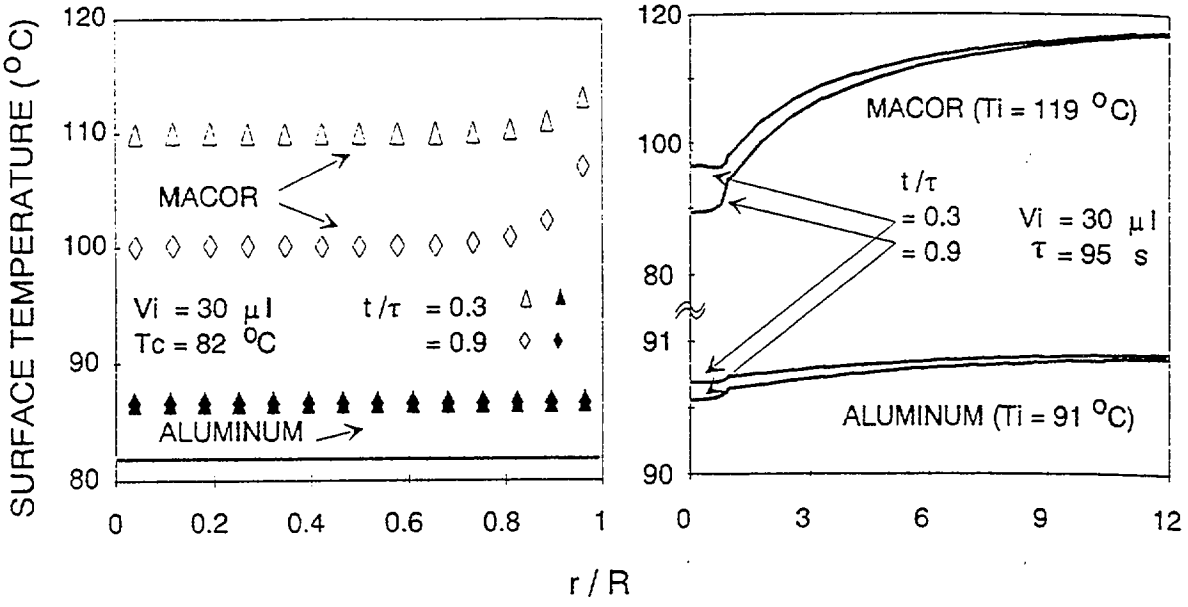

FIGURE 4 - Calculated solid surface temperature profiles on Macor and Aluminum

for Macor the temperatures vary almost 30 °C. This fact is further elucidated in the plot (to the left) at the solid-liquid interface which is shown for various times and locations under the droplet. The results presented in the plot to the left are for a 30 μl droplet which, deposited both on Macor (at T_i = 140 °C; τ = 66 s) and aluminum (at T_i = 87 °C; τ = 105 s), generates the same calculated contact temperature of 82 °C. It is clear that the hypothesis of uniform and constant temperature at the solid-liquid interface is excellent for aluminum and unacceptable for Macor.

Further, in the simplified model for high conductivity solids, the interfacial temperature was assumed equal to the contact temperature. This assumption is rather fortuitous in that the error made is within ten per cent, notwithstanding the lack of fundamental basis for the correlation between these two temperatures.

Figure 5 shows the relative magnitude of the axial and radial component of the heat flux for various droplet sizes, solid materials, initial solid surface temperatures, locations within the droplet and elapsed evaporation time. These results show that the assumption of dominant axial conduction is reasonable since the axial heat flux is more than 90 per cent of the total heat flux in most cases. The points to the right side of the figure are taken at the droplet edge for Macor and show axial heat fluxes of slightly less than 90 per cent of the total heat flux. This result is to be expected considering the temperature distribution at the edge of the liquid-solid interface as depicted in Fig. 4.

In conclusion, a powerful and complex model for the prediction of the thermal transient behavior of water droplets deposited on hot solids is demonstrated. Some of the computed results provide insight on the limits of the simplified model presented earlier [1,2]. Better understanding of the processes involved in dropwise evaporative cooling is achieved. Further work to resolve the details of the initial portion of the thermal transient is required although its contribution to the total evaporation process is small [2].

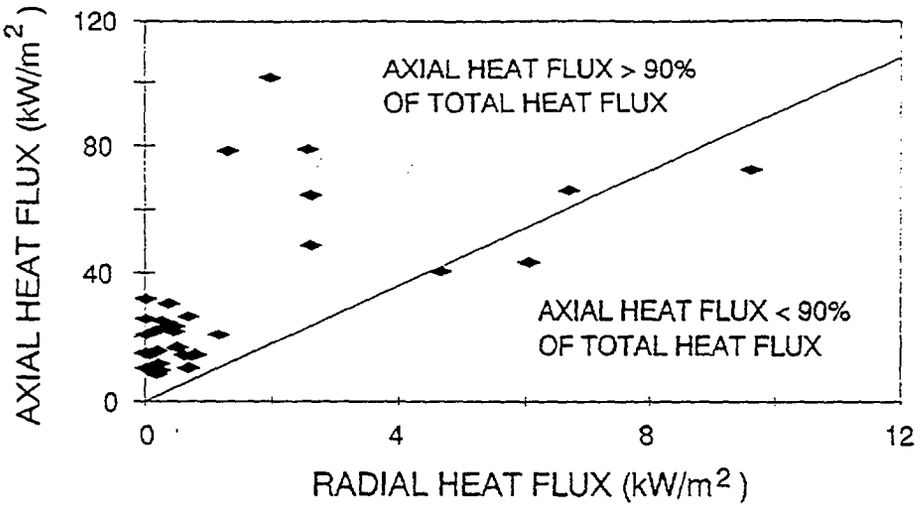

FIGURE 5 - Calculated axial and radial heat flux components

ACKNOWLEDGEMENTS

This research is supported by a grant of the National Institute for Standards and Technology with contributions by the Computer Science Center of the University of Maryland. The authors wish to acknowledge the contribution of Mr. F. Kavoosi for the BEM formulation and Mr. M. Klassen for the infrared thermography.

NOMENCLATURE

c_p	specific heat
D	steam water mass diffusivity
$\tilde{f}$	forcing and unknown vector
G	Green's function
h_a	convective heat transfer coefficient ($\approx$ 12 W/m^2 °C, see [8])
h_{fg}	latent heat of vaporization
k	thermal conductivity
$L_o(z)$	Bessel function: $e^{-z} I_o(z)$
Le	Lewis number: $(D/\alpha)^{2/3}$
$\hat{n}$	unit vector normal to the surface
q	heat flux
r	radial coordinate
r_i	radius of influence (see Fig. 1)
R	radius of the solid wetted region
s	surface
t	time
t_o	recollection time
T	temperature
T_a	far field air temperature
T_c	contact temperature defined by Seki [4]
T_i	initial solid surface temperature
u	transformed temperature
v	volume
$\tilde{v}$	position vector
V_i	initial droplet volume
W	weight matrix

x_a	far field steam in air molar fraction
x_i	interfacial steam in air molar fraction
z	axial coordinate
α	thermal diffusivity
Δr_o	spatial step
Δt_o	time step
ϵ	solid surface total emittance
σ	Stefan-Boltzmann constant
τ	total evaporation time

Subscripts:

l	liquid
o	generic point index
r	in the radial direction
s	solid
z	in the axial direction

REFERENCES

1. diMarzo, M. and Evans, D.D., "Dropwise Evaporative Cooling of High Thermal Conductivity Materials", Heat and Technology, 5: 1-2, 126-136, 1987.

2. diMarzo, M. and Evans, D.D., "Evaporation of a Water Droplet Deposited on a Hot High Thermal Conductivity Solid Surface", ASME Journal of Heat Transfer, 111: 210-213, 1988.

3. Michiyoshi, I. and Makino, K., "Heat Transfer Characteristics of Evaporation of a Liquid Droplet on Heated Surfaces", International Journal of Heat and Mass Transfer, 21: 605-613, 1978.

4. Seki, M., Kawamura, H. and Sanokawa, K., "Transient Temperature Profile of a Hot Wall Due to an Impinging Liquid Droplet", ASME Journal of Heat Transfer, 100: 167-169, 1978.

5. Carslaw, H.S. and Jaeger, J.C., Conduction of Heat in Solids, Oxford University Press, 1959.

6. Pina, H.L.G. and Fernandes, J.L.M., "Applications in Transient Heat Conduction", Topics in Boundary Element Research, ed. C.A. Brebbia, 1: 2, pp. 41-58, Springer-Verlag, 1984.

7. Wrobel, L.C. and Brebbia, C.A., "A formulation of the Boundary Element Method for Axisymmetric Transient Heat Conduction", International Journal of Heat and Mass Transfer, 24: 843-850, 1981.

8. Chapman, A.J., Heat Transfer Macmillan Publishing Co., 1984.

9. Corning, Macor Machinable Glass Ceramic Manufacturer Literature

PAPER # 6

HEAT and TECHNOLOGY
CALORE e TECNOLOGIA
Vol. 10 • No. 3-4 • 1992

THE SOLID-LIQUID INTERFACIAL CONDITIONS FOR DROPWISE EVAPORATIVE COOLING

P. Tartarini (*), M. di Marzo (*)

ABSTRACT

A thecretical research is carried out to describe the thermal behavior of a solid surface subjected to droplet evaporative cooling. The objective of this study is the analysis of various simplified boundary conditions which can be used to generate predictions of the thermal behavior of the solid surface. This study is part of a more general research conducted in order to individuate the global cooling effect of a spray impinging a hot solid surface. A number of numerical algorithms are used to obtain solutions of the governing equations for the various cases examined. Results are presented for the different boundary conditions.

INTRODUCTION

A large number of theoretical and experimental studies have been conducted to investigate the cooling of hot surfaces by droplet sprays. Multi-droplet systems were studied by Bonacina [1]. He concurred with Toda's [2] conclusion that conduction is the dominant heat transfer mode in absence of nucleate boiling. Grissom and Wierum [3] further developed these concepts to define a range of conditions for spray evaporative cooling.

In order to evaluate the thermal behavior of a hot solid surface subjected to dropwise evaporative cooling, the effect of a single impinging droplet has to be accurately determined. Detailed description of the droplet evaporation phenomenology and of the solid surface temperature behavior is provided by diMarzo [4,5] and by Klassen [6]. Experimental data were collected by infrared thermography on Macor (a low thermal conductivity, glass-like material).

Analytical models for the prediction of the thermal behavior of a semi-infinite solid subjected to cooling induced by droplet evaporation have been proposed by Seki [7], Rizza [8] and Kavoosi [9]. All these models are based on the simplifying assumption of uniform and constant temperature at the solid-liquid interface. This assumption is reasonable if one considers solid materials with high thermal conductivity such as metals. Experimental data

(*) Mechanical Engineering Department, University of Maryland, College Park, MD 20742 U.S.A.

by Michiyoshi [10,11,12] show that this uniform temperature is also constant throughout the evaporation process. The behavior of materials characterized by lower thermal conductivity is completely different, as it was demonstrated by Klassen [6] in the above mentioned infrared thermography experiments conducted on Macor. For high thermal conductivity solids, Seki [7] considers that the interfacial temperature can be obtained using the exact solution available for two semi-infinite solids, which yields:

$$T_c = \frac{T_l\sqrt{\rho_l c_l k_l} + T_s\sqrt{\rho_s c_s k_s}}{\sqrt{\rho_l c_l k_l} + \sqrt{\rho_s c_s k_s}} \tag{1}$$

MODEL FORMULATION

The conduction equation describes the thermal transient in a solid and in a motionless liquid. The full description of the problem requires the identification of all the boundary conditions and the coupling of the liquid and solid regions at the wetted surface under the droplet. The conduction equation for both the liquid and the solid, keeping in mind that the thermal diffusivity should be changed accordingly, can be written as follows:

$$\frac{\partial T}{\partial t} = \alpha \nabla^2 T \tag{2}$$

The liquid region is bounded by a liquid-vapor interface where the mass transfer is coupled with the heat transfer as extensively described in previous papers [4,5]. This boundary condition can be cast as:

$$-k_l \nabla T + h_a (T_a - T) = 0.624\, h_a \left(\frac{D}{\alpha_a}\right)^{\frac{2}{3}} \frac{\Lambda}{c_a} \frac{x_i - x_a}{1 - x_i} \tag{3}$$

The liquid-solid boundary conditions, expressing the continuity of the temperature and the conservation of energy across the interface, are written as:

$$\begin{aligned} T_l &= T_s \\ k_l \nabla T_l &= k_s \nabla T_s \end{aligned} \tag{4}$$

The boundary condition at the solid-air interface accounts for the convective and radiative heat transfer contributions, namely:

$$-k_s \nabla T = h_a (T - T_a) + \sigma \varepsilon (T^4 - T_a^4) \tag{5}$$

The axisymmetric nature of the problem grants that the gradient of T is zero on the vertical axis through the center of the wetted region coincident with the origin of the cylindrical coordinate system. The initial condition can be a linear one-dimensional temperature distribution in the solid and uniform temperature in the liquid or uniform temperature in both liquid and solid.

In order to describe the thermal behavior of different materials subjected to the cooling effect of an evaporating droplet, a solid-liquid coupled model is proposed by diMarzo [13]. In a coupled model the boundary conditions at the solid-liquid interface express the matching of liquid and solid temperatures and the conservation of energy across the interface at any time. These conditions require a complex analytical model, as described in details by Tartarini [14]. The main characteristic of the computer code based on the coupled model consists of the simultaneous use of a Boundary Element Method (BEM) for the solid region and a Control Volume Method (CVM) for the liquid droplet.

The numerical predictions of this code are in excellent agreement with the experimental data related to the droplet evaporation time and the solid surface temperature distributions. The code validation is extensively described in previous papers (see diMarzo [13] and Tartarini [14]). A comparison between experimental data and corresponding predictions provided by the code is shown in Fig. 1.

The mathematical and numerical complexity of the coupled model suggests that simplified solutions should be sought in order to analyze the solid thermal behavior when a multi-droplet system is taken into consideration. The analysis of the multi-droplet scenario is handled by using a code for the solid which calculates the simultaneous influence of various droplets on a single point of the hot surface. In this code, the presence of an evaporating liquid droplet is represented by a circular region over which the appropriate boundary conditions are applied to simulate the solid-liquid interactions.

The solid governing equation is solved by applying the same BEM used in the coupled model, as extensively described by Kavoosi [9]. This method requires an adjoint equation to Eq. (2) (see Wrobel [15]). That is:

$$\frac{\partial G}{\partial t} = -\alpha \nabla^2 G \tag{6}$$

which is satisfied by the following Green's function:

$$G(r,z,t;r*,z*,t*) = (4\pi\alpha_s t*)^{-3/2}\left[e^{-\frac{(r-r*)^2+(z-z*)^2}{4\pi t*}} + e^{-\frac{(r-r*)^2+(z+z*)^2}{4\pi t*}}\right] \tag{7}$$

A linear combination of Eq. (2) and Eq. (6) is integrated over the spatial and the temporal domain. The integral of the transient terms is reduced to two spatial integrals at the initial time and at the present time. The spatial integral at the present time is simply the integrand since the Green's function reduces to a Dirac function. The integral at the initial time is eliminated with a proper choice of a transformed temperature such as:

$$u(r,t) = T - T_s - \frac{qz}{k_s} \tag{8}$$

By using the Gauss theorem, one obtains:

$$u(r,t) = \int_0^t \int_0^\infty \nabla u(r*,t*)\, r*\, t*^{-3/2}\, L_0\left(\frac{2rr*}{4\alpha_s t*}\right) e^{-\frac{(r-r*)^2}{4\alpha_s t*}}\, dr*\, dt* \tag{9}$$

In the coupled model, Eq. (9) is combined in matrix form with the integral equation for the liquid. By inverting the matrix, one obtains the transient temperature and heat flux distribution in the liquid and over the solid surface. In a solid-only model, a fundamental assumption in terms of interfacial boundary conditions is required to solve the problem. The only variable that can be considered as always known is the heat flux on the exposed solid surface, which is given by:

$$\frac{dT}{dz} = \frac{h}{k_s}(T - T_a) \tag{10}$$

At the solid-liquid interface, temperature and heat flux distributions are not both known. Therefore, in order to satisfy the mathematical requirements of the differential equation describing the solid, either the interfacial temperature or the interfacial heat flux distributions should be provided. The different boundary conditions are presented and discussed in the following.

BOUNDARY CONDITIONS

The following cases are considered and the specific code used in each case is identified.

Coupled model solution

The coupled model is used: the distribution of temperature in the liquid and in the solid is calculated simultaneously at each time step. All the boundary conditions described in the previous section [Eqs.(2)-(4)] have to be taken into account. Data obtained with the coupled model have been published in previous papers [13,14], providing an extensive validation of the computer code for different materials and initial conditions (see as an

example Fig. 1). The coupled model solution can be taken as a reference term of comparison in order to check the validity of simplified and approximate solutions.

Uniform and constant heat flux solution

The solid model is used: the distribution of temperature on the solid surface is obtained by imposing the boundary condition of constant and uniform solid-liquid interfacial heat flux, which is calculated as:

$$q_0 = \frac{\rho_l V \Lambda}{\pi R^2 \tau} \tag{11}$$

The convective boundary condition given by Eq. (10) is applied on the exposed solid surface. Thus, one has:

$$\begin{aligned} \bar{q} = q_0 = const \qquad & at \quad r \le R \\ q = -\frac{h}{k_s}\frac{du}{dz} \qquad & at \quad r > R \end{aligned} \tag{12}$$

The inadequacy of this boundary condition is evident if one considers that the real heat flux at the interface between a solid surface and an evaporating droplet is always higher near the droplet edge and increases with time during the final phase of the transient. The typical behavior of the normalized interfacial heat flux during the transient and that of its corresponding spatial average is shown in Fig. 2.

One should expect that the use of a constant and uniform heat flux can only lead to smooth the predicted distribution of temperature by underestimate the temperature values in the solid region and overestimating them in the interfacial region. Numerically, this solution offers the remarkable advantage of being totally explicit.

Analytical solution

A closed form solution is used: In an effort to normalize the relevant parameters, an approximate, closed-form solution not involving the computer code was sought. Carslaw and Jaeger [16] show that, for a semi-infinite solid with a constant and uniform heat flux applied over a disk of radius R and no heat transfer on the remainder of the surface, the transient temperature profile on the solid surface is:

$$T_s - T = \frac{qR}{k_s}\int_0^\infty J_0(\lambda r)\, J_1(\lambda R)\, erf(\lambda\sqrt{\alpha_s t})\,\frac{d\lambda}{\lambda} \tag{13}$$

One can normalize this equation by defining:

$$\delta = \frac{\sqrt{\alpha_s t}}{R} \quad ; \qquad \eta = \frac{r}{R} \tag{14}$$

By setting q equal to q_0, one obtains the following equation for the normalized temperature θ:

$$\theta = JA\left(\frac{\rho_s}{\rho_l}\right)\delta^2\,\beta^3 = \frac{4}{3}\int_0^\infty J_0(\zeta\eta)\,J_1(\zeta)\,erf(\zeta\,\delta)\,\frac{d\zeta}{\zeta} \tag{15}$$

where β is the shape parameter defined by Bonacina [1] and JA is the Jakob number. These two parameters can be expressed as follows:

$$\beta = R\left(\frac{4\pi}{3V}\right)^{1/3} \quad ; \qquad JA = \frac{c_s(T_s - T)}{\Lambda} \tag{16}$$

The assumptions that are made to obtain this solution are almost the same which characterize the application of the uniform and constant heat flux boundary condition previously described. The only difference is in the exposed surface heat flux, which is assumed to be zero in the closed-form solution, while it is still calculated by Eq.(9) in the solid program solution. Note that the heat flux evaluated at the solid-air interface is clearly negligible with respect to the solid-liquid one, thus the numerical and analytical solutions basically coincide.

Uniform and constant temperature solution

The solid model is used: the temperature distribution on the exposed solid surface and the heat fluxes at the interface are calculated by using the boundary condition prescribing constant and uniform interfacial temperature. The convective heat flux boundary condition is applied to the exposed solid surface. That is:

$$\begin{aligned} T &= T_c = const \qquad && at \quad r \le R \\ q &= -\frac{h}{k_s}\frac{du}{dz} \qquad && at \quad r > R \end{aligned} \tag{17}$$

The interfacial temperature is assumed to be the theoretical contact temperature defined by Eq. (1). This interfacial temperature at the initial liquid-solid contact is obtained considering the exact solution for two semi-infinite solids.

RESULTS AND DISCUSSION

The coupled model and the code for the solid with different boundary conditions are used to calculate the solid surface temperature distribution for evaporation on Macor at initial surface temperature of 145°C and 165°C. The results are presented in Figs. 3 to 5. In all these plots, temperature profiles are shown at five different times during the transient (t/τ = 0.1, 0.3, 0.5, 0.7 and 0.9 respectively). The comparisons refer to: a) coupled model, whole set of boundary conditions; b) solid model, constant and uniform interfacial heat flux; c) solid model, constant and uniform interfacial temperature (i.e., theoretical contact temperature).

Figures 3 and 4 show the temperature distributions obtained for two evaporating droplets with an initial volume of 10μl (R = 1.871 mm) and 20 μl (R = 2.357 mm) respectively. The initial temperature of the solid surface is 165°C in both cases. The high similarity between the two figures is an evident consequence of the effectiveness of the spatial normalization. In other words, given an initial solid surface temperature, the temperature profiles during the transient depend on the distance from the wetted area expressed in terms of droplet radii.

In order to examine the influence of the initial solid surface temperature, Fig. 5 is shown, which takes into consideration a 20 μl droplet on a surface whose initial temperature is 145°C. In both the 20μl cases (see Figs. 4 and 5), note the dip in the temperature near the edge of the droplet, due to the very low conductivity of Macor which enhances the local temperature gradients. In all cases note that the temperature at the edge of the droplet is higher than the spatial averaged value. Also note the different behavior of the surface temperature distributions outside the wetted area and, in particular, the radial distance where the effect of the droplet cooling becomes negligible.

It is quite evident that the assumption of uniform and constant temperature is the one which provides results more similar to those of the coupled model in terms of shape of the temperature profiles. However, the temperature profiles obtained with the coupled model show that the solid-liquid interfacial temperature varies during the transient and reaches a value close to the theoretical contact temperature only in the last phase of the evaporative process. Of course, the uniform and constant temperature solution cannot follow this evolution during the transient. Therefore, this solution underestimates the exposed surface temperatures, because the portion of solid near the droplet edge is forced to be in contact with a wetted area whose temperature is lower than the actual one until the last moments of the evaporation. However, the results obtained for high thermal conductivity solids are valid over a wide range of materials (copper, aluminum, steel), because those solid surfaces are subjected to very small variations of temperature both in time and in space. In all these cases, uniform and constant interfacial temperature can be assumed.

The uniform and constant interfacial heat flux solution provides much smoother temperature profiles, as expected, and it appears to be not suitable for a correct evaluation of the evaporative cooling effect on the solid. This is basically due to the harshness of the approximation obtained under this boundary condition, as it is evident from the

consideration of the actual heat flux profiles versus radial distance and time (see Fig. 2). With the assumption of uniform and constant interfacial heat flux, one does not consider the big increase of the flux values near the edge of the droplet; moreover, the sudden increase of the heat flux with time in the final 20% of the transient is also neglected. Consequently, one obtains temperature profiles which tend asymptotically toward a final value, while the coupled model solution shows that the variations of temperature in the interfacial region increase with time.

In the initial portion of the transient ($t/\tau < 0.1$) both the experimental data obtained by infrared thermography [6] and the solution of the coupled code show extremely strong temperature gradients under the droplet. In the code, this results in high initial oscillations of the heat flux calculation, which affect the correct evaluation of the interfacial temperature during the first 10 per cent of the transient. The physical phenomena which are related to these observations are not yet completely understood. The apparent discrepancies of the temperature profiles in Figs. 3 to 5, part a) and part b), have to be interpreted in light of these considerations.

CONCLUSIONS

This paper reviews the different boundary conditions which can be applied in a solid model to calculate the temperature distribution on a hot solid surface subjected to dropwise evaporative cooling. The results obtained with these boundary conditions are compared with the predictions provided by a coupled model solid-liquid code presented and validated in previous works by the same authors. The coupled model solution is clearly more suitable and accurate, thus justifying the use of a complex numerical code instead of approximate or analytical solutions. However, the use of a solid model with simplified interfacial assumption is strongly recommended when dealing with a larger solid surface and when the influence of an increased number of droplets has to be considered. In this case, the numerical complexity of the coupled model solution requires high CPU time and a very fine grid nodalization in order to keep the same level of accuracy. On the other hand, the solid-only solutions are subjected to accuracy problems related to the averaging, which has to be implemented.

ACKNOWLEDGEMENTS

This study was made possible by a grant of the Center for Fire Research of the National Institute of Standards and Technology. Partial funding of the computational expenditures was provided by the Computer Science Center of the University of Maryland at College Park.

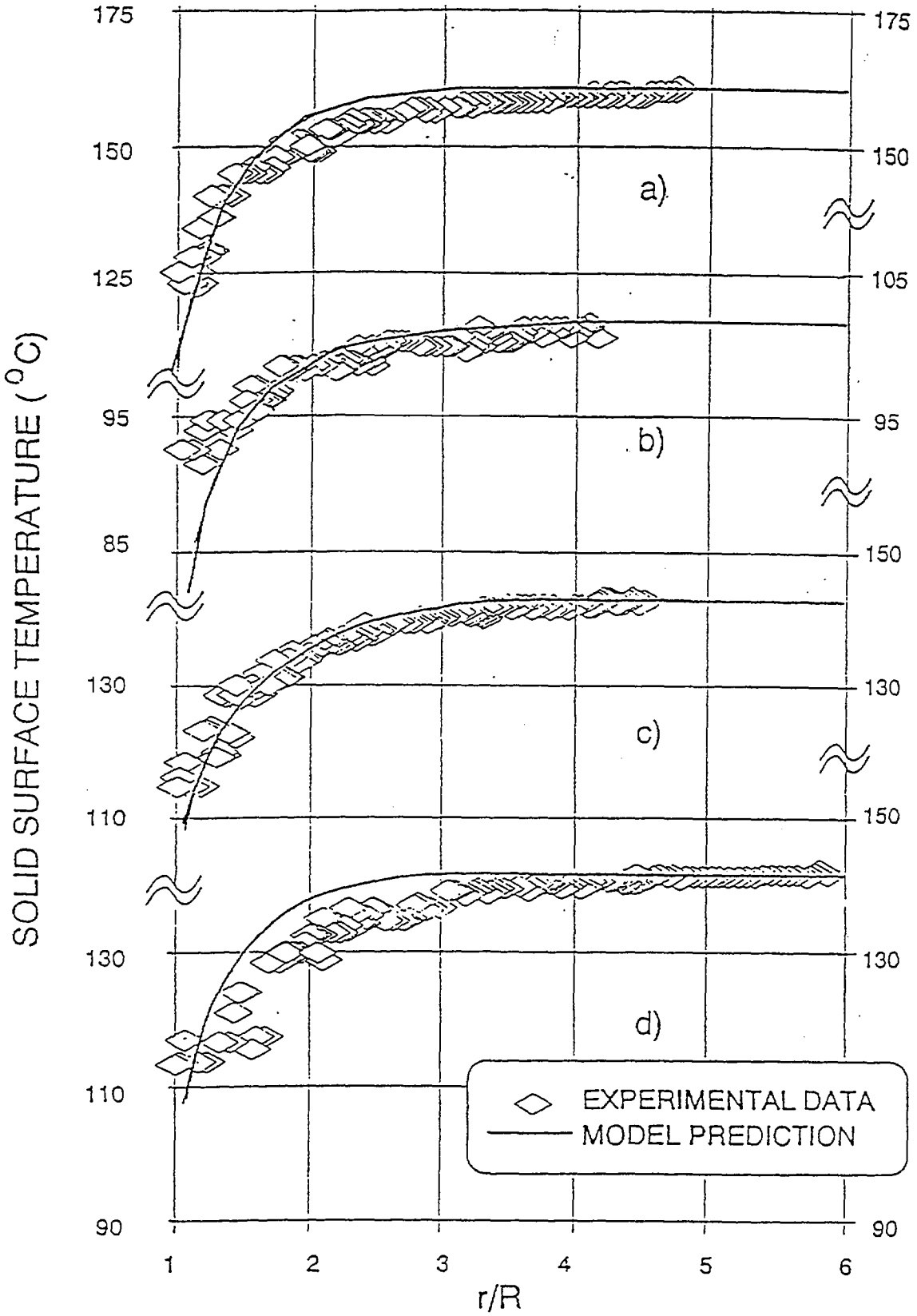

FIGURE 1 Coupled model validation: solid surface temperatures for water on Macor at t/τ = 0.9 with a) V = 30 μl, T_s = 160 °C; b) V = 30 μl, T_s = 101 °C; c) V = 10 μl, T_s = 143 °C and d) V = 30 μl, T_s = 143 °C

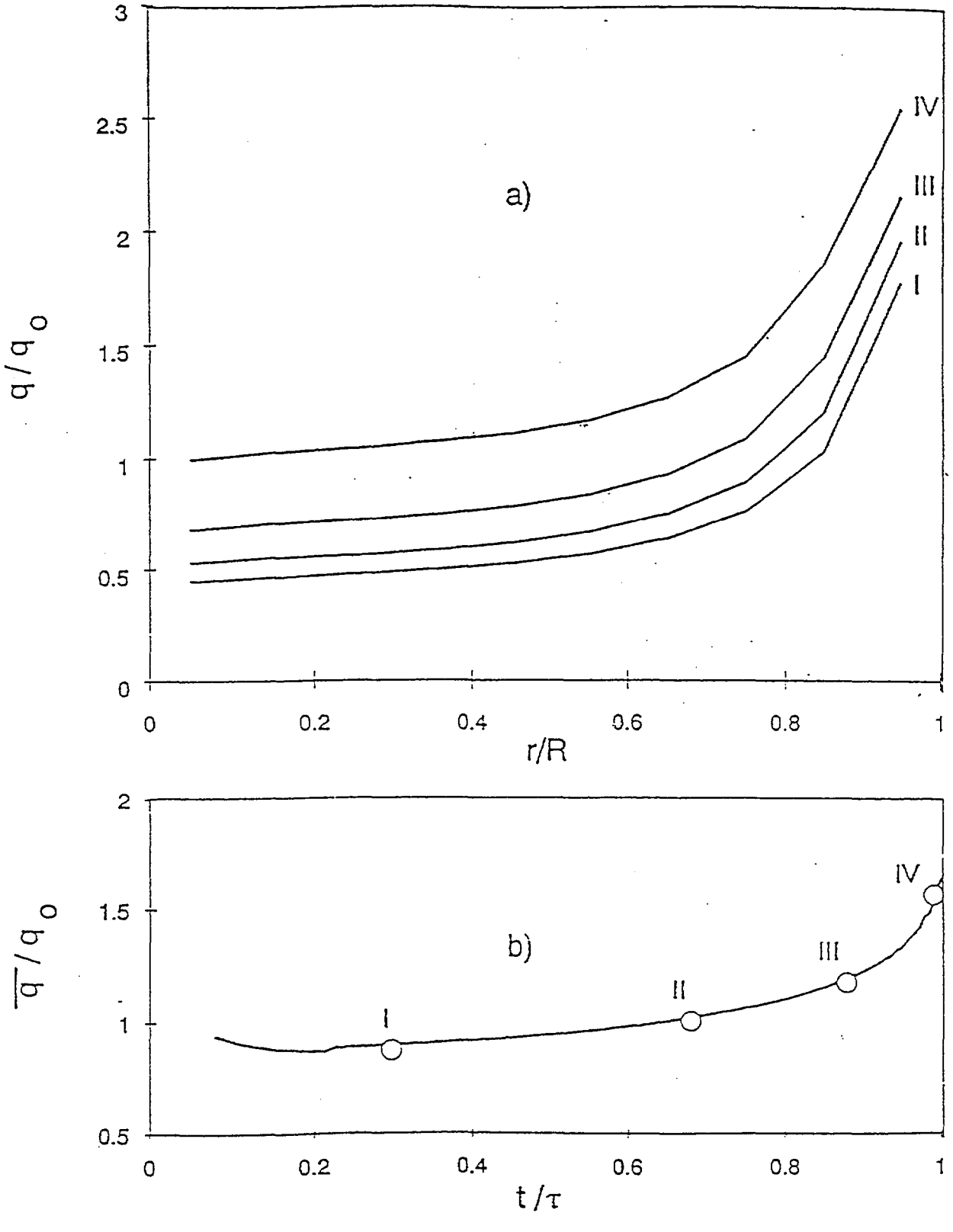

FIGURE 2 Liquid-solid interfacial fluxes for water droplet with V = 30 μl on Macor with T_s = 143 °C and τ = 64s: a) normalized interfacial fluxes at I) $t/\tau = 0.3$, II) $t/\tau = 0.7$, III) $t/\tau = 0.9$, IV) $t/\tau = 0.98$; b) normalized spatial averaged heat flux.

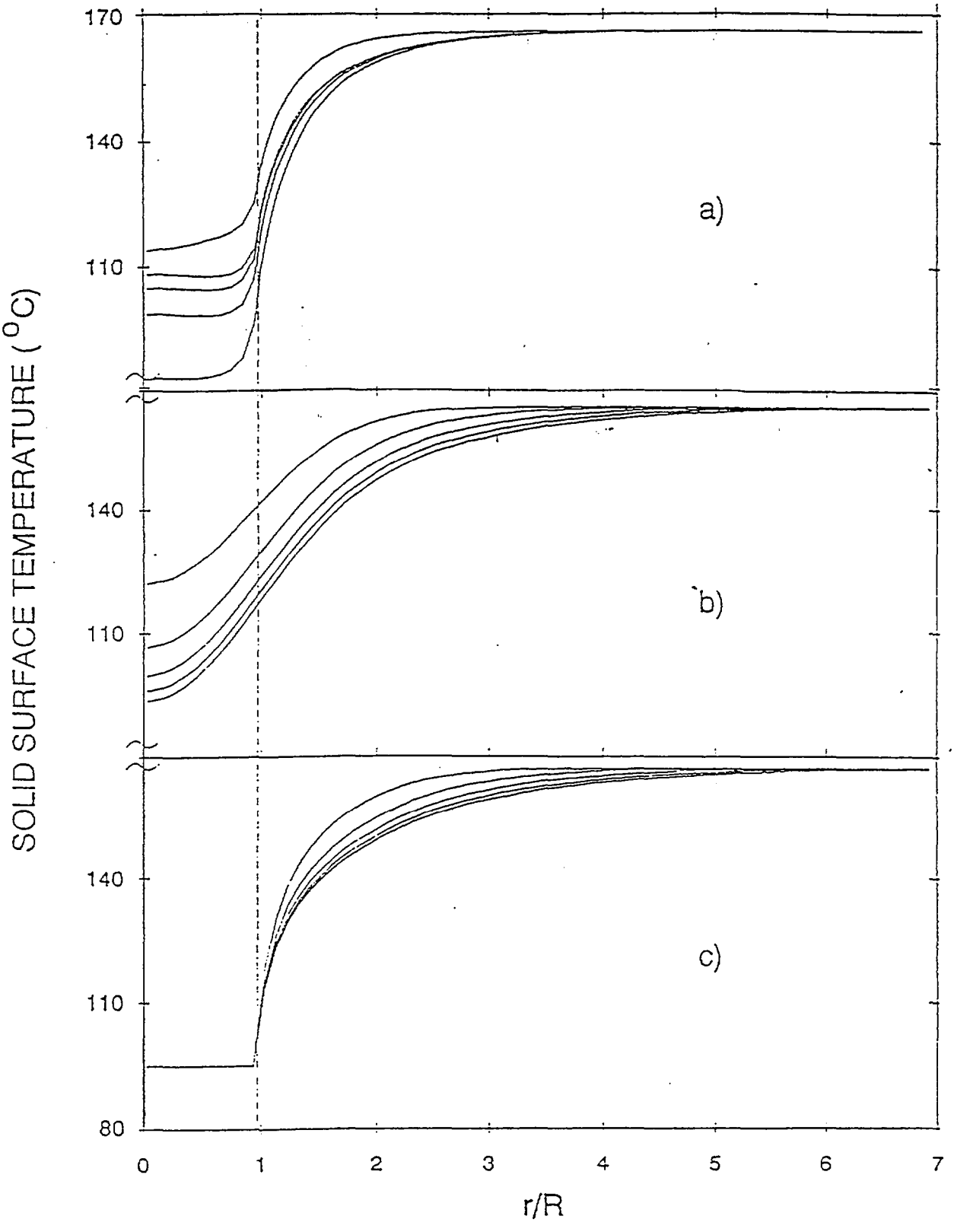

FIGURE 3 Typical solid surface temperature profiles for a water droplet with V = 10 μl on Macor with T_s = 165 °C at t/τ = 0.1, 0.3, 0.5, 0.7 and 0.9 : a) coupled code; b) solid code with constant and uniform interfacial heat flux; c) solid code with constant and uniform interfacial temperature.

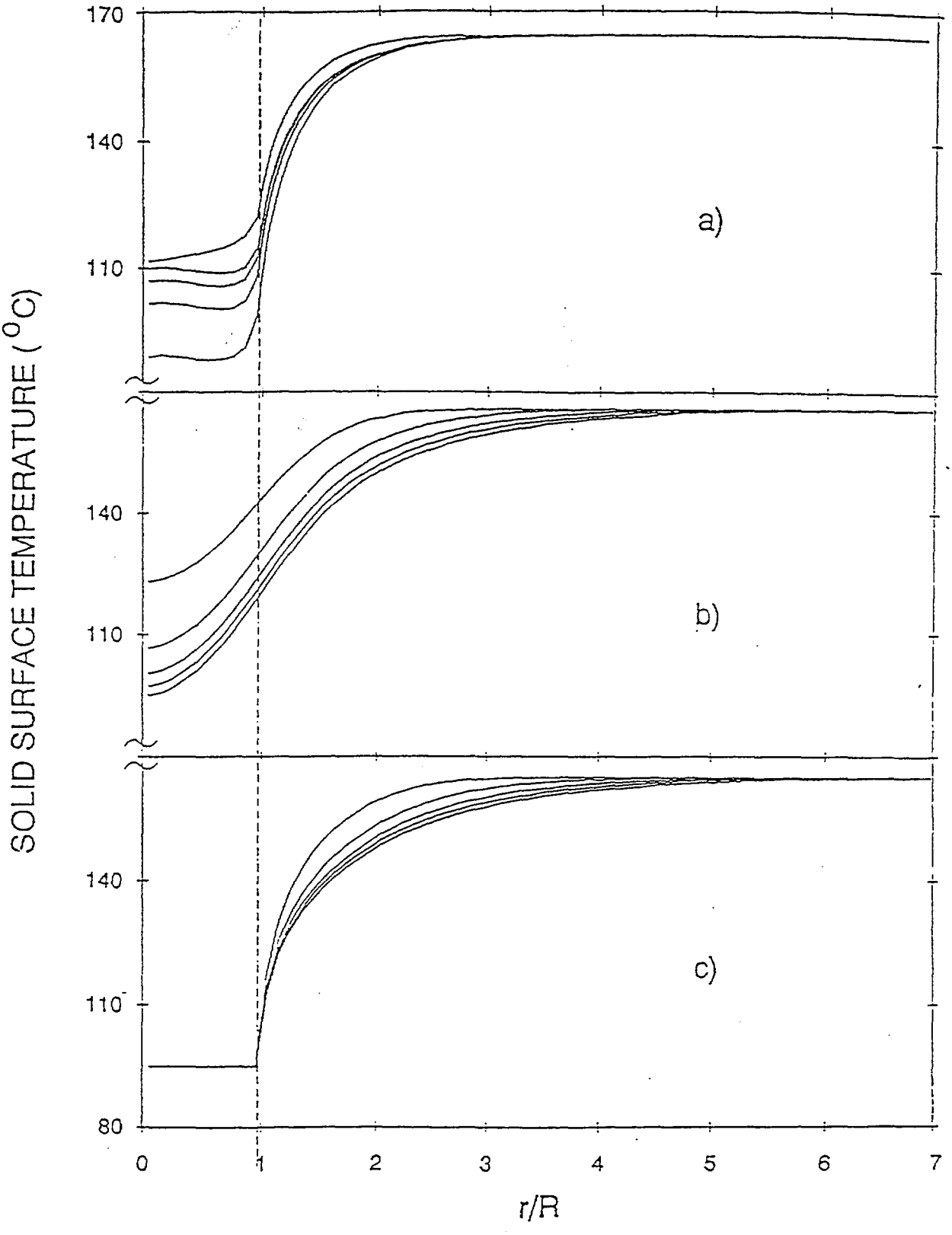

FIGURE 4 Typical solid surface temperature profiles for a water droplet with V = 20 μl on Macor with T_s = 165 °C at t/τ = 0.1, 0.3, 0.5, 0.7 and 0.9 : a) coupled code; b) solid code with constant and uniform interfacial heat flux; c) solid code with constant and uniform interfacial temperature.

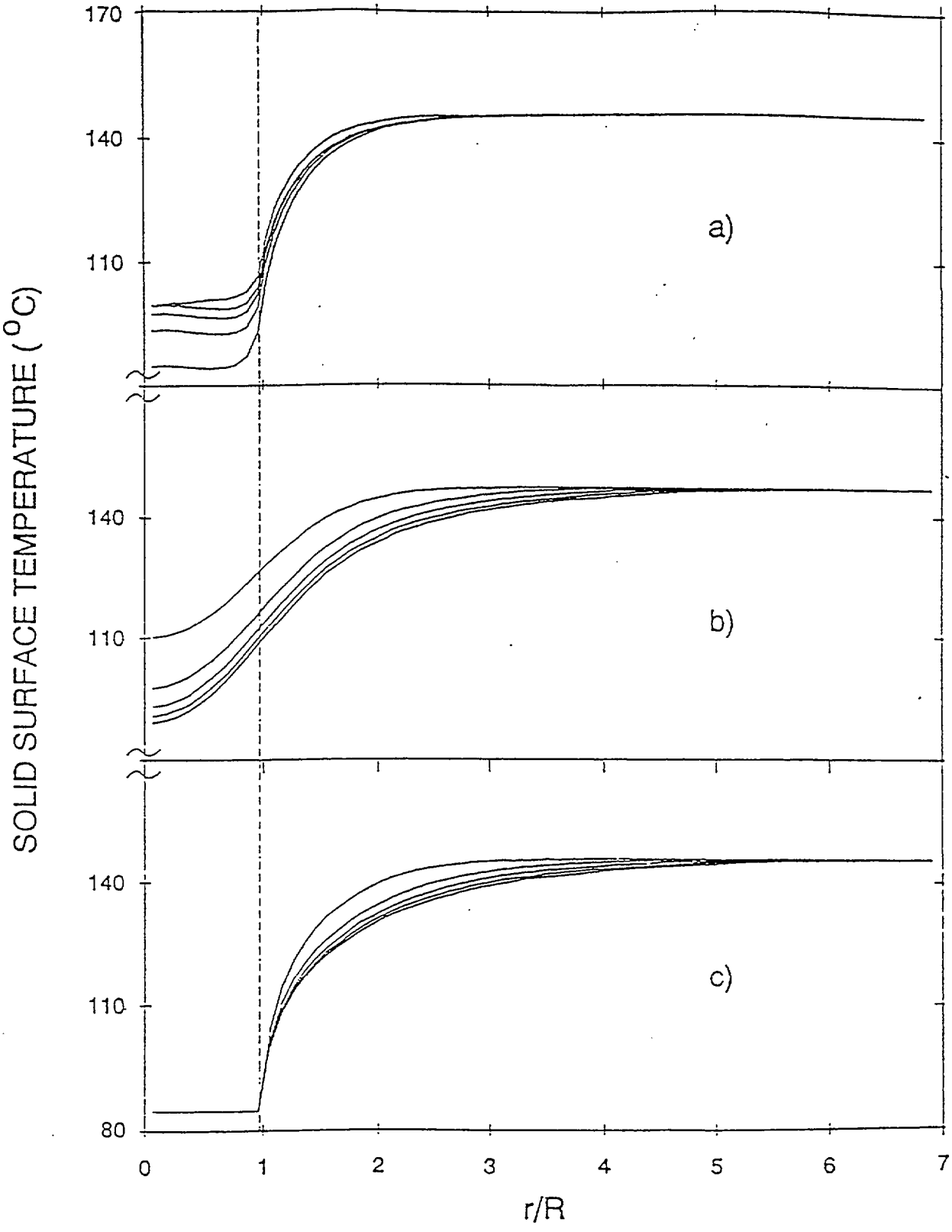

FIGURE 5 Typical solid surface temperature profiles for a water droplet with V = 20 μl on Macor with T_s = 145 °C at t/τ = 0.1, 0.3, 0.5, 0.7 and 0.9 : a) coupled code; b) solid code with constant and uniform interfacial heat flux; c) solid code with constant and uniform interfacial temperature.

NOMENCLATURE

c	specific heat
D	air-steam mass diffusivity
erf	error function
G	Green's function; see Eq. (7)
h	overall heat transfer coefficient
J_0, J_1, I_0	Bessel's functions
JA	Jakob number; see Eq. (16)
k	thermal conductivity
L_0	modified Bessel's function: $e^{-\zeta} I_0(\zeta)$
q	axial heat flux
$\bar{q}$	spatial averaged heat flux
r	radial coordinate
R	radius of the wetted area
t	time
T	temperature
T_c	contact temperature; see Eq. (1)
u	transformed temperature; see Eq. (8)
V	droplet volume
x	molar fraction of steam in air
z	axial coordinate
α	thermal diffusivity
β	shape parameter; see Eq. (16)
δ	normalized time; see Eq. (14)
ϵ	solid surface emissivity
ζ, λ	dummy variables
η	normalized radius: r/R
θ	normalized temperature; see Eq. (15)
Λ	liquid latent heat of vaporization
ρ	density
σ	Stefan-Boltzmann constant
τ	total evaporation time

subscripts

a	air, ambient
i	interfacial
l	liquid
s	solid
0	initial
*	Green's function argument

REFERENCES

[1] Bonacina, C., Del Giudice, S., Comini, G., Dropwise Evaporation, *ASME Journal of Heat Transfer*, Vol. 101, pp.441-446 (1979).

[2] Toda, S., A Study of Mist Cooling. First Report: Investigation of Mist Cooling, *Heat Transfer Japanese Research*, Vol. 1, No. 3, pp.39-50 (1972).

[3] Grissom, W.M., Wierum, F.A., Liquid Spray Cooling of a Heated Surface, *International Journal of Heat and Mass Transfer*, Vol. 24, pp.261-271, (1981).

[4] diMarzo, M., Evans, D., Dropwise Evaporative Cooling of High Thermal Conductivity Materials, *International Journal of Heat and Technology*, Vol.5, No. 1-2, pp. 126-136 (1987).

[5] diMarzo, M., Evans, D., Evaporation of a Water Droplet Deposited on a Hot High Conductivity Solid Surface, *ASME Journal of Heat Transfer*, Vol.111, pp.210-221 (1989).

[6] Klassen, M., diMarzo, M., Sirkis, J., Infrared Thermography of Dropwise Evaporative Cooling, *ASME HTD*, Vol. 141, pp. 117-121 (1990).

[7] Seki, M., Kawamura, H., Sanokawa, K., Transient Temperature Profile of a Hot Wall Due to an Impinging Liquid Droplet, *ASME Journal of Heat Transfer*, Vol.100, pp.167-169 (1978).

[8] Rizza, J.J., A Numerical Solution to Dropwise Evaporation, *ASME Journal of Heat Transfer*, Vol.103, pp.501-507 (1981).

[9] Kavoosi, F., diMarzo, M., Baum, H., Evans, D., An Application of Boundary Element Method to a Transient Axisymmetric Heat Conduction Problem, *ASME HTD*, Vol.110, pp. 79-85 (1989).

[10] Michiyoshi, I., Makino, K., Heat Transfer Characteristics of Evaporation of a Liquid Droplet on Heated Surface, *International Journal of Heat and Mass Transfer*, Vol. 21, pp. 605-613 (1978).

[11] Michiyoshi, I., Makino, K., The Behavior of a Water Droplet on Heated Surfaces", *International Journal of Heat and Mass Transfer*, Vol. 27, No. 5, pp. 781-791, 1985.

[12] Michiyoshi, I., Makino, K., Discussions of Transient Heat Transfer to a Water Droplet on Heated Surfaces under Atmospheric Pressure, *International Journal of Heat and Mass Transfer*, Vol. 30, No. 9, pp. 1895-1905 (1987).

[13] diMarzo, M., Tartarini, P., Liao, Y., Evans, D., Baum, H., Dropwise Evaporative Cooling, accepted for presentation at the *27th ASME/AIChE/ANS National Heat Transfer Conference* to be held in Minneapolis, MN, on July 28-31, 1991.

[14] Tartarini, P., Liao, Y., diMarzo, M., Transient Cooling of a Hot Surface by Droplets Evaporation, *UMCP Mechanical Engineering Report*, No. 90-6 (1990).

[15] Wrobel, L.C., Brebbia, C.A., A Formulation of the Boundary Element Method for Axisymmetric Transient Heat Transfer Conduction, *International Journal of Heat and Mass Transfer*, Vol. 24, pp. 843-850 (1981).

[16] Carslaw, H.S., and Jaeger, J.C., 1959, *Conduction of Heat in Solids*, Clarendon Press, Oxford, pp. 214-217 and 264.

PAPER # 7

Int. J. Heat Mass Transfer. Vol. 36. No. 17. pp. 4133–4139. 1993
Printed in Great Britain

0017–9310 93 $6.00 + 0.00
Pergamon Press Ltd

Evaporative cooling due to a gently deposited droplet

M. DI MARZO, P. TARTARINI and Y. LIAO
Mechanical Engineering Department, University of Maryland, College Park, Maryland 20742, U.S.A.

and

D. EVANS and H. BAUM
Building and Fire Research Laboratory, National Institute of Standards and Technology, Gaithersburg, Maryland 20899, U.S.A.

(*Received* 9 *March* 1993 *and in final form* 21 *May* 1993)

Abstract—The transient thermal behavior of a single water droplet gently deposited on the surface of a semi-infinite solid is investigated. A coupled model that solves simultaneously the transient conduction equation for the solid and the liquid to yield the surface temperature and heat flux distributions as well as the description of the droplet evaporation transient is proposed. The predictions of the evaporation time are compared with experimental data. An additional model is presented which assumes constant heat flux at the liquid–solid interface. This model provides a closed form solution for the solid surface transient temperature distribution.

INTRODUCTION

THE COOLING of hot solid surfaces by droplet evaporation has been studied extensively. Multi-droplet systems were investigated both theoretically and experimentally over several years; see for example the work of Toda [1], Bonacina *et al.* [2] and Tio and Sadhal [3]. Single droplet systems were described by Inada *et al.* [4], Makino and Michiyoshi [5, 6] and Takano and Kobayashi [7] among others.

The droplet configuration upon impacting a solid surface has been discussed in great detail by Chandra and Avedisian [8] while the droplet shape during the last stages of evaporation was examined by Zhang and Yang [9].

In this paper general models are derived for the case of a water droplet gently deposited over the surface of a semi-infinite solid. A typical photographic description of the evaporative transient, which is consistent with a similar record provided by Xiong and Yuen [10], is shown in Fig. 1. The initial solid surface temperature is below the limit at which onset of nucleate boiling is observed. The formulation of a model to predict both the evaporation time and the transient thermal behavior of the solid surface is the first step in formulating more comprehensive predictive tools for multi-droplet evaporative cooling.

The transient thermal behavior of a high conductivity semi-infinite solid has been modeled by imposing a constant uniform temperature at the solid–liquid interface [11, 12]. The models based on this assumption yield good predictions for cases where the surface temperature is not experiencing major changes during the process which is most common for high thermal conductivity solids. However, these models are unable to predict the solid thermal behavior for low thermal conductivity materials which exhibit large temperature variations during the drop evaporating process. De-coupling the liquid from the solid (by imposing that artificial boundary condition at the solid–liquid interface) means that the liquid droplet is assumed to behave independently of the substrate (i.e. the solid). The interfacial temperature at the initial liquid–solid contact is approximated by the exact solution available for the contact temperature of two semi-infinite solids. Seki *et al.* [11] based their analysis on this consideration and suggested that the interfacial temperature can be obtained as:

$$T_c = \frac{T_l\sqrt{(\rho_l c_l k_l)} + T_s\sqrt{(\rho_s c_s k_s)}}{\sqrt{(\rho_l c_l k_l)} + \sqrt{(\rho_s c_s k_s)}}. \qquad (1)$$

The constant temperature model does not conserve energy at the liquid–solid interface since there is no energy conservation constraint. This constitutes a major barrier to the extension of these results to the multi-droplet formulation because the overall heat balance for multiple droplet solid cooling cumulates the single droplet inaccuracies.

THEORETICAL MODELS

Coupled model description

Inspection of Fig. 1 reveals that the liquid–solid receding angle (which has been found to be 7° for aluminum and water) is reached when a small fraction of the original water in the droplet is left [13]. Therefore, it is reasonable to assume that the surface of the wetted area is constant throughout the evaporative process as can be deduced from the figure.

Visual inspection of a tracer and the measurements reported by Ostrach and Pradhan [14] indicate that

NOMENCLATURE

c	specific heat
d	diameter of the wetted region
D	*air-steam mass diffusivity*
erf	error function
G	Green's function; see equation (12)
h	overall heat transfer coefficient
h_{conv}	convective heat transfer coefficient
J_0, J_1, I_0	*Bessel's functions*
JA	Jakob number; see equation (20)
k	thermal conductivity
L_0	modified Bessel's function, $e^{-\zeta}I_0(\zeta)$
q	heat flux
q_r	*reference heat flux*, $\Lambda\rho_l V_l/(\pi R^2\tau)$
r	radial coordinate
R	radius of the wetted area; see Fig. 2
S	surface; see equation (15)
t	time
T	*temperature*
T_c	contact temperature; see equation (1)
u	transformed temperature; see equation (13)
V	droplet volume or volume; see equation (15)
x	molar fraction of steam in air
z	axial coordinate.

Greek symbols

α	thermal diffusivity
β	*shape parameter; see equation (19)*
δ	normalized time, $(\alpha_s t)^{1/2}/R$
δ_τ	normalized evaporation time, $(\alpha_s\tau)^{1/2}/R$
ζ, λ	dummy variables
η	normalized radius, r/R
η_ϕ	radius of influence associated with the constant ϕ
θ	normalized temperature; see equation (17)
Λ	liquid latent heat of vaporization
ρ	density
τ	total evaporation time
ϕ	arbitrary constant.

Subscripts

a	*far-field air property*
i	liquid–vapor interfacial property
l	liquid property at the liquid–solid interface
o	solid initial property
s	*solid surface property*
*	Green's function argument; equations (12) and (14).

little convective motion is present in the water droplet. Therefore, one can assume that the dominant mechanism of heat transfer in the water droplet is conduction. This assumption is common to most previous models [1, 11, 12, 15]. The shape of the water droplet in Fig. 1 can be described with good approximation as a segment of a sphere of fixed base and decreasing apex [12]. This geometrical representation of the deposited droplet is accurate while the liquid–solid contact angles exceeds the receding angle [13] as previously discussed. The modeling of the coupled solid and liquid thermal behavior is described by the transient conduction equation for both domains with the appropriate boundary conditions.

The governing equations, with respect to the coordinate system depicted in Fig. 2, are:

$$\frac{\partial T}{\partial t} = \alpha_s\nabla^2 T, \quad \frac{\partial T}{\partial t} = \alpha_l\nabla^2 T. \qquad (2, 3)$$

The initial and boundary conditions are as follows:

$$\text{at } t = 0, \quad \text{for the solid}: \quad T = T_0 - \frac{q_0 z}{k_s}$$

$$\text{and for the liquid}: \quad T = T_s \qquad (4, 5)$$

at $0 \leqslant r \leqslant R$, $z = 0$:

$$T_s = T_l, \quad k_s\left(\frac{\partial T}{\partial z}\right)_s = k_l\left(\frac{\partial T}{\partial z}\right)_l$$

at $r > R$, $z = 0$:

$$k_s\left(\frac{\partial T}{\partial z}\right)_s = h(T_s - T_a) \qquad (6, 7, 8)$$

at $z \to -\infty$ for all r's

$$-k_s\left(\frac{\partial T}{\partial z}\right)_s = q_0$$

at $r \to \infty$, $z \leqslant 0$:

$$\left(\frac{\partial T}{\partial r}\right)_s = 0. \qquad (9, 10)$$

At the liquid–vapor interface, a small portion of the heat conducted from below through the liquid is transferred to the ambient by convection and by radiation. Most of the heat evaporates the liquid.

The conservation of energy at the liquid–vapor interface provides the remaining boundary condition needed for equation (3). To account for the evaporation, the vapor diffusion in the air is considered. Details of the derivation of this liquid–vapor interfacial condition are given by di Marzo and Evans [12]. In the derivation the mass transfer coefficient is related to the convective heat transfer h_{conv} by the Chilton–Colburn analogy [16].

The final formulation of the boundary condition at the liquid–vapor interface can be written as:

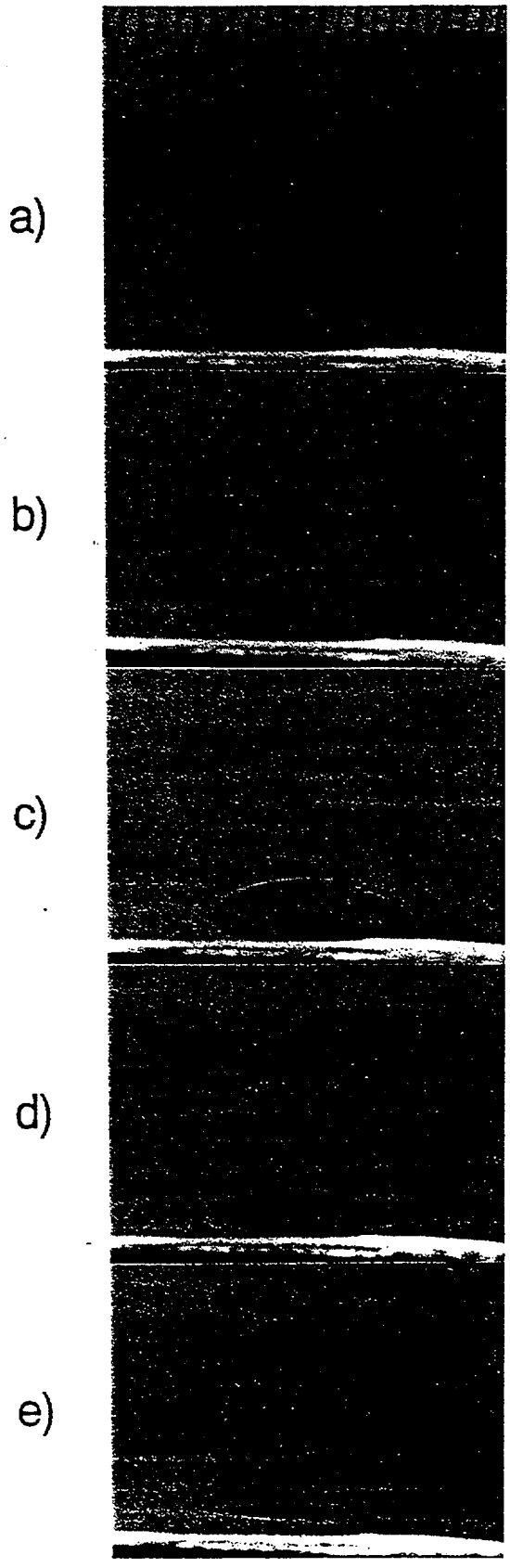

FIG. 1. Typical photographic record of a 30 μl droplet on aluminum ($T_s = 92$ C, $\tau = 86$ s) at (a) $t/\tau = 0$; (b) $t/\tau = 0.21$; (c) $t/\tau = 0.38$; (d) $t/\tau = 0.62$ and (e) $t/\tau = 0.85$.

$$-k_l \nabla T \cdot \hat{n} - h(T_i - T_a) = 0.624 h_{conv} \left(\frac{D}{\alpha_a}\right)^{2/3} \frac{\Lambda}{c_a} \frac{x_i - x_a}{1 - x_a} \quad (11)$$

where the temperature gradient is taken normal to the liquid vapor interface. The grid geometry shown in Fig. 2 is such that this gradient is normal to the upper boundary of the computational domain for the liquid region.

Extremely strong local thermal gradients at the droplet edge, during the initial transient, pose some difficulties to the solution of this problem with conventional finite difference schemes. In the present study, the solution of the transient conduction equation in the solid is obtained by using a Boundary Element Method (BEM). This is combined with a finite volume treatment of the liquid droplet. The BEM is described in detail by Kavoosi *et al.* [17]. The adjoint equation to equations (2) is satisfied by the following Green's function [18]:

$$G(r, z, t; r^*, z^*, t^*) = (4\pi\alpha_s t^*)^{-3/2} \times \{e^{-[(r-r^*)^2+(z-z^*)^2]/(4\alpha_s t^*)} + e^{-[(r-r^*)^2+(z+z^*)^2]/(4\alpha_s t^*)}\}. \quad (12)$$

A linear combination of equation (2) and of its adjoint equation, is integrated over the solid and temporal domain. By applying the Gauss theorem on the volume integral, one obtains the following relationship between the solid temperature and its normal derivative at the solid surface:

$$u(r, t) = T - T_s - \frac{q_0 z}{k_s} = \int_0^t \int_0^\infty \nabla u(r^*, t^*) r^* t^{*-3/2} L_0\left(\frac{2rr^*}{4\alpha_s t^*}\right) \times e^{-(r-r^*)^2/(4\alpha_s t^*)} \, dr^* \, dt^*. \quad (13, 14)$$

The governing equation for the liquid is cast in the following form:

$$\int_V \frac{\partial T}{\partial t} dv = \alpha_l \int_S \nabla T \cdot \hat{n} \, ds \quad (15)$$

which is integrated for each elementary volume of the discretized liquid domain. The volume elements are defined in terms of the coordinates shown in Fig. 2. Details on the treatment of the liquid domain are given by Liao [19]. These two equations, equations (14) and (15), represent the energy conservation in the solid and liquid respectively. In their discretized form they become matrix equations for the transient temperature and heat flux distribution in the liquid and over the solid surface.

A computer code has been developed to solve these equations [19]. The input to the code must prescribe: (a) the droplet initial volume; (b) the droplet shape parameter β as defined by Bonacina *et al.* [2]; (c) the initial surface temperature; (d) the overall heat transfer coefficient and (e) the convective heat transfer

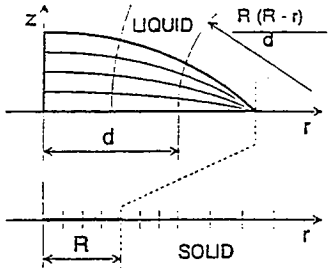

FIG. 2. Coordinate system and nodalization.

coefficient. The shape parameter and the two heat transfer coefficients are provided by correlations based on experimental data. The code predicts: (a) the transient temperature profiles on the solid surface and throughout the liquid; (b) the heat fluxes at all points of the liquid domain and on the solid surface; (c) the total evaporation time and (d) the transient liquid inventory.

The shape parameter is reported for various solid materials and evaporating fluids by several investigators [2, 8, 12, 20]. The overall heat transfer coefficient has been measured by Klassen and di Marzo [21] and correlations are available in the literature to estimate the convective heat transfer coefficient.

Constant flux model

This model is of interest because its relative simplicity makes it a candidate for use in multi-droplet evaporative cooling studies. Carslaw and Jaeger [22] show that, for a semi-infinite solid with a surface heat flux constant and uniform applied over a disk of radius R and no heat transfer on the remainder of the surface, the transient temperature profile on the solid surface is given by

$$T_0 - T_s = \frac{q_s R}{k_s} \int_0^\infty J_0(\lambda r) J_1(\lambda R) \operatorname{erf}\left(\lambda \sqrt{(\alpha_s \tau)}\right) \frac{\mathrm{d}\lambda}{\lambda}. \tag{16}$$

By introducing the normalized radius $\eta = r/R$ and the normalized evaporation time $\delta_s = (\alpha_s \tau)^{1/2}/R$ and by setting q_s equal to the spatial and temporal averaged heat flux due to droplet evaporation, one obtains:

$$0 = JA \left(\frac{\rho_s}{\rho_l}\right) \delta_s^2 \beta^3 = \frac{4}{3} \int_0^\infty J_0(\zeta\eta) J_1(\zeta) \operatorname{erf}(\zeta\delta) \frac{\mathrm{d}\zeta}{\zeta} \tag{17, 18}$$

where β is the shape parameter defined by Bonacina *et al.* [2] and JA is the Jakob number. These two parameters can be expressed as follows:

$$\beta = R \left(\frac{4\pi}{3V_l}\right)^{1/3}, \quad JA = \frac{c_s(T_0 - T_s)}{\Lambda}. \tag{19, 20}$$

In order to quantify the extent of the solid surface region affected by the droplet cooling, a significant parameter is the radial heat flux at the surface at any given location. The presence of the droplet is felt when this radial heat flux is greater than a fraction of the reference value identified as the spatial and temporal averaged heat flux, that is:

$$k_s \frac{\partial T_s}{\partial r} \geqslant \phi \frac{\Lambda \rho_l V}{\pi R^2 \tau}. \tag{21}$$

By using equations (18) and (19), this condition, in terms of normalized quantities, becomes:

$$-\frac{\partial \theta}{\partial \eta} \geqslant \frac{4}{3}\phi$$

$$\int_0^\infty J_1(\zeta\eta) J_1(\zeta) \operatorname{erf}(\zeta\delta)\, \mathrm{d}\zeta \geqslant \phi \tag{22, 23}$$

where ϕ is an arbitrary constant. Equation (23) can be used to define the radius of influence η_ϕ ($= r_\phi/R$) as the minimum value of η that satisfies the inequality. The radius of influence can be defined for $\phi = 0.1$ which relates the radial heat flux to 10% of the spatial and temporal averaged heat flux (see equation (21)). With this definition one implies that a radial heat flux of less than 10% of the reference heat flux is considered small. At such distance from the droplet and beyond, the evaporative cooling effect is considered equally small. Note that the definition of the radius of influence is based on the arbitrary constant ϕ. Therefore, it can be used only on a comparative basis.

MODELS VALIDATION

Coupled model

A comparison of the coupled model with the experimental data is obtained by looking at the evaporation times for aluminum [12] and for macor [20]. Figure 3 shows the calculated and measured evaporation time for both materials for various initial solid surface temperatures and droplet sizes. The agreement is

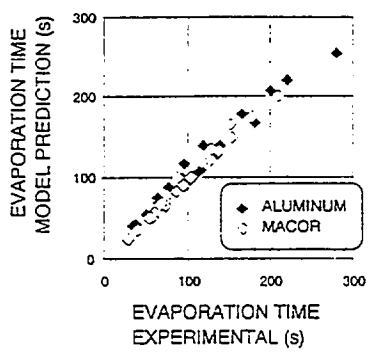

FIG. 3. Model validation: total evaporation time for droplets with $V = 10, 30, 50\ \mu l$ on aluminum with $T_s = 75$–102 C and on macor with $T_s = 101$–208 C (data for aluminum from ref. [12], data for macor from ref. [20]).

remarkable in light of the fact that the experimental data are repeatable within 10% of the indicated value.

The cooling effect, due to the droplet, is strongly dependent on the properties of the solid. Figure 4 illustrates this point by comparing the temperature distributions for a 30 μl droplet which evaporates in 95 s on aluminum and macor. To achieve the same time averaged heat flux, the initial surface temperatures are obviously different: for aluminum $T_s = 91°C$ and for macor $T_s = 119°C$. The curves shown in the figure are at 29 and 86 s after deposition. Note the minimal temperature excursion for aluminum and the rather deep temperature drop for macor. Further, the cooling effect is felt over a large portion of the aluminum surface (more than nine droplet radii) while the effect is rather contained on the macor surface (about three droplet radii) albeit much more intense. The other aspect, that emerges from the analysis of the code computation, is the unidimensionality of the heat transfer in the liquid region. The radial heat flux, at various locations and at various stages of the evaporative process, amounts to less than 5% of the total heat flux in most cases. Only for a few locations at the droplet edge, for low thermal conductivity materials, toward the end of the process, does its contribution exceed 10% of the total heat flux. This observation allows the simplifications of the model for the liquid layer, which will be particularly important in future studies of multi-droplet heat transfer.

The measured transient temperature distribution over the solid surface is illustrated in Fig. 5. These data are obtained via infrared thermography of the surface by Klassen *et al.* [20]. The temperature profiles shown in the figure are over a line (on the solid surface) passing through the center of the wetted region. The readings over the surface covered by the liquid

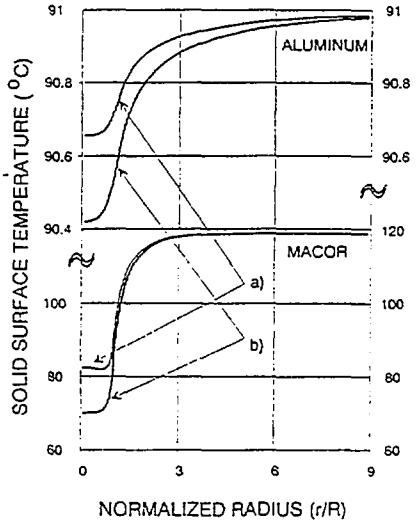

FIG. 4. Typical solid surface temperature profiles for a water droplet ($V = 30$ μl, $\tau = 95$ s) deposited on aluminum ($T_s = 91$ C) and macor ($T_s = 119$ C) for (a) $t/\tau = 0.3$ and (b) $t/\tau = 0.9$.

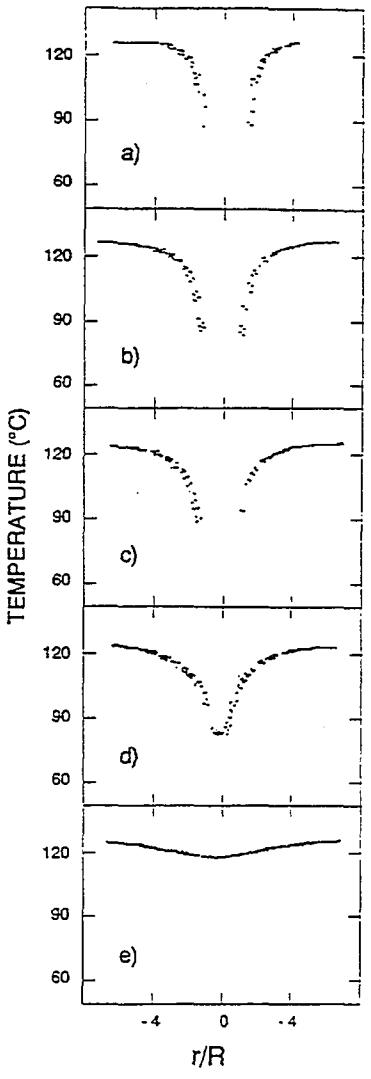

FIG. 5. Typical surface temperature distribution for a 30 μl droplet on macor (data from ref. [20] for $T_s = 124$°C and $\tau = 100$ s) at (a) $t/\tau = 0.1$; (b) $t/\tau = 0.7$; (c) $t/\tau = 0.9$; (d) $t/\tau = 1.0$ and (e) $t/\tau = 1.1$.

(i.e. plots a, b, c for $r/R < 1$) cannot be related to a temperature scale due to the infrared radiation absorption of the water layer. Note that the last two plots (i.e. plots d, e) describe the surface temperature after the complete droplet vaporization.

Figure 6 compares the experimental data (shown as shaded regions) with the models previously described. Case (a) shows the results of the coupled model; case (b) illustrates the predictions of the constant flux model while case (c) is related to previous simplified models reported in the literature [11, 12].

The overall performance of the coupled model is quite reasonable. It slightly over-predicts the data while capturing well the temperature at the droplet edge ($r = R$). The radius of influence is under-estimated by this model. Both the droplet evaporation and the solid cooling are modeled and the simultaneous thermal transient description is obtained.

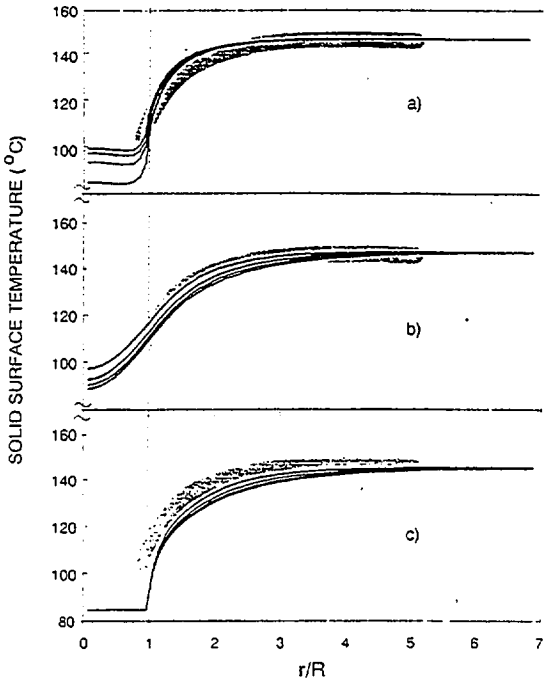

FIG. 6. Typical solid surface temperature profiles for droplets deposited on macor compared with data from ref. [21] with $0.3 \leqslant t/\tau \leqslant 0.9$ for (a) the coupled model; (b) the constant flux model and (c) the constant temperature model ($V = 30$ μl; $T_s = 145$°C; at $t/\tau = 0.3$; $t/\tau = 0.5$; $t/\tau = 0.7$ and $t/\tau = 0.9$).

Constant flux model

The constant flux model is able to predict the data well as shown in Fig. 6 (case b) where it slightly under-predicts the measured temperature profile while preserving the general trends. This closed-form solution over-estimates the droplet cooling effect.

Figure 7 shows the liquid–solid interfacial fluxes, calculated from the coupled model, for a typical case. It is important to note that the heat flux is not uniform nor constant during the evaporative process. The spatial distribution indicates that most of the evaporation takes place at the outer edge of the droplet. Therefore, it is not surprising that the constant heat flux model exhibits some discrepancies with the data for the temperature gradient at $r = R$ (or, in non-dimensional variables, for $\eta = 1$) as it can be seen in Fig. 6.

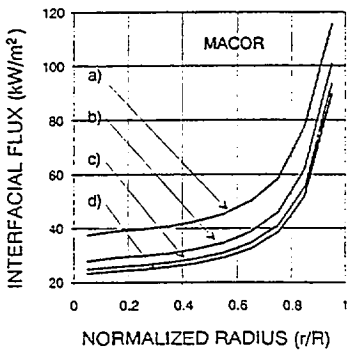

FIG. 7. Liquid–solid interfacial fluxes for water droplet with $V = 30$ μl on macor with $T_s = 145$°C at (d) $t/\tau = 0.3$; (c) $t/\tau = 0.5$; (b) $t/\tau = 0.7$; (a) $t/\tau = 0.9$ and $\tau = 64$ s (coupled model computations).

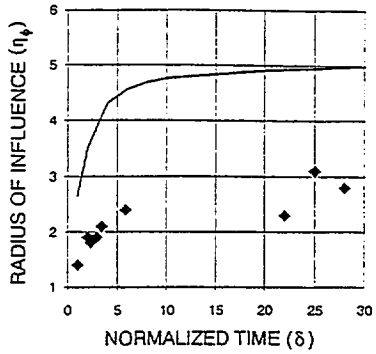

FIG. 8. Radius of influence vs normalized time with $\phi = 0.1$: —— constant flux model; ◆ coupled model.

The constant flux model provides a very good quantitative representation of the temperature profiles on the solid surface. However, it fails to capture the qualitative details of the transient behavior. Figure 5 shows that the measured temperature profile is almost constant throughout the process after a rapid initial transient. This behavior is well represented by the coupled model while the constant flux model exhibits an ever changing temperature profile as time progresses.

Concerning the cooling effect, the solution of equation (23), for $\phi = 0.1$, is shown in Fig. 8. The predictions of the coupled model, at selected values, are also shown in the figure for comparison. By inspecting Fig. 6, one can conclude that the actual radius of influence lies between the predictions of the coupled model and of the constant flux model. Note that the cylindrical coordinate system will favor the coupled model when the area of the surface influenced by the droplet is compared.

The fundamental difference between the coupled

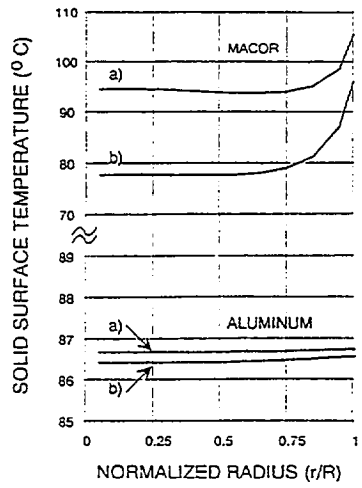

FIG. 9. Typical liquid–solid interfacial temperatures for macor and aluminum with $T_s = 82$°C for water droplets with $V = 30$ μl at (a) $t/\tau = 0.3$ and (b) $t/\tau = 0.9$ (coupled model computations).

model and the constant flux model is in that *the coupled model provides a complete description of the phenomena while the constant flux model requires the droplet evaporation time (as an independent input) in order to estimate the spatial and temporal averaged heat flux* q_t.

Finally, the model based on the constant and uniform temperature at the solid–liquid interface underpredicts the surface temperature while over-predicting the surface cooling. Figure 9 illustrates the transient temperature distribution (obtained with the coupled model) at the liquid–solid interface for aluminum and macor when a 30 μl droplet is deposited on the solid with an initial solid surface temperature (T_s) which will yield a calculated contact temperature $T_c = 82°C$ from equation (1). As one can readily observe, this calculated contact temperature has no relation with the results shown in Fig. 9 since the solid–liquid interfacial temperature is changing with time as well as spatially.

CONCLUSIONS

This paper briefly reviews the formulation of two models for the prediction of the thermal behavior of the droplet–solid interaction during evaporative cooling. The coupled model, which solves simultaneously the liquid and the solid transient conduction equations, is validated over a wide range of parameters.

The constant flux model is also described. This model de-couples the liquid from the solid by introducing a simplified boundary condition at the liquid–solid interface (i.e. constant and uniform heat flux). A comprehensive discussion of the two models in comparison with experimental data outlines their relative merits: the coupled model provides the full solution for the solid surface cooling and for the droplet evaporation while the constant flux model predicts the transient surface temperature distribution reasonably well.

The multi-droplet model, which will be the subject of future studies, is based on the super-position of the transient surface thermal behavior due to a single evaporating droplet. Therefore, these two models provide the basis for its development.

Acknowledgements—This study was made possible by a grant of the Building and Fire Research Laboratory, National Institute of Standards and Technology. Partial funding of the computational expenditures was provided by the Computer Science Center of the University of Maryland at College Park.

REFERENCES

1. S. Toda, A study of mist cooling. First report: investigation of mist cooling, *Heat Transfer-Jap. Res.* 1(3), 39–50 (1972).
2. C. Bonacina, S. Del Giudice and G. Comini, Dropwise evaporation, *Trans. ASME, J. Heat Transfer* **101**, 441–446 (1979).
3. K. K. Tio and S. S. Sadhal, Thermal analysis of droplet spray evaporation from a heated solid surface, *Trans. ASME, J. Heat Transfer* **114**, 220–233 (1992).
4. S. Inada, Y. Mikasaka and K. Nishida, Transient heat transfer for a water drop impinging on a heated surface, *Bull. JSME* **28**(246), 2675–2681 (1985).
5. K. Makino and I. Michiyoshi, Effects of the initial size of water droplet on its evaporation on heated surfaces, *Int. J. Heat Mass Transfer* **22**, 979–981 (1979).
6. K. Makino and I. Michiyoshi, The behavior of a water droplet on heated surfaces, *Int. J. Heat Mass Transfer* **27**, 781–791 (1984).
7. T. Takano and K. Kobayashi, Vaporization behavior of a single droplet impinging on a heated surface with a flame-spayed ceramic coating, *Heat Transfer—Jap. Res.* **20**, 1–17 (1991).
8. S. Chandra and C. T. Avedisian, On the collision of a droplet with a solid surface, *Proc. R. Soc.* **432**, 13–41 (1991).
9. N. Zhang and W. J. Yang, Natural convection in evaporating minute drops, *Trans. ASME, J. Heat Transfer* **104**, 656–662 (1982).
10. T. Y. Xiong and M. C. Yuen, Evaporation of a liquid droplet on a hot plate, *Int. J. Heat Mass Transfer* **34**, 1881–1894 (1991).
11. M. Seki, H. Kawamura and K. Sanokawa, Transient temperature profile of a hot wall due to an impinging liquid droplet, *Trans. ASME, J. Heat Transfer* **100**, 167–169 (1978).
12. M. di Marzo and D. D. Evans, Evaporation of a water droplet deposited on a hot high thermal conductivity surface, *Trans. ASME, J. Heat Transfer* **111**, 210–213 (1989).
13. F. F. Simon and Y. Y. Hsu, Wetting dynamics of evaporating drops on various surfaces, *NASA TM X-67913* (1971).
14. S. Ostrach and A. Pradhan, Surface-tension induced convection at reduced gravity, *AIAA J.* **16**(5), 419–424 (1978).
15. J. J. Rizza, A numerical solution to dropwise evaporation, *Trans. ASME, J. Heat Transfer* **103**, 501–507 (1981).
16. T. H. Chilton and A. P. Colburn, Mass transfer (absorption) coefficients prediction data on heat transfer fluid motion, *Ind. Engng Chem.* **26**, 1183–1187 (1934).
17. F. Kavoosi, M. di Marzo, H. R. Baum and D. D. Evans, An application of boundary element methods to a transient axisymmetric heat conduction problem, *ASME HTD* **110**, 79–85 (1989).
18. L. C. Wrobel and C. A. Brebbia, A formulation of the boundary element method for axisymmetric transient heat transfer conduction, *Int. J. Heat Mass Transfer* **24**, 843–850 (1981).
19. Y. Liao, Dropwise evaporative cooling of solid surfaces, Ph.D. Thesis, University of Maryland, College Park, Maryland (1992).
20. M. Klassen, M. di Marzo and J. Sirkis, Infrared thermography of dropwise evaporative cooling, *ASME HTD* **141**, 117–121 (1990).
21. M. Klassen and M. di Marzo, Transient cooling of a hot surface by droplets evaporation, *NIST-GCR* 90-575 (1990).
22. H. S. Carslaw and J. C. Jaeger, *Conduction of Heat in Solids*, pp. 214–217 and 264, Clarendon Press, Oxford (1959).

PAPER # 8

Mixed numerical scheme solution for dropwise evaporative cooling

P. Tartarini[a] & M. di Marzo[b]

[a]*Istituto di Fisica Tecnica, Università di Bologna, viale Risorgimento, 2, Bologna 40136, Italy*

[b]*Department of Mechanical Engineering, University of Maryland, College Park, Md 20742, USA*

ABSTRACT

A numerical code for the prediction of evaporative cooling of solid surfaces induced by a gently deposited water droplet is presented. The code is based upon a solid-liquid coupled model which predicts the droplet evaporation and the solid surface cooling for materials with thermal conductivity spanning over more than two orders of magnitude. The numerical solution of the conduction equation, which links a control volume method (CVM) used for the liquid and a boundary element method (BEM) used for the solid, is presented. The necessity of using the BEM for the solid domain is particularly stressed.

INTRODUCTION

The evaporation of a liquid droplet on a hot solid surface is a subject of practical interest in many industrial areas, such as spray cooling of solid in steel industries, vaporization process in internal combustion engines, cooling of turbine blades, and many others. The solid and liquid thermal behavior, the heat transfer phenomena involved and the relevant parameters governing the evaporative transient constitute the main objectives of the studies conducted in this field. Many experimental and theoretical investigations [1-5] have been carried out for liquid droplets on a high temperature solid surface. DiMarzo *et al.* [6,7] developed a mathematical model to describe the thermal transient due to a single droplet evaporating on a solid surface. In this model, an integral Control Volume Method (CVM) is applied for the droplet while Boundary Element Method (BEM) is used for the solid. Although the droplet and the solid are treated separately by different numerical methods, the temperature in the droplet and along the solid surface are solved

simultaneously at each time step by coupling the CVM and the BEM in the numerical model, which is presented in the following paragraphs.

GOVERNING EQUATION AND BOUNDARY CONDITIONS

The conduction equation can be written for both the liquid and the solid region, provided that the thermal diffusivity, α, is changed accordingly:

$$\frac{\partial T}{\partial t} = \alpha \nabla^2 T \tag{1}$$

Three interfaces are involved in this evaporative cooling phenomenon: a) the liquid-air interface, b) the liquid-solid interface and c) the solid-air interface. The boundary conditions applying to each of them must be given to solve the governing equation. At the liquid-air interface one has:

$$-k_l \nabla T = h\,(T - T_a) + 0.624\, h_c \left(\frac{D}{\alpha_a}\right)^{\frac{2}{3}} \frac{\lambda_{fg}}{c_a} \frac{x_i - x_a}{1 - x_a} \tag{2}$$

At the liquid-solid interface, the continuity boundary conditions are:

$$\begin{aligned} T_l &= T_s \\ k_l \nabla T_l &= k_s \nabla T_s \end{aligned} \tag{3}$$

The boundary condition for the solid-air interface takes into account the convective and radiative heat transfer contributions:

$$k_s \nabla T = h(T_s - T_a) + \sigma \varepsilon (T_s^4 - T_a^4) \tag{4}$$

Because of the axisymmetric nature of the droplet, the gradient of temperature is zero on the vertical axis through the origin of either spherical or cylindrical coordinates. Furthermore, the gradient of temperature can be set equal to zero at points far away from the droplet since the evaporative cooling effect becomes negligible. When the droplet is deposited on the solid surface, the liquid and the solid have uniform temperature distribution. Therefore, from the physical point of view, uniform and constant temperature for the droplet and the solid surface respectively can be used as initial conditions.

NODALIZATION AND NUMERICAL METHODS

In order to approach numerically the thermal evaporative transient, an accurate discretization of the solid-liquid domain has to be chosen. Under the assumptions that the wetted area remains constant and that the droplet keeps a spherical segment shape during the whole transient, the volume of the droplet can be expressed as a function of its radius and

thickness. The appropriate coordinate system to be used is cylindrical. After some algebra, the coordinates (r,z) of all the points in the droplet can be defined for $0 \le r \le R$ and $0 \le z \le a$. In order to improve the accuracy of the model in the interfacial regions, two additional ("virtual") layers for the droplet are defined, one underneath the liquid-solid interface and the other above the liquid-air interface. The coordinates (r,z) of the points of the first virtual layer can be determined by symmetry about the interface with the liquid points immediately above it. The coordinates of the points of the second virtual layer are calculated as geometrically belonging to the droplet. The liquid droplet domain is discretized by a staggered grid, in which the geometric coordinates are defined at each corner of a mesh and the physical variable (temperature) is defined at the center (Fig. 1). A special nodalization is also required for the exposed solid surface. Since the temperature gradient near the droplet edge is very large, a refined discretization in this region is needed to describe the sharp variation of temperature. This refinement can be progressively reduced as the distance from the droplet edge becomes larger (Fig. 2). The cooling effect becomes negligible, for all materials, at a distance corresponding to 5-6 times the radius of the droplet; this result dictates the size of the domain of discretization in the code.

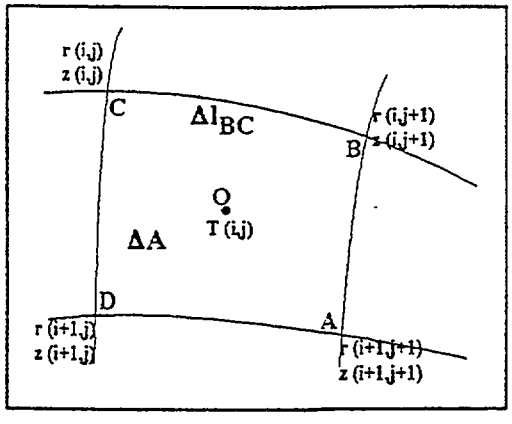

Figure 1

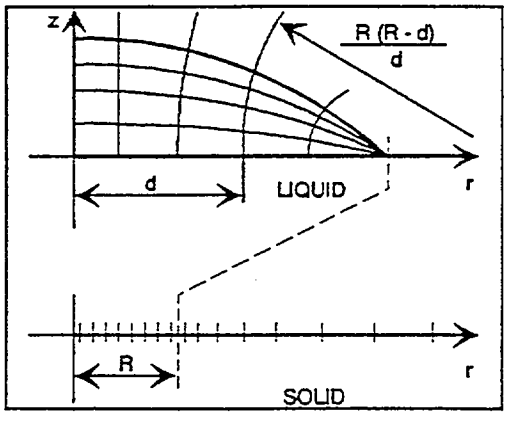

Figure 2

Two different numerical techniques are applied to study the droplet and the solid behaviors during the evaporative transient. CVM is used for the droplet, while the BEM is used for the solid. The CVM consists of an integration of the conduction equation over the liquid droplet. By integrating over the volume of the droplet and applying the Gauss' theorem for the right-hand-side, the discretized governing equation in cylindrical coordinates becomes:

$$r_0 \frac{\Delta T}{\Delta t} \Delta A = \alpha \sum_j \frac{\Delta T_j}{\Delta \bar{r}_j} r_j \Delta l_j \qquad (5)$$

where all the coefficients are time dependent since the droplet geometry

varies with time. By applying a Crank-Nicolson scheme, one can obtain an equation where all the T_{ij}'s at the time step $n+1$ are the only unknowns.

The BEM is used to solve the conduction equation in the solid (see also [8]). There are two advantages implicit in this methodology: a) since the relevant events take place on the surface of the domain, only this area is considered in the calculations; b) in order to analyze sharp localized changes in the temperature gradients, an integral approach is more effective than a method based on differentiation. To solve the conduction equation for the solid, an adjoint equation in terms of the Green's function G is defined as:

$$\frac{\partial G}{\partial t} = -\alpha \nabla^2 G \tag{6}$$

By multiplying Eqs. (1) and (6) by G and T respectively, then combining them together and integrating over the domain by using Gauss' theorem, one obtains:

$$\int_t \int_V \frac{\partial (TG)}{\partial t} dV\, dt = \alpha \int_t \oint_A (T\nabla G - G\nabla T)\cdot \vec{n}\, dA\, dt \tag{7}$$

The Green function is chosen as:

$$G(r,z,t,r_0,z_0,t_0) = (4\pi\alpha_s t_0)^{-\frac{3}{2}} \left(e^{-\frac{(r-r_0)^2+(z-z_0)^2}{4\pi t_0}} + e^{-\frac{(r-r_0)^2+(z+z_0)^2}{4\pi t_0}} \right) \tag{8}$$

and the following variables are also defined for convenience:

$$u = T - T_0 + \frac{q_0 z}{k_s} \quad ; \qquad f = \frac{du}{dz} \quad . \tag{9}$$

In cylindrical coordinates, the equation is further simplified since the angular integration can be expressed in terms of Bessel functions. The final forms results in a double integral in time and along the radius r:

$$u(r,t) = \frac{1}{\sqrt{4\pi\alpha}} \int_0^t \int_0^\infty \nabla u(r_0,t_0)\, r_0 t_0^{-\frac{3}{2}} L_0\left(\frac{2rr_0}{4\alpha t_0}\right) e^{-\frac{(r-r_0)^2}{4\alpha t_0}}\, dr_0 dt_0 \tag{10}$$

In order to simplify the task of handling these complex surface integrations, the following form is used:

$$u = \sum_{i=1}^{n} W_i \cdot \vec{f}_i + W_0 \cdot \vec{f}_0 \tag{11}$$

where W is a weight matrix and f is the vector of the forcing and unknown functions. The summation term is known since it involves previously calculated parameters. The second term on the right-hand-side contains unknown functions and the specified boundary conditions. Once the

weights are assigned for each pair of points they do not change throughout the computation. A new time scale must be introduced, which has its origin at the present time t and stretches its positive axis toward the past. Due to this set-up, t_0 is identified as the "recollection time". It represents the "memory" of the system in terms of heat fluxes. While the actual time is elapsing as the evaporative cooling process takes place, the recollection time is always zero at the present time. Then, since the effect of past forcing functions fades as actual time increases, hence the corresponding weights keep decreasing and after a few time steps they become negligible. This shows that the system recollection time can be considered for a limited number of time steps, even if its theoretical extension corresponds to the time elapsed from the beginning of the transient to the present time. From the computational point of view, this results in a summation in time which can be truncated as the corresponding values of the weight matrix become negligible. Since the weight function depends on the diffusivity of the material constituting the solid surface, the temporal sensibility of the system also varies according to the chosen materials. It is found that a recollection time of 10 to 20 seconds can be imposed in the code, from a conservative point of view, for any material. At the liquid-solid interface, the forcing function, f, constitutes the main parameter in the liquid-solid coupling, since it represents the term which accounts for the continuity of heat flux in terms of boundary conditions. By definition the forcing function can be written as $f = du/dz$, yielding two different expressions in the solid-air interfacial region and in the solid-liquid interfacial region.

In order to find the new coordinates for the droplet nodal points at each time step, the variation of the droplet volume has to be calculated by using the temperature distribution at the current time step, in particular the temperature along the liquid-air interface. After calculating the new droplet volume and coordinates, one can perform again all the computations concerning temperatures and heat fluxes until when the complete evaporation is reached. The variation of the droplet volume with time is obtained at each step by using the following expression:

$$\frac{dV}{dt} = \frac{2\pi(0.624)h}{\rho_w c_a}\left(\frac{D}{\alpha_a}\right)^{\frac{2}{3}} \int_0^L \frac{x_i - x_a}{1 - x_a} r\, dl \qquad (12)$$

and the new volume is calculated accordingly:

$$V_{new} = V_{old} - \frac{dV}{dt} \cdot \Delta t \qquad (13)$$

Once the new current volume of the droplet is given, another set of grid points for the droplet can be formed to proceed into the transient with the calculation of temperatures and fluxes. The cycle stops when the droplet volume becomes zero, i.e. when the droplet is completely evaporated.

CODE FORMULATION

The equations for T - written for the solid, the liquid and the interfacial regions - are regrouped to form a linear system that has to be solved at each time step during the transient. Although two different numerical methods are used for the droplet and the solid surface, they can be applied together to form the following matrix equation:

$$B \cdot \underline{T} = \underline{R} \tag{14}$$

where T is the vector of the temperatures at the current time step. The matrix B and the vector R contain the information on the evolution of the droplet shape and on the droplet temperature at the last time step in the liquid domain. On the solid surface, B becomes the matrix of the coefficients derived from the spatial and temporal integration required by the BEM, while R contains all the known surface temperatures and/or heat fluxes at the previous time steps which are taken into consideration depending on the chosen size of the recollection time. The dimension of the matrix B in the code is 216x216, resulting from the following choice of parameters: a 16x11 grid for the liquid, 40 points in the exposed solid surface. The matrix B is pentadiagonal in the liquid region and full in the solid region. In order to find a solution for T at each time step, the matrix of the coefficients, B, has to be inverted and multiplied by the vector of the known terms, R (a normalization of the matrix B is necessary in order to obtain a diagonal dominant coefficient matrix). After this intermediate step, the current temperature T can be calculated directly as:

$$\underline{T} = B^{-1} \cdot \underline{R} \tag{15}$$

From the mathematical point of view, there is a singularity when time is zero. Numerical fluctuations in temperature and heat flux can be expected if the initial temperature distribution is not properly chosen. In order to minimize these fluctuations, an iterative scheme can be used. The program runs for a small time interval (1 second) with very small time steps (no more than 0.1s each), until a reasonable temperature distribution in the droplet and in the solid is achieved; then, the calculations are restarted with this temperature distribution used as a new initial condition. This procedure is justified by the temporal characteristics of the evaporative transient, since the most relevant events occur in the final part of the process.

Two different constant values of the heat transfer coefficient are used in the code, one for the droplet and air interface, and another for the exposed solid surface. Both heat transfer coefficients are obtained from the investigation of experimental measurements. The assumption of constant heat transfer coefficients is reasonable for the regions where the temperature varies in a relatively small range along the surfaces, but it creates a mathematical discontinuity near the droplet edge. The

temperature in this region, both in the droplet and along the exposed solid surface, changes very rapidly. Some fluctuations in the temperature and in the heat flux can be expected because of the constant heat transfer coefficients applied near the edge.

CONCLUSIONS

A numerical code for the prediction of evaporative cooling of solid surfaces induced by a gently deposited water droplet has been presented. The code can be used to predict the evaporation time and the temperature distribution in the droplet and along the solid surface. Numerical tests have been conducted over a wide range of materials constituting the hot solid surface. Besides the numerical investigation, the model has been validated on the basis of the comparison between its numerical predictions and many experimental tests obtained with the infrared apparatus described in [9]. A direct comparison between numerical predictions and experimental results is possible for the evaporation time and for the distributions of temperature on the exposed solid surface. Therefore, a very large number of data from tests on aluminum and Macor has been collected, in a broad range of initial solid surface temperatures, and all the corresponding evaporation times have been calculated by the code and compared with the experimental values. The comparison between experimental data and code predictions has been extensively shown and discussed in [10]. A remarkable agreement has been observed, and, on the basis of the satisfactory results obtained by the single-droplet code, a multi-droplet model has been recently formulated.

ACKNOWLEDGEMENTS

This study was made possible by a grant of the Building and Fire Research Laboratories of the National Institute of Standards and Technology. Partial funding of the computational expenditures was provided by the Computer Science Center of the University of Maryland at College Park. The Italian C.N.R. and M.U.R.S.T. also provided partial funding for this research. The authors wish to acknowledge Dr. H. Baum for his inestimable mathematical advices.

REFERENCES

1. Seki, M., Kawamura, H. and Sanokawa, K., 'Transient Temperature Profile of a Hot Wall Due to an Impinging Liquid Droplet', *ASME J. Heat Transfer*, Vol.100, pp.167-169, 1978.
2. Bonacina, C., Del Giudice, S. and Comini, G., 'Dropwise

Evaporation', *ASME J. Heat Transfer*, Vol. 101, pp. 441-446, 1979.

3. Rizza, J.J., 'A Numerical Solution to Dropwise Evaporation', *ASME J. Heat Transfer*, Vol.103, pp.501-507, 1981.
4. Grissom, W.M. and Wierum, F., 'Liquid Spray Cooling of a Heated Surface', *Int. J. Heat Mass Transfer*, Vol.24, pp.261-271, 1981.
5. Makino, K. and Michiyoshi, I., 'The Behavior of a Water Droplet on Heated Surfaces', *Int. J. Heat Mass Transfer*, Vol.27, pp.781-791, 1985.
6. diMarzo, M. and Evans, D., 'Prediction of Droplet Evaporation Time and Temperature Distribution in the Solid', *Int. J. Heat & Technology*, Vol.5, No.1-2, pp. 126-136, 1987.
7. diMarzo, M. and Evans, D., 'Evaporation of a Water Droplet Deposited on a Hot High Thermal Conductivity Surface', *ASME J. Heat Transfer*, Vol.111, pp.210-213, 1989.
8. Kavoosi, F., diMarzo, M., Baum, H. and Evans, D., 'An Application of Boundary Element Method to a Transient Axisymmetric Heat Conduction Problem', *ASME HTD*, Vol.110, pp. 79-85, 1989.
9. Klassen, M., diMarzo, M. and Sirkis, J., 'Infrared Thermography of Dropwise Evaporative Cooling', *ASME HTD*, Vol.141, pp.117-121, 1990.
10. diMarzo, M., Tartarini, P., Liao, Y., Evans, D. and Baum, H., 'Evaporative Cooling Due to a Gently Deposited Droplet', *Int. J. Heat Mass Transfer*, Vol.36, pp. 4133-4139, 1993.

NOMENCLATURE

A	surface area
B	matrix of coefficients
c	specific heat
D	mass diffusivity
$\underline{f}$	forcing functions vector
G	Green's function
h	heat transfer coefficient
k	thermal conductivity
L_0	modified Bessel's function
l	length
q	heat flux
r	radial coordinate
R	wetted region radius
$\underline{R}$	vector of known terms
t	time
t_o	recollection time
T	temperature
u	transformed temperature
V	volume
W	weight matrix
x	steam mass fraction
z	axial coordinate

Greek letters

α	thermal diffusivity
ϵ	solid surface emissivity
λ_{fg}	latent heat of vaporization
ρ	density
σ	Stefan-Boltzmann constant
τ	evaporation time

subscripts

a	ambient, air
c	convective
i	interface
l	liquid
r	radial direction
s	solid
z	axial direction
0	initial

PART THREE

To be consistent with fire protection scenarios, the heat input should be by radiation from above the solid surface to simulate a fire environment. This introduces a dual evaporative mechanism: a) by direct radiant input at the liquid-vapor interface; and b) by conduction at the solid-liquid interface. Additionally, the heat input at the liquid-vapor interface has a very strong influence on the droplet shape since it changes the liquid surface tension by increasing its temperature at the liquid-vapor interface. These are the major results of this portion of the study:

1. The direct radiative input at the liquid-vapor interface relaxes the surface tension and the liquid spreads more on the solid surface. The droplet configuration exhibits a lower initial contact angle (i.e. at the droplet edge).
2. The flatter configuration of the water on the solid surface results in an early receding condition for the liquid. Therefore, the wetted region shrinks significantly during the later portion of the evaporative transient.
3. The heat input by direct radiation increases at a slower rate than the heat input by conduction. Therefore, conduction at the solid-liquid interface becomes the major contributor as the overall heat input increases.

M. diMarzo, C.H. Kidder & P. Tartarini, Infrared thermography of dropwise evaporative cooling of a semi-infinite solid subjected to radiant heat input, Experimental Heat Transfer 5 (1992) 101-114.

P. Tartarini & M. diMarzo, Dropwise evaporative cooling in radiative field, in Heat Transfer 1994 6 (1994) 277-282

G. White, S. Tinker & M. diMarzo, Modeling of dropwise evaporative cooling on a semi-infinite solid subjected to radiant heat input, in Fire Safety Science, IAFSS (1994) 217-228.

PAPER # 9

Experimental Heat Transfer, vol. 5, pp. 101–114, 1992

INFRARED THERMOGRAPHY OF DROPWISE EVAPORATIVE COOLING OF A SEMIINFINITE SOLID SUBJECTED TO RADIANT HEAT INPUT

M. diMarzo, C. H. Kidder, and P. Tartarini
Mechanical Engineering Department, University of Maryland, College Park, Maryland 20742

A single droplet is gently deposited on the surface of a semiinfinite body and the evaporative cooling transient is recorded. This study is limited to the evaporative phenomena, therefore, the temperature range selected is such that nucleate boiling or film boiling is not observed. The solid (a glasslike material) is heated from above by two radiant electric panels, and it is placed on a chilled plate held at near-ambient, constant, and uniform temperature. The transient temperature distribution over the semiinfinite solid surface is monitored by infrared thermography. Image-processing techniques are used to eliminate undesired information and to retain the data, which are then converted into surface temperature readings. Droplet sizes in the range of 10 to 50 μl are used with initial solid surface temperatures between 90 and 180°C. The results are compared with similar experiments performed with the semiinfinite solid heated from below by conduction to gain insight into the competing mechanisms of evaporation by direct radiation from above and by conduction at the solid–liquid interface. The droplet aspect ratio is a dominant parameter in the conduction-controlled evaporative component. Therefore, particular care is taken in assessing the behavior of the droplet shape during the transient. The direct radiation from above strongly reduces the surface tension of the liquid and thus allows the drop to spread on the surface more than for the conduction case.

INTRODUCTION

Quenching of metals, spray cooling, and fire suppression with sprinklers are a few of the applications that inspired numerous theoretical and experimental investigations. A global approach to spray–surface interactions is addressed in the early investigations by Toda [1] and Bonacina [2]. More detailed numerical and experimental studies followed. In particular, the contributions of Rizza [3], Seki et al. [4], Inada et al. [5], and diMarzo and Evans [6, 7] are based on the integration of the transient conduction equation in the solid with a simple boundary condition at the liquid–solid interface that prescribes constant and uniform temperature throughout the vaporization process. Grissom and Wierum [8] determined experimentally the lowest surface temperature possible for the existence of spray evaporative cooling and presented a conduction-controlled analytical model of droplet evaporation.

Other experimental work reinforced these modeling assumptions for solids characterized by high thermal conductivity. In particular, Sadhal and Plesset [9] described the droplet shape behavior when the liquid thins and breaks up; Pedersen [10] presented a large number of experimental data showing that, for impinging droplets,

NOMENCLATURE

r	radial coordinate on the solid surface	t	time
R	radius of the wetted region [$f(t)$ in the radiation case]	T_0	initial solid surface temperature
		V	volume of the droplet at deposition
R_0	radius of the wetted region at deposition	β	shape parameter ($= R/R_s$)
R_s	radius of a sphere with equal volume of the droplet at deposition	τ	total evaporation time

approach velocity is a dominant variable affecting droplet heat transfer; Choi and Yao [11] studied the heat transfer characteristics of impacting sprays, with special attention to the differences between sprays impacting horizontally and vertically. Makino and Michiyoshi [12–15] investigated the onset of nucleate boiling and the corresponding behavior of the droplets during the different stages of the evaporating process, with particular interest on the influence of the governing parameters such as the droplet size and the initial surface temperature. These investigations span the full range of vaporization phenomena, including evaporation, nucleate boiling, and film boiling. Detailed information on the droplet shape [9, 13] and on the solid thermal transient [12, 14, 15] are given.

Recent studies by Abu-Zaid and Atreya [16], diMarzo and Evans [6, 7], and Klassen et al. [17] concentrated on the evaporative phenomena with temperature ranges below the onset of nucleate boiling. Low-thermal-conductivity solids are heated from below and the evaporation of a single droplet is investigated [6, 7, 17]. The behavior of porous and nonporous materials with similar thermal properties is compared [16], and porous materials show higher evaporative cooling rates.

This work is part of a long-term research effort aimed at modeling the extinguishment of a solid fuel fire. Water, used as an extinguishing agent, is a primary cause of secondary fire damage. By understanding and predicting fire extinguishment mechanisms, one can optimize the water application (droplet sizes, mass fluxes) and thus minimize the damage associated with the extinguishment process. Previous studies focused on the evaporation of water droplets deposited on surfaces that were heated by conduction from below. Klassen et al. [17] studied droplet evaporation from Macor (a glasslike material), and diMarzo [6, 7] reported on the evaporative cooling of aluminum. Most of these data refer to the range where only evaporation takes place and nucleate boiling is fully suppressed. Some data points are also taken in the nucleate boiling range. In the present study, the heat input is provided by radiant panels located above the Macor to simulate a fire environment. Data are compared with previous experiments by Klassen et al. [17] to determine the differences in the evaporation process due to the heat input characteristics (i.e., radiation from above versus conduction from below). Klassen et al. [17] developed an infrared thermographic technique to obtain transient temperature profiles on the solid surface during the droplet evaporation. This technique is nonintrusive and has no response lag. The primary purposes of this work are (1) to gather data that will be used to validate models of the evaporation phenomena and (2) to provide insight into dropwise evaporative cooling.

EXPERIMENTAL APPARATUS

The experimental apparatus (shown schematically in Fig. 1) consists of a Macor tile (of squared shape with 15.2-cm sides and 2.54 cm thick) mounted onto a steel chilled plate. Contact between the tile and the chilled plate is enhanced by a conductive paste. The Macor is located under two radiant panels facing each other and oriented toward the Macor surface. An infrared camera is mounted above the tile at a 45° angle from the vertical axis and looks through a chilled pipe at the Macor surface. A mechanized droplet dispenser rolls in and out of the heated region and is designed to dispense metered water volumes at a precise location and in a repeatable manner (for details, see [6]).

The radiant panels are used to simulate the heat flux output of a fire. These panels are powered by a three-phase 220-V power supply, which is controlled by a 0–10 V output temperature controller. The panel surface temperatures provide the feedback to the controller.

A chilled plate is placed under the Macor tile and is kept at near ambient temperature by controlling the water flowing through it. The heat flux in the vertical direction overwhelms the heat losses through the side of the tile. This setup is designed to obtain (prior to the droplet deposition) a uniform Macor surface temperature by reducing the radial temperature gradients and by providing a linear temperature profile across the tile in the vertical direction.

The infrared camera (model 525 Infrared Thermal Imaging System by Inframetrics) is used to observe the temperature distribution on the Macor tile surface. The camera is connected to a videocassette recorder (VCR) that records the transient infrared temperature distribution of the portion of the Macor surface affected by the water droplet. The video image is recorded in real time. A chilled pipe is used to minimize the amount of extraneous infrared radiation that reaches the camera lens. This chilled pipe is constructed with a water-cooled copper coil. The interior of the chilled pipe is coated with a high-emissivity black paint to minimize the amount of reflection.

A mechanized droplet dispenser is used to place the water droplets onto the Macor surface. The dispenser rolls in and out of the experimental apparatus quickly and easily, so that almost no disruption of the radiant heat flux is observed. A microdispenser (Drummond Scientific Corporation 550) is used to measure the droplet volume and to dispense it on the Macor surface. The dispenser is operated by a motor-driven cam to obtain a repeatable droplet shape on the surface after deposition.

Macor properties are listed in Table 1. In particular, note that it has high emissivity, which minimizes reflection from the surface. Macor can withstand repeated thermal shocks, and its surface is smooth and cracks free.

EXPERIMENTAL PROCEDURES

An extensive test matrix is implemented following an identical experimental protocol. These experiments are conducted for droplet sizes of 10, 30, and 50 μl at surface temperatures of 90, 110, 130, 145, 150, 155, and 164°C. The droplet sizes are a compromise between the sprinkler-delivered droplets ($\simeq 1$ μl) and reasonably large volumes to achieve easy repeatable dispensing (> 10 μl). Note that surface tension impairs

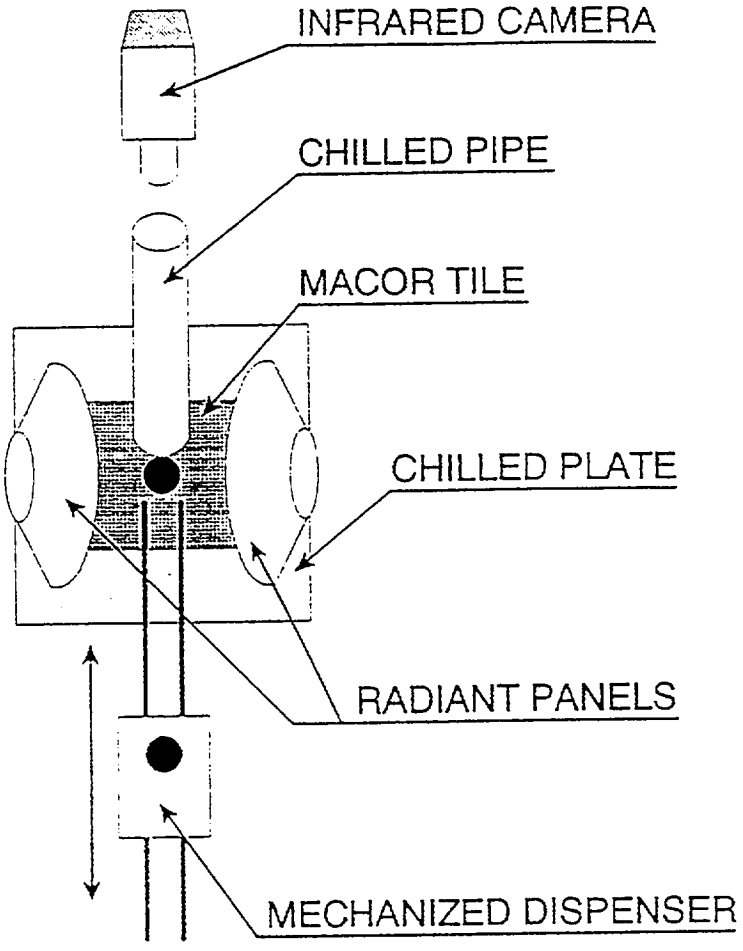

Fig. 1 Experimental apparatus (top view).

the delivery of smaller single droplets under the sole gravitational forces. The temperatures are mostly in the evaporative range, since onset of nucleate boiling is observed at and above 155 °C. The experimental protocol consists of five steps, as described below.

Water Conditioning

The water used in the experiment is de-ionized and must be completely degassed. De-ionized water is used to maintain a clean, deposit-free Macor surface. Complete degassing must be achieved to avoid degassing during the evaporative process. If gasses come out of solution during the evaporation, they may alter the droplet shape and therefore its behavior or they can even shatter the droplet or trigger nucleate boiling.

Degassing is obtained by repeatedly freezing and thawing water kept under vacuum. The water is then removed from the degassing container by bringing it to boil and

Table 1 Macor Properties

Density (kg/m^3)	2520
Thermal conductivity (W/m °C)	1.297
Specific heat (J/kg °C)	888.9
Emissivity	0.94

by extracting the liquid with a syringe. The syringe is then used to load the mechanized dispenser.

Infrared Camera, Radiant Panels, Chilled Plate, and Pipe

The radiant panels and the chilled plate are activated and the Macor tile is brought to thermal steady state. The infrared camera sensing enclosure is constantly monitored to ensure that adequate cooling by liquid nitrogen is available (a liquid nitrogen charge lasts about 45 min). The chilled pipe is also activated and the infrared picture of the Macor surface is obtained. The infrared camera provides a two-dimensional picture where the vertical axis relates to a radiance reading while the horizontal axis is the actual position of the radiance reading on a line that can be arbitrarily set on the Macor surface. This line is carefully positioned through the center of the wetted area (i.e., the liquid–solid interfacial area).

Temperature Calibration

The radiant panels control set point is adjusted and adequate time is allowed for the system to reach thermal steady state. The infrared picture needs to be calibrated to relate the radiance readings to temperatures. The temperature scale is provided by the infrared camera manufacturer and is also calibrated independently by using a blackbody source. The temperature scale is referenced with one radiance/temperature point. This reference point is obtained by measuring the surface temperature with a hand-held probe (OMEGA surface probe series 68000) until a constant reading is observed. By quickly removing the probe while recording the infrared picture of the probe location, one obtains an instantaneous reading of the same location with the infrared camera and with the temperature probe. Note that the temperature at the probe location changes after the probe removal and that only the picture immediately after probe removal provides the desired information. Since 30 frames per second are acquired with the VCR, there is no problem in selecting the appropriate frame.

Droplet Deposition

Prior to droplet deposition, the surface is cleaned with alcohol and with de-ionized water. When the cleaning water is evaporated, the droplet is deposited. The line on which the temperatures are scanned is adjusted to pass exactly through the center of the wetted region. This is a fine-tuning adjustment, since the mechanized dispenser places the droplet within fractions of a millimeter of the desired location. The evaporative process is then recorded and set aside for postprocessing. Each experiment is repeated at least 10 times to build sufficient confidence in its repeatability.

Test Record

A regular black-and-white camera is used to record (on the same VCR tape) the experimental conditions. In particular, droplet size, Macor surface temperature, chilled plate temperature, and radiant panels temperatures are recorded. In addition, an infrared picture of a small coin placed on the Macor surface is also recorded to determine the

length scale of the infrared image. All this information is recorded at the beginning and at the end of a 10-test sequence (which relate to the same droplet size and initial temperature conditions).

DATA PROCESSING

After a sequence of 10 tests is completed, data processing is performed. The evaporation time τ for each experiment is measured from the VCR record. The size of the wetted region is identified and the droplet shape is inferred. Extensive visual observations and photographic records show that the droplet shape can be approximated by a segment of a sphere [6, 9]. By inspecting the droplet shape and evaporation time information, one representative test is selected out of the 10-test sequence. The rationale for this selection is based on the following concepts.

1. The droplet evaporation time increases as solid–liquid interfacial area decreases. Since the droplet geometry is reasonably approximated by a segment of a sphere, a shape parameter, β [2, 6, 9], is defined as the radius of the wetted area over the radius of an equal-volume droplet of spherical shape. An averaged and most repeatable shape parameter identifies the representative droplet.
2. In spite of the dispenser accuracy, some of the water will cling to the inside of the droplet dispenser. The longer a droplet takes to evaporate, the greater is the likelihood that less water is left in the dispenser.
3. The droplet does not always fall in the same location. Sometimes the temperature scanned line is not positioned exactly through the droplet center. Further, the wetted region shrinks during the evaporation, and the center of the wetted region may drift from its initial position. If this occurs, the image may show complete evaporation when water is still present.

These three concepts are the guidelines for the selection of the most representative droplet. Usually there are four or five identical tests. In a few cases, a decision must be made based on item 1 with some bias toward higher evaporation times to account for items 2 and 3.

Images from the record for the selected droplet are obtained at 10, 30, 50, and 100% of the evaporation time, and a few images are also analyzed to describe the surface temperature recovery after the evaporation. These images are digitized by a PC-based 641H $\times$ 201V frame grabber (by Computer Eyes, which also provides the required software). The spatial resolution in the horizontal axis may vary depending on the camera field of view. Usually a pixel corresponds to 0.05 mm. The temperature scale is of about 100 °C, and the typical thermographic trace is 2 pixels thick. Therefore, a resolution of 1–2 °C is achieved in the vertical axis (i.e., the temperature scale).

The digitized image is processed with a thresholding and subsequent erosion techniques, which are described at length by Klassen et al. [17]. In summary, the intensity of the thermographic traces is differentiated from unwanted noise by thresholding. This technique identifies as noise the pixels with intensities above a set value and retains the pixels with intensity below this set threshold. In addition, thresholding binarizes the resulting image by assigning the maximum and minimum intensity value, respectively, to

data pixels or "blank" pixels. Further elimination of noise is achieved by erosion, which consists of a pixel-by-pixel inspection of the neighboring information to differentiate between isolated information (which is most likely noise) and clustered information (which is most likely useful data). These techniques are applied by trial and error, and visual inspection of the images confirms their effectiveness.

The data points isolated by the image-processing techniques are then compacted by folding the right side of the image (about the droplet center) onto the left side of the image. Since the temperature profile is symmetric about the droplet center, superimposing one half of the profile on the other half produces twice as many data points to be analyzed and allows a more accurate determination of the symmetry axis through the center of the wetted region. Figure 2 shows the typical transient data after processing. Note that in the figures prior to the complete evaporation ($t < \tau$), the temperature profiles are plotted for $r \geq R$. The radiance signal in the solid surface region covered by the droplet cannot be translated into a significant temperature reading, since water is a radiation-participating medium. The temperature distributions in the range $0.3\tau \leq t \leq 0.9\tau$ do not change appreciably, and the surface temperature recovers its initial value for $t \geq 1.5\tau$.

RESULTS AND DISCUSSION

Phenomenology

To set the results and their discussion in the appropriate context, it is necessary to review briefly the major differences in the thermal behavior between the case of radiant heat input (from above the surface) and the case of conductive heat input (from below the surface). The experimental study of the evaporative cooling due to droplets deposited on Macor heated by conduction from below has been reported in a previously published article [17]. It is important to note that, for the droplet sizes under investigation, the heat transfer mechanisms in the liquid are conduction and radiation. Convection does not play a significant role, since Rayleigh-Benard instabilities require times longer than the evaporative time to develop and Marangoni surface tension-driven flows generate very slow motion for these experimental conditions [18].

The droplet is vaporized by direct radiation and by conduction from the solid. The contribution of the direct radiation provides up to a third of the overall vaporization energy requirements. The radiation input is absorbed throughout the liquid layer and also transmitted to the solid under the droplet. One of the major by-products of the radiation contribution is the increase in temperature at the liquid–vapor interface, which affects the surface tension and the droplet shape. In fact, the surface tension is decreased and the liquid spreads to a larger extent on the solid surface. This in turns reduces the liquid layer thickness and enhances the heat transfer by conduction. The net result is a decrease in the vaporization time, since the direct radiation and the conduction enhancement offset the reduced heat input from the depth of the solid as shown in Fig. 3 (all the data points are within 4% of the plotted values). Note that for the case of radiant heat input, the initial vertical temperature gradient in the solid shows a higher temperature at the surface and a lower temperature at the chilled plate. The droplet tends to reduce the heat transfer in the vertical direction, since it decreases the vertical temperature gradient. In the case of conductive heat input, the initial vertical temperature gradient is

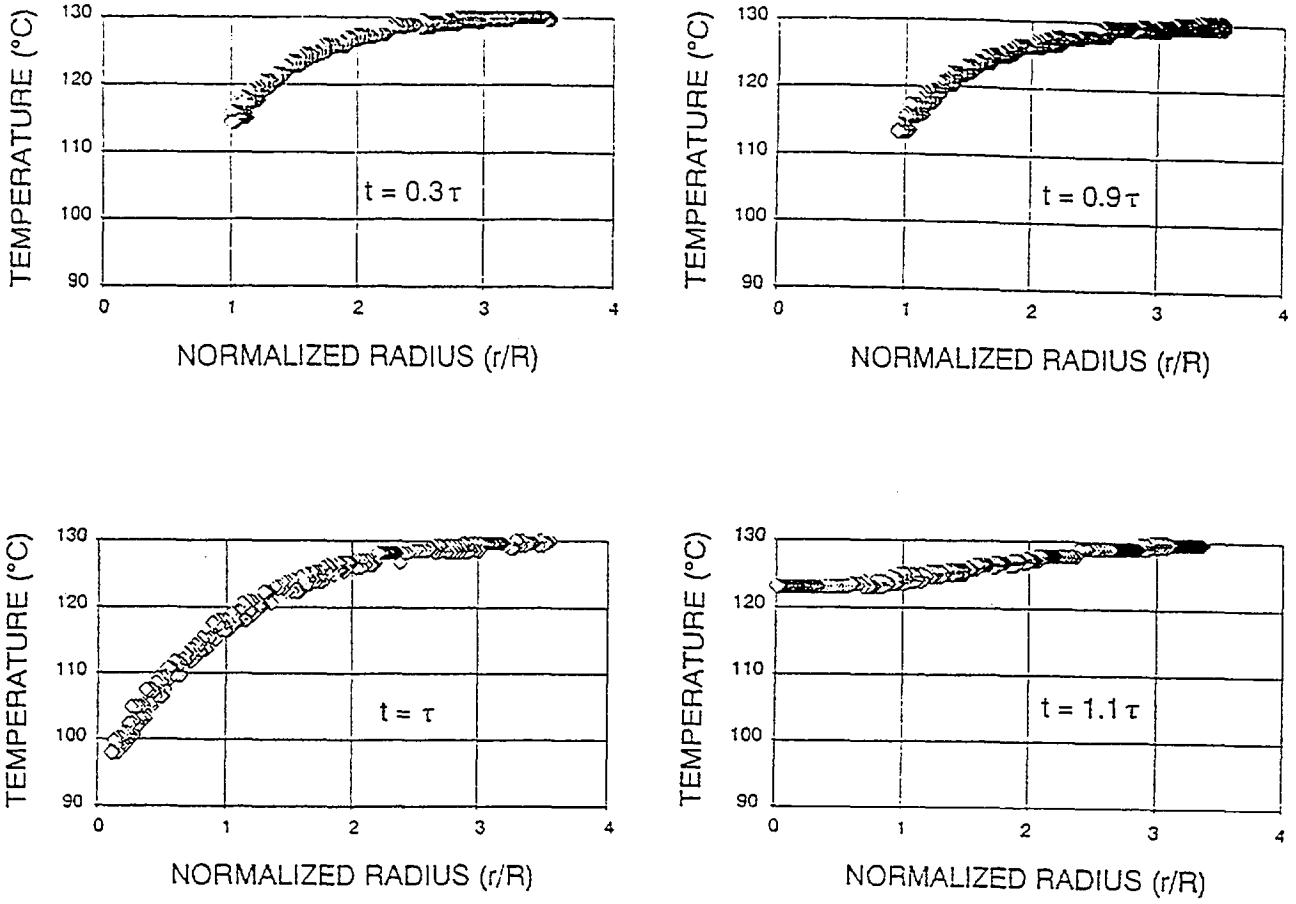

Fig. 2 Transient temperature distribution (T_0 = 130°C; V = 30 μl; τ = 60 s).

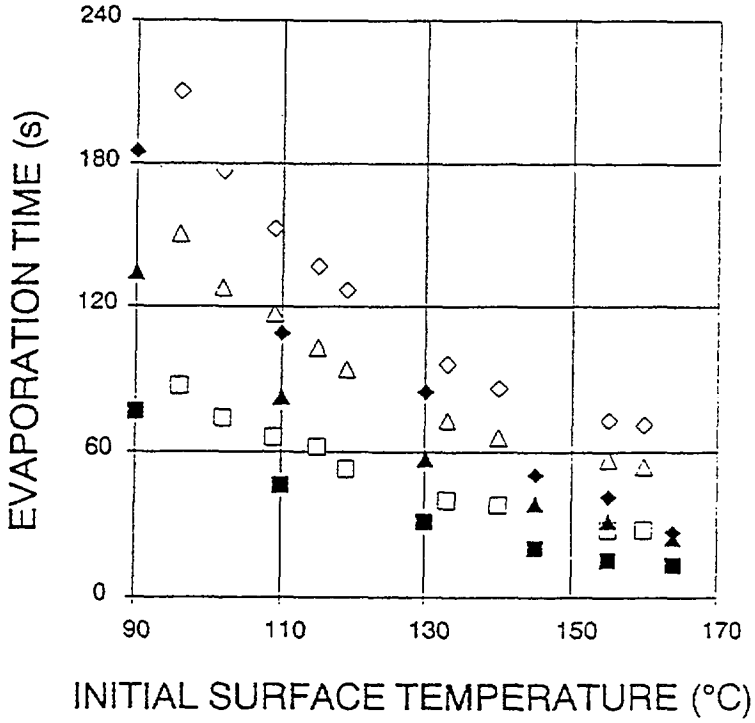

Fig. 3 Evaporation time (solid symbols for radiation case; open symbols for conduction case; ◇, V = 50 μl: △, V = 30 μl; □, V = 10 μl).

opposite, since the temperature increases with depth. Droplet cooling increases the heat transfer in the vertical direction, since it increases the vertical temperature gradient. This means that the portion of the solid under the droplet contributes greatly to the evaporation of a droplet in the conduction case while it has a lesser role in the radiation case. For both cases the amount of heat required to evaporate a given size droplet is the same.

To better characterize the radiant heat input, consider that the radiant panels behave as blackbodies. The view factor of a small portion of the Macor surface is 0.089 for each radiant panel. Table 2 summarizes the total irradiation fluxes and the initial steady-state Macor surface temperature associated with various radiant panel temperatures. At these temperatures the maximum emission of the blackbody spectrum occurs in the 3- to 3.5-μm range [19]. Water has its maximum absorption coefficient of 11,400 cm^{-1} at a wavelength of 3 μm and maintains an elevated value at all wavelengths in the near infrared above 2.6 μm [19]. The absorption coefficient determines the exponential attenuation of the light intensity. By multiplying the absorption coefficient by the thickness of the water layer, one obtains a nondimensional exponent that determines how much radiant energy is transmitted through the water. Figure 4 shows the percentage of incident radiation that is absorbed by water (10-, 30- and 50-μl droplets) at various initial solid surface temperatures, corresponding to various radiant panels temperatures. The line in the figure is the linear regression of the data. The temperature distribution at the exposed solid surface is shown in Fig. 5 for both the radiation and the conduction case. Curves a and b represent, respectively, a radiation and a conduction case with the same initial surface temperature, while curve c shows the temperature distribution for a radiation case in which the evaporation time is the same as the conduction case b. All curves are obtained for a 30-μl droplet. These three curves are for $t = .03\tau$, since thereafter the droplet shrinks in the radiation case and a graphical representation of the temperature profiles would be quite intricate due to the time dependence of the normalizing parameter R.

A direct comparison of the radial heat flux is not possible due to the uncertainty associated with the data at the droplet edge ($r = R$). However, it is apparent that the cooling effect is less pronounced for the radiation case, since radiation contributes directly to the vaporization process, thus reducing the conduction contribution.

Shape Parameter

Figure 6 shows the shape parameter, β, for various droplet sizes and initial solid surface temperatures. The shape parameter is defined as $\beta = R/R_s$, where R is the radius of the wetted region under the deposited droplet and R_s is the radius of a spherical droplet of the same volume. Note that an experimental measurement of β is possible only at the beginning of the evaporative transient, because it is not possible to obtain information about the droplet volume during the evaporation, thus R_s cannot be determined after the initial time t = 0.

The droplet size is not significantly affecting β. This holds true for the conduction case. The scatter is overwhelming for temperatures above 155 °C. This temperature corresponds to the onset of nucleate boiling. For the conduction case, nucleate boiling is observed at 164 °C and above. Klassen et al. [17] measured β values that ranged from 1.2 to 1.5. These values are significantly lower than the values measured for the radiation case. Klassen et al. also showed constant radii of the wetted region. Similar results

Table 2 Radiant Panels Temperature and Total Irradiation

Initial solid surface temperature (°C)	Radiant panels temperature (°C)	Total irradiation flux (kW/m^2)
180	750	11
164	730	10
155	715	9.6
150	702	9.1
145	675	8.2
130	655	7.5
110	635	6.9
90	525	4.1

were obtained by diMarzo and Evans [6] for a quartz surface. Both these results were obtained for the conduction case. It appears that, for the conduction case, increasing the solid surface temperature does not affect the water-vapor interfacial temperature. This is reasonable, since the heat can only be conducted from the solid surface through the liquid layer.

For the radiation case, β average values range from 1.4 at an initial solid surface temperature of 90 °C to 2.5 at an initial solid surface temperature of 155 °C. This may be due to the direct radiation from above the droplet. The absorption coefficients are high for water in the spectra produced by the radiant panels. This results in substantial amounts of energy absorbed by the surface of the water, causing the droplet surface to heat up and therefore reducing its surface tension. This in turn may cause the droplet to spread out. The higher the temperature of the heaters, the greater is the amount of heat

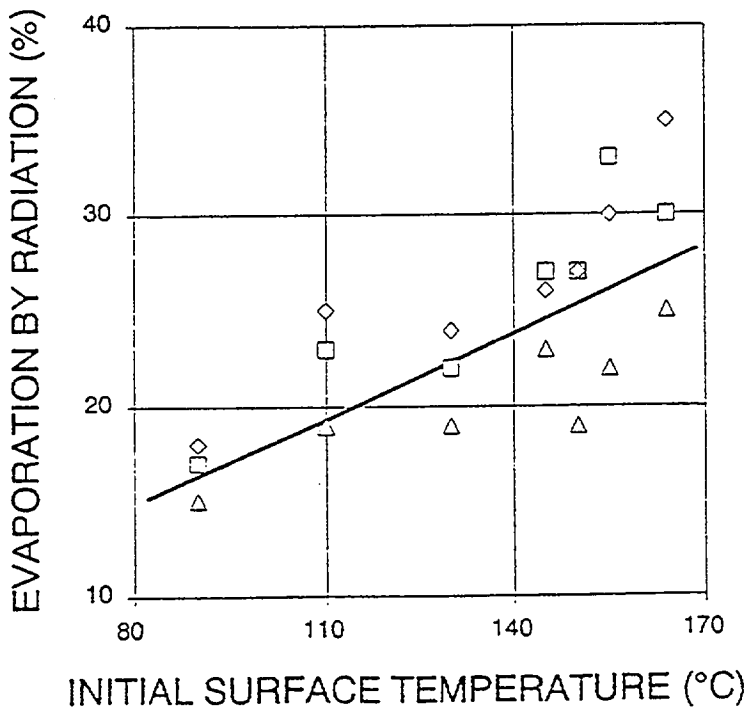

Fig. 4 Percentage of vaporization heat by direct radiation (△, V = 50 μl; ◇, V = 30 μl; □, V = 10 μl).

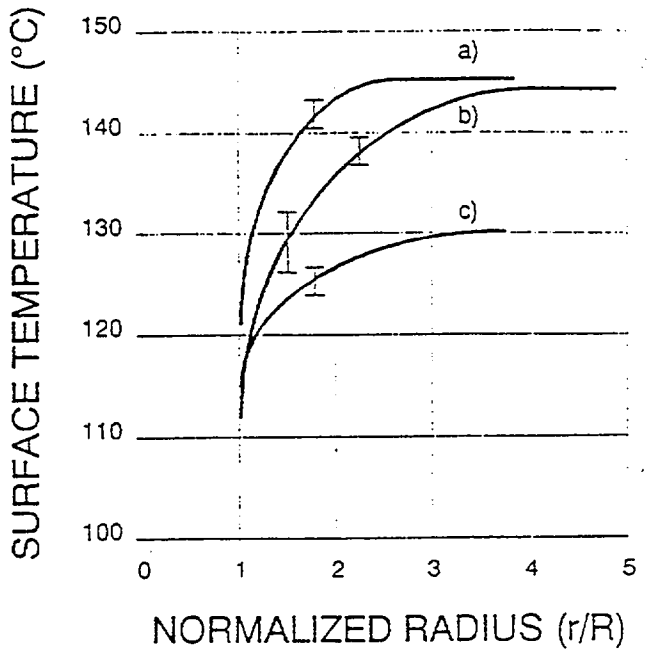

Fig. 5 Cooling effect: comparison between radiation and conduction (V = 30 μl; a: radiation T_0 = 145 °C, τ = 40 s; b: conduction T_0 = 145 °C, τ = 60 s; c: radiation T_0 = 130 °C, τ = 60 s).

absorbed by the droplets, which lowers the surface tension and contributes to a wider spreading of the droplet. Note that for temperatures above 150 °C, the scatter in the initial shape factor data becomes overwhelming. This is due to the disruption of the droplet shape caused by the onset of nucleate boiling.

Figure 7 shows how the radius of the wetted region changes during the evapora-

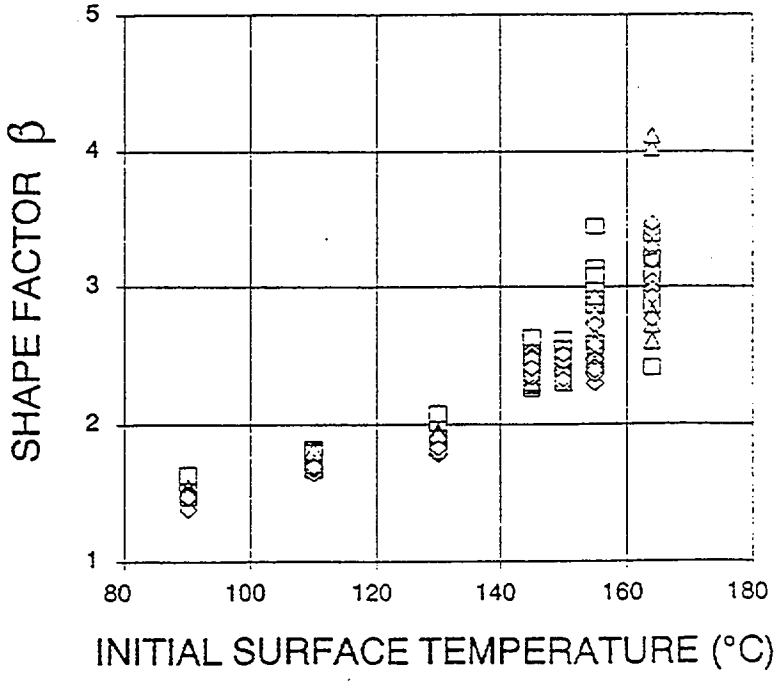

Fig. 6 Shape factor (◇, V = 50 μl; △, V = 30 μl; □, V = 10 μl).

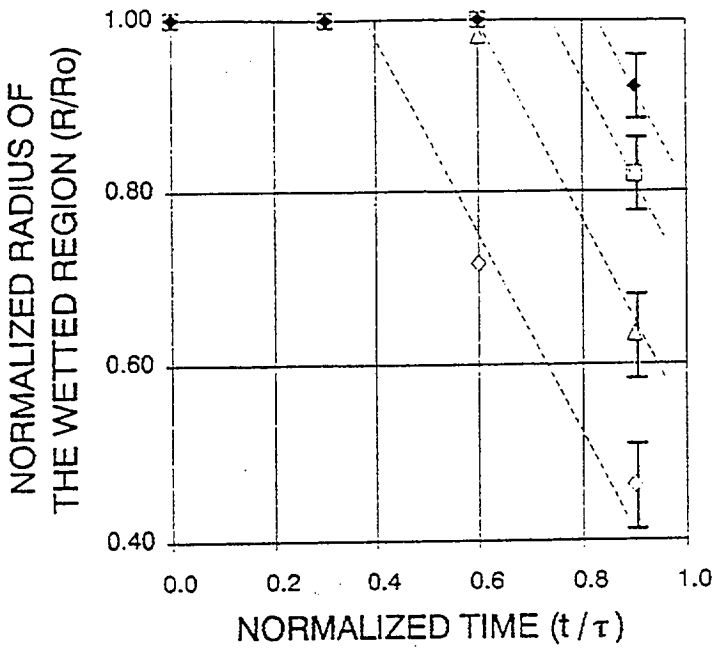

Fig. 7 Normalized radius of the wetted region (♦, T_0 = 130°C; □, T_0 = 155°C; △, T_0 = 164°C; ◇, T_0 = 180°C).

tion process for various initial solid surface temperatures. Note that the radius of the wetted region R is normalized with its value at deposition R_0. At higher initial surface temperatures (i.e., at the onset of boiling), a marked decrease in the radius of the wetted region is observed as the evaporation progresses. To explain this phenomenon, one must refer to the theory and experimental studies performed by Simon and Hsu [20], which are summarized briefly hereafter. A sessile drop shape can be approximated as a segment of a sphere, and during the evaporation process three phases are identified: phase I, where the liquid–solid angle exceeds the receding angle, the area of the wetted region remains constant, and the droplet apex decreases; phase II, where the liquid–solid angle equals the receding angle, the droplet aspect ratio remains constant, and the wetted region shrinks; and phase III, where the vaporization process nears the end and the liquid layer quickly breaks down. The receding angle for water deposited on Macor is measured with photographic techniques and is found to be 7°. Dashed lines are added to Fig. 7 to provide some indication of the transition from phase I to phase II as the receding angle is reached. Note that as the initial value of the shape parameter increases, the receding angle is reached earlier in the vaporization process.

Although there are many differences between the solid thermal response for the conduction and radiation cases, there are also some similarities. Both cases show an onset of nucleate boiling when the initial surface temperature is in the 155–164 °C range. Both cases show that nucleate boiling drastically disrupts the droplet geometry with large variations of β.

CONCLUSIONS

The experiments describe some aspects of the behavior of a low-thermal-conductivity material heated by radiation from above when a water droplet is placed on

its surface. The results are different from analogous results obtained with the same material heated by conduction from below.

Water absorbs near infrared radiation. More than 95% of the radiant heat supplied from the radiant panels is in the near infrared spectrum. It is estimated that 20–30% of the heat of vaporization is supplied to the water droplet from direct absorption of the incident radiation. The remainder is from conduction across the liquid–solid interface.

The shape parameter increases as the surface temperature increases. A contributing factor is the effect of surface tension at different temperatures. For the conduction case, the constant value of β is an indicator that the temperature at the exposed water droplet surface is not affected by the initial solid surface temperature.

The evaporation times for the radiation case are shorter than for the conduction case. The water droplets on the radiatively heated surface are heated from both below and above. Further, the radiatively heated droplets spread across the surface more than in the conduction case, thus providing a large surface area to absorb heat from above and a thinner layer to transfer heat from below by conduction.

REFERENCES

1. S. Toda, A Study of Mist Cooling. 1st Report: Investigation of Mist Cooling, *Heat Transfer Jap. Res.*, vol. 1, pp. 39–50, 1972.
2. C. Bonacina, S. Del Giudice, and G. Comini, Dropwise Evaporation, *J. Heat Transfer,* vol. 101, pp. 441–446, 1979.
3. J. J. Rizza, A Numerical Solution to Dropwise Evaporation, *J. Heat Transfer,* vol. 103, pp. 501–507, 1981.
4. M. Seki, H. Kawamura, and K. Sanokawa, Transient Temperature Profile of a Hot Wall Due to an Impinging Liquid Droplet, *J. Heat Transfer,* vol. 100, pp. 167–169, 1978.
5. S. Inada, Y. Miyasaka, and K. Nishida, Transient Heat Transfer for a Water Drop Impinging on a Heated Surface, *Bull. JSME,* vol. 28, no. 245, pp. 2675–2681, 1985.
6. M. diMarzo and D. D. Evans, Dropwise Evaporative Cooling of High Thermal Conductivity Materials, *Heat and Technology,* vol. 5, no. 1–2, pp. 126–136, 1987.
7. M. diMarzo and D. D. Evans, Evaporation of a Water Droplet Deposited on a Hot High Thermal Conductivity Solid Surface, *J. Heat Transfer,* vol. 111, pp. 210–213, 1989.
8. W. M. Grissom and F. A. Wierum, Liquid Spray Cooling of a Heated Surface, *Int. J. Heat Mass Transfer,* vol. 24, pp. 261–271, 1981.
9. S. S. Sadhal and M. S. Plesset, Effect of Solid Properties and Contact Angle in Dropwise Condensation and Evaporation, *J. Heat Transfer,* vol. 101, pp. 48–54, 1979.
10. C. O. Pedersen, An Experimental Study of the Behavior and Heat Transfer Characteristics of Water Droplets Impinging upon a Heated Surface, *Int. J. Heat Mass Transfer,* vol. 13, pp 369–381, 1970.
11. K. J. Choi and S. C. Yao, Mechanism of Film Boiling Heat Transfer of Normally Impacting Spray, *Int. J. Heat Mass Transfer,* vol. 30, no. 2, pp. 311–318, 1987.
12. K. Makino and I. Michiyoshi, Heat Transfer Characteristics of Evaporation of a Liquid Droplet on Heated Surfaces, *Int. J. Heat Mass Transfer,* vol. 21, pp. 605–613, 1978.
13. K. Makino and I. Michiyoshi, Effects of Initial Size of Water Droplet on Its Evaporation on Heated Surfaces, *Int. J. Heat Mass Transfer,* vol. 22, pp. 979–981, 1979.
14. K. Makino and I. Michiyoshi, The Behavior of a Water Droplet on Heated Surfaces, *Int. J. Heat Mass Transfer,* vol. 27, no. 5, pp. 781–791, 1984.
15. K. Makino and I. Michiyoshi, Discussion of Transient Heat Transfer to a Water Droplet on

Heated Surfaces Under Atmospheric Pressure, *Int. J. Heat Mass Transfer*, vol. 30, no. 9, pp. 1895–1905, 1987.

16. M. Abu-Zaid and A. Atreya, Effect of Water on Piloted Ignition of Cellulosic Materials, *Natl. Inst. Stds. and Technol. Interagency Rep.*, NIST-GCR-89-561, 1989.
17. M. Klassen, M. diMarzo, and J. Sirkis, Infrared Thermography of Dropwise Evaporative Cooling, *ASME HTD*, vol. 141, pp. 117–121, 1990; also to appear on *Experimental Thermal and Fluid Science*, vol. 5, no. 1, pp. 136–141, 1992.
18. S. Ostrach and A. Pradhan, Surface-Tension Induced Convection at Reduced Gravity, *AIAA J.*, vol. 16, no. 5, pp. 419–424, 1978.
19. R. Siegel and J. R. Howell, *Thermal Radiation Heat Transfer*, 2nd ed., Hemisphere, New York, 1981.
20. F. F. Simon and Y. Y. Hsu, Wetting Dynamics of Evaporating Drops on Various Surfaces, *NASA Tech. Memo.*, NASA TM X-67913, 1971.

PAPER # 10

DROPWISE EVAPORATIVE COOLING IN RADIATIVE FIELD

P. Tartarini*, M. di Marzo+

* Istituto di Fisica Tecnica
Universita' di Bologna
viale Risorgimento, 2
Bologna, Italy 40136

+ Mechanical Engineering Department
University of Maryland
College Park, Md, U.S.A. 20742

ABSTRACT

This paper investigates the evaporative cooling of solid surfaces induced by the impingement of single water droplets. The solid surface is heated by radiant panels from above; therefore, the radiant heat absorbed directly by the evaporating droplet has to be considered. A theoretical model is presented, which calculates the droplet evaporation time and the solid surface cooling for materials with thermal conductivity spanning over more than two orders of magnitude. In particular, results concerning droplet evaporation on Macor (low thermal conductivity material) are reported and discussed. The model accurately predicts the total evaporation time. It is further validated with transient surface temperature measurements obtained by infrared thermography. The predictions are in excellent agreement with the experimental data. The interfacial heat flux distribution under the evaporating droplet is studied. These single droplet results are currently being used to study the cooling strategies for different materials, and constitute the basis for the formulation of a multi-droplet comprehensive model.

1. INTRODUCTION

The study of the evaporation of a liquid droplet on a hot solid surface is a subject of practical interest in many industrial applications, such as spray cooling of metals in steel industries, vaporization process in internal combustion engines, cooling of turbine blades, and many others. The solid and liquid thermal behavior, the heat transfer phenomena and the relevant parameters governing the evaporative transient constitute the main objectives of the studies conducted in this field.

It is generally recognized that droplet evaporation can be classified into three categories, which depend on the degree of superheat of the solid surface (with respect to the liquid saturation temperature). Therefore, different approaches can be used to study the evaporative transient under conditions of low, intermediate and high superheat respectively. In the regimes of intermediate and high superheat, nucleate or film boiling are the dominant heat transfer modes. A large number of experimental and theoretical investigations have been carried out for liquid droplets deposited on a very high temperature solid surface and, in general, it could be said that a higher number of papers have been published about the regimes of high rather than low superheat. Baumeister & Simon (1973) studied the Leidenfrost transition for liquids as water and liquid metals. More recently, many other contributions on the Leidenfrost evaporation were provided (e.g., Sadhal and Plesset 1979, Avedisian & Koplik 1987). Multi-droplet systems have been investigated by Toda (1972) and by Bonacina *et al.* (1979). These works showed that conduction in the liquid is the relevant heat transfer mode in absence of nucleate boiling. Rizza (1981) provided another numerical investigation for spray evaporation on a hot surface. A two-dimensional transient conduction equation was solved for the solid alone with an arbitrary surface temperature as the boundary condition. Grissom & Wierum (1981) further developed these concepts to define a range of conditions for spray evaporative cooling. Rizza's main assumption of uniform and constant solid-liquid interfacial temperature had already been made by Seki *et al.* (1978), and it was supported by the extensive experimental observations of Makino & Michiyoshi (1978, 1984, 1987). Makino & Michiyoshi (1984) provided a full range of the boiling curve associated with the evaporation of a water drop on a heated surface. Zhang & Yang (1982) observed the interfacial flow patterns of evaporating droplets and discussed the stability of different flow structures at the liquid and air interface. They pointed out that, in steady conditions, the droplet is shaped as a spherical segment with a very smooth surface. This is a basic assumption that will be used in the present study.

A simple model for a single droplet evaporation was proposed by diMarzo and Evans (1987, 1989). This model was limited to evaporation at the liquid-vapor interface in complete suppression of nucleate boiling. Photographic inspection of evaporating droplets (diMarzo & Evans 1987) confirmed that the droplet shape can be approximated by a segment of a sphere.

Most of the above mentioned studies focused on water droplets deposited on high thermal conductivity materials. In that case, the assumption of uniform and constant solid-liquid interfacial temperature is reasonable and the modeling of the liquid region can be de-coupled from the treatment of the solid. This is not the case for dropwise evaporative

cooling taking place on low thermal conductivity materials. Abu-Zaid & Atreya (1989) measured the interfacial temperature at various locations and confirmed that the temperature changes during the transient.

DiMarzo *et al.* (1989, 1992) reported a series of experiments on droplet evaporation on a relatively low temperature solid surface. These studies provided a large amount of data for single water droplets evaporating on solid surface with thermal conductivities ranging from aluminum to Macor, a glass-like material. Many observations, including the evaporation time, the surface temperature distribution and the spatial and temporal behavior of the heat flux on the surface, were given.

The objective of this paper is to provide a basis for the modeling of the cooling effect due to droplet evaporation under radiant input conditions. Extending the range of analysis of a previous model by the same authors, a computer code which describes the coupled thermal behavior of solid and liquid during the evaporative transient is formulated. The predictions of the model are presented and compared with the experimental results. Further analysis of numerical and experimental results is carried out to provide more insight into the evaporative cooling mechanism.

2. PHENOMENOLOGY

Some detailed descriptions of the droplet evaporation phenomenology and of the solid surface temperature behavior were provided by diMarzo and Evans (1987, 1989) and by Klassen *et al.* (1990). Experiments were conducted on aluminum (k = 180 W/m·C) and on Macor (k = 1.3 W/m·C). The thermal conductivity more than the thermal diffusivity of the materials is the main parameter characterizing the evaporative cooling behavior.

In the previous works by diMarzo & Evans (1987, 1989) and by Klassen *et al.* (1990), the operative conditions were those of a single droplet gently deposited on a solid surface heated by conduction from below. All these experiments showed that the wetted area can be considered as constant for the entire evaporative transient. Experiments conducted by Kidder (1990) and by diMarzo *et al.* (1992) showed that the same assumption is not realistic when the solid surface is heated by radiation from above, since the droplet visibly shrinks, in this case, during the transient. This phenomenon had been early observed and studied by several researchers (Adam & Jessop 1925, Herzberg & Marian 1970, Simon & Hsu 1971). They showed that, when a liquid droplet impinges a hot solid surface, the solid-liquid contact angle is characterized by a critical value, dependent on the physical properties of both materials. Below this critical value, called receding angle, the droplet contact area cannot remain constant and it starts to shrink. Since the shape of a droplet gently deposited on a solid surface has been shown to be that of a segment of sphere, the receding angle results to be related to the shape parameter β, defined as $\beta = R/R_{sph}$, where R is the radius of the wetted area and R_{sph} is the radius of the spherical droplet of equal volume.

When the droplet impinges the solid surface and the evaporative transient begins, the initial value of the shape parameter, β_0, is directly observed. When heat is supplied by radiation from above, the amount of heat absorbed directly by the water upper layer causes the droplet to spread out under the effect of decreasing surface tension. This difference in the initial droplet shape is confirmed by the experiments conducted by Klassen *et al.* (1990) and by Kidder (1990) on Macor heated by conduction from below and by radiation from above respectively. Figure 1 shows the behavior of the initial value of the shape parameter, β_0, under both conductive and radiative heat input conditions for the same values of the initial solid surface temperature.

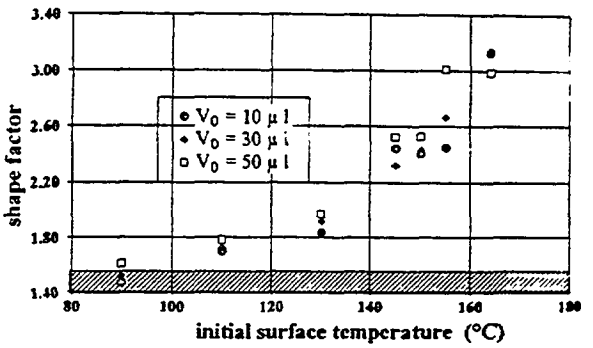

Fig. 1 Shape factor (β_0) versus initial surface temperature for Macor. Shaded area = solid surface heated by conduction; o, ◇, □ = solid surface heated by radiation.

3. THEORETICAL MODEL

3.1 Previous Work

The original model by diMarzo *et al.* (1987, 1989) was used to gain insight into the evaporative process mechanism in the special case of droplets laid on solid surfaces heated by conduction from below. The evaporative cooling behavior for different conductivity materials (spanning over more than two orders of magnitude, from Macor to aluminum) was analyzed for an identical heat sink. As a result of these studies, it was found that a constant and uniform interfacial temperature can be assumed for high conductivity materials and leads to meaningless results for a low thermal conductivity solid (Tartarini & diMarzo 1991). The conductive version of the model by diMarzo *et al.* (1987, 1989) was also used to investigate the interfacial temperatures and heat fluxes under the droplet, where direct measurements are unavailable. An important result of previous analyses consisted in observing that the heat flux is not uniform nor constant during the evaporative process. The spatial distribution also indicated that most of the evaporation takes place at the outer edge of the droplet.

Some basic assumptions are made in the model formulation:

- Heat conduction is assumed to be the only heat transfer mechanism in the liquid droplet and in the solid. Nucleate or film boiling are not present.
- The wetted area on the solid surface covered by the

cooling taking place on low thermal conductivity materials. Abu-Zaid & Atreya (1989) measured the interfacial temperature at various locations and confirmed that the temperature changes during the transient.

DiMarzo *et al.* (1989, 1992) reported a series of experiments on droplet evaporation on a relatively low temperature solid surface. These studies provided a large amount of data for single water droplets evaporating on solid surface with thermal conductivities ranging from aluminum to Macor, a glass-like material. Many observations, including the evaporation time, the surface temperature distribution and the spatial and temporal behavior of the heat flux on the surface, were given.

The objective of this paper is to provide a basis for the modeling of the cooling effect due to droplet evaporation under radiant input conditions. Extending the range of analysis of a previous model by the same authors, a computer code which describes the coupled thermal behavior of solid and liquid during the evaporative transient is formulated. The predictions of the model are presented and compared with the experimental results. Further analysis of numerical and experimental results is carried out to provide more insight into the evaporative cooling mechanism.

2. PHENOMENOLOGY

Some detailed descriptions of the droplet evaporation phenomenology and of the solid surface temperature behavior were provided by diMarzo and Evans (1987, 1989) and by Klassen *et al.* (1990). Experiments were conducted on aluminum (k = 180 W/m·C) and on Macor (k = 1.3 W/m·C). The thermal conductivity more than the thermal diffusivity of the materials is the main parameter characterizing the evaporative cooling behavior.

In the previous works by diMarzo & Evans (1987, 1989) and by Klassen *et al.* (1990), the operative conditions were those of a single droplet gently deposited on a solid surface heated by conduction from below. All these experiments showed that the wetted area can be considered as constant for the entire evaporative transient. Experiments conducted by Kidder (1990) and by diMarzo *et al.* (1992) showed that the same assumption is not realistic when the solid surface is heated by radiation from above, since the droplet visibly shrinks, in this case, during the transient. This phenomenon had been early observed and studied by several researchers (Adam & Jessop 1925, Herzberg & Marian 1970, Simon & Hsu 1971). They showed that, when a liquid droplet impinges a hot solid surface, the solid-liquid contact angle is characterized by a critical value, dependent on the physical properties of both materials. Below this critical value, called receding angle, the droplet contact area cannot remain constant and it starts to shrink. Since the shape of a droplet gently deposited on a solid surface has been shown to be that of a segment of sphere, the receding angle results to be related to the shape parameter β, defined as $\beta = R/R_{sph}$, where R is the radius of the wetted area and R_{sph} is the radius of the spherical droplet of equal volume.

When the droplet impinges the solid surface and the evaporative transient begins, the initial value of the shape parameter, β_0, is directly observed. When heat is supplied by radiation from above, the amount of heat absorbed directly by the water upper layer causes the droplet to spread out under the effect of decreasing surface tension. This difference in the initial droplet shape is confirmed by the experiments conducted by Klassen *et al.* (1990) and by Kidder (1990) on Macor heated by conduction from below and by radiation from above respectively. Figure 1 shows the behavior of the initial value of the shape parameter, β_0, under both conductive and radiative heat input conditions for the same values of the initial solid surface temperature.

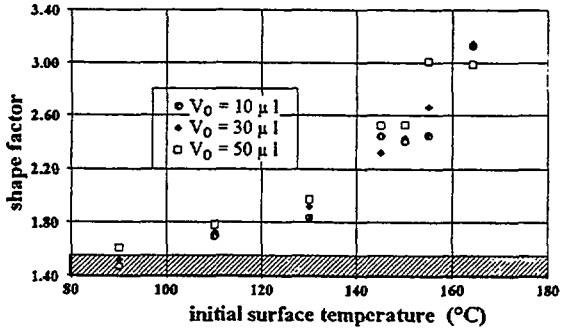

Fig. 1 Shape factor (β_0) versus initial surface temperature for Macor. Shaded area = solid surface heated by conduction; o, ◇, □ = solid surface heated by radiation.

3. THEORETICAL MODEL

3.1 Previous Work

The original model by diMarzo *et al.* (1987, 1989) was used to gain insight into the evaporative process mechanism in the special case of droplets laid on solid surfaces heated by conduction from below. The evaporative cooling behavior for different conductivity materials (spanning over more than two orders of magnitude, from Macor to aluminum) was analyzed for an identical heat sink. As a result of these studies, it was found that a constant and uniform interfacial temperature can be assumed for high conductivity materials and leads to meaningless results for a low thermal conductivity solid (Tartarini & diMarzo 1991). The conductive version of the model by diMarzo *et al.* (1987, 1989) was also used to investigate the interfacial temperatures and heat fluxes under the droplet, where direct measurements are unavailable. An important result of previous analyses consisted in observing that the heat flux is not uniform nor constant during the evaporative process. The spatial distribution also indicated that most of the evaporation takes place at the outer edge of the droplet.

Some basic assumptions are made in the model formulation:

- Heat conduction is assumed to be the only heat transfer mechanism in the liquid droplet and in the solid. Nucleate or film boiling are not present.
- The wetted area on the solid surface covered by the

droplet remains constant for contact angles greater than the value of the receding angle, regardless of droplet volume decreasing.

- The model generating the transient droplet shape also assumes that, at the receding angle, the droplet has reached a spherical cap configuration. This is reasonable because, in order for the surface tension to shrink the wetted surface, the liquid-vapor surface configuration must maximize the bounded volume. This receding angle configuration identifies the aspect ratio of the droplet which will be preserved for all the remaining portion of the transient. Chandra and Avedisian (1991) showed that, for an evaporating droplet, this angle is less than 90°.

3.2 The Experimental Apparatus

The radiant heat input is provided by two panels mounted above the surface of a Macor square tile (0.1524 x 0.1524 x 0.0254 m). The panels can reach temperatures in excess of 800°C and can be approximated to black bodies. They are conical in shape with an external diameter of about 0.2 meters. These two panels are positioned above the Macor tile, on two opposite sides of the tile with their axis at 30° from the vertical and facing the tile surface. The panels are fed by a three-phase power supply which is controlled on a temperature feedback, and are held at a constant temperature set point. The Macor tile is pasted onto a chilled plate which is kept at near ambient temperature by a water flow. The radiant boundary condition as well as the thermal condition at the lower surface of the tile are designed to obtain a linear temperature profile in the tile depth and to insure that the tile exposed surface is isothermal over the droplet impingement region, prior to the initiation of the transient. The Macor tile transient surface temperature distribution is recorded by an infrared camera. The infrared image is correlated to a temperature distribution. The 256 shades of gray are related to a temperature scale of about 120°C. The scale is set by simultaneously measuring the temperature of a given surface point with a thermocouple probe and via the infrared camera reading. The spacial resolution is about 10 pixel/mm and the temperature resolution is 2°C/gray-shade which yields an accuracy of about ±1°C. The transient temperature distribution is recorded on a VCR and selected frames during the transient are grabbed by a PC to be analyzed.

3.3 Model Formulation

The modeling of the coupled solid and liquid thermal behavior is described by the transient conduction equation for both domains with the appropriate boundary conditions:

$$\textit{solid domain}: \quad \frac{\partial T}{\partial t} = \kappa_s \nabla^2 T - H_{\mu,z}\big|_{z=0} \tag{1}$$

$$\textit{liquid domain}: \quad \frac{\partial T}{\partial t} = \kappa_l \nabla^2 T - H_{\mu,z} \tag{2}$$

Assuming that both diffusion and reflection at the bottom of the droplet are negligible, one can write the volumetric heat generation in the liquid layer as:

$$\frac{\partial F}{\partial z} = H_{\mu,z} = \int_0^{\infty} E_\lambda \alpha_\lambda \times \times \int_0^{\pi/2} \frac{2}{\mu} \Phi_{\lambda,\theta} \sin\theta \cos\theta \, e^{-\frac{\alpha_\lambda z}{\mu}} (1-\rho_{\lambda,\theta}) d\lambda \, d\theta \tag{3}$$

The absorption coefficient α is a very strong function of the wave length λ (Siegel & Howell 1981), the direction cosine μ is given by the Snell's law, the fractional surface area coverage Φ depends on the geometrical configuration of the radiant heat source, and the reflectivity ρ is less than 0.1 for θ less than 65 and it is given by the electromagnetic theory. For the typical experimental conditions (Kidder 1990, diMarzo *et al.* 1992), the panels temperature is less than 750°C. The direct radiation contribution is maximum at the liquid-vapor interface; however, the contribution of the radiant heat input in the layer thickness is not negligible, and the model takes it into account for each value of the axial coordinate z.

By introducing an overall heat transfer coefficient h at the exposed solid surface, the boundary conditions at the liquid-vapor interface can be written as:

$$-k_l \nabla T + q_{top} = h(T_i - T_a) + 0.624\, h_c \left(\frac{D}{\kappa_a}\right)^{\frac{2}{3}} \frac{\Lambda}{c_a} \frac{x_i - x_a}{1 - x_a} \tag{4}$$

where q_{top} denotes the radiant heat flux that is absorbed by the top layer of the liquid.

The set of boundary conditions at the liquid-solid interface and at the exposed solid surface can be written as follows:

$$at \;\; 0 \le r \le R,\; z=0: \quad T = T_0 \;;\; k_s \frac{\partial T}{\partial z} = k_l \frac{\partial T}{\partial z} + q_{z=0} \tag{5}$$

$$at \;\; r > R,\; z=0: \quad k_s \frac{\partial T}{\partial z} = h(T_{s,0} - T_a) + \varepsilon_s \sigma (T_s^4 - T_a^4) \tag{6}$$

In order to evaluate the amount of radiant heat that is directly absorbed by the droplet and the percentage that reaches the solid-liquid interface, experimental tests and numerical simulations have been carried out.

The heat flux incident on the water droplet surface, q_{inc}, was measured (Kidder 1990) with a radiometer at various heaters temperatures. It was found that the heat flux on the surface was about 18% of the flux produced by the heaters, that is:

$$q_{inc} = 0.18\, \varepsilon\, \sigma\, T_H^4 \tag{7}$$

In the numerical code, the conical heaters have been simulated as a series of separate rectangular shaped panels, each at a different angle to the droplet (Kidder 1990).

Since the heaters surface area, the total absorption coefficient, the incident heat flux and the droplet surface area are all known, Eq. (3) allows one to calculate the amount of incident energy (from the i-th rectangular heater element) that is absorbed by each mesh of the droplet. This is possible because the coordinates of each mesh are known step by step, and Eq. (3) can be applied as if every mesh consisted of a disk of known thickness and position inside

the whole droplet.

Also under radiant heat input conditions, as well as in the conductive case (see Tartarini *et al.* 1990), extremely strong local thermal gradients at the drop initial contact preclude the solution of this problem with conventional finite difference schemes. The solution is obtained by using a Boundary Element Method (BEM) for the solid region and a Control Volume Method (CVM) for the liquid region. The BEM is described in detail by Wrobel & Brebbia (1981), while the CVM used here is described by Tartarini *et al.* (1990). Although the droplet and the solid are treated separately by different numerical methods, the temperatures in the droplet and along the solid surface are solved simultaneously at each time step by coupling the CVM and the BEM in the numerical model.

4. RESULTS AND DISCUSSION

In the present work, a computer code has been formulated on the basis of the previously described theoretical model. Validation has been obtained by numerous comparisons between numerical predictions and experimental data provided by Kidder (1990) and by diMarzo *et al.* (1992). The droplet evaporation time and the solid surface transient temperature distribution are the main parameters which provide an estimate of the effectiveness of the numerical predictions. The comparison between experimental data and numerical prediction for the total evaporation time is presented in Fig. 2.

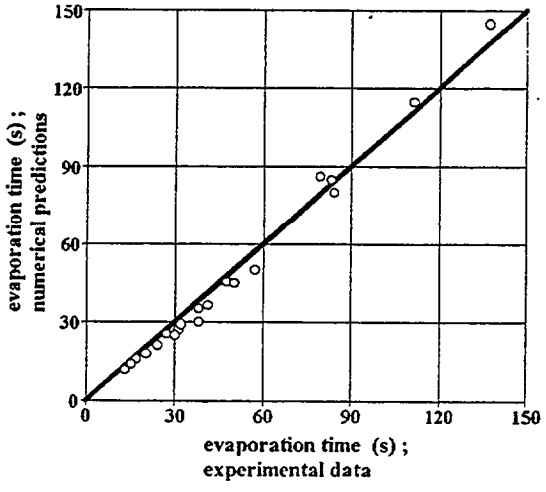

Fig. 2 Model validation: total evaporation time for droplets with V_0 = 10, 30 and 50 µl on Macor; comparison between experimental data and numerical predictions.

In this figure, data and numerical results concerning droplets of 10, 30 and 50 µl are reported. The experiments were conducted with the initial surface temperature of the Macor tile ranging from 90°C to 165°C. The agreement between data and numerical predictions is generally within 5%. Some discrepancies were observed for evaporation times greater than 160 s (low surface temperatures and big initial volumes) and for high surface temperatures (some experiments were also carried out with T_s= 180°C). Both these conditions, however, are in conflict with the initial assumptions of the present work: in fact, very low evaporation times coincide with the onset of convective motion inside the droplet, while Macor temperatures over 160°C induce nucleate boiling.

In Fig. 3 and Fig. 4, experimental and numerical surface temperature curves are reported. They show four reference cases of surface temperature distribution after 30% and 90% of the total evaporation time respectively. Initial droplet volumes of 10 and 30 µl, subjected to initial surface temperatures of 110, 130 and 145 °C, are considered here, and in all cases a very satisfactory accuracy of the numerical simulation is observed. This is consistent with the results (Tartarini & diMarzo 1990) which had been provided by the previous code version for solid surfaces heated by conduction from below.

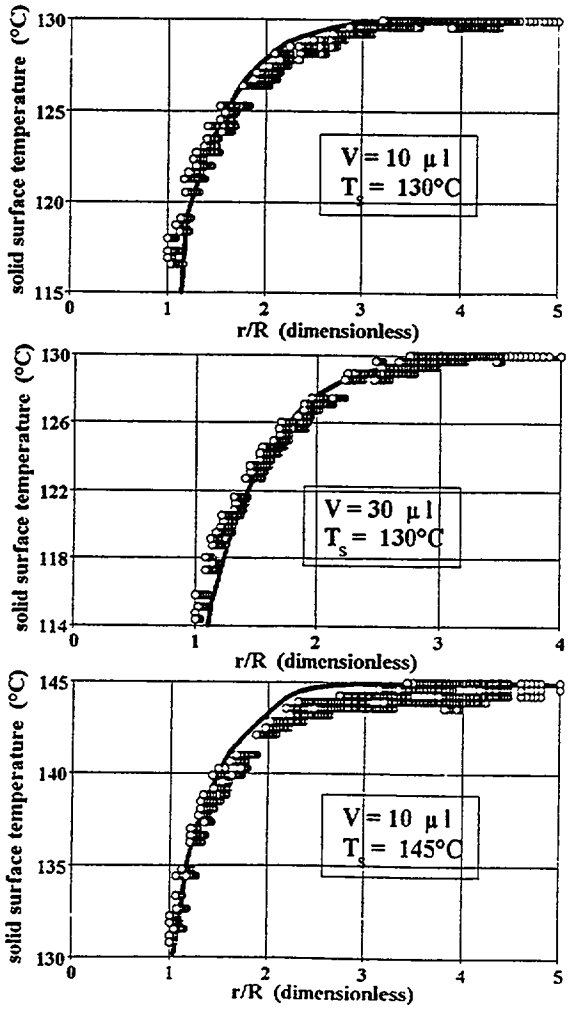

Fig. 3 Model validation: solid surface temperatures for water on Macor at t = 0.3 τ. Solid line = numerical simulation; o = experimental data.

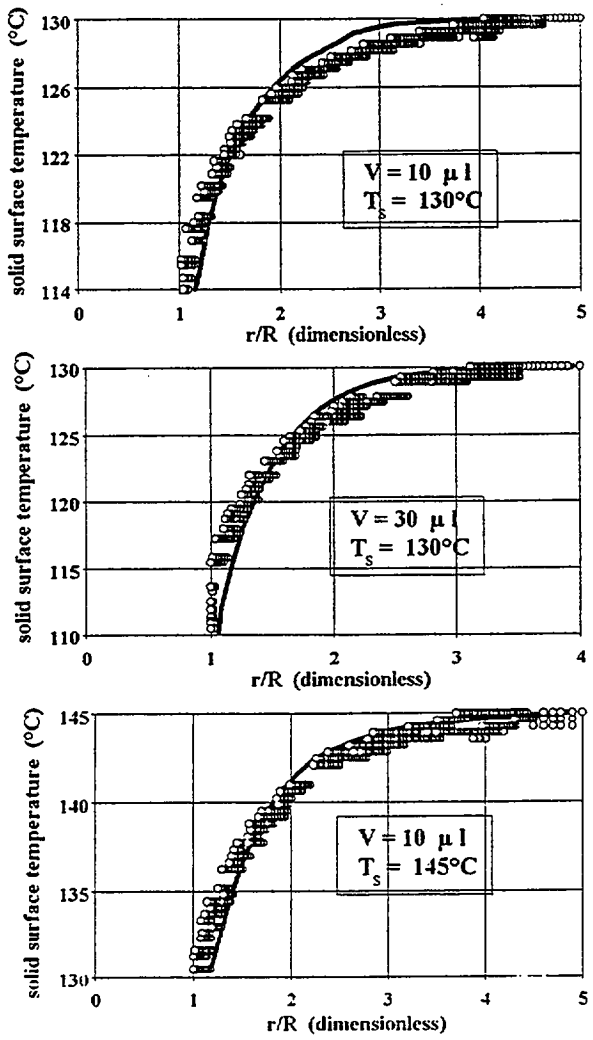

Fig. 4 Model validation: solid surface temperatures for water on Macor at t = 0.9 τ. Solid line = numerical simulation; O = experimental data.

The code accuracy in both situations is remarkable if one considers the very different behavior of the droplets in terms of initial and transient values of the wetted area for conductive and radiative heating of the solid surface.
A useful information that is provided by the code, and that is needed for the multi-droplet extension of the model, consists of the calculation of the solid-liquid interfacial heat flux during the evaporative transient. Two examples of the interfacial heat flux behavior are reported in Fig. 5, which also confirms that the interfacial heat flux between water and low conductivity materials like Macor is not constant nor uniform during the evaporative transient.
These observations provide some insight on the cooling strategies to be used for different materials, and constitute the basis for the formulation of a multi-droplet comprehensive model.

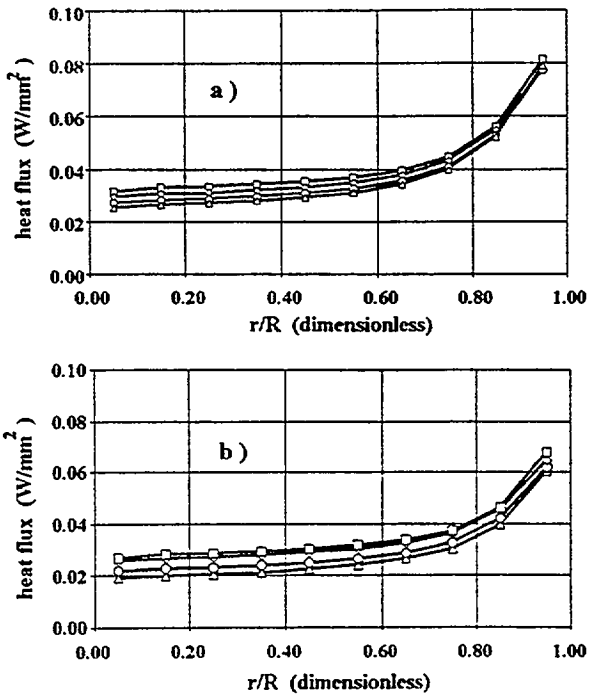

Fig. 5 Liquid-solid interfacial fluxes for water droplets with T_s = 130°C on Macor;
a) V = 10 µl - t=0.3 τ (Δ); t=0.5 τ (O); t=0.7 τ (◇) and t=0.9 τ (□);
b) V = 30 µl - t=0.3 τ (Δ); t=0.5 τ (O); t=0.7 τ (◇) and t=0.9 τ (□).

5. CONCLUSIONS

The cooling effect due to the evaporation of a liquid droplet on a hot solid surface heated by radiation from above has been investigated. The theory for the formulation of a model for the prediction of the thermal behavior of the droplet-solid interaction has been reviewed. On the basis of a large number of experimental results, the model has been presented and validated over various parameters. Model predictions for a variety of conditions are used to gain insight into the evaporative process mechanism.
The new model, now including both conductive and radiative heat input options, constitutes a validated instrument to analyze the single-droplet evaporative cooling for a wide range of materials. Its extension to multi-droplet systems (sprays) is currently in progress.

ACKNOWLEDGEMENTS

This study was made possible by a grant of the Building and Fire Research Laboratory, National Institute of Standards and Technology. Funding of the computational expenditures was provided by the Italian M.U.R.S.T. and C.N.R.

NOMENCLATURE

c	specific heat
D	air-steam mass diffusivity
E_λ	spectral radiative flux
F	total radiative flux
H	radiative heating rate
h	overall heat transfer coefficient
h_c	convective heat transfer coefficient
k	thermal conductivity
q	heat flux
r	radial coordinate
R	radius of the wetted area
t	time
T	temperature
x	molar fraction of steam in air
z	axial coordinate
Greek letters	
α_λ	spectral absorption coefficient of water
β	shape parameter
ϵ	emissivity
θ	polar angle
κ	thermal diffusivity
Λ	liquid latent heat of vaporization
λ	wavelength
μ	direction cosine
ρ_λ	reflectivity of the air-water interface
σ	Stefan-Boltzmann constant
τ	total evaporation time
Φ	fractional surface area
Subscripts	
a	air
H	heaters
i	interfacial
l	liquid
s	solid
0	initial

REFERENCES

Abu-Zaid, M. & Atreya, A. 1989, Effect of Water on Piloted Ignition of Cellulosic Materials, NIST Rpt., GCR-89-561.

Adam, N. & Jessop, G. 1925, Angles of Contact and Polarity of Solid Surfaces, J. Chem. Soc., vol. 127, pp. 1863-1868.

Avedisian, C.T. & Koplik, J. 1987, Leidenfrost Boiling of Methanol Droplets on Hot Porous/Ceramic Surfaces, Int. J. Heat Mass Transfer, vol. 30, pp. 379-393.

Baumeister, K.J. & Simon, F.F. 1973, Leidenfrost Temperature - Its Correlation for Liquid Metals, Cryogens, Hydrocarbons and Water, ASME J. Heat Transfer, vol. 95, pp. 166-173.

Bonacina, C., Del Giudice, S. & Comini, G. 1979, Dropwise Evaporation, ASME J. Heat Transfer, vol. 101, pp. 441-446.

Chandra, S. & Avedisian, C.T. 1991, On the Collision of a Droplet With a Solid Surface, Proc. of the Royal Society of London, vol. 432, pp. 13-41.

diMarzo, M. & Evans, D.D. 1987, Dropwise Evaporative Cooling of High Thermal Conductivity Materials, Int. J. Heat & Technology, vol. 5 (1-2), pp. 126-136.

diMarzo, M. & Evans, D.D. 1989, Evaporation of a Water Droplet Deposited on a Hot Thermal Conductivity Surface, ASME J. Heat Transfer, vol. 111, pp. 210-213.

diMarzo, M., Kidder, C.H. & Tartarini, P. 1992, Infrared Thermography of Dropwise Evaporative Cooling of a Semiinfinite Solid Subjected to Radiant Heat Input, Int. J. Exp. Heat Transfer, vol. 5, pp. 101-114.

Grissom, W.M. & Wierum, F.A. 1981, Liquid Spray Cooling of a Heated Surface, Int. J. Heat Mass Transfer, vol. 24, pp. 261-271.

Herzberg W.J. & Marian, J.E. 1970, The Receding Contact Angle, J. Colloid Interface Science, vol. 33, pp. 164-171.

Kidder, C. 1990, Dropwise Evaporative Cooling of a Ceramic Solid Surface Heated by Radiation, MS Thesis, University of Maryland, Dept. of Mechanical Engineering.

Klassen, M.S., diMarzo, M. & Sirkis, J. 1990, Infrared Thermography of Dropwise Evaporative Cooling, ASME HTD, vol. 141, pp. 117-121.

Makino, K. & Michiyoshi, I. 1978, Heat Transfer Characteristics of Evaporation of a Liquid Droplet on Heated Surfaces, Int. J. Heat Mass Transfer, vol. 21, pp. 605-613.

Makino, K. & Michiyoshi, I. 1984, The Behavior of a Water Droplet on Heated Surfaces, Int. J. Heat Mass Transfer, vol. 27, pp. 781-791.

Makino, K. & Michiyoshi, I. 1987, Discussion of Transient Heat Transfer to a Water Droplet on Heated Surfaces Under Atmospheric Pressure, Int. J. Heat Mass Transfer, vol. 30, pp. 1895-1905.

Rizza, J.J. 1981, A Numerical Solution to Dropwise Evaporation, ASME J. Heat Transfer, vol. 103, pp. 501-507.

Sadhal, S.S. & Plesset, M.S. 1979, Effect of Solid Properties and Contact Angle in Dropwise Condensation and Evaporation, ASME J. Heat Transfer, vol. 101, pp. 48-54.

Seki, M., Kawamura, H. & Sanokawa, K. 1978, Transient Temperature Profile of a Hot Wall Due to an Impinging Liquid Droplet, ASME J. Heat Transfer, vol.100, pp 167-169.

Siegel, R. & Howell, J.R. 1981, Thermal Radiation Heat Transfer, Hemisphere Publishing Corporation, New York.

Simon, F.F. & Hsu, Y.Y. 1971, Wetting Dynamics of Evaporating Drops on Various Surfaces, NASA Technical Memorandum, NASA TM X-67913.

Tartarini, P. & diMarzo, M. 1990, The Solid-Liquid Interfacial Conditions for Dropwise Evaporative Cooling, Int. J. Heat & Technology, vol. 10 (3-4), pp. 130-144.

Tartarini, P., Liao, Y. & diMarzo, M. 1990, Transient Cooling of a Hot Surface by Droplets Evaporation, UMCP Mechanical Engineering Report, No. 90-6.

Toda, S. 1972, A Study of Mist Cooling. First Report: Investigation of Mist Cooling, Heat Transfer Japanese Research, vol. 1 (3), pp. 39-50.

Wrobel, L.C. & Brebbia, C.A. 1981, A Formulation of the Boundary Element Method for Axisymmetric Transient Heat Transfer Conduction, Int. J. Heat Mass Transfer, vol. 24, pp. 843-850.

Zhang, N. & Yang, W.-J. 1982, Natural Convection in Evaporating Minute Drops, ASME J. Heat Transfer, vol. 104, pp. 656-662.

PAPER # 11

Modelling of Dropwise Evaporative Cooling on a Semi-infinite Solid Subjected to Radiant Heat Input

G. WHITE, S. TINKER and M. DI MARZO
Mechanical Engineering Department
University of Maryland
College Park, MD 20742 USA

ABSTRACT

A model for the prediction of dropwise evaporative cooling over hot solid surfaces is proposed for the case of radiant heat input. A detailed representation of the droplet shape during the transient is provided. The direct radiant contribution to the evaporative process is expressed as a liquid-vapor interfacial term and a constant heat absorption term within the liquid layer. The liquid layer is treated with a one-dimensional heat conduction approximation justified by previous results and three sub-models are used to describe it during the transient. A boundary element method for the solid thermal behavior, previously developed, is extended to this case. The results obtained from a closed-form solution, with simplified solid-liquid interfacial boundary conditions, are also included. Comparisons with the experimental data illustrate the adequacy of the model and the performance of the closed-form solution.

KEYWORDS: cooling, evaporation, drops.

NOMENCLATURE

A,B	constants
c	specific heat
$E_{b\lambda}$	blackbody spectral hemispherical emissive power
f_ϕ	fractional surface area coverage
F	radiant flux absorbed near the liquid-vapor interface
h	overall heat transfer coefficient
h_c	convective heat transfer coefficient
H	radiant volumetric heat absorption in the water layer
J_0, J_1	Bessel's functions
k	thermal conductivity
Le	Lewis number
$\hat{n}$	normal to the liquid-vapor interface

FIRE SAFETY SCIENCE—PROCEEDINGS OF THE FOURTH INTERNATIONAL SYMPOSIUM, pp. 217–228

q_o	initial steady state heat flux through the solid
q_c	average heat flux at the solid-liquid interface: see Eqs. (4, 5)
q_r	heat flux by direct radiation
r	coordinate: see Fig. 1
R	radius of the wetted region under the droplet
t	time
T	temperature
V	initial droplet volume
x	vapor molar fraction
z	coordinate: see Fig. 1
α	thermal diffusivity
β	shape parameter: $R / (3V/4\pi)^{1/3}$
δ	droplet thickness
θ	liquid-vapor-solid contact angle
κ_λ	water absorption coefficient
Λ	latent heat of vaporization
λ	wave length or dummy variable
μ	direction cosine in the water
ρ_ϕ	water air reflectivity
τ	total evaporation time
ϕ	polar angle

Subscripts

a	air or far field
i	liquid-vapor interface
l	liquid
o	initial condition
r	receding condition
s	solid or at the solid-liquid interface

INTRODUCTION

Cooling of hot surfaces by droplet sprays has been the subject of numerous investigations. Early experiments of spray cooling by Toda [1] and Bonacina [2] provided insight in the effectiveness of this technique. Detailed studies of single droplets evaporating over hot surfaces heated from below were reported among others by Inada [3], Makino [4] and Takano [5]. In an attempt to extend this information to the fire safety field, a set of dropwise evaporative cooling experiments were performed with radiant heat sources from above the solid surface. DiMarzo [6] investigated single droplets behavior while Dawson [7] provided information on multi-droplet arrays.

Models are proposed for single and multi-droplet systems by a number of investigators. Early models by Seki [8] and diMarzo [9] assumed a constant liquid-vapor interfacial temperature set at an arbitrary value dictated by the solution for two semi-infinite solids brought into sudden contact. This assumption allowed a decoupled treatment of the solid and the liquid. The results of these models are reasonable only for high thermal conductivity solids. More recently, models by Tio [10] and by diMarzo [11] have coupled the liquid and the vapor behavior, thus providing adequate predictions for all non-porous solid materials. However, both these models are for heat input by conduction from below the solid.

This paper addresses the modelling of the droplet evaporative process with radiant heat input from above the solid surface. The model makes use of some of the techniques previously developed by diMarzo [11] and of some of the results obtained for that case.

PHENOMENOLOGY

The initial temperature and thermal properties of the solid surface determine how the dropwise evaporation will occur. Evaporation, nucleate boiling and film boiling are the three possible modes observed. This modelling effort is limited to the evaporative mode which is observed at relatively low initial surface temperatures.

A brief overview of the phenomena is provided to explain the rationale for the various assumptions used in the derivation of the model. In the liquid droplet, heat is transferred by conduction since negligible convective motion is observed during the transient [12]. Two major remarks should be made for the specific case of radiant heat input from above the solid surface: a) the droplet vaporization is due in part to the direct radiant input and b) the droplet shape is greatly affected by direct radiation. These two observations are presented and discussed in detail by diMarzo [6]. The first observation is expected, and the contribution of the direct radiation to the evaporative process will be quantified. The second issue is more subtle since the droplet configuration has a very important impact on its evaporation. In the following, it will be shown that relatively low-frequency direct radiation from above is mostly absorbed in a very thin liquid layer at the liquid-vapor interface. This heat input has a strong effect in relaxing the liquid surface tension thus allowing the droplet to spread on the surface. The consequent increase of the wetted region and the thinning of the liquid layer are great contributors to the enhancement of the heat transfer between the solid-liquid interface and the liquid-vapor interface where evaporation takes place.

A last important consideration must be made concerning the solid thermal behavior. When the heat input is supplied by conduction through the solid, the temperature increases with depth in the normal direction to the solid surface. For the radiant heat input case, the maximum temperature of the solid is at its exposed surface and the temperature decreases with depth. Therefore, an evaporating droplet increases the heat flux toward the wetted region for the conduction case while it decreases the flux for the radiation case. This consideration is very important since it implies that, during the radiant transient, the contribution to the droplet evaporation due to the heat input from below the droplet is depressed. The enhanced heat transfer through the thinner droplet and the direct radiation oppose this effect and the overall evaporation time depends on the combination of all these compensating effects.

MODEL FORMULATION

Droplet Transient Configuration

One of the most relevant input parameters to the model is the description of the transient droplet configuration on the solid surface. Two seminal contributions by Chandra [13] and by Zhang [14] illustrate the droplet behavior at the beginning and at the end of the evaporative process. Based on this information, the original assumption (common to all the previous models) of a droplet which has a segment of a sphere geometry for the duration of the evaporative transient must be revised. This

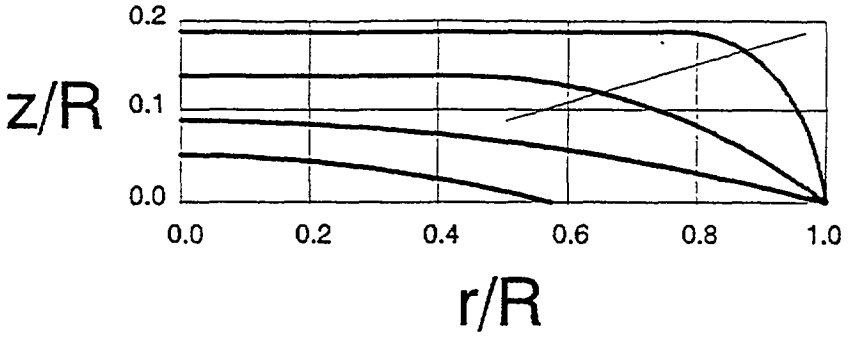

FIGURE 1 Modelled transient geometrical configuration of the droplet.

configuration is fully characterized by a single shape parameter β (defined by Bonacina [2] as the ratio of the radius of the wetted area under the deposited droplet and of the equivalent spherical radius of the droplet prior to deposition). This representation needs to be updated, especially in the early portion of the transient, in light of the evidence compiled by Chandra [13] which clearly demonstrated that a flattened shape exists after deposition. This modification of the droplet shape configuration requires the introduction of a second parameter, namely the liquid-vapor-solid contact angle θ.

The resulting shape with these two parameters has been characterized by considering the value of the parameter β at deposition and the values of the parameter θ at deposition and at the onset of the shrinkage of the wetted region which occurs when θ reaches its receding value. The receding angle, θ_r, is defined as the minimum liquid-vapor-solid contact angle consistent with the balance of the surface tension and surface adhesion forces. When the contact angle reaches this limiting value, additional reduction in the droplet volume will cause shrinkage of the wetted surface.

The first assumption in modelling the transient droplet configuration is that the droplet shape can be characterized as a segment of a sphere once θ reaches the receding value. This assumption is reasonable since the surface tension must first reconfigure the liquid-vapor interface (to minimize its surface area) before it can shrink the solid-liquid interface. The initial value of the parameter β_o identifies the radius (i.e., the area) of the solid-liquid interface up to the receding conditions. Therefore, the value of θ_r (given the solid-liquid interfacial area) identifies a unique volume of liquid at the receding conditions. This droplet configuration is used as a milestone in the transient configuration since, for any subsequent times, the droplet will retain the same aspect ratio; thus, it is fully characterized.

The second assumption in the modelling of the transient droplet configuration is needed to unequivocally define the gradual transition from the initial configuration to the configuration at the receding conditions. This assumption states that the droplet apex will always be less or equal to its initial value. Therefore, the droplet apex at the receding condition constitutes a minimum value for the initial value of the droplet apex and thus a maximum bound for the angle θ_o. Note that another upper bound of θ_o is obtained by Chandra [13] at 90° for evaporating and boiling droplets (nucleate boiling).

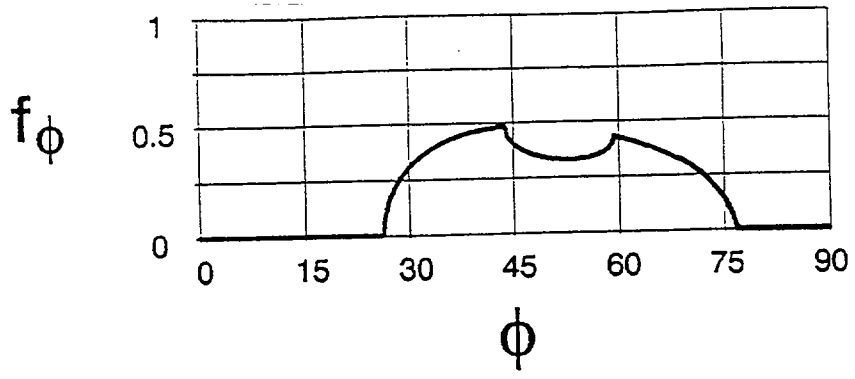

FIGURE 2 Fractional surface area coverage (data from [6]).

The minimum value of the angle θ_o is obtained if a spherical segment configuration is assumed at deposition. To unequivocally set the initial droplet configuration, one may want to neglect the small recoiling effect described by Chandra [13] and conclude that θ_o should be the largest possible. This final assumption leaves two possibilities open; the value of θ_o is equal to the smaller of: a) its maximum bound set by the value of the droplet apex at the receding conditions or b) $\theta_o = 90°$. Note that, for the second case, it follows that the droplet apex at deposition is larger than at the receding conditions.

Consider the intersection of the tangents to the droplet liquid-vapor interface at the droplet apex and at the liquid-vapor-solid contact point. One can identify such an intersection point at deposition and a similar point at the receding conditions. For case a) a straight line connecting these two points is horizontal while for case b) it is depicted in Fig. 1. By constraining the intercept of the two tangents to be on this line, one obtains a condition that insures a gradual change in the droplet geometrical configuration which is reasonably consistent with the experimental observations [13]. Figure 1 provides a set of geometrical configurations that illustrate the typical results of this model.

Direct Radiation in the Liquid Layer

A significant effort has been devolved to capture the main features of the direct radiation contribution to the water droplet evaporation while retaining a simple approach amenable to the model formulation. The first step is to characterize the specific radiant source. For the data obtained by diMarzo [6], the geometry of the radiant heat source has been described in Fig. 2 where two electric radiant panels are located above the surface and are identified in terms of their respective fractional surface area coverage at various polar angles ϕ above the solid surface. The following assumptions are made: a) the radiant panels behave as black bodies; b) the radiation scattering within the water droplet is negligible; c) the liquid-vapor interface is horizontal and flat; and d) the radiation reaching the liquid-solid interface is completely absorbed by the solid. The volumetric heat absorption in the liquid layer is given as:

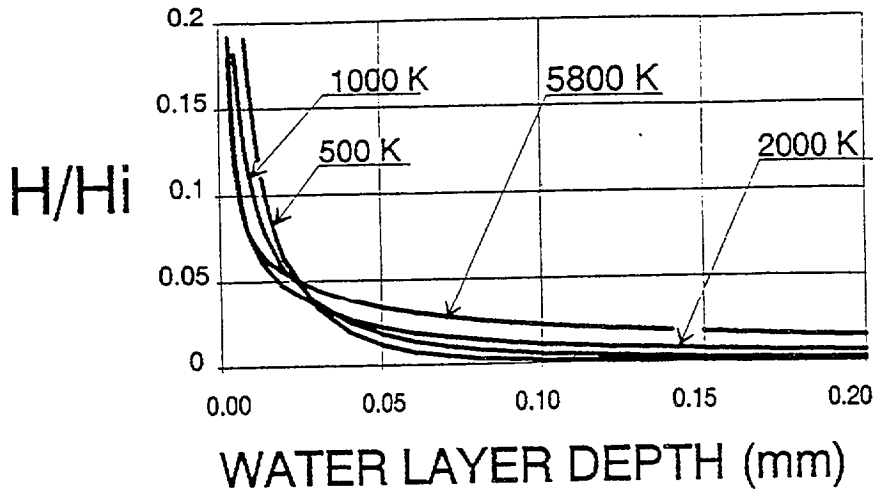

FIGURE 3 Normalized heat absorption in the liquid due to direct radiation (data from [6]).

$$H = 2\int_0^{\infty} E_{b,\lambda}\,\kappa_\lambda \int_0^{\pi/2} \frac{1}{\mu} f_\phi \cos\phi \sin\phi\,(1-\rho_\phi)\, e^{-\frac{\kappa_\lambda(\delta - z)}{\mu}}\, d\phi\, d\lambda \qquad (1)$$

The absorption coefficient κ_λ is a very strong function of the wave length λ, the direction cosine μ is given by the Snell's law, the fractional surface area coverage f_ϕ is obtained from Fig. 2, and the reflectivity ρ_ϕ is less than 0.1 for ϕ less than 65° and is given by the electromagnetic theory. The direct radiation into the water layer for the geometrical configuration used by diMarzo [6] is shown in Fig. 3. The volumetric heat absorption is high in a thin layer near the liquid-vapor interface (consider a layer thickness of about 0.05 mm). This is true over a broad range of the radiant surface temperature. Therefore, one can split the direct radiation in three parts: a) an interfacial flux term F (which is the integral of H over the thin layer thickness); b) a volumetric heat absorption term H which can be considered a constant, uniformly distributed heat source throughout the liquid layer; and c) a residual term which accounts for the incoming radiation at the solid-liquid interface. This last term is evaluated from an energy balance by deducting from the incoming radiant flux at the liquid-vapor interface the two previous terms.

Careful consideration must be given to the fact that the liquid-vapor interface is not flat. The flat surface assumption is useful to obtain simple results as shown in Fig. 3. However, a significant error can be introduced in the evaluation of the total incoming radiation when significant radiant surfaces are present at large polar angles ($\phi > 60°$). To rectify this problem, a multiplier must be introduced which accounts for the liquid-vapor interface orientation given the transient geometrical configuration of the droplet.

Modelling of the Liquid Layer

The results of the coupled model proposed by diMarzo [11] show that the heat transfer by conduction in the liquid layer is mostly one-dimensional in the direction normal to the solid-liquid interface. This is true everywhere and at all times with the exception of the region in the immediate proximity of the droplet edge where the radial component of the flux may be as large as ten percent of the total flux. The thinner geometrical configuration of the droplet subjected to the direct radiant field reinforces the assumption that the liquid may be treated as a one-dimensional conduction medium with generation (uniform internal generation is used to account for the residual contribution of the direct radiation not absorbed in the proximity of the liquid-vapor interface).

The one-dimensional modeling of the transient heat conduction in the liquid region encompasses three sub-models: a) initial contact closed-form solution; b) full transient diffusion equation; and c) quasi-steady state conduction equation. In the early portion of the transient, the liquid layer behaves as a semi-infinite solid while the heat wave propagates through its thickness. The solution of this problem is the classical solution for two semi-infinite solids (initially at different temperatures) brought into sudden contact [15]. Note that this solution is valid for a very short time (fraction of a second) especially where the liquid layer is thin (i.e. at the droplet edge). The relevance of this sub-model is to provide a smooth temperature profile in the liquid and a heat flux at the solid-liquid interface to initiate the numerical computations.

When the heat wave through the liquid reaches the liquid-vapor interface, the full transient diffusion equation sub-model is used. The diffusion equation written for the liquid yields a tri-diagonal matrix solution (with the one-dimensional heat flux approximation used here). At the time when this full transient solution is first used, the temperature profile is given by the closed-form solution for the two semi-infinite solids brought into sudden contact. At any subsequent time, the temperature at $z = 0$ is given by the solution of the semi-infinite solid which will be discussed in the following. The liquid-vapor boundary condition at $z = \delta$ (where $\delta(r)$ is given by the transient droplet configuration model) can be written as [11]:

$$-k_l \nabla T \cdot \hat{n} = 0.62 \left(\frac{h_c \Lambda}{c_a Le^{2/3}} \right) \frac{x_i - x_a}{1 - x_i} + h (T_i - T_a) - F \qquad (2)$$

Note the term F which describes the direct radiation contribution absorbed near the liquid-vapor interface. This term is configured as an interfacial heat flux since the layer thickness of 0.05 mm (see Fig. 3) is much smaller than the computational grid size.

When the liquid heat capacity term becomes small (i.e: the transient solution and the quasi-steady state solution are within less than 3 percent), the quasi-steady state conduction equation sub-model takes over. This third sub-model provides a very fast solution for the liquid layer. At the solid-liquid interface, the quasi-steady state conduction equation (with the constant heat source term discussed previously) yields a heat flux given by:

$$-k_s \frac{\partial T}{\partial z} = \frac{k_l}{k_l + A\delta}\left(\frac{A H \delta^2}{2 k_l} + H\delta - A T_s - B\right) \qquad (3)$$

The vapor-liquid boundary condition on the right hand side of Eq. (3) is linearized as a function of the interfacial temperature T_i (i.e.: $A\ T_i + B$). Note that the vapor molar fraction at the liquid-vapor interface is a function of the interfacial temperature. By expanding the boundary condition in a two-term series and by making use of the Clausius-Clapeyron relationship to differentiate the molar fraction with respect to the interfacial temperature, A and B are obtained analytically.

The coupling of these solutions for the liquid region with the solid solution is done with a simple predict-correct method where the heat flux distribution is the input to the solid solution and the interfacial solid-liquid temperature distribution is the output. To this effect, note the formulation of Eq. (3) which readily provides the heat flux at the solid surface as a function of the interfacial temperature T_s.

To provide a general indication of the role played by the three sub-models, consider that: a) the first sub-model is applicable for a very short time at the initiation of the transient; b) the full transient sub-model is used for about sixty per cent of the transient thereafter; and c) the quasi-steady state sub-model takes over for the last forty percent of the transient.

Modelling of the Semi-Infinite Solid

The solid thermal behavior is described by the transient two-dimensional (r,z) diffusion equation. The boundary conditions provide full coupling at the solid-liquid interface and state that the droplet effect is negligible in the far field. The solution of this equation is obtained with a boundary element method previously used for the conduction case [11]. The details of this method have been presented in the cited reference and in a number of previous publications.

Closed-Form Solution

In addition to the previous model, a closed-form solution for the transient surface temperature distribution is presented. By assuming that the solid-liquid interfacial heat flux is constant and uniform, one can obtain the following expression [15]:

$$T_{s,0} - T = \frac{(q_c - q_o) R}{k_s} \int_0^\infty J_0(\lambda r) J_1(\lambda R)\, erf(\lambda \sqrt{\alpha_s t})\, \frac{d\lambda}{\lambda} \qquad (4)$$

This form is used during the evaporation transient (i.e., $t < \tau$). Thereafter, the following modified form is used:

$$T_{s,0} - T = \frac{(q_c - q_o) R}{k_s} \int_0^{\infty} J_0(\lambda r) J_1(\lambda R) \{erf(\lambda \sqrt{\alpha_s t}) - erf[\lambda \sqrt{\alpha_s (t-\tau)}]\} \frac{d\lambda}{\lambda} \qquad (5)$$

This solution is in good agreement with the experimental data and the numerical computations for the conduction case [11]. For the case under consideration here, the closed-form solution refers to the heat associated with the droplet volume vaporized by conduction. The portion of the liquid vaporized by direct radiation will be excluded from the term q_c which represents the average heat flux transferred to the droplet during the whole evaporative transient through the solid-liquid interface (i.e., πR_o^2). Note that this solution requires as input the total evaporation time τ as well as the fraction of the vaporization heat input due to direct radiation which are outputs of the previous model.

MODEL VALIDATION

The results of the model are compared with the experimental findings of diMarzo [6]. The measured and calculated total evaporation times are within less than 10 percent (which is the scatter of the experimental data).

The surface temperature distribution of the model is compared with the experimental measurements [6] in Fig. 4. The data are for two initial solid surface temperatures and for the same droplet volume. Some discrepancies are observed during the transient after the droplet evaporation. However, as time passes (i.e., $t > 1.3\ \tau$), they tend to disappear.

Overall, the model predictions are in good agreement with the data. Additionally, the temperature distributions obtained with the closed-form solution are also plotted (dashed lines) to show that Eqs. (4) and (5) provide a reasonable representation of the phenomena. The total evaporation time and the evaporative component due to the direct radiation must be known in advance to use the closed-form solution. The relevance of this solution is for its use in the formulation of multi-droplet models for the prediction of the performance of sparse sprays. Therefore, the closed-form solution should be regarded as a useful fitting function to concisely represent the transient surface temperatures.

Note that the infrared thermography, used to acquire the data, is unable to provide data for the temperature at the solid-liquid interface. It is interesting to note the different behavior of the closed-form solution and of the model in the wetted region. The results are consistent with the different boundary conditions (i.e., uniform flux for the closed-form and a coupled liquid-solid condition for the model).

DISCUSSION

The validated model can be used to gain additional insight into the evaporative transient phenomena. One aspect worth considering is the effect of the initial value of the liquid-gas-solid contact angle. As pointed out previously, there is a range of values which is bounded by a flattened shape and a spherical cap. The first question concerns the

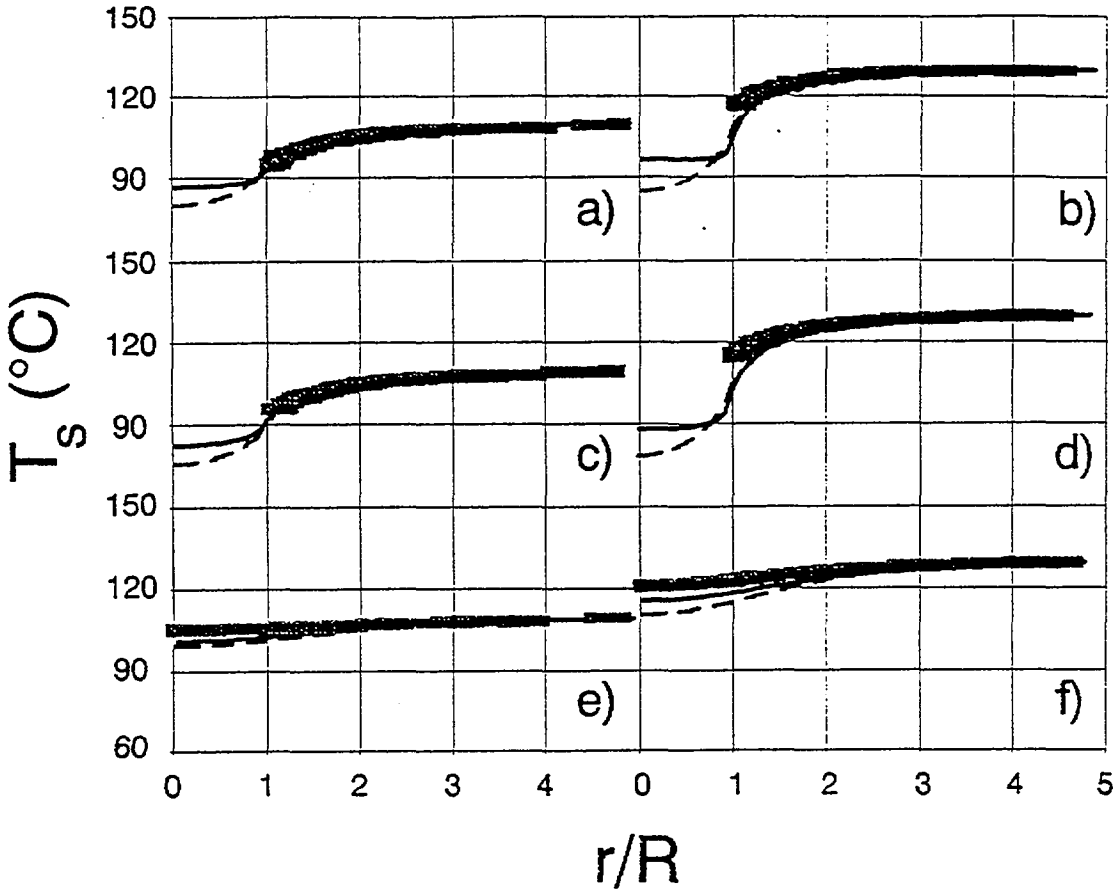

FIGURE 4 Model and closed-form solution validation (V = 10 μl). Data (from [6]): shaded; model: solid line; closed-form: dashed line. a),c) and e): $T_{s,o}$ = 110 °C at 0.3, 0.9 and 1.1 t/τ. b), d) and f): $T_{s,o}$ = 130 °C at 0.3, 0.9 and 1.1 t/τ.

sensitivity of the results with the initial value of the contact angle. The model indicates that little effect is observed in the overall evaporation time. Figure 5 illustrates the transient behavior of β, of the ratio R/R_o (which characterizes the shrinkage of the wetted region) and of θ for the maximum and minimum initial values of this parameter. Note that the uniqueness of the value at the receding conditions and the invariance of the total evaporation time with θ_o is reflected in the independence of the shape parameter and radius of the wetted region from the initial value of the contact angle. Chandra [13] reports values of the contact angle at deposition between 32° and 90° for conditions similar to the one reported here. The data from diMarzo [6] are in reasonable agreement with the model estimates.

Another relevant aspect is the direct radiation contribution to the evaporative process which has been discussed previously. According to the model computations, the evaporative component by direct radiation grows more slowly than the solid-liquid interfacial flux with increasing initial solid surface temperatures. Table 1 summarizes these findings and also provides the total evaporation time for the various cases.

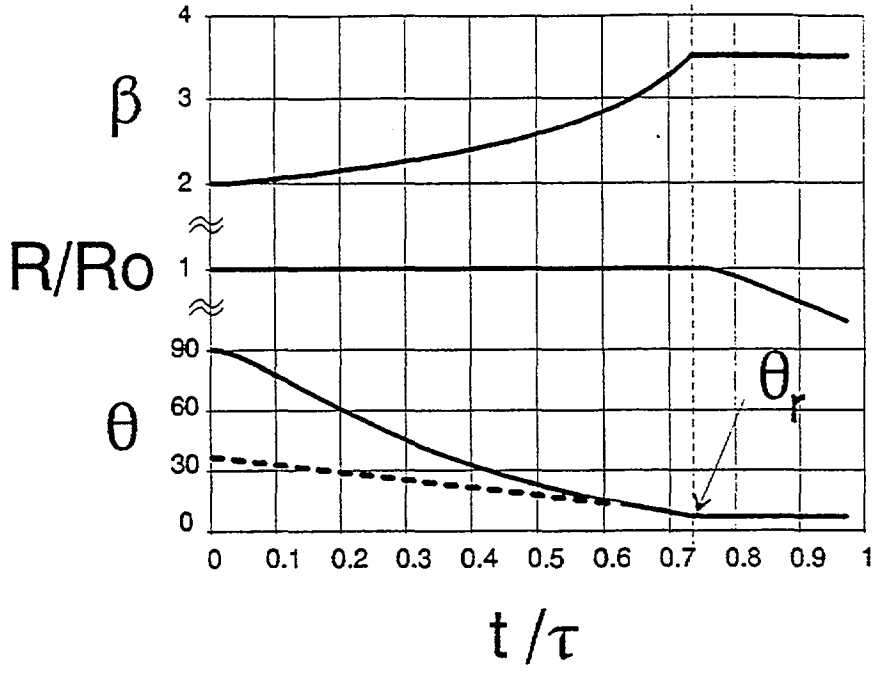

FIGURE 5 Transient behavior of the parameters governing the droplet shape ($T_{s,o}$ = 130 °C; V = 10 μl) θ_o maximum: solid line; θ_o minimum: dashed line

TABLE 1 Evaporation time, radiant and conductive heat fluxes for various $T_{s,o}$

$T_{s,o}$ [°C]	τ [s]	q_c [kW/m^2]	q_r [kW/m^2]
90	103	5.0	5.5
100	78	9.1	5.8
110	58	12.6	6.1
120	46	17.3	6.5
130	37	22.8	6.9
140	31	28.4	7.2

CONCLUSIONS

A model has been presented which predicts the transient thermal behavior of the coupled droplet-solid system for evaporative cooling due to radiant heat input. The transient droplet shape is modeled introducing a shape parameter and the liquid-gas-solid contact angle. The model predicts the total evaporation time and the transient temperature distribution over the solid surface. A closed-form solution is suggested as a simple fitting routine to represent the solid surface thermal behavior. The closed-form solution and the model results are in good agreement with the experimental data. The closed-form solution will be used to represent the solid surface temperature distribution

in multi-droplet models which simulate the cooling effect of sparse sprays.

ACKNOWLEDGEMENTS

This study has been supported by the Building and Fire Research Laboratory of the National Institute of Standards and Technology. The authors wish to express their gratitude to Drs. Baum and Evans for their guidance and encouragement.

REFERENCES

1. Toda, S., "A Study of Mist Cooling. First Report: Investigation of Mist Cooling," Heat Transfer, Japanese Research, 1: 3, 39-50, 1972.
2. Bonacina, C., Del Giudice, S. and Comini, G., "Dropwise Evaporation," Transactions ASME, Journal of Heat Transfer, 101: 441-446, 1979.
3. Inada, S., Mikasaka, Y. and Nishida, K., "Transient Heat Transfer for a Water Drop Impinging on a Heated Surface," Bulletin of JSME, 28: 246, 2675-2681, 1985.
4. Makino, K. and Michiyoshi, I., "The Behavior of a Water Droplet on Heated Surfaces," International Journal of Heat and Mass Transfer, 27: 781-791, 1984.
5. Takano, T. and Kobayasi, K., "Vaporization Behavior of a Single Droplet Impinging on a Heated Surface With a Flame-Sprayed Ceramic Coating," Heat Transfer, Japanese Research, 20: 1-17, 1991.
6. diMarzo, M., Kidder, C.H. and Tartarini, P., "Infrared Thermography of Dropwise Evaporative Cooling of a Semi-Infinite Solid Subjected to Radiant Heat Input," Experimental Heat Transfer, 5: 101-114, 1992.
7. Dawson, H.F., and diMarzo, M., "Multi-Droplet Evaporative Cooling: Experimental Results," AIChE Symposium Series, 89: 26-35, 1993.
8. Seki, M., Kawamura, H. and Sanokawa, K., "Transient Temperature Profile of a Hot Wall Due to an Impinging Liquid Droplet," Transactions ASME, Journal of Heat Transfer, 100: 167-169, 1978.
9. diMarzo, M. and Evans, D.D., "Evaporation of a Water Droplet Deposited on a Hot High Thermal Conductivity Surface," Transactions ASME, Journal of Heat Transfer, 111: 210-213, 1989.
10. Tio, K.K. and Sadhal, S.S., "Thermal Analysis of Droplet Spray Evaporation from a Heated Solid Surface," Transactions ASME, Journal of Heat Transfer, 114: 220-233, 1992.
11. diMarzo, M., Tartarini, P., Liao, Y., Evans, D. and Baum, H., "Evaporative Cooling Due to a Gently Deposited Droplet," International Journal of Heat and Mass Transfer, 36: 4133-4139, 1993.
12. Ostrach, S. and Pradhan, A., "Surface-Tension Induced Convection at Reduced Gravity," AIAA Journal, 16: 5, 419-424, 1978.
13. Chandra, S. and Avedisian, C.T., "On the Collision of a Droplet With a Solid Surface," Proceedings of the Royal Society, 432: 13-41, 1991.
14. Zhang, N. and Yang, W.J., "Natural Convection in Evaporating Minute Drops," Transactions ASME, Journal of Heat Transfer, 104: 656-662, 1982.
15. Carslaw, H.S., and Jaeger, J.C., Conduction of Heat in Solids, Clarendon Press, Oxford, 87-88, 214-216 and 264, 1959.

PART FOUR

Experiments describing the cooling effect of a sparse spray with uniform droplet size are conducted. The sparse spray model is based on the superposition of the cooling effects of the single droplets. The single droplet cooling effects are evaluated as follows:

1. In the near-field, the closed-form solution, based on constant and uniform heat flux at the solid-liquid interface, is modified to account for the contribution of the direct radiation and to the effect of direct radiation on the droplet shape.
2. In the far-field, an instantaneous point sink is used to approximate the effect of the evaporating droplets.

The sparse spray model is the main product of the research program. Note that this model requires the input of the single droplet model described in the PART THREE.

H.F. Dawson & M. diMarzo, Multi-droplet evaporative cooling: experimental results, AIChE Symposium Series 89 (1993) 26-35.
P. Tartarini, Y. Liao & M. diMarzo, Numerical simulation of multi-droplet evaporative cooling, Heat and Technology 11 (1993) 98-107.
M. diMarzo & S. Tinker, Evaporative cooling due to a sparse spray (1995) unpublished manuscript.

PAPER # 12

Multi-Droplet Evaporative Cooling: Experimental Results

H. F. Dawson and M. di Marzo

Mechanical Eng. Dept., University of Maryland, College Park, MD 20742

Experimental results concerning the evaporative cooling of a Macor tile subjected to a random droplet distribution are reported. The heat input is provided by three radiant panels above the solid surface. The spatial transient temperature distribution over the solid surface and its average surface temperature history are described.

INTRODUCTION

There are a number of engineering and safety applications in which a hot surface is subject to a spray of water droplets. Fire suppression in nuclear powerplants, in process chemical storage, and in fuel storage facilities is a primary application which has inspired a number of experimental and theoretical studies on the phenomena associated with spray cooling. Schoen and Droste [1] investigated the spray cooling of flame engulfed LPG storage tanks to guard against bursting. Davenport [2] also recognized the importance of water spray systems in a study of LPG storage tanks exposed to a fire environment, while Ramskill [3] included spray cooling effects in the computer modeling of exposed tanks. Atallah and Schneider [4] considered the use of water spray curtains as a means of vapor dilution of liquid natural gas in accident situations.

Extensive work has been conducted on the more fundamental aspects of water droplets evaporation. Klassen and diMarzo [5] and Klassen et al. [6] provide a thorough investigation of the evaporation rate of a single droplet gently deposited on low thermal conductivity ceramic surface heated by conduction from below. DiMarzo et al. [7] extended the single droplet experiments to the case of radiant heat input which models more realistically a fire environment. In these studies, the droplet configuration on the solid surface (described by Chandra and Avedisian [8]) is related to the evaporation time, yielding shorter times under conditions of radiant heating.

Research covering the full range of vaporization has been done by Makino and Michiyoshi [9]. DiMarzo and Evans [10,11] formulated the transient conduction problem for an evaporating droplet heated from below by using a simplified, constant and uniform temperature boundary condition at the liquid-solid interface during evaporation. Seki [12] used a similar boundary condition in a study of the transient temperature profile of a hot wall. Numerical integration of the equations in the work by diMarzo and Evans was obtained successfully by diMarzo et al. [13].

The present work constitutes part of a long-term study aimed at modeling the extinguishment of solid fuel fires. In particular, the research presented here investigates the cooling of a radiantly heated solid surface by multiple water droplets evaporation. It is an extension of the previous research efforts given in References [5,6,7]. This study is concerned only with cooling phenomena in a radiant, fire-like environment, where no combustion (hence, no extinguishment) is present. The heated material used is Macor, a glass-like ceramic.

The purposes of this study are: a) to investigate both the temporal and spatial behavior of the surface

temperature of a low thermal conductivity material subject to spray cooling and radiant heat input; b) to continue development of the digital image analysis techniques applied to infrared thermography; c) to gain additional insight into evaporative cooling phenomena, especially for the case of multiple water droplets and d) to obtain data for the validation of a computer code modeling multi-droplet evaporative cooling with radiant heat input.

EXPERIMENTAL APPARATUS

The experimental apparatus is shown in Figure 1. A droplet generator hangs vertically and works in conjunction with a positioning mechanism. Water droplets ejected from the generator impinge upon the Macor tile (square shape with 15.2 cm sides and 2.54 cm thickness) mounted below. The tile rests on a chilled plate to provide a controlled boundary condition at its lower surface. Two radiant panels are positioned on opposite sides of the tile and radiate downward onto the surface at an angle of 30° to the vertical. A third radiant panel surrounds the perimeter of the tile to provide uniform heating to the sides of the Macor. An infrared camera is mounted above and to the side of the tile at an angle of 30° from vertical, and views the surface through a water cooled chilled pipe positioned at the same angle.

The droplet generator produces water droplets with an average volume of 10 ± 1 μl. The primary mechanism for droplet formation is a water filled cavity internal to the generator. A solenoid driven piston produces an indentation in a plastic disk which seals the top of the water filled cavity, thus ejecting a droplet from the generator. The mass flux of the water impinging on the surface is controlled by a time delay relay connected to the solenoid.

A random distribution of water droplets on the surface is achieved by a positioner for the droplet generator. The positioner consists of an aluminum plate with a 25.4 cm hole in the center. Three solenoid driven plastic bumpers are situated around the perimeter of the hole, and simultaneously move radially inward when the solenoids are energized. The droplet generator hangs vertically by four wires in the center of the hole, and motion of the generator is produced when it collides with the moving bumpers. Both the shape of the bumpers and the frequency at which they are activated are optimized to produce a random distribution. The droplets impinge over

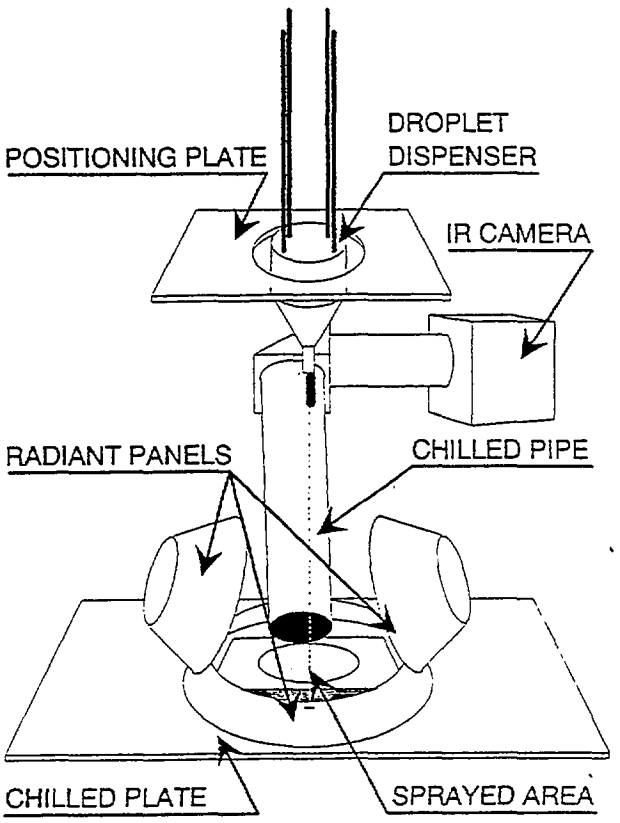

Figure 1. Experimental Apparatus

a circular region with an area of 0.38 cm^2. A typical droplet distribution is shown in Figure 2. This distribution is obtained by marking the landing site of about 200 consecutive droplets delivered by the droplet generator.

The radiant panels used to provide heat input to the surface simulate the heating conditions encountered in an actual fire environment. All three panels are conical in shape and capable of temperatures in excess of 800 °C. Furthermore, they may be approximated to radiate as black-bodies. The panels are connected in a delta circuit and powered by a 208 volt three-phase supply. A temperature feedback loop between the panels and an Omega CN-7100 digital controller maintains the set point temperature of the panels.

An Inframetrics Model 525 infrared camera is the primary data acquisition instrument. The camera uses a 0.61 m focal length closeup lens, and is positioned to view the droplet impingement region of

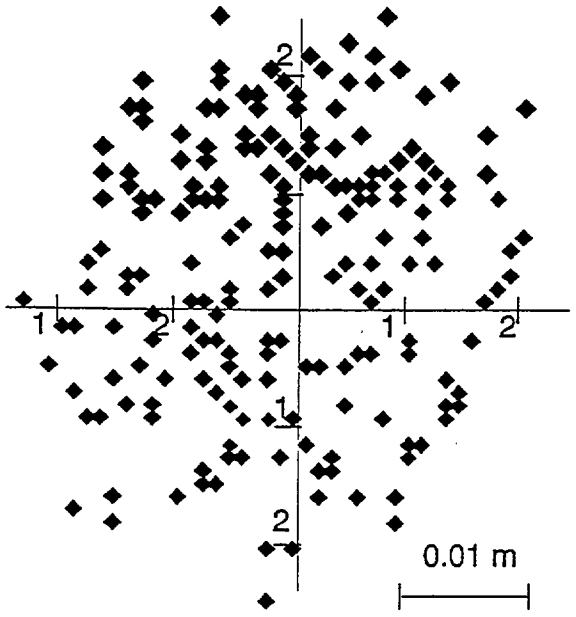

Figure 2. Typical Droplet Distribution

the surface. It produces a real time, monochrome thermal image of the relative temperature distribution on the surface. This image is recorded with a Sony high resolution 8 mm VCR (Hi8) over the duration of an experimental run, producing a complete record of the thermal phenomena occurring on the surface. The geometric orientation of the chilled pipe and the radiant panels is such that reflected radiation from the panels hits the cool, black inner wall of the chilled pipe and is absorbed before reaching the infrared camera. This is important to ensure that only emitted radiation from the surface is recorded as data.

The Macor tile is attached to the chilled plate using Dow Corning silicone heat sink compound. Cold water circulates through the chilled plate, holding the bottom surface temperature of the Macor at a constant value of about 30 °C. This establishes a linear temperature profile between the upper and lower surfaces of the tile, and a uniform temperature on the upper surface before droplets begin to fall.

The relevant properties of Macor are listed in Table 1. Important to note are its relatively high emissivity and low thermal conductivity. Additionally, it has the ability to withstand high thermal stresses, giving a smooth, crack free surface.

Table 1. Macor Properties

Density (kg/m^3)	2520
Thermal Conductivity ($W/m \cdot °C$)	1.297
Specific heat ($J/kg \cdot °C$)	888.9
Emissivity	0.84

EXPERIMENTAL PROCEDURE

The parameters being varied in the experiments are the mass flux of the impinging spray and the initial surface temperature of the solid. In order to ensure consistent thermal conditions, experiments at three different mass fluxes are performed at the same initial temperature in one experimental session. Five initial temperatures of 110 °C, 130 °C, 150 °C, 160 °C, and 180 °C are investigated, while the mass fluxes at each temperature are chosen to preclude the possibility of a surface flooding condition. Over the set of all experiments, these range from .24 $g/m^2 \cdot s$ to 1.6 $g/m^2 \cdot s$. These mass fluxes are nearing the flooding conditions set by the criterion of Grissom and Wierum [14]. It should be noted that the initial temperature of 160 °C corresponds to the onset of nucleate boiling for the Macor surface, while that of 180 °C is in the full nucleate boiling regime. The remaining initial temperatures fall in the evaporative region. The major steps of the experimental procedure are given below.

The water used in the experiments is deionized and degassed. The removal of condensible gasses from the water prior to experiment initiation is essential to obtaining the most controllable experimental conditions. Gasses coming out of solution during the droplet evaporation might alter the configuration of the droplet upon the surface or trigger the onset of nucleate boiling in ways which can be unwieldy to quantify. Water degassing is achieved by consecutive cycles of freezing, vacuum pumping, and thawing. Droplets are tested for bubbles by viewing their evaporation upon a heated surface, and deemed acceptable when no bubbles appear. A sealed water feed to the droplet generator prevents atmospheric gasses from degrading the purity of the final degassed water.

To allow the surface to reach the desired initial temperature, the radiant panels are activated at least two hours prior to experiment initiation. This allows the heater temperature to stabilize to the temperature set on the controller, and most importantly ensures

that the temperature of the solid has reached a steady state condition. The surface temperature is monitored with an Omega thermocouple probe (K-type) read by an Omega digital thermocouple readout. The probe is present on the surface during the heating transient to allow equalization of the probe and surface temperatures.

The infrared camera and all additional electronics (power supply and video components) are also activated two hours prior to experiments to minimize effects of thermal drift. Additionally, water is allowed to begin circulating through the chilled plate and chilled pipe at the time the radiant panels and electronics are turned on. At steady state, before droplets begin to fall, an infrared image of the surface at the initial temperature is recorded. This video image is then digitized using computer resident frame grabbing apparatus (to be described in detail) to assign an actual value to the shades of gray in the image. Ideally, since the surface temperature is uniform, the gray values of the image at each point on the surface are equal, with the exception of random deviations introduced by electronic noise. The average gray value of the surface is then correlated with the initial surface temperature reading to yield a linear relationship of the following form between the temperature at any point on the surface and the gray value at that location. The following expression provides the calibration for a particular initial surface temperature:

$$T = 1.165\ I + T_i \qquad (1)$$

The droplet volume is measured before every run at a given set of conditions. To do this, the droplet generator is turned on and allowed to run for approximately ten minutes to allow the system to stabilize. Fifty droplets are then collected in a beaker of known mass which is quickly capped to avoid evaporation of the droplets. A Metler electronic balance is used to obtain the mass of the water droplets and beaker, ultimately yielding the volume of the droplets. Over the set of all experiments run, droplet volumes range from 8.8 to 11 μl.

Ethyl alcohol is used to clean the surface between each experiment at a different mass flux to remove any impurities or film present. Alcohol sprayed on the surface is allowed to evaporate, and the surface is then rinsed with distilled water. This is repeated and the surface is then given time to return to the initial temperature.

For each experiment conducted at a particular set of conditions, droplets impinge upon the heated surface for a period of twenty five minutes while the infrared image is recorded onto videotape. During this time, the image being recorded can be viewed on a video monitor. For a few seconds before each recorded run on the videotape, a regular TV camera is used to record a portion of a blackboard containing pertinent information about the run (droplet volume, initial surface temperature, mass flux, heater temperature, ambient temperature, and chilled plate temperature). The information contained on the videotape is then sufficient to determine both transient and spatial temperature information about the surface in the experimental data processing and reduction.

DATA PROCESSING AND REDUCTION

At the completion of one set of experiments at a given initial temperature, data processing is performed. Two types of information can be obtained from the video record: a) the transient behavior of the average surface temperature and b) the spatial temperature distribution on the surface at any time into the transient. Common to both analyses is the video digitization system used to extract gray values from the recorded image. A Matrox MVP-AT frame grabber is used to digitize individual frames, of duration 1/30 of a second, into a discrete number of gray shades. Subroutine libraries included with the frame grabber (Imager-AT software) are linked with user written source code to access the gray value of each pixel of the digitized image individually. This value is then correlated with a temperature to perform the desired analysis. The specific method of analysis for each case is now discussed.

The transient behavior of the average surface temperature is obtained by digitizing individual frames of the recorded surface at intervals of 30 seconds starting at the beginning of the run. A computer program is used to average the gray values of every fifth pixel in the image, corresponding to 3717 pixels over a 5 cm x 5 cm region of the surface. An average pixel value for the surface at that particular time during the transient is thus obtained, which is then used with Equation (1) to determine the average surface temperature.

The resulting data are fit to a decaying exponential curve of the following form:

$$T = (T_i - T_{ss})\, e^{-t/\tau} + T_{ss} \qquad (2)$$

where τ is the time constant of the fit and T_{ss} the steady state temperature. Both of these parameters are adjusted to obtain the best fit. A total of 130 gray shades are used to resolve an average temperature range of 100 °C, resulting in a thermal resolution of 0.76 °C/gray shade.

To obtain the spatial distribution of the temperature at a specific time into the transient, each pixel in a digitized frame is accessed individually. From knowledge of the area of the viewed region and the pixel location in the image, an cartesian coordinate is determined along with the gray shade for each pixel. The temperature at a particular location is then determined from Equation (1). This is done for the same number of pixels as in the transient analysis, and the results plotted as a three dimensional surface of the temperature versus the cartesian coordinates (i.e. x and y). The spatial resolution achieved using these techniques is 0.14 mm/pixel, corresponding to a 512 (horizontal) x 480 (vertical) pixel image of a viewed region 7.2 cm x 6.7 cm. Note that the area of the viewed region is somewhat smaller than the wetted area. This is necessary to achieve the best focus with the infrared camera.

RESULTS AND DISCUSSION

Three dimensional plots of the temperature distribution on the Macor surface are shown in Figures 3(a-c), 4(a-c), and 5(a-c) for the indicated initial temperatures and mass fluxes. The results are especially notable in that they represent a detailed description of the temperature at any point on the surface, obtained with highly non-intrusive techniques. Each sequence of plots shows the surface temperature distribution at three different times; 1) early in the transient, 2) further on in the transient, and 3) at or approaching steady state. The most distinct features are the large dips in the temperature, especially at times early in the transient. These are regions where individual droplets have landed, and caused a rapid local cooling effect. The average surface temperature is seen to be still very near the initial value. At later times, the average surface temperature begins to drop

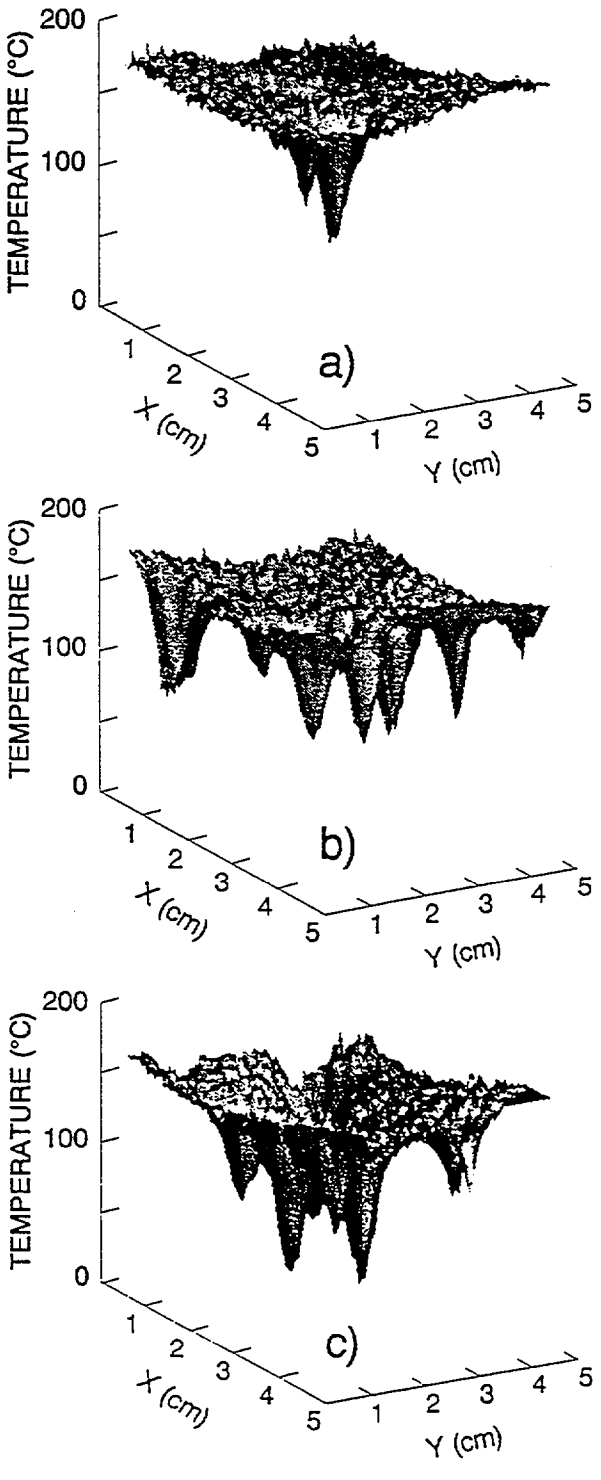

Figure 3. Solid Surface Temperature Distribution for T_i = 182 °C and G = 0.86 g/m²s (a: t = 5s; b: = 240s; c: = 600s)

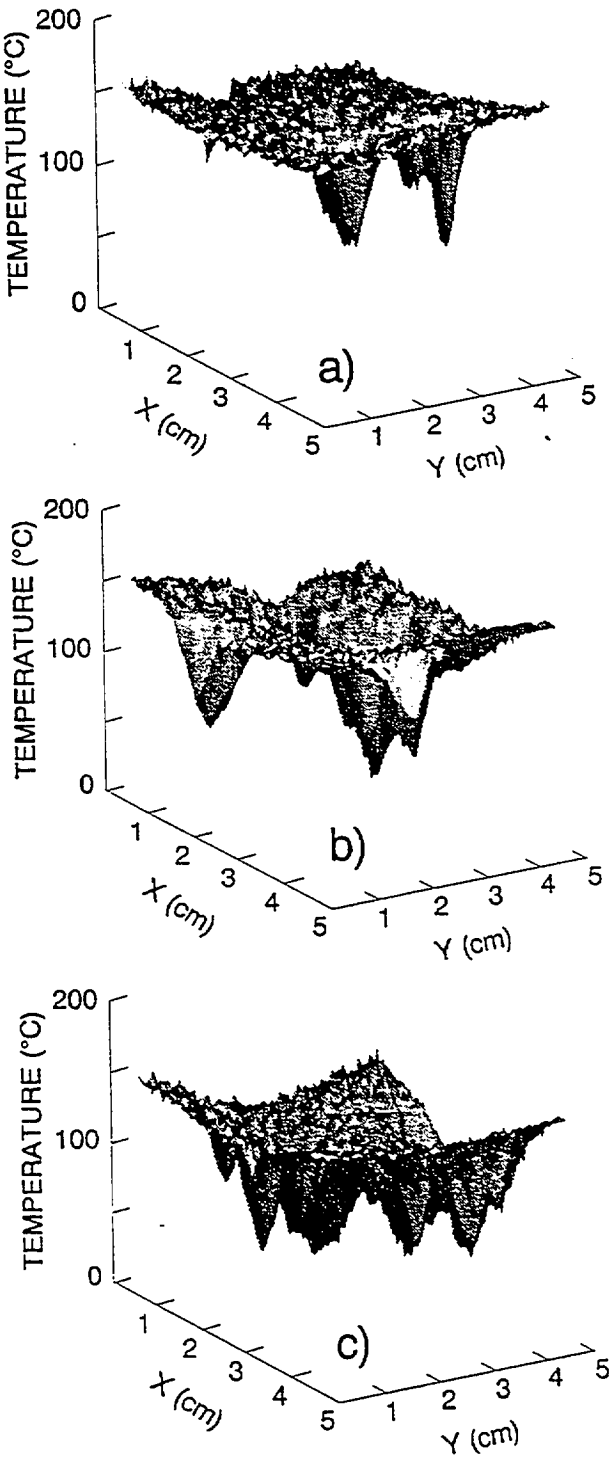

Figure 4. Solid Surface Temperature Distribution for T_i = 162 °C and G = 0.97 g/m^{2}s (a: t = 5s; b: = 240s; c: = 600s)

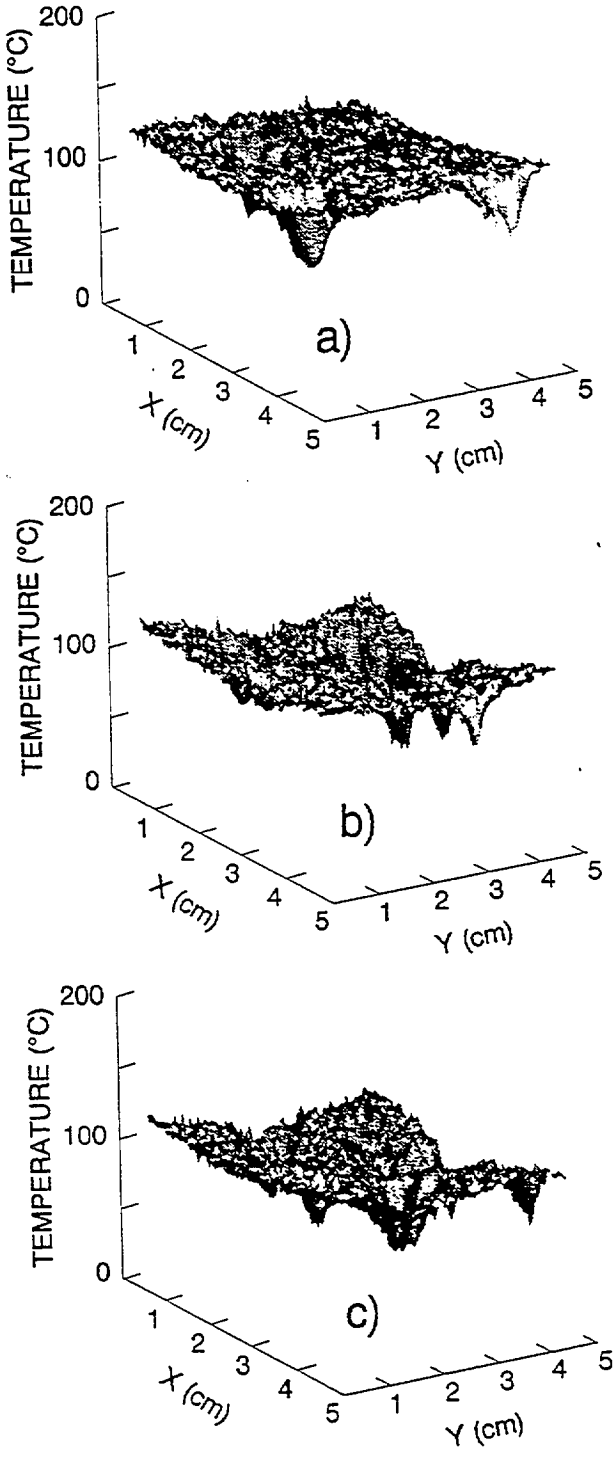

Figure 5. Solid Surface Temperature Distribution for T_i = 131 °C and G = 0.50 g/m^{2}s (a: t = 5s; b: = 240s; c: = 600s)

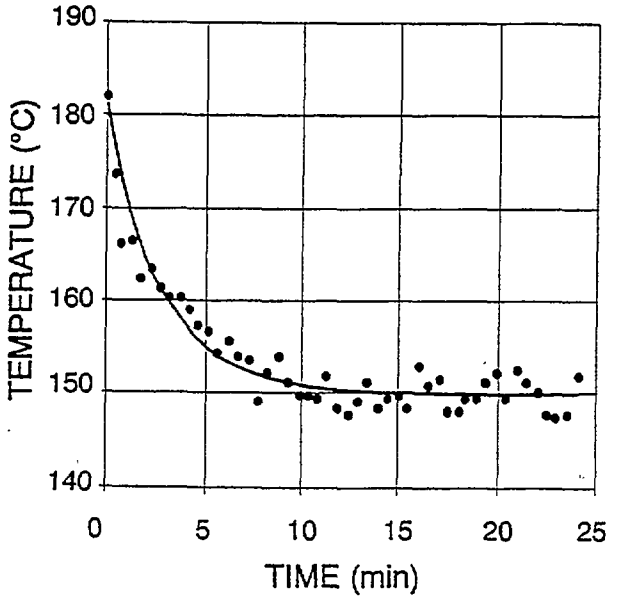

Figure 6. Transient Average Surface Temperature for T_i = 182 °C and G = 0.86 g/m^{2}s

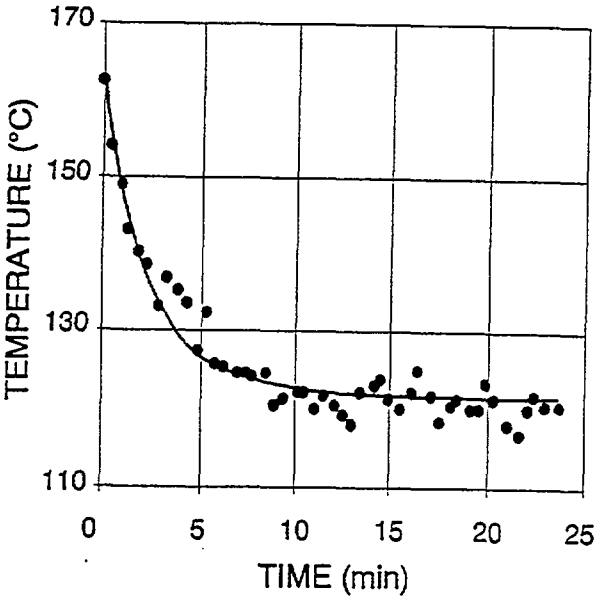

Figure 7. Transient Average Surface Temperature for T_i = 162 °C and G = 0.97 g/m^{2}s

from the initial value, since the droplets have cooled the surface sufficiently such that the effects of individual droplets tend to superimpose with one another for more uniform cooling. As the surface temperature approaches a steady state, the individual droplets become more difficult to discern and the plot surface more wave-like. An error of ± 2 °C is evident from the plots, and results primarily from variations in pixel intensity caused by surface irregularities and electronic noise.

Graphical results of the average surface temperature versus time are shown in Figures 6, 7, and 8. The raw data are shown along with the best fit exponential decay for each case. The initial temperatures shown include both convective and nucleate boiling. Examination of the plots reveals important features which can be seen in all the cases. The most significant is the clear decay to a steady state temperature. In all cases a steady state condition is reached at a time no later than ten minutes after initial droplet deposition. A comment on the oscillatory nature of the average surface temperature is necessary. Such behavior arises because only a portion of the actual sprayed area is viewed by the infrared camera. Therefore, at any time, there may be a different number of droplets

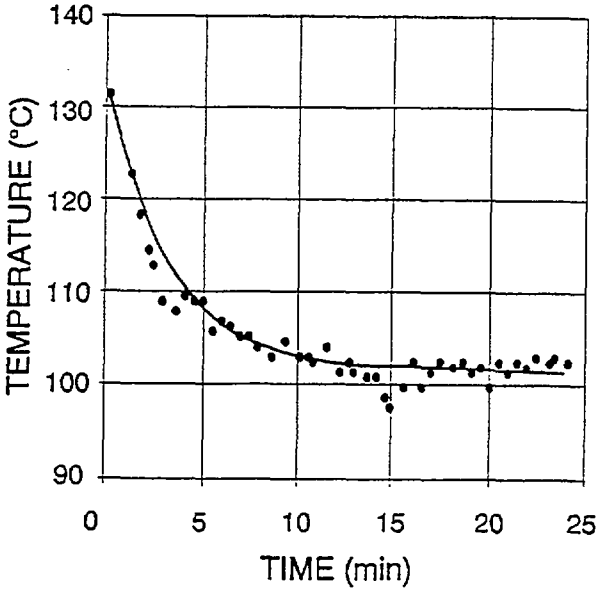

Figure 8. Transient Average Surface Temperature for T_i = 131 °C and G = 0.50 g/m^{2}s

on the surface than at other times, resulting in overall pixel intensity variations in the image.

An energy balance is performed on the hot surface to provide verification of the results by calculating a steady state temperature. Equating the heat input from the radiant panels to the heat released from the Macor by radiative exchange, convection, and conduction yields the following balance of terms:

$$\epsilon \sigma F T_h^4 = h(T_i - T_\infty) + \frac{k}{d}(T_i - T_b) \quad (3)$$

Note that the net conductance h embodies both convective and radiative mechanisms. Additionally, Kirchoff's Law for a gray surface has been used. At steady state the same energy balance is written as:

$$\epsilon \sigma F T_h^4 - \lambda G = h(T_{ss} - T_\infty) + \frac{k}{d}(T_{ss} - T_b) \quad (4)$$

By subtracting Equation (4) from Equation (3), one obtains:

$$\lambda G = h(T_i - T_{ss}) + \frac{k}{d}(T_i - T_{ss}) \quad (5)$$

Rearrangement provides an analytical expression for the steady state temperature:

$$T_{ss} = T_i - \frac{\lambda G}{h + \frac{k}{d}} \quad (6)$$

With h calculated from Equation (3) and used in Equation (6), the measured steady state temperature versus the calculated value is shown in Figure 9. Agreement of the best fit straight line is best at higher temperatures and deviates slightly at lower values. A likely explanation is that the view factor between the heaters and the surface, F = 0.26 (obtained by measuring the incident radiation), is slightly in error, which can have a significant effect on h and thus T_{ss}. Another possible source of error is that the temperature underneath individual droplets

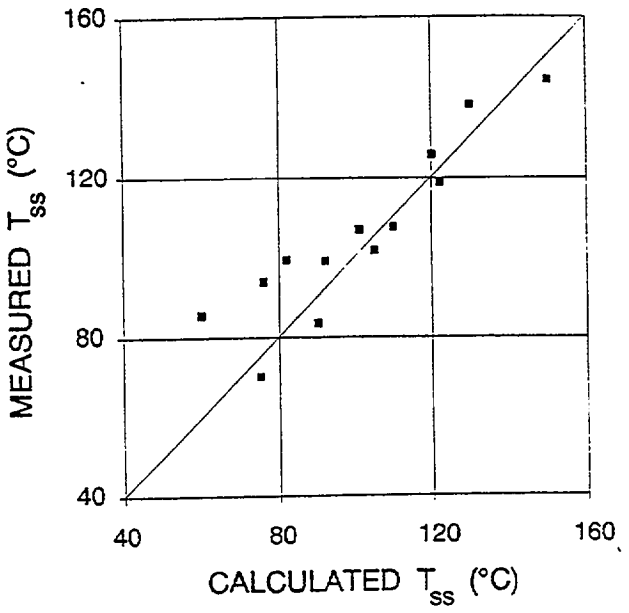

Figure 9. Experimental and Calculated Steady State Temperature

is under-estimated. This would occur because the calibration used to obtain the temperatures is only valid for the Macor surface. When the camera records a water droplet that has not yet evaporated, the calibration no longer applies since a water droplet and not the surface is being viewed. Approximately 10% of the surface is covered at a given time. This percentage of the average temperature drop underneath a droplet, approximately 40 °C, gives an estimate of 4 °C by which the average temperature is in error.

The best fit curve to the transient data is determined by inspection of the data to ascertain the steady state temperature used in the fit. The time constant τ is then adjusted to introduce the least spread in the points around the curve. It might be expected that at higher mass fluxes, τ would be smaller due to the increased cooling capacity of the higher flux spray. Accordingly, the time constants (deduced from the best fit of the data) from each experiment are plotted versus the mass flux in Figure 10. From the figure, no apparent relationship is evident, suggesting that the properties of the Macor may be the more dominant factors influencing the time scale of the phenomenon. Pursuing this idea, a general expression for the penetration depth in the

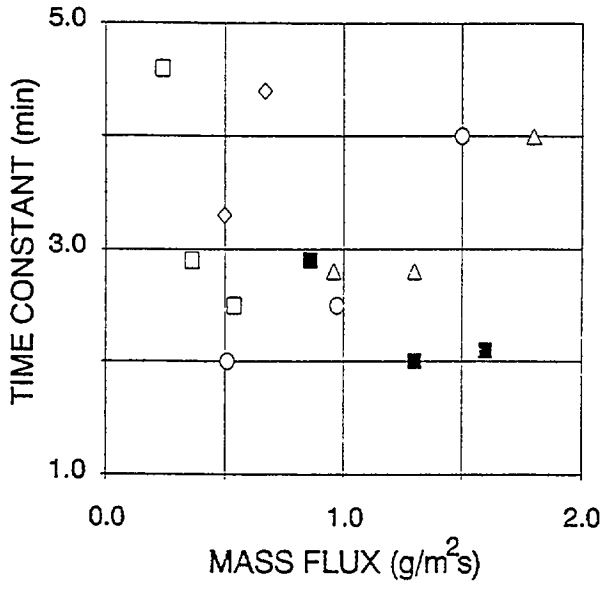

Figure 10. Transient Time Constant for Various Water Mass Fluxes and Initial solid Surface Temperatures (■: T_i = 182 °C; ○: T_i = 162 °C; △: T_i = 151 °C; ◇: T_i = 131 °C; □: T_i = 111 °C)

solid is given by:

$$\delta = \sqrt{\alpha \tau} \qquad (7)$$

Substituting 5.8 x 10^{-7} m^2/s for the thermal diffusivity of Macor, and an average τ of 170 seconds from Figure 10 yields δ = 1 cm. This can be compared to the radius of influence of a single droplet, as discussed by Klassen and diMarzo [5]. Essentially, it is a measure of the cooling effect a single droplet has upon the region surrounding it. On Macor, this corresponds to a circular region four times the radius of a droplet on the surface, or 0.5 cm. This is on the same order as δ, and suggests that the time constant is more closely linked to thermophysical properties of the material than to the impinging mass flux.

CONCLUSIONS

The spatial and temporal behavior of the temperature of a radiantly heated, low thermal conductivity surface cooled by multiple water droplets evaporation was experimentally investigated over a range of different initial surface temperatures and mass fluxes. For all conditions, the average surface temperature decreases exponentially with time before reaching a steady state value. The measured steady state temperature agrees well with that calculated from an energy balance, with the best agreement achieved by considering small variations in the view factor between the heaters and surface. Slight variations in the view factor, due to small inaccuracies in spatial measurements used to determine it, can result in over-estimation of the overall heat transfer coefficient, resulting in lowered calculated temperatures.

The spatial distribution of the surface temperature shows a decrease in the average temperature, as suggested by the transient results, and provides a thorough description of the temperature at a point on the surface at any time. There appears to be no strong correlation between the impinging mass flux and the time constant of the exponential temperature decay. A length scale determined using properties of the solid material suggests that the characteristic time scale of the phenomenon is more likely a function of these properties.

The data acquisition system used, employing digital image analysis and infrared thermography, provides a high degree of thermal and spatial resolution. Additionally, it represents a novel approach to non-intrusive temperature measurement for this type of application.

ACKNOWLEDGEMENTS

This research has been sponsored by a grant of the Building and Fire Research Laboratory of the National Institute of Standards and Technology.

NOTATION

d	thickness of Macor tile
F	view factor between radiant panels and surface
G	water mass flux
I	average gray value
h	overall heat transfer coefficient
k	thermal conductivity of Macor
T	temperature
T_b	Macor bottom surface temperature
T_i	initial solid surface temperature
T_h	radiant panel temperature

T_{ss} steady state surface temperature
T_∞ ambient temperature
t time

α thermal diffusivity of Macor
δ penetration depth
ϵ emissivity of Macor
λ water latent heat of vaporization
σ Stefan-Boltzman constant
τ time constant

LITERATURE CITED

1. Schoen, W. and B. Droste, "Investigation of Water Spraying Systems for LPG Storage Tanks by Full Scale Fire Tests," *Journal of Hazardous Materials*, 20, 73-82, (1988).

2. Davenport, J., "Hazards and Protection of Pressure Storage and Transport of LP-GAS," *Journal of Hazardous Materials*, 20, 3-19, (1988).

3. Ramskill P.K., "A Description of the "ENGULF" Computer Codes - Codes to Model the Thermal Response of an LPG Tank Either Fully or Partially Engulfed by Fire," *Journal of Hazardous Materials*, 20, 177-196, (1988).

4. Atallah, S., and A.L. Schneider, "LNG Safety Research in the USA," *Journal of Hazardous Materials*, 8, 25-42, (1988).

5. Klassen, M. and M. diMarzo, "Transient Cooling of a Hot Surface by Droplet Evaporation," *National Institute of Standard and Technology Report*, NIST-GCR-90-575, (1990).

6. Klassen, M., M diMarzo and J. Sirkis, "Infrared Thermography of Dropwise Evaporative Cooling," *ASME-HTD*, 141, 117-121, (1990).

7. diMarzo, M., C.H. Kidder, and P. Tartarini, "Infrared Thermography of Dropwise Evaporative Cooling of A Semi-Infinite Solid Subjected to Radiant Heat Input," *Experimental Heat Transfer*, 5, 101-104, (1992).

8. Chandra, S. and C.T. Avedisian, "On the Collision of a Droplet with a Solid Surface," *Proceedings of the Royal Society of London*, 432, 13-41, (1991).

9. Makino, K. and I. Michiyoshi, "The Behavior of a Water Droplet on Heated Surfaces," *International Journal of Heat and Mass Transfer*, 27, 781-791, (1984).

10. diMarzo, M. and D.D. Evans, "Dropwise Evaporative Cooling of High Thermal Conductivity Materials," *Heat and Technology*, 5, (1-2), 126-136, (1989).

11. diMarzo, M. and D.D. Evans, "Evaporation of a Water Droplet Deposited on a Hot High Thermal Conductivity Solid Surface," *Journal of Heat Transfer*, 111, 210-213, (1989).

12. Seki, M., H. Kawamura and K. Sanokowa, "Transient Temperature Profile of a Hot Wall Due to an Impinging Liquid Droplet," *Journal of Heat Transfer*, 100, 167-169, (1978).

13. diMarzo, M., P. Tartarini, Y. Liao, D.D. Evans and H. Baum, "Dropwise Evaporative Cooling," *ASME-HTD*, 166, 51-58, (1991).

14. Grissom, W.M. and F.A. Wierum, "Liquid Spray Cooling of a Heated Surface," *International Journal of Heat and Mass Transfer*, 24, 261-271, (1981)

PAPER # 13

HEAT and TECHNOLOGY
CALORE e TECNOLOGIA
Vol. 11 • No. 1-2 • 1993

NUMERICAL SIMULATION OF MULTI-DROPLET EVAPORATIVE COOLING

P. Tartarini (*), Y. Liao (**), M. di Marzo (**)

ABSTRACT

A theoretical study is carried out to predict the thermal behavior of a solid surface subjected to multi-droplet evaporative cooling. A single-droplet numerical code, which has been previously presented and validated, is used here to gain insight into the behavior of a surface subjected to dropwise evaporative cooling. On the basis of the single-droplet results, a generalized model is presented and a novel numerical code is formulated, which analyzes the effects of a multi-droplet evaporative transient on a low thermal conductivity solid surface. The main parameters that characterize the evaporative transient behavior are identified. Some numerical results obtained with this new model are presented and discussed.

INTRODUCTION

Dropwise evaporative cooling of a hot surface is a widely used technique in many engineering applications. For instance, it is commonly found in metallurgical, nuclear and electronic industries. Recently, it has also been used in the space station thermal control systems for equipment cooling.

The single-droplet cooling of hot surfaces has been studied extensively by many researchers. Numerous experimental works provide the basic understanding of the droplet cooling phenomena. Great emphasis has been given to the case of high solid surface temperature where nucleate and film boiling are the dominant heat transfer modes. Makino and Michiyoshi [1][2][3] provide the full range of the boiling curve for the evaporation of a water droplet on a heated surface. The heat transfer rate in the nucleate, transition and film boiling regions is presented as a function of the solid surface superheat. Detailed observations of evaporation time versus initial solid surface temperature, time averaged heat flux and transient temperature distribution are also provided by these authors. In the film boiling region, Seki [4] describes the solid-liquid thermal interaction and measures the rapid change of surface temperature during the formation of the vapor layer below the liquid drop. Contributions concerning the effect of the droplet impact momentum are provided in the experimental studies conducted by Pedersen [5]. These experiments show that the approaching velocity is the dominant parameter in the droplet heat transfer during the film boiling process, while the surface temperature has little effect on it.

For the case of low surface temperatures, experimental data have been collected by diMarzo and Evans [6][7] with photographic inspection of evaporating droplets, and by

(*) Istituto di Fisica Tecnica, Università di Bologna, Viale Risorgimento 2, 40136 Bologna.
(**) Department of Mechanical Engineering, University of Maryland, College Park, MD 20742, USA.

Klassen *et al.* [8] with infrared thermographic techniques. In these works, the influence of the solid thermal properties is emphasized, and predictions are made for materials spanning over two orders of magnitude in terms of thermal conductivity, i.e. from Macor (k = 1.29 W/m°C) to aluminum (k = 180 W/m°C).

In the more general field of spray cooling, early works by Toda [9] and Bonacina *et al.* [10] give a first insight into the phenomena associated with a complex multi-droplet scenario. Their research provides measurements of the heat transfer in mist cooling for low values of the solid surface superheat. Bonacina *et al.* also developed a mathematical model to correlate the experimental data. In all these models, it is pointed out that, at low temperatures, nucleate and film boiling can be neglected since heat conduction through the liquid layers is the dominant heat transfer mechanism.

Rizza [11] provides a numerical investigation for spray evaporation on a semi-infinite solid. A two dimensional transient conduction equation is solved for the solid alone under the assumption of constant surface temperature as a boundary condition. The results from a single-droplet model are used to develop the spray evaporation cooling model. This analysis shows that, in spray cooling, the fraction of the heat transfer surface area on the hot solid covered by the droplets is relatively small.

Among the latest contributions in the field of numerical simulation of dropwise evaporation, a simple model for single-droplet evaporation has been introduced by diMarzo and Evans [7]. It describes the evaporation at the liquid-vapor interface under complete suppression of nucleate boiling and calculates the solid surface temperature distribution with satisfactory accuracy, as confirmed by the comparison between numerical predictions and experimental data (diMarzo and Evans [7], diMarzo *et al.* [12], Tartarini *et al.* [13]). The validated code based on this model is used in the present work to obtain the single-droplet results which lead to the formulation of a comprehensive multi-droplet model for evaporative spray cooling.

MODEL FORMULATION

In order to evaluate the thermal transient due to dropwise evaporation on a hot solid surface, the transient heat conduction equation has to be solved for the liquid and the solid simultaneously and the rate of change of the droplet volume has to be calculated step by step during the entire process. A numerical procedure based on the Boundary Element Method (BEM) for the solid domain and on the Control Volume Method (CVM) for the liquid domain is used to formulate a single-droplet code whose characteristics and validation are extensively described by Tartarini *et al.* [13].

The single-droplet model provides the evaporation time and the solid surface temperature distribution for a droplet evaporating on non-porous materials with thermal conductivity ranging over more than two orders of magnitude. Experiments were conducted on Macor (non-porous, glass-like material, k = 1.29 W/m°C) and aluminum (k = 180 W/m°C), and the results were compared with the numerical predictions. The excellent agreement between experimental data and numerical simulation allows one to use the single-droplet code as an effective basis to build up the more general and complex multi-droplet code.

The transient conduction equation for the liquid and the solid is:

$$\frac{\partial T}{\partial t} = \alpha \nabla^2 T \qquad (1)$$

In analogy with the single-droplet model, the multi-droplet initial conditions can be expressed as:

$$T = T_0 - \frac{q_0}{k_s} z \qquad at \quad t = 0 \tag{2}$$

In a multi-droplet situation, however, the value of the initial surface temperature is a function of the deposition time and location for each droplet. This condition can be written as:

$$T = T_{i,o} \qquad i\text{-}th \ droplet; \qquad t = t_{i0}; \qquad i = 1,...,N \tag{3}$$

where N is the total number of droplets deposited on the solid surface. This implies that the initial surface temperature T_{is0} must be considered uniform in the small region where the droplet is deposited. Such an assumption is reasonable if both the droplet size and the surface temperature gradient in the deposition region are small. The surface temperature profiles obtained from the single-droplet model show that large temperature gradients on the solid surface occur only near the droplet edge.

For each droplet, let T_{is0} be the uniform initial surface temperature and U_i the transformed temperature, which is defined as:

$$U_i = T_i - T_{i,o} + \frac{q_0}{k_s} z \tag{4}$$

From the single-droplet model, one can write the governing equation and the associated boundary and initial conditions for the i-th droplet as follows:

$$\frac{\partial U_i}{\partial t} = \alpha \nabla^2 U_i \qquad U_i = 0 \quad at \quad t = t_{io}$$

$$\frac{\partial U_i}{\partial r} = 0 \quad at \quad r \to \infty \qquad \frac{\partial U_i}{\partial z} = 0 \quad at \quad z \to \infty$$

$$k_s \left(\frac{\partial U_i}{\partial z} \right)_s = k_l \left(\frac{\partial U_i}{\partial z} \right)_l \qquad at \quad z = 0, \ r \le R$$

$$k_s \frac{\partial U_i}{\partial z} = h U_i \qquad at \quad z = 0, \ r > R$$

(5,6,7,8,9,10)

The formulation of the multi-droplet model is based on the partition of the droplet cooling domain into a near-field and a far-field. In such a way, the near-field temperature distribution can be obtained from the single-droplet calculations (which are compiled in a data base), while the far-field temperature distribution is obtained from a closed form solution. The solid surface temperature is then calculated by superimposing the values from the data base or the closed form solution.

In the near-field the single-droplet results are directly applied. A typical temperature distribution from the droplet center to the far-field at different times during the evaporative transient is shown in Fig. 1. When the distance from the droplet is large enough, the cooling effect propagation time becomes greater than the droplet

evaporation time. On Macor, at a distance r equal to ten times the droplet radius (i.e. $r \approx 1$ cm) this propagation time can be estimated as:

$$t \sim \frac{r^2}{\alpha_s} \approx \frac{10^{-4}}{10^{-7}} = 1000\ s \tag{11}$$

while the evaporation times for the ranges of values mentioned above span between 10 and 100 seconds.

Therefore, in the far-field (for distances greater than 10 droplet radii) the surface temperature distribution can be calculated by a closed form solution (by Carslaw and Jaeger [14]), which approximates the droplet transient behavior as an instantaneous point sink. That is:

$$\Delta T = T - T_{s0} = \frac{Q}{8(\pi \alpha_s t)^{3/2}}\, e^{-\frac{r^2}{4\alpha_s t}} \tag{12}$$

where the "strength" of the instantaneous point sink Q is:

$$Q = -2 V_0 \frac{\rho_l}{\rho_s} \frac{\Lambda}{c_{p_s}} \tag{13}$$

This instantaneous point sink is generated at time t, while for the evaporation of a single droplet the heat removal is spread over the evaporation time τ. By calculating the spatial averaged heat flux and its mean value over the evaporation time (see Fig. 2), one can find that the instantaneous point sink can be set at a time t equal to 60 percent of the evaporation time τ for Macor. This corresponds to a delay of $0.6\ \tau$ in the deposition time. Therefore, for each droplet, the expression of the temperature difference in the far-field points is given by:

$$\Delta T = T - T_{s0} = -\frac{V_0 \frac{\rho_l}{\rho_s} \frac{\Lambda}{c_{p_s}}}{4[\pi \alpha_s (t - 0.6\tau)]^{\frac{3}{2}}}\, e^{-\frac{r^2}{4\alpha_s (t - 0.6\tau)}} \tag{14}$$

Figure 3 shows the difference between the temperature calculated by the single-droplet model and the closed form solution at different times as a function of the radial distance for Macor. The error is within an acceptable range for $r/R \geq 10$. Figure 4 shows the same temperature difference calculated at $r/R = 10$ as a function of time for three different cases of initial surface temperature. One can see that the difference is always bound within less than ± 0.1°C.

Due to the linearity of the conduction equation, the principle of superposition can be invoked in the multi-droplet model, and one can write:

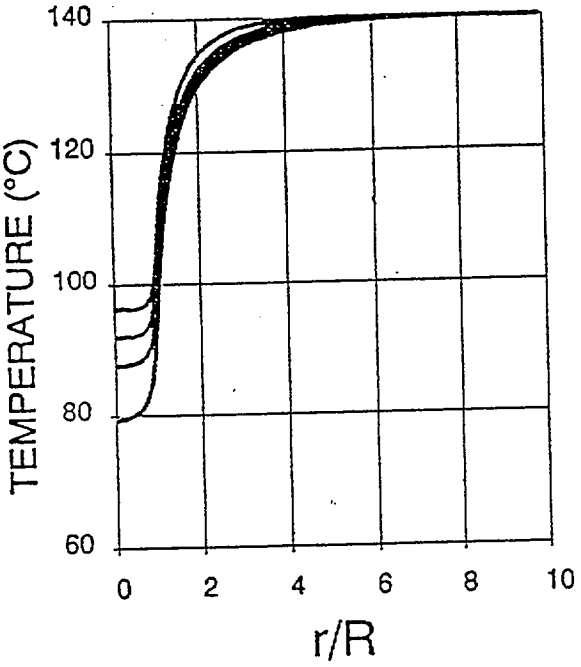

FIGURE 1 - Single-droplet model: Typical solid surface temperature profiles during the evaporative transient (T_{s0}=140 °C; t/τ = 0.3, 0.5, 0.7 and 0.9 top-to-bottom; V_0 = 10 μl on Macor)

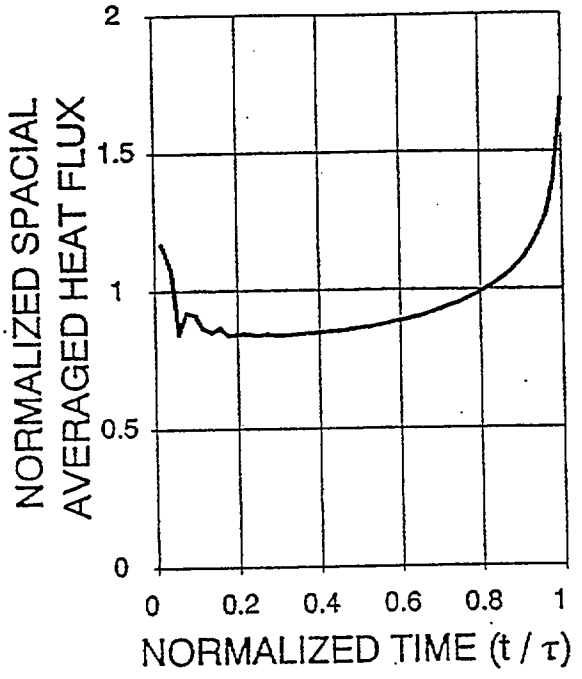

FIGURE 2 - Single-droplet model: Normalized heat flux at the solid-liquid interface versus normalized time for a 10 μl drop evaporating on Macor at T_{s0}=140 °C.

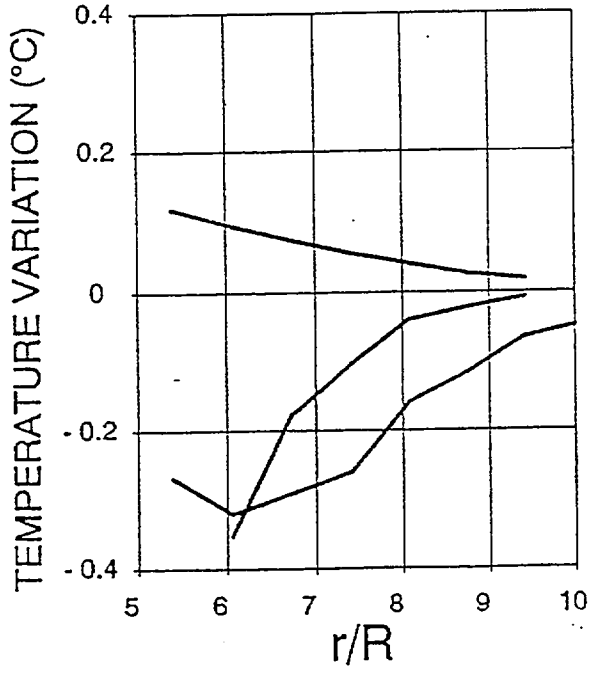

FIGURE 3 - Spatial behavior of the temperature difference between single-droplet model calculations and closed form solution.

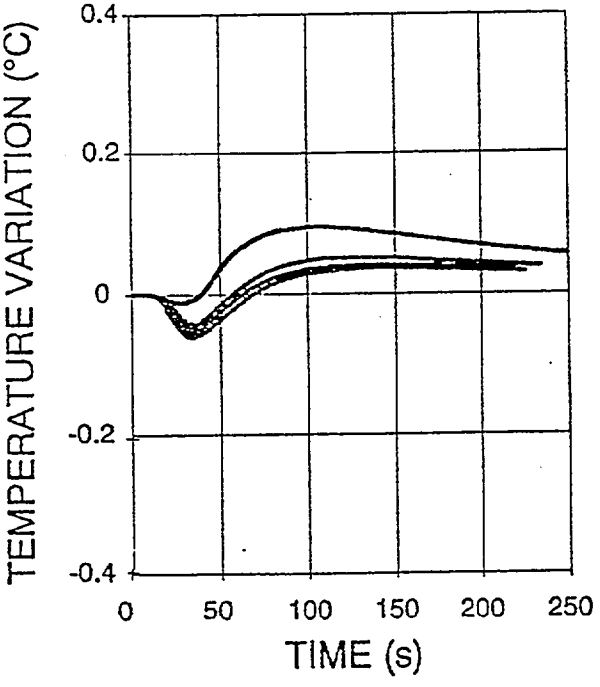

FIGURE 4 - Temporal behavior of the temperature difference between single-droplet model calculations and closed form solution.

$$U = \sum_{i=1}^{N} U_i \tag{15}$$

The transformed temperature U, as defined in Eq.(15), is the solution of the multi-droplet cooling problem. Thus the temperature T can be expressed as:

$$T = T_{s0} + \sum_{i=1}^{N} \left(T_i - T_{i_{s0}} \right) \tag{16}$$

The droplet distribution pattern on the solid surface is determined by a simple numerical program. It simulates the action of a dispenser that releases droplets of fixed volume with assigned frequency at random locations. A typical droplet pattern is shown in Fig. 5. Given this distribution pattern, all cooling effects from each droplet are superimposed. The summation provides a detailed temperature distribution as a function of time in a multi-droplet evaporative cooling transients.

The most useful parameter to describe the temperature distribution in multi-droplet cooling is a spatial average temperature of the calculation domain which is defined as follows:

$$T_{ave} = \frac{\iint T\,dx\,dy}{\iint dx\,dy} = \frac{\sum_{i=1}^{N_{pi}} \sum_{j=1}^{N_{pj}} T_{ij}\,\Delta x_i \Delta y_j}{\sum_{i=1}^{N_{pi}} \sum_{j=1}^{N_{pj}} \Delta x_i \Delta y_j} \tag{17}$$

Further simplification can be made if the size of every mesh is the same. Then the spatial average temperature can be interpreted as the summation of the temperatures of all the specified points on the surface divided by the total number of the grid points N_p:

$$T_{ave} = \frac{\sum_{k=1}^{N_p} T_k}{N_p} \tag{18}$$

The controlling parameters for the multi-droplet cooling include the initial solid surface temperature, the properties of the solid and the mass flux of the liquid spray. Even if only Macor has been used during this study, any other material can be considered by inserting the appropriate data base. The only limit to the initial surface temperature is set by the operating condition of full suppression of nucleate boiling (for Macor the maximum temperature that can be reached before the onset of nucleate boiling is about 160°C). The liquid mass flux is defined as:

$$\dot{m} = \frac{\rho f V_0}{A} \tag{19}$$

and, given a fixed droplet volume and the liquid density, it is a function of the droplet deposition frequency f and of the spray impingement area A.

RESULTS AND DISCUSSION

The main objective of a spray cooling analysis is to evaluate the temperature distribution on the solid surface as a function of time during the multi-droplet evaporative process. As previously described, the temperature at any point of the solid surface can be obtained by superimposing the results of many single-droplet calculations. Given an initial solid surface temperature and a pre-determined droplet distribution pattern, the temperature distribution at any selected time can be predicted by the code.

Figures 6 to 8 show some three-dimensional temperature plots for a portion of the solid surface at different times. These figures pertain to the transient with an initial solid surface temperature of 160°C and a liquid mass flux of $3x10^{-4}$ kg/m^{2}s. At the beginning of the transient, the region influenced by one droplet is easily identifiable. The temperature variation is very sharp in the area where the droplet is evaporating. When more droplets are deposited on the solid surface, the temperature at any point is the result of the cooling effect caused by all the droplets and the single droplet contribution becomes less evident.

Figures 9 and 10 show the average solid surface temperature versus time in two typical cases analyzed by the multi-droplet model. The fluctuations of the average temperature are related with the random distribution pattern of the droplets on the solid surface. These plots show a rapid decrease in the initial phase of the process. Note that the evaporation time on Macor given the initial conditions of the reported cases ranges from 25 to 100 seconds. During this time interval, the solid surface is constantly cooled down by the evaporating droplets, and the average temperature steadily decreases. When a droplet is completely evaporated, the corresponding surface points show a temperature recovery. The initial volume of the droplets used here is constant ($V_0=5\mu l$).

CONCLUSIONS

A dropwise evaporation model is presented, which calculates the transient temperature distribution on a hot solid surface subjected to the cooling effect of an evaporating water spray. The numerical simulation can be applied to a broad range of solid non-porous materials. A single-droplet model, provides accurate predictions of the droplet evaporation time, of the temperature distribution and of the heat fluxes inside the droplet and on the solid surface. These results are used as a basis for the formulation of the multi-droplet numerical code.

By applying the linear characteristic of the conduction equation, the principle of superposition is used in the multi-droplet model. The combination of the thermal effects due to a pre-determined droplet pattern generates surface temperature distributions as a function of time.

A spatial average temperature is used to describe the cooling mechanism on the solid surface. The spray mass flow rate and the initial solid temperature are identified as the governing parameters in the multi-droplet evaporation process.

Further work to evaluate the influence of different surface materials on the evaporative spray cooling is in progress.

ACKNOWLEDGEMENTS

This study was made possible by a grant of the Building and Fire Research Laboratory of the National Institute of Standards and Technology. The authors are indebted to Dr. H. Baum (BFRL-NIST) for his guidance and suggestions.

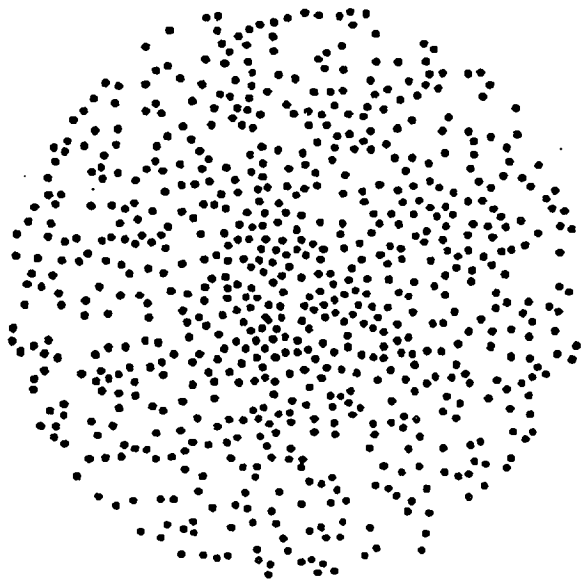

IMPACTED AREA RADIUS = 10 cm

FIGURE 5 - Multi-droplet model: Typical droplet distribution on the solid surface as simulated by the code.

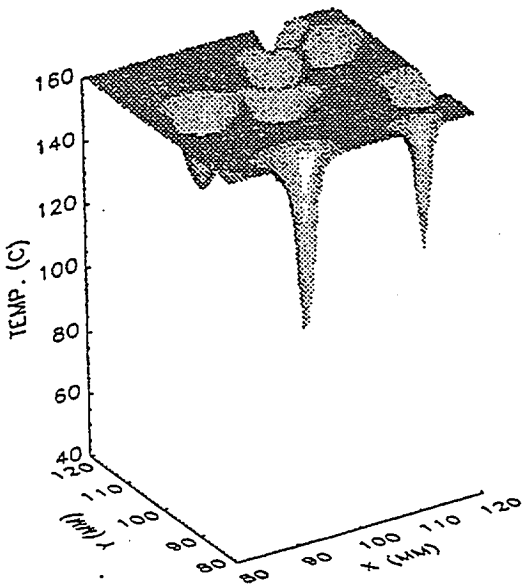

FIGURE 6 - Multi-droplet model: Temperature distribution on the solid surface after 5 seconds (V_0 = 5 μl; T_{s0} = 160 °C; $\dot{m}$ = 0.0016 kg/m^{2}s)

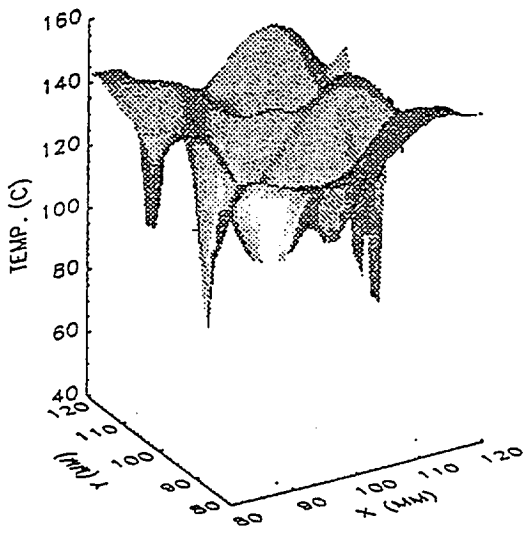

FIGURE 7 - Multi-droplet model: Temperature distribution on the solid surface after 60 seconds (V_0 = 5 μl; T_{s0} = 160 °C; $\dot{m}$ = 0.0016 kg/m^{2}s)

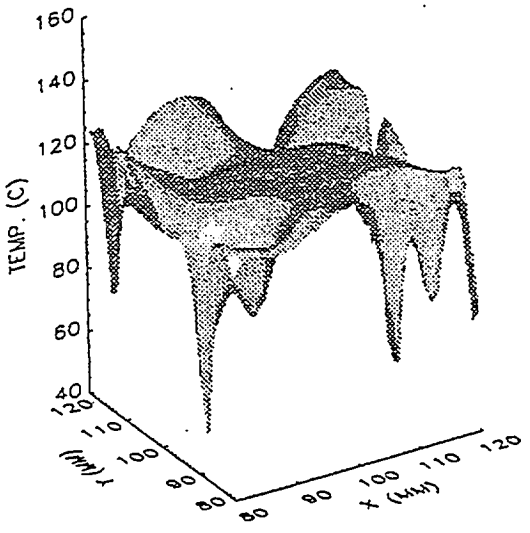

FIGURE 8 - Multi-droplet model: Temperature distribution on the solid surface after 200 seconds (V_0 = 5 μl; T_{s0} = 160 °C; $\dot{m}$ = 0.0016 kg/m^{2}s)

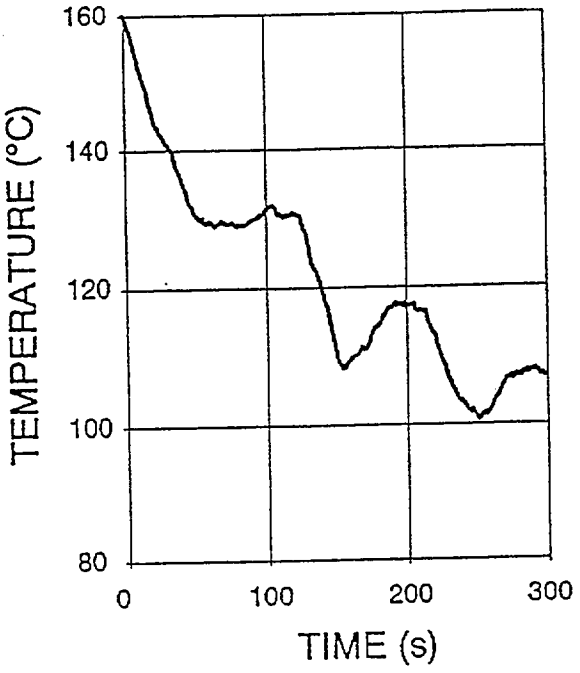

FIGURE 9 - Multi-droplet model: Average solid temperature distribution versus time (V_0 = 5 μl; T_{s0} = 160 °C; $\dot{m}$ = 0.0016 kg/m^{2}s)

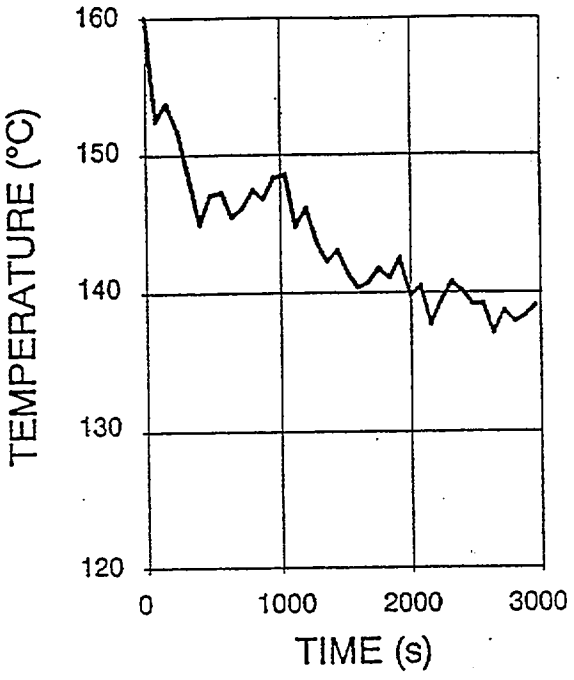

FIGURE 10 - Multi-droplet model: Average solid temperature distribution versus time (V_0 = 5 μl; T_{s0} = 160 °C; $\dot{m}$ = 0.0008 kg/m^{2}s)

NOMENCLATURE

A	spray impingement area
c_p	specific heat
d	droplet distribution density
f	droplet deposition frequency
h	overall heat transfer coefficient
k	thermal conductivity
m	mass flux
N	total number of droplets
N_p	number of grid points
Q^p	strength of the instantaneous point sink
q	axial heat flux
$\bar{q}$	spatial averaged heat flux
R	radius of the wetted area
r	radial coordinate
T	temperature
t	time
U	transformed temperature
V	droplet volume
x,y	cartesian coordinates
z	axial coordinate

α	thermal diffusivity
Λ	latent heat of vaporization
ρ	density
τ	evaporation time

subscripts

ave	average
l	liquid
s	solid
0	initial

REFERENCES

[1] Makino, K., Michiyoshi, I., Heat Transfer Characteristics of Evaporation of a Liquid Droplet on Heated Surfaces, *Int. J. Heat Mass Transfer*, Vol.21, pp.605-613 (1978).

[2] Makino, K., Michiyoshi, I., The Behavior of a Water Droplet on Heated Surfaces, *Int. J. Heat Mass Transfer*, Vol.27, pp.781-791 (1984).

[3] Makino, K., Michiyoshi, I., Discussion of Transient Heat Transfer to a Water Droplet on Heated Surfaces Under Atmospheric Pressure, *Int. J. Heat Mass Transfer*, Vol.30, pp.1895-1905 (1987).

[4] Seki, M., Kawamura, H., Sanokawa, K., Transient Temperature Profile of a Hot Wall Due to an Impinging Liquid Droplet, *ASME J. Heat Transfer*, Vol.100, pp.167-169 (1978).

[5] Pedersen, C.O., An Experimental Study of the Behavior and Heat Transfer Characteristics of Water Droplets Impinging Upon a heated Surface, *Int. J. Heat Mass Transfer*, Vol.13, pp.369-381 (1970).

[6] di Marzo, M., Evans, D.D., Dropwise Evaporative Cooling of High Thermal Conductivity Materials, *Int. J. Heat & Technology*, Vol.5, pp.126-136 (1987).

[7] di Marzo, M., Evans, D.D., Evaporation of a Water Droplet Deposited on a Hot High Conductivity Solid Surface, *ASME J. Heat Transfer*, Vol.111, pp.210-221 (1989).

[8] Klassen, M., di Marzo, M., Sirkis, J., Infrared Thermography of Dropwise Evaporative Cooling, *ASME HTD*, Vol.141, pp.117-121 (1990).

[9] Toda, S., A Study of Mist Cooling. First Report: Investigation of Mist Cooling, *Heat Transfer Japanese Research*, Vol.1, pp.39-50 (1972).

[10] Bonacina, C., Del Giudice, S., Comini, G., Dropwise Evaporation, *ASME J. Heat Transfer*, Vol.101, pp.441-446 (1979).

[11] Rizza, J.J., A Numerical Solution to Dropwise Evaporation, *ASME J. Heat Transfer*, Vol.103, pp.501-507 (1981).

[12] di Marzo, M., Tartarini, P., Liao, Y., Evans, D.D., Baum, H., Dropwise Evaporative Cooling, *28th ASME/AIChE/ANS National Heat Transfer Conference*, Minneapolis, Minnesota, HTD Vol.166, pp.51-58 (1991).

[13] Tartarini, P., Liao, Y., di Marzo, M., Transient Cooling of a Hot Surface by Droplets Evaporation, *UMCP Mechanical Engineering Report*, No.90-6 (1990).

[14] Carslaw, H.S., Jaeger, J.C., *Conduction of Heat in Solids*, Clarendon Press, Oxford, pp. 214-217 and 264 (1959).

PAPER # 14

Evaporative Cooling Due to a Sparse Spray

M. di Marzo & S. Tinker

Mechanical Engineering Department
University of Maryland
College Park, MD 20742

ABSTRACT

The cooling effect of a sparse spray impinging on a semi-infinity solid is investigated. Experiments are conducted by monitoring, via infrared thermography, the surface of the solid heated by radiation and cooled by sprays of uniform size droplets until steady state conditions are reached. The surface temperature field in the proximity of a single droplet is modeled with a closed-form solution based on the hypothesis of constant and uniform heat flux at the solid-liquid interface. In the far-field, an instantaneous point-sink solution is adequate to represent a single droplet cooling effect. These closed-form solutions are used to fit the results of a coupled model, previously developed, which solves the liquid and solid temperature field for the evaporative transient. Inputs from this model are necessary for the formulation of both the closed-form solutions. The spray model formulation is based on the superposition of the cooling effect of all the droplet deposited on the surface. The transient surface temperature distributions and the average surface temperature are compared for the data and computations. The results are in good agreement for similar random droplet distributions of the order of one g/m^{2}s with initial solid surface temperatures ranging between 130 and 160 °C.

NOTATION

c	specific heat of the solid
D	cumulative droplet distribution in the region bounded by r^*
erf	error function
J_0, J_1	Bessel's functions
k	thermal conductivity of the solid
r	generic radial coordinate
r^*	normalized radius of the spray: see Eq. (1)
R	radius of the wetted region under an evaporating droplet
q_c	average heat flux at the solid-liquid interface
q_0	steady state heat flux in the solid prior to the spray activation
T	solid surface temperature
T_0	solid surface temperature prior to the spray application
α	thermal diffusivity of the solid
β	droplet shape parameter after deposition
θ	contact angle receding value
λ	dummy variable of integration
ρ	density of the solid
τ	droplet evaporation time

INTRODUCTION

Spray cooling finds application in quenching processes, in surface coating, in cooling towers and in a number of other industrial processes. The large heat removal associated with the water vaporization is the key characteristic of spray cooling. Several researchers have studied the fundamental mechanism of single droplet and multi-droplets evaporation. Early investigations by Toda [1] and Bonacina [2] provide the fundamental insight in the performance of water sprays and mists. Models of the cooling effect of sprays are proposed by Tio and Sadhal [3] and Rizza [4].

In the specific area of fire protection, sprinkler and mist technologies are based on spray cooling. The sprinklers are designed to effectively extinguish a developing fire and typically involve significant water fluxes. With the elimination of alogenated agents, due to environmental concerns, a more sophisticated usage of light water sprays and mists may find application in the protection of valuable items. Especially in locations exposed to a developing fire, there might be a need to protect items exposed to radiant heat input. In this case, the temperature levels on the solid surfaces are low enough to confine the vaporization processes to evaporative cooling. This implies that the surface temperatures are such that onset of nucleate boiling is not observed. The potential for water damage is higher at these low temperature since the water vaporization rate is reduced.

The motivation for this study is to investigate the behavior of a water spray in these conditions, which require water fluxes of the order of 1 g/m^2s. Note that these water fluxes are about one order of magnitude less than the mist water fluxes required for extinguishment [5]. The droplet size used are one order of magnitude larger than those used in mists applications to insure that the water will reach the solid surface thus protecting it from the fire exposure.

A progression of studies provides the basic understanding to construct a multi droplet model which encompasses: a) the detailed description of the evaporative mechanism and b) a simple representation of each droplet cooling effect. To achieve these objectives, single droplet evaporative transients are investigated with increasingly complex boundary conditions.

At first the droplet is evaporated on a high conductivity material heated from below [6]. In this case, the solid-liquid interfacial condition is almost isothermal and Seki [7] estimates the "contact temperature" from the classical closed-form solution of two infinite solids brought in sudden contact. The study of single droplets deposited on high thermal conductivity materials focusses on the validation of two hypotheses: a) the liquid-vapor boundary condition is dictated by a simultaneous heat and mass transfer, and b) the effect of convective motion in the liquid is negligible. The validity of the second hypothesis is confirmed also by other investigators [8] and allows the treatment of the liquid with a simple heat conduction equation.

Experiments and modeling of evaporation on low thermal conductivity solids provide the description of the solid-liquid boundary [9]. The coupling of the solid and liquid thermal domains is not amenable to finite difference integration due to the sharp temperature gradients in the proximity of the droplet outer edge. The use of boundary element methods circumvents this difficulty. Two major findings results from these studies: a) the realization that the liquid thermal behavior is nearly one-dimensional, in the direction orthogonal to the solid surface, and b) the favorable comparison of the model predictions with those obtained with a closed-form solution based on uniform and constant heat flux under the droplet. Note that the closed-form solution provides an overall temperature distribution on the solid surface which understates the cooling effect under the droplet while exhibiting a slightly broader cooling effect away from the droplet. In the following, the overall effect

of these discrepancies will be outlined the comparison of the spray model prediction with the infrared thermographic data. An additional outcome of these experimental investigations is the development of non-intrusive infrared thermography for the monitoring of the solid surface transient thermal behavior [10]. This measurement technique enables the validation of the model for this case and for all the subsequent more complex situations.

The application of evaporative cooling to fire protection suggests the use of radiant heat input from above rather than the conductive boundary condition previously used. Experimental and theoretical studies are performed in a radiant environment with the same infrared instrumentation [11] and with models which incorporate the effect of the direct radiation as well as the heat input by conduction from the solid [12,13]. These models, validated against a large experimental database, constitute the background information necessary to formulate the multi-droplet model that will be described in the following.

The objective of this paper is to describe: a) the experimental results for the evaporative cooling of a solid subjected to the impingement of a sparse spray and b) the formulation of a model for the prediction of the thermal transients observed experimentally.

EXPERIMENTS

The experimental apparatus is depicted in Fig. 1. The droplet generator is suspended by four cables and is oscillating within a circular region while three bumpers, which move in and out radially at a given frequency, collide randomly with it. Both the shape and the motion frequency of the bumpers are optimized to produce a random motion of the droplet generator. The water droplets, ejected from the generator, have uniform size and impinge upon a Macor tile (square in shape with 15.2 cm sides

and 2.54 cm thickness) mounted below. Macor is a glass-like material with density of 2520 kg/m^3, thermal conductivity of 1.297 W/m °C, specific heat of 888.9 J/kg °C and emissivity of 0.84. The tile lower surface is maintained at a constant temperature of about 30 °C by a chilled plate to provide a controlled thermal boundary condition.

The heat input is provided by three radiant panels. Two of which are mounted symmetrically with respect to the Macor surface at an angle of 30° and the third, lower in aspect ratio, surrounds the Macor tile. The panels are capable of temperatures in excess of 800 °C and they can be approximated to radiate as black-bodies. A 208 V three-phase electric supply is used to power them via a feedback controller which monitors the temperature of the panels heating elements. The position of the panels is important to avoid direct reflection of the incoming radiation to the infrared camera (Inframetrics Model 525). To eliminate additional sources of stray radiation, the camera focusses on the Macor surface through a chilled pipe. The monochrome infrared image is recorded by a high-resolution 8-mm VCR.

The test procedure prescribes a surface cleaning routine and the subsequent exposure of the Macor tile for long period of time (i.e. about two hours) to the radiant heat input. Steady-state conditions are reached and the infrared instrumentation is also brought on-line and stabilized over a long period of time. A reservoir of degassed, deionized water is connected to the droplet generator. A special oil-sealed system is used to prevent gasses (i.e. air) from dissolving in the water. A frequency of droplet deposition is selected and measurements of the water flow rate are obtained to insure the steadiness of the spray dispensing system.

The typical droplet size used in these experiments is of 10 ± 1 μl. The droplet frequency ranges from 0.07 to 0.6 which corresponds to mass fluxes between 0.2 and 1.6 g/m^{2}s over the spray

surface. The droplet distribution is characterized in separate tests using the same equipment. To describe the droplet distribution, a polynomial function is defined which satisfies the following conditions: a) at the center of the spray the droplet distribution is proportional to the surface area; b) at a normalized spray radius of 0.6 the distribution reaches its maximum since for larger radii, the effect of the bumpers is increasingly restricting the droplet generator motion; c) at the outermost radius the generator is nil since it is impossible for the distributer to reach that location due to the presence of the bumpers; d) the distribution is normalized over the spray area. With these conditions the integrated distribution is:

$$D = 1.83\ r^5 - 5.66\ r^4 + 3.83\ r^3 + r^2 \qquad (1)$$

Where the radius is normalized with respect to the spray radius of 0.034 m. This expression fits reasonably well the experimental data as can be seen in Fig. 2.

The correlation between the infrared and temperature scales is obtained by measurements of a black body source in a separate calibration routine. Prior to the activation of the spray, the initial uniform solid surface temperature is detected with a thermocouple probe and this information is used to reference the infrared readings. The details of the calibration procedure are given by Klassen [10]. The infrared thermography is non-intrusive, provides a reasonable temperature resolution and an excellent spatial resolution. The resulting database is extensive since each test lasts for 15 minutes approximately. About 30,000 frames are available for each transient. Each infrared frame can be grabbed and digitized pixel-by pixel yielding about 240,000 independent temperature readings per frame. The uncertainty associated with the temperature readings is of ± 2 °C and the typical spatial resolution is of about 100 μm. The raw data for one frame, where one out of five pixel is sampled,

is presented in Fig. 3. Each square in the figure represents a surface area of 0.40 mm^2. The dark region is bounded by two isothermal lines at 130 °C and 100 °C respectively.

Five initial solid surface temperatures, with several water fluxes, have been investigated for a total of 14 transients. The onset of nucleate boiling for a water droplet deposited on Macor is observed at about 163 °C. The initial solid surface temperatures investigated are: 111, 131, 151, 162 and 182 °C. The water fluxes used are compatible with these temperature levels. This means that lower water fluxes are used with the lower temperatures in order to avoid flooding of the surface.

The results indicates that for several tests at the high water fluxes, the long-term average surface temperature drops well below 100 °C. Therefore, these tests are of limited interest here and will not be considered for the model validation. Note that the spray model cannot be applied to the 182 °C test where nucleate boiling is present. The cooling effect associated with nucleate boiling is completely different from the one modeled here. The spray model will be compared with three sets of data at 131 °C, 151 °C and 162 °C respectively.

MODELING

The modeling of the evaporative transient for a single droplet has been completed and reported in a series of publications [9,12,13]. In particular, a closed-form solution, which describes the transient thermal behavior of a solid surface in the proximity of an evaporative droplet, has been derived as:

$$T_0 - T = \frac{(q_c - q_0)\, R}{k} \int_0^\infty J_0(\lambda r)\, J_1(\lambda R)\, erf(\lambda \sqrt{\alpha t})\, \frac{d\lambda}{\lambda} \qquad (2)$$

$$T_0 - T = \frac{(q_c - q_0)\, R}{k}$$

$$\times \int_0^\infty J_0(\lambda r)\, J_1(\lambda R)\, \{erf(\lambda\sqrt{\alpha t}) - erf[\lambda\sqrt{\alpha (t-\tau)}]\}\, \frac{d\lambda}{\lambda} \qquad (3)$$

This closed-form solution is obtained applying a constant and uniform condition over a circular portion of the surface of a semi-infinite body. The second equation describes the surface temperature distribution after the heat flux has been removed (i.e. after the complete evaporation of the droplet) as the surface recovers its original state.

This solution has been modified for the case of a water droplet subjected to radiant heat input, while evaporating on a the surface of a solid with low thermal conductivity [13]. The effect of direct radiation on the droplet is to decrease the surface tension and to increase the droplet spreading on the surface [11]. The flatter droplet configuration results in the early decrease of the contact angle to its receding value. Thereafter, the wetted region under the droplet shrinks. A multiplier has been introduced to account for this droplet shrinkage during the later portion of the evaporative transient. A solid-liquid coupled model which uses a boundary element method for the solid domain and a 1-D solution for the liquid, has been developed previously [13]. This model has been described in detailed in previous papers and for the discussion of its features, the reader can consult those references. Note that this model requires two inputs from the experiments: a) the droplet shape parameter, β; b) the receding angle, θ. The droplet shape parameter and the receding angle are obtained experimentally for single droplets deposited over any given solid surface. In general, while sufficiently repeatable, these parameters are strong functions of the surface condition and of the experimental procedures.

Typically, the receding angle is a constant value while the shape parameter may have some minor dependency on the initial solid surface temperature. The coupled model results are reasonably fitted by the closed-form solution if 0.9 R is used instead of R in the term preceding the integral on the right hand side of Eqs. (2) and (3).

Note that, in order to apply the closed-form solution previously described, two parameters must be known: a) the single droplet evaporation time, τ; and b) the portion of the heat flux which contributes to evaporative process by conduction from below the droplet, q_c. The coupled model is used to determine these two parameters. Figure 4 depicts the evaporation time and the conduction heat flux for water droplets of 10 µl deposited on Macor. The closed-form solution obtained in this way approximates reasonably well the coupled model solution up to region under the droplet where discrepancies are observed. This is obvious since the uniform and constant heat flux condition given by the closed-form solution is a poor match for the complex solid-liquid thermal interactions. However, the overall error associated with these discrepancies is very small since the surface involved compared to the overall spray surface is small (less than one percent).

The closed-form solution previously described is used to characterize the surface temperature in the proximity of the droplet. At larger distances ($r > 5$ R, for Macor), a simple, instantaneous point-sink closed-form solution is given as [14]:

$$T_0 - T = \frac{q_c R^2 \tau}{4 \alpha (t - 0.6\tau)^{3/2} \sqrt{\pi \rho c k}} e^{\frac{-r^2}{4\alpha(t-0.6\tau)}} \qquad (4)$$

For this solution, the evaporative heat flux contributed by conduction is used. Note that the time of

droplet deposition is augmented by 60 percent of the total evaporation time in order to better approximate the instant when the time-averaged heat removal has occurred. The cut-off between the closed-field and the far-field solution is determined by comparing the two solutions. It is found that for r = 5 R, the maximum difference between the surface temperature computed with the two solutions is of the order of 0.1 °C. Within the uncertainties of the measurements, this would amount to a combined effect of 20 droplets within 5 radii from a given site. Such a droplet density exceed by far the conditions characterized as a sparse spray.

The computational technique for the sparse spray is based on the superposition of the cooling effect of the droplets with respect to the point of concern. This means that each droplet evaporating transient is based on the solid surface temperature at deposition and is not accounting for mutual droplet interactions. This assumption is realistic for the fire protection application which is considered here. In an extinguishment situation, where the droplet density required is higher, this assumption may not apply.

In order to determine the site of deposition for the various droplets, a pairs of random numbers (between 0 and 1) is used to determine each droplet polar position. The first number is used to generate a random azimuthal angle from the center of the spray. The second number is used to generate a radial position for the droplet. The radial position is obtained by solving Eq. (1) while setting the integrated distribution equal to the random number. From Fig. 2 observe that for small values of this number, the droplet is moved to outer positions while for large values of the number the droplet is moved to inner positions. At about 0.6 the number coincides with the actual radial position.

In summary, upon determining the various droplet landing sites and times of deposition, the

superposed effect of all the deposited droplets is evaluated at each point of the computational domain and the temperature of any given point is obtained for any given instant of the transient.

DISCUSSION

The solid surface temperatures within the field of view depicted in Fig. 3 are independently computed with the spray model and the results are shown in Fig. 5 . The computations and the infrared thermography are in reasonable qualitative agreement. There are six droplets on both surfaces at this time and the region bounded by the 130 °C isothermal is slightly smaller in the data plot while the isothermal at 100 °C bounds a larger surface in the same plot the thus yielding an analogous average surface temperature. This is consistent with the slight discrepancies associated with the closed-form solution for the near-field described previously. Note that similar times in the transient have been selected for the data and the model computation. The droplets distribution are independently random and they only match the water flux and droplet distribution but by no mean are identical in droplet deposition sites. The portion of the solid surface considered is identical for the experiment and for the model to insure a similar behavior of the average temperature by considering a similar portion of the spray distribution.

To provide a more quantitative comparison, the average surface temperature is plotted over the duration of the transient for three different tests in Figs. 6 through 8. The oscillatory nature of the temperature is due to the fact that only a portion of the spray area is viewed by the infrared camera. Therefore, at any time, there may be a different number of droplets in the field of view than at other times, resulting in overall variation exhibited in these plots. These comparisons are for tests with initial solid surface temperatures of 131, 151 and 162 °C. They sufficiently demonstrate the

adequacy of the model. Note that for all these plots the transient thermal response of the solid is similar and it exhibits a time constant of about 3 minutes. This result elicits the dominant effect of the substrate heat capacity.

A similar conclusion is derived from considerations of the solid surface temperature behavior for the case with an initial nucleate boiling transient. Figures 9 depicts the average surface temperature during the cooling transient for a test at a low water flux (i.e. 0.50 g/m^2s) with an initial solid surface temperature of 162 °C. For this test, the data up to 3 minutes and for average surface temperatures above 145 °C, exhibit a sharp drop in average surface temperature due to nucleate boiling. Then, upon returning to the evaporative heat transfer regime, the average surface temperature briefly increases (see the arrow in the figure). Thereafter, the temperature resumes its decay at a less steep rate. This phenomenology outlines the significant role played by the stored heat in the solid. Note the marginal upward trend of the data after 7 minutes into the transient. It will take approximately one hour for the steady-state to be reached as the average surface temperature slowly climbs. From these observations it is clear that this set of data is not applicable for model validation since the initial nucleate boiling transient completely changes the thermal behavior of the solid surface.

CONCLUSIONS

A model for the prediction of the cooling effect of a sparse spray applied to a solid surface subjected to radiant heat input is proposed. The model is based on the superposition of the cooling effect of each droplet deposited on the surface. The cooling effect of a single droplet is evaluated by two closed-form solutions for the near and far-field respectively.

The near-field solution assumes uniform and constant heat flux at the solid-liquid boundary

under the evaporating droplet. This closed-form solution is obtained by comparing it with a previously validated coupled-model which describes the vaporization transient. This closed-form solution exhibits slight discrepancies which are reflected in the overall predictions of the spray model. Nonetheless, the overall transient behavior of the solid surface is consistently predicted over a range of conditions.

A few notes concerning the effect of nucleate boiling under the deposited droplet and the realization that the overal time constant is not a strong function of the water flux indicate that the substrate properties play a dominant role on the cooling transient.

ACKNOWLEDGMENTS

This research is sponsored by the Building and Fire Research Laboratory of the National Institute of Standards and Technology (BFRL-NIST). The authors are grateful to Dr. H. Baum (BFRL-NIST) for his guidance in the formulation of the multi-droplet model.

REFERENCES

1. Toda, S., A study of mist cooling. First report: investigation of mist cooling, *Heat Transfer-Jap. Res.* **1** (1972) 39-50.
2. Bonacina,C., Del Giudice, S. & Comini, G., Dropwise evaporation, *Trans. ASME, J. Heat Transfer* **101** (1979) 441-446.
3. Tio, K.K. & Sadhal, S.S., Thermal analysis of droplet spray evaporation from a heated solid surface, *Trans. ASME, J. Heat Transfer* **114** (1992) 220-233.
4. Rizza, J.J., A numerical solution to dropwise evaporation, *Trans. ASMR, J. Heat Transfer* **103**

(1981) 503-507.

5. Milke, J.A., & Gerschefski, C.E., Overview of water mist research for library applications, *ICFRE*, 1995, ed. D.P. Lund - SFPE, pp. 133-138.

6. diMarzo, M. & Evans, D.D., Evaporation of a water droplet deposited on a hot high thermal conductivity surface, *Trans. ASME, J. Heat Transfer* **111** (1989) 210-213.

7. Seki, M., Kawamura, H. & Sanokawa, K., Transient temperature profile of a hot wall due to a impinging liquid droplet, *Trans. ASME, J. Heat Transfer* **100** (1978) 167-169.

8. Ostrach, S. & Pradhan, A., Surface-tension induced convection at reduced gravity, *AIAA J.***16** (1978) 419-424.

9. diMarzo, M., Tartarini, P., Liao, Y., Evans, D. & Baum, H., Evaporative cooling due to a gently deposited droplet, *Int. J. Heat Mass Transfer* **36** (1993) 4133-4139.

10. Klassen, M., diMarzo, M. & Sirkis, J., Infrared thermography of dropwise evaporative cooling, *Experimental Thermal and Fluid Sci.* **5** (1992) 136-141.

11. diMarzo, M., Kidder, C.H. & Tartarini, P., Infrared thermography of dropwise evaporative cooling of a semi-infinite solid subjected to radiant heat input, *Experimental Heat Transfer* **5** (1992) 101-114.

12. Tartarini, P. & diMarzo, M., Dropwise evaporative cooling in radiative field, *Heat Transfer*, 1994, ed. G.F. Hewitt **6**, pp. 277-282.

13. White, G., Tinker, S. & diMarzo, M., Modelling of dropwise evaporative cooling on a semi-infinite solid subjected to radiant heat input, *Fire Safety Science*, 1994, ed. T. Kashiwagi , pp. 217-228.

14. Carslow, H.S. & Jaeger, J.C., *Conduction of Heat in Solids*, 1959, Oxford Press, pp. 256-258.

CAPTIONS

Figure 1 - Experimental apparatus.

Figure 2 - Integrated droplet distribution: data and curve fit.

Figure 3 - Typical solid surface temperature distribution from the infrared thermographic data: T_o = 151 °C; G = 0.96 g/m^{2}s; t = 300 s (each square represents 0.40 mm^2).

Figure 4 - Evaporation time and conductive heat flux: coupled-model results (**x**) and curve fits.

Figure 5 - Typical solid surface temperature distribution from the spray model predictions: T_o = 151 C; G = 0.96 g/m ^{2}s; t = 300 s (each square represents 0.40 mm^2).

Figure 6 - Average surface temperature transient: T_o = 131 C; G = 0.50 g/m ^{2}s (the open symbols represent the experimental data and the closed ones represent the spray model computations).

Figure 7 - Average surface temperature transient: T_o = 151 C; G = 0.96 g/m ^{2}s (the open symbols represent the experimental data and the closed ones represent the spray model computations).

Figure 8 - Average surface temperature transient: T_o = 162 C; G = 0.97 g/m ^{2}s (the open symbols represent the experimental data and the closed ones represent the spray model computations).

Figure 9 - Average surface temperature transient: T_o = 162 C; G = 0.50 g/m ^{2}s (the open symbols represent the experimental data and the closed ones represent the spray model computations).

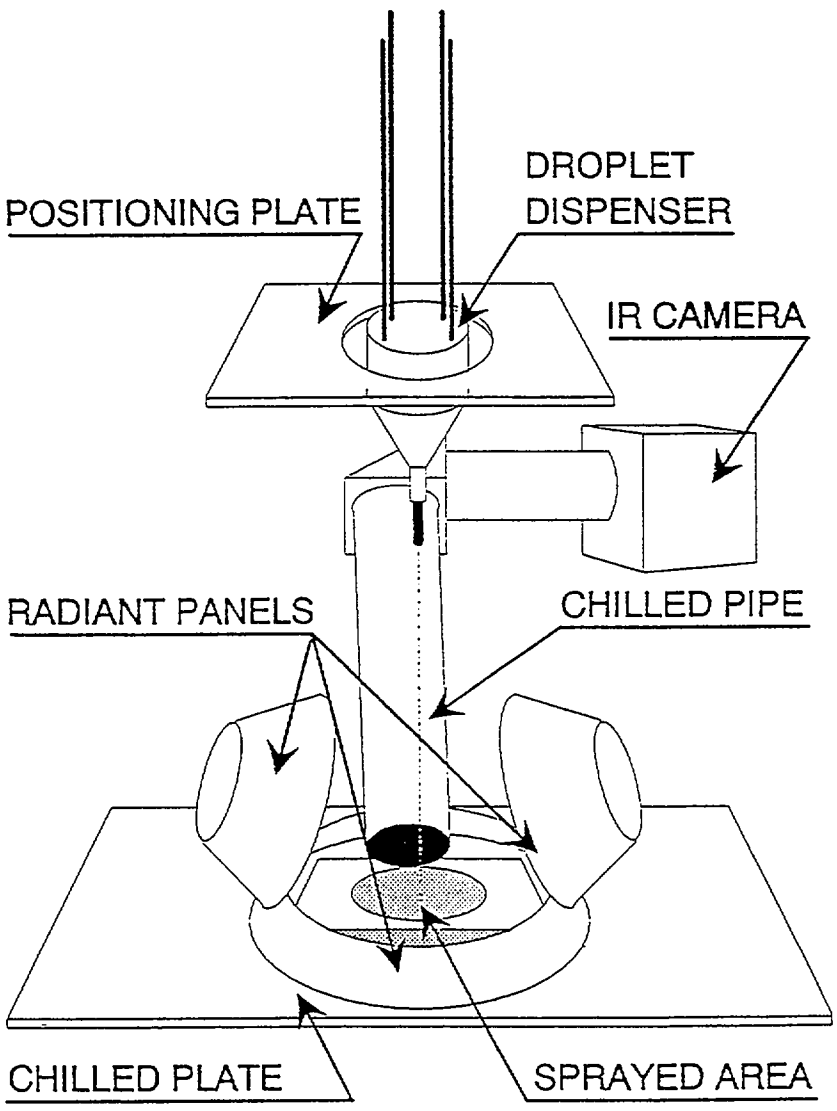
POSITIONING PLATE
DROPLET DISPENSER
IR CAMERA
RADIANT PANELS
CHILLED PIPE
CHILLED PLATE
SPRAYED AREA

FIGURE 1

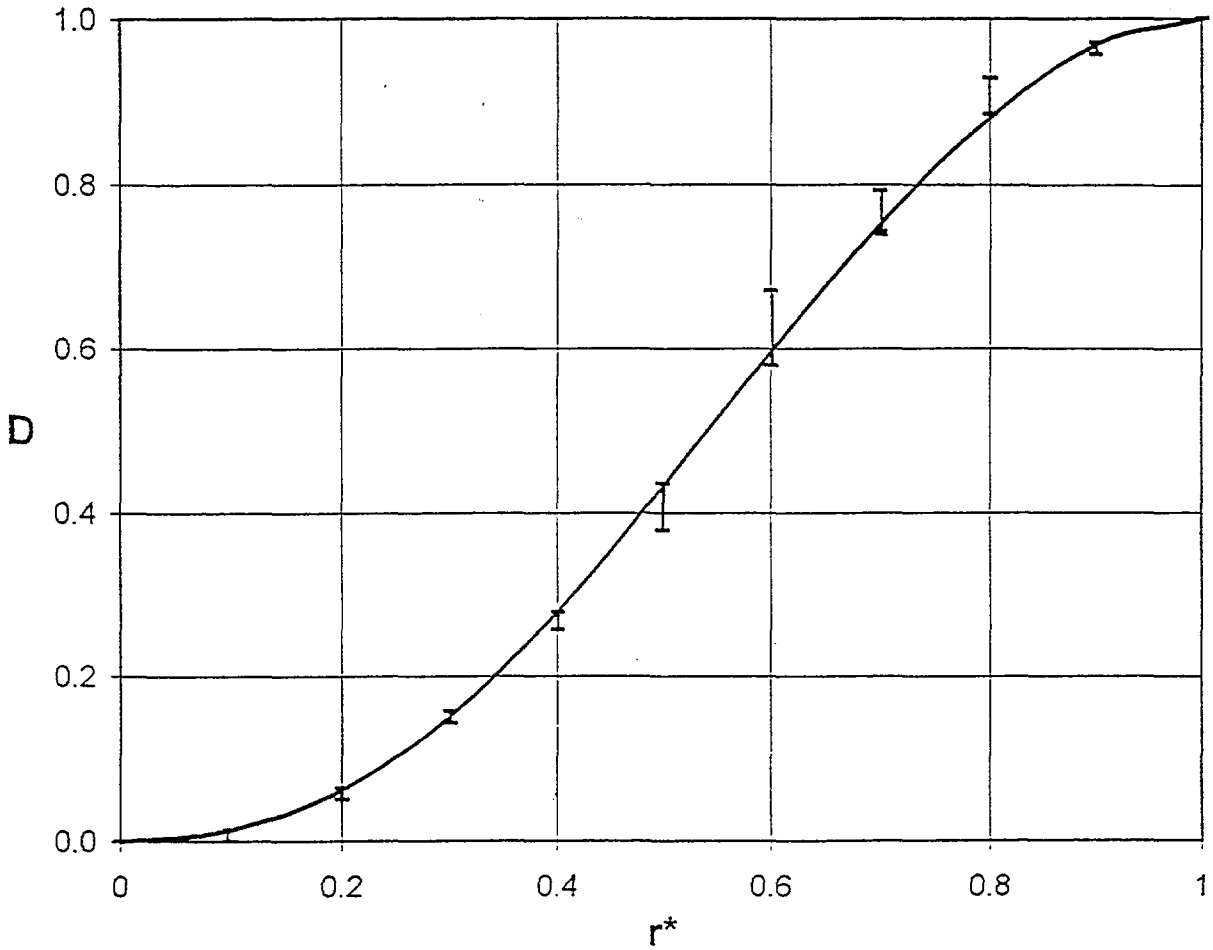

FIGURE 2

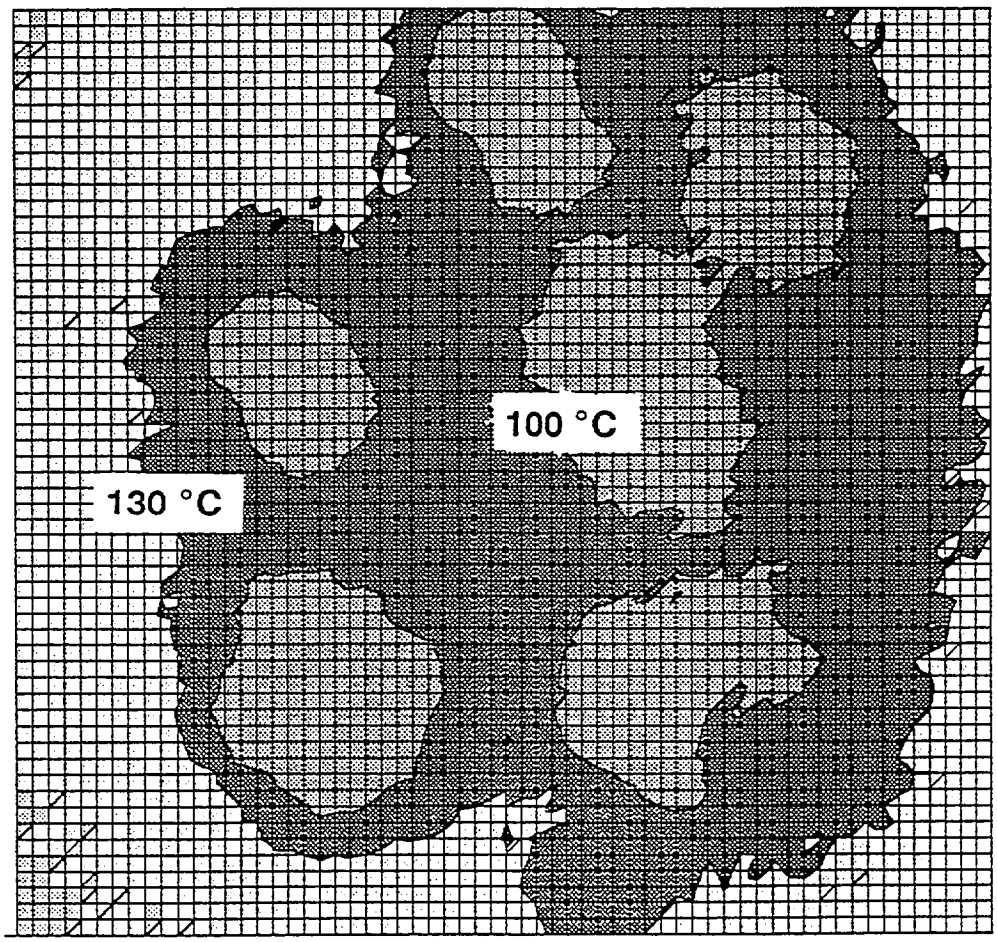

FIGURE 3

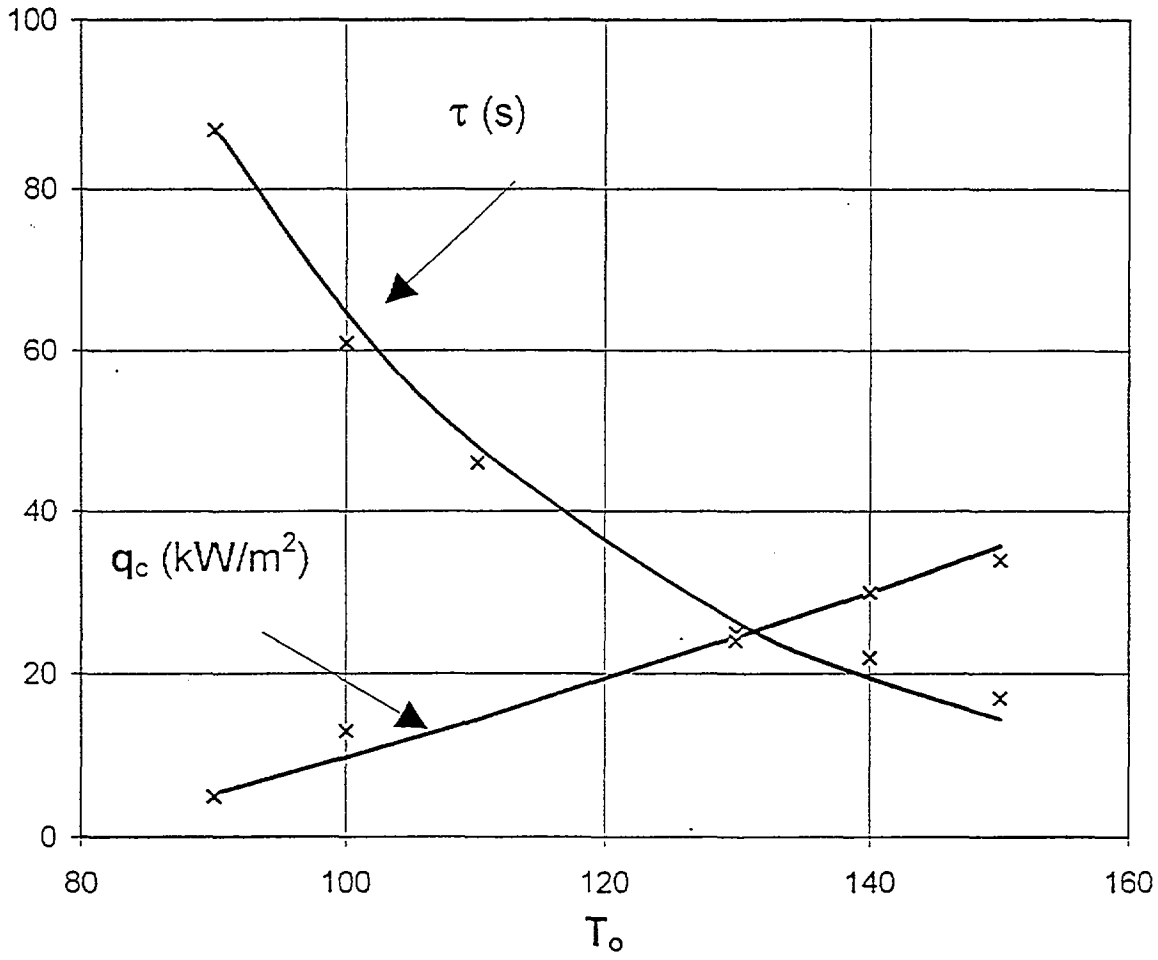

FIGURE 4

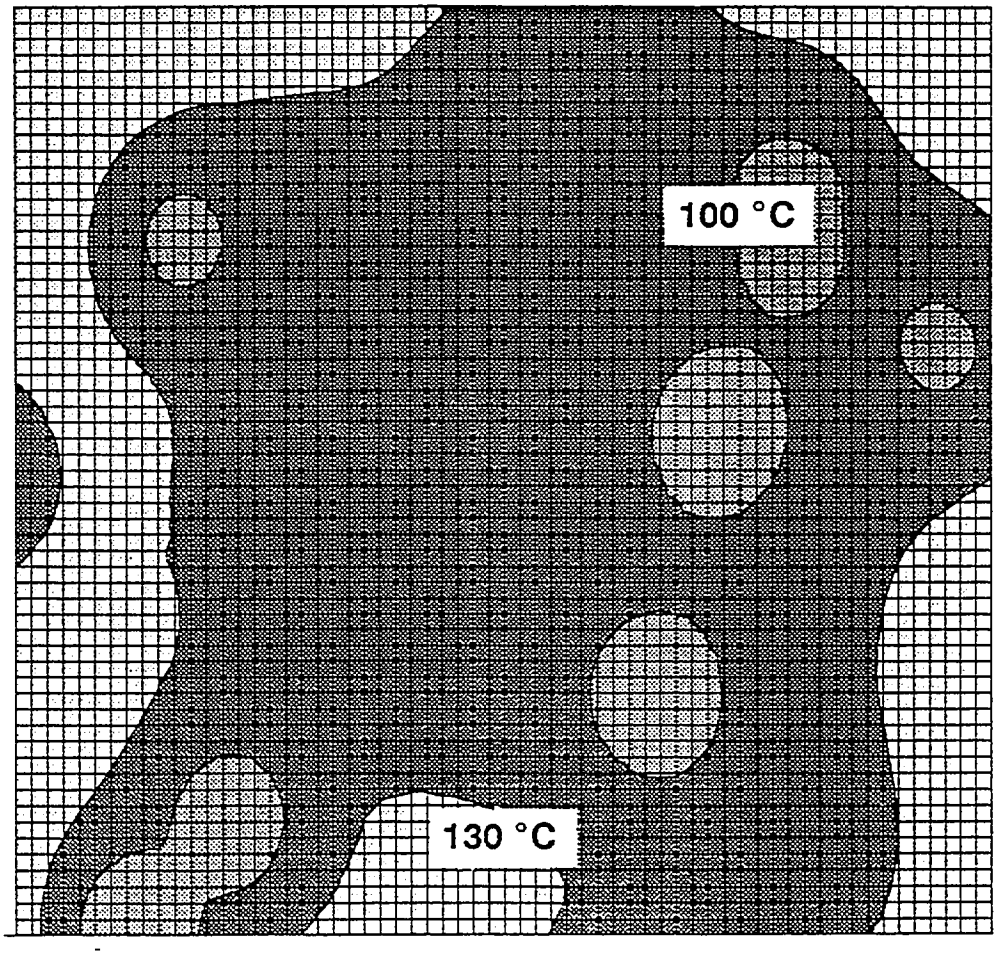

FIGURE 5

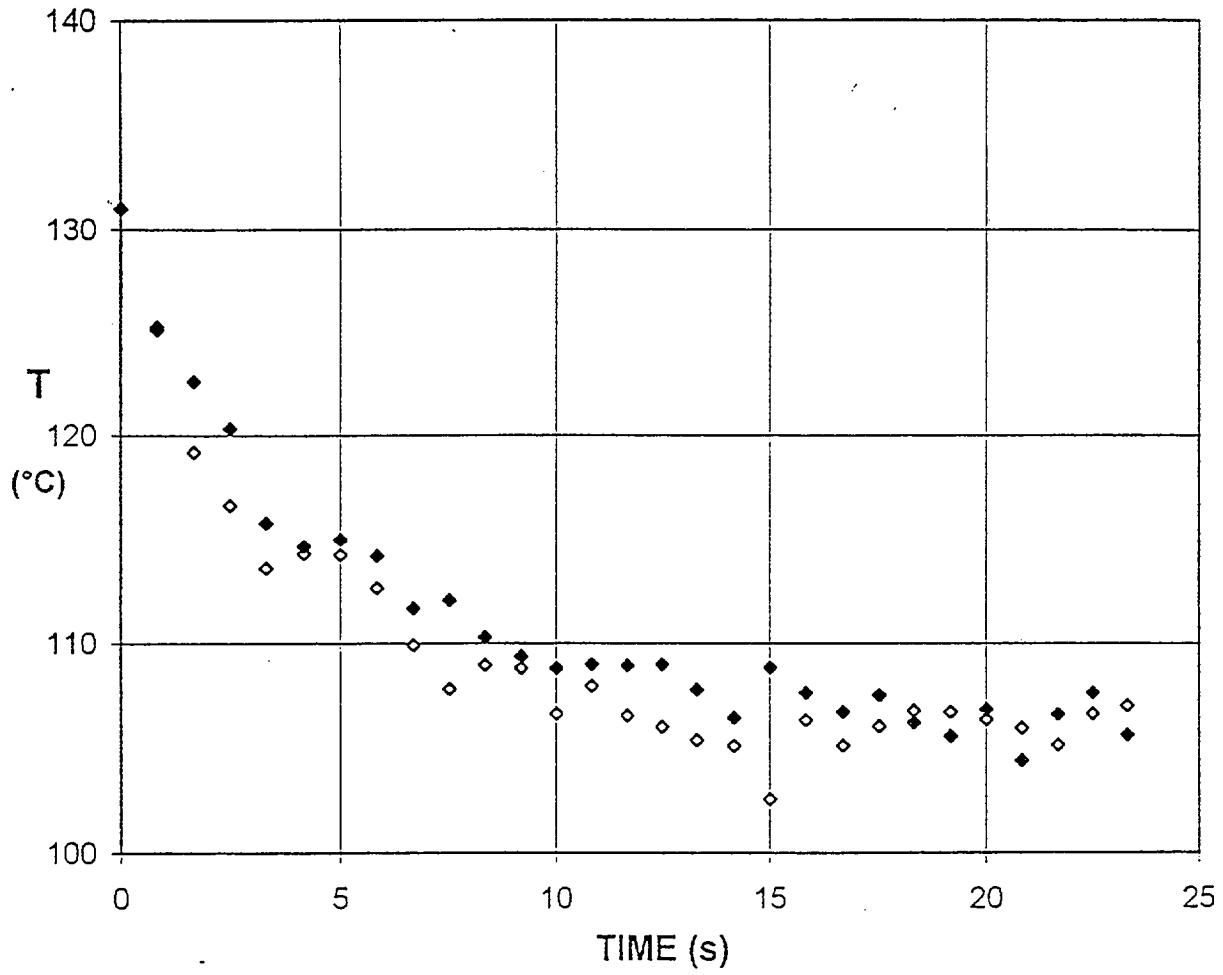

FIGURE 6

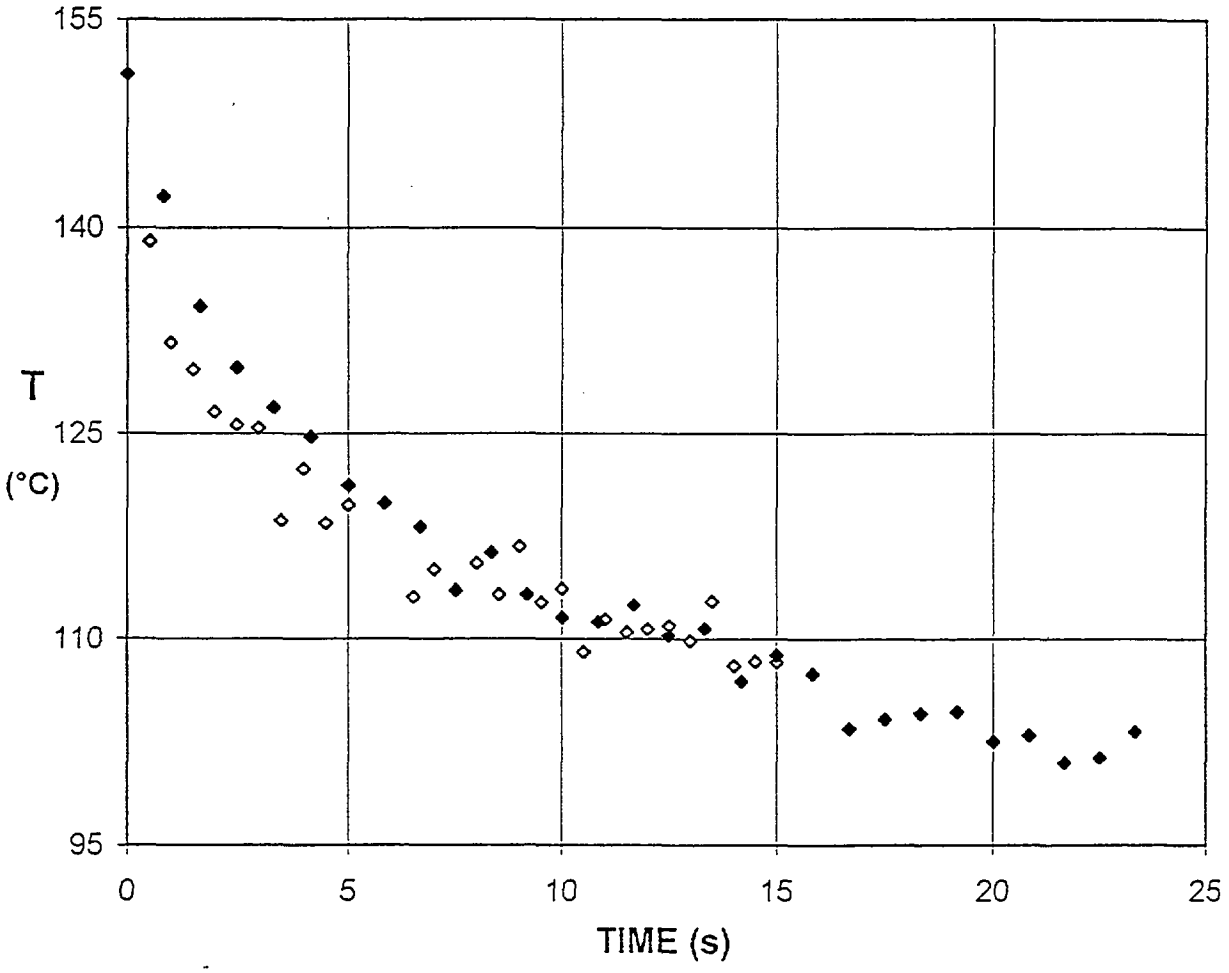

FIGURE 7

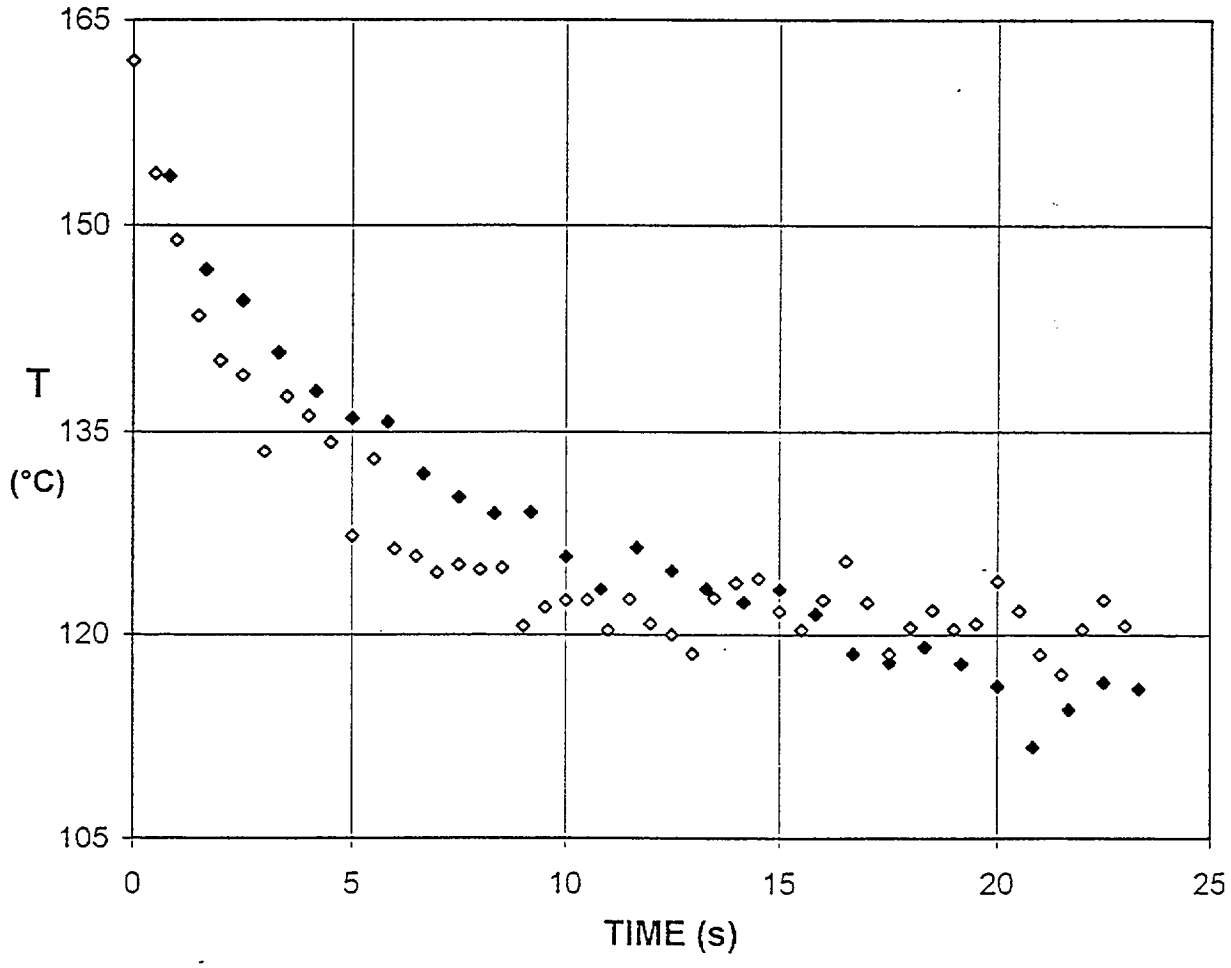

FIGURE 8

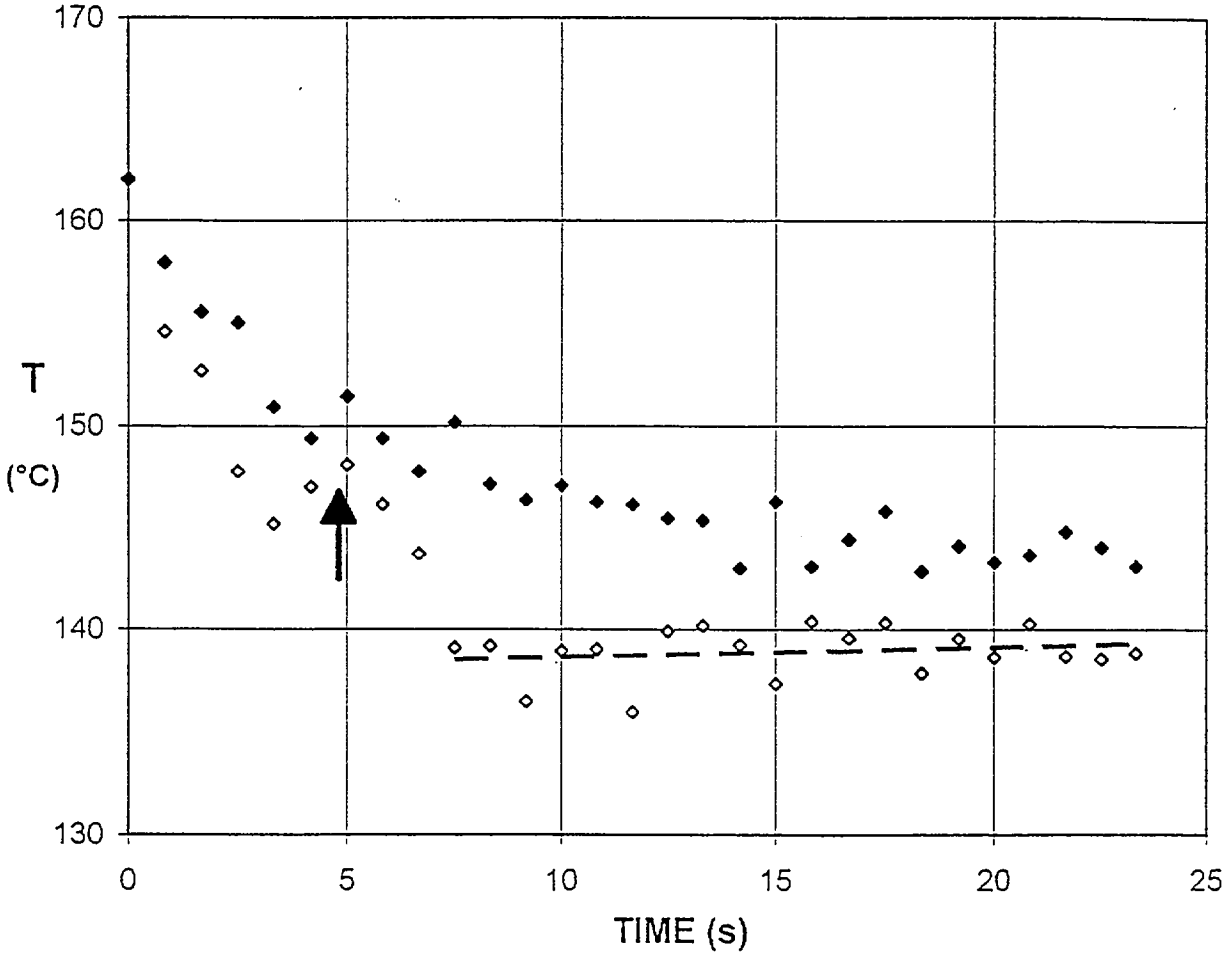

FIGURE 9

APPENDIX A:

Effect of surfactants in the water

S. Chandra, M. diMarzo, Y.M. Qiao & P. Tartarini, Effect of solid-liquid contact angle on droplet evaporation (1995) unpublished manuscript.

PAPER # 15

Effect of Liquid-Solid Contact Angle on Droplet Evaporation

S. Chandra[1], M. di Marzo[2], Y.M. Qiao[1], P. Tartarini[3]

[1] Mechanical Engineering Department
University of Toronto
Toronto, Ontario, Canada M5S 1A4

[2] Mechanical Engineering Department
University of Maryland
College Park, Md, U.S.A. 20742

[3] Istituto di Fisica Tecnica
Universita` di Bologna
viale Risorgimento, 2 - Bologna, Italy 40136

ABSTRACT

The effect of varying initial liquid-solid contact angle on the evaporation of single droplets of water deposited on a stainless steel surface is studied using both experiments and numerical modelling. Contact angle is controlled in experiments by adding varying amounts of a surfactant to water. The evolution of contact angle and liquid-solid contact diameter is measured from a video record of droplet evaporation. The computer model is validated by comparison with experimental results. Reducing contact angle increases contact area between the droplet and solid surface, and also reduces droplet thickness, enhancing heat conduction through the droplet. Both effects increase droplet evaporation rate. Decreasing the initial contact angle from 90° to 20° reduces droplet evaporation time by approximately 50%. The computer model is used to calculate surface temperature and heat flux variation during droplet evaporation: reducing contact angle is shown to enhance surface cooling.

INTRODUCTION

One of the most effective ways of cooling a hot, solid surface is to spray it with liquid droplets. Water sprays are widely used for fire suppression, both to extinguish flames on burning objects and to prevent flame spread by cooling surfaces that have still not ignited. Using excessive amounts of water in fighting fires can, however, cause considerable secondary fire damage, which has motivated research into finding methods to reduce water usage. There is also renewed interest in water as an environmentally benign alternative to halons for fire extinguishment on board aircraft and vehicles, where the weight of liquid that can be carried on board is limited and it is important to minimize water requirements. Efforts to maximize spray cooling efficiencies and optimize water application methods have led to the formulation of models[1-5] to predict heat transfer from a hot surface to an impinging spray. All such simulations incorporate sub-models that describe the evaporation of a single droplet on a hot surface. Several experimental studies have been carried out to observe droplet evaporation[6-13], and both numerical[14,15] and analytical[16-18] models of single droplet evaporation have been developed.

Di Marzo and Evans[14] proposed a model applicable to droplets evaporating on a high thermal conductivity surface at temperatures below those required to initiate nucleate boiling. The analysis was simplified by assuming the solid surface temperature to be constant during droplet evaporation, equal to the contact temperature of two semi-infinite solids. Droplet geometry was described (based on measurements from photographs) by a spherical cap, so that droplet shape was completely specified by the volume of liquid and the liquid-solid contact angle. The reliability of predictions from this model depends both on a correct selection of the initial contact angle and accurate description of its evolution during evaporation. Di Marzo and Evans[14] assumed that the contact angle decreased continuously during droplet evaporation, while the diameter of the wetted region under the droplet remained constant. Observation of water droplets evaporating on an aluminum surface showed this to be a valid assumption over most of the droplet lifetime. However, the assumption of constant liquid-solid contact diameter may not always be accurate. Studies of evaporating droplets[6] have shown that the contact angle cannot decrease beyond a

minimum value, called the receding contact angle[19]. Once this angle has been reached the contact angle remains constant, while the surface area wetted by the droplet decreases. Sadhal and Plesset's model [17] assumes constant contact angle during the entire evaporation process, which is an accurate description of the last stage of droplet evaporation after the receding contact angle is reached. Their results, however, are applicable only to droplets for which the liquid-vapor interface temperature equals that of the ambient vapor.

The contact angle may also be affected by thermal radiation incident upon a droplet. Di Marzo et al.[13] found that infrared radiation is absorbed at the surface of an evaporating droplet, heating it and reducing surface tension. This causes droplets to spread out, increasing liquid-solid contact area and decreasing droplet evaporation time. Such effects may be significant in modelling fire extinguishment by water droplets, and have to be accounted for.

A study of the effect of contact angle on droplet evaporation is important not only in formulating accurate models, but also in suggesting strategies to improve cooling efficiencies by enhancing surface wetting. For example, it is known that the addition of "wetting agents", which are typically surfactant solutions that reduce surface tension, significantly increases the fire extinguishing capabilities of water[20]. Large scale tests have shown that addition of a wetting agent reduces by up to 60% the volume of water required to extinguish fires on wood, cotton bales and rubber tires. Though wetting agents have been used for about 40 years, little information is available on the mechanism by which surfactants enhance heat transfer from a hot surface to impinging droplets in water sprays.

In the present work the effect of varying the initial liquid-solid contact angle on the evaporation of single droplets of water on a hot surface is investigated, using both experiments and numerical modelling. The contact angle is reduced progressively from 90° (the equilibrium value for pure water) to 20°, by adding increasing amounts of surfactant to the liquid. The surface temperature varies from 60°C to 110°C, low enough that nucleate boiling does not occur. In the experiments the initial droplet diameter is held constant (2.05 ± 0.03 mm), as well as surface material (stainless steel), ambient temperature (~20 °C) and ambient pressure (atmospheric). A

stainless steel surface is used since it resists oxidation when heated and can be cleaned easily after deposition and evaporation of droplets, allowing a constant surface condition to be maintained. Stainless steel has a low enough thermal conductivity that the surface cannot be assumed to be isothermal during droplet evaporation: temperature measurements under a droplet evaporating on a low thermal conductivity surface show both spatial and temporal variation[12]. Therefore, the numerical model of di Marzo et al.[15], which couples the solution of the heat conduction equation in both droplet and substrate, is used here to provide a numerical simulation of droplet evaporation.

The main objectives of the present study are: *a*) to investigate experimentally the effect of varying contact angle on the evaporation rate of water droplets; *b*) to measure the evolution of contact angle, contact diameter, and droplet volume during evaporation; *c*) to verify that the numerical model of droplet evaporation accurately predicts the effect of contact angle variation; *d*) to study, using the model, how heat transfer from the solid surface changes with contact angle; and *e*) to examine the possibility of improving spray cooling efficiencies by enhancing surface wetting by droplets.

EXPERIMENTAL METHOD

In the experiments described here, liquid surface tension and liquid-solid contact angle are reduced by dissolving a surfactant, sodium dodecyl sulfate (Malinckrodt Speciality Chemicals), in water. Three surfactant concentrations are used: 0 ppm (i.e., pure water), 100 ppm, and 1000 ppm by weight. Solutions are prepared by adding measured amounts (0.08 g or 0.8 g) of powdered surfactant to 800 g of distilled water. The measured equilibrium contact angle for pure water on a stainless steel surface is 90°; adding 100 ppm and 1000 ppm of surfactant reduces this angle to 55° and 20° respectively. Surfactant concentrations are low enough that other thermophysical properties remain unchanged.

A glass syringe with a plunger driven by a syringe pump is used to form droplets. Water or water/surfactant solution is pumped through stainless steel tubing to a hypodermic needle, at whose tip it accumulate until the weight of liquid exceeds surface tension forces attaching the drop

to the needle. Addition of surfactant reduces the surface tension; the needle diameter is increased to form uniform sized droplets. A 33 gauge needle is used for pure water and 100 ppm solutions, and 30 gauge for 1000 ppm solution droplets. Droplets with diameters of 2.05 mm (pure water), 2.02 mm (100 ppm) and 2.07 mm (1000 ppm) are formed by this method.

Droplets fall from a height of 50 mm onto a stainless steel surface. The droplet impact velocity (1.0 m/s) is low enough that drops remain intact after impact. The stainless steel plate, 50.8 mm square and 6.35 mm thick, is mounted on a copper block in which are housed two 125 W cartridge heaters. The solid surface temperature is measured by a chromel-alumel thermocouple inserted into a hole drilled into the plate. A temperature controller regulates power to the heaters so as to hold the surface temperature prior to droplet deposition constant within $\pm 0.5^\circ$ C.

Measurements of liquid-solid contact angles are sensitive to surface finish and the presence of any contaminants. The stainless steel surface is prepared by polishing with 600 grit emery cloth and metal polish. After the deposition and evaporation of each drop, traces of any residue are removed by cleaning the test surface first with a cotton swab dipped in acetone and then with distilled water. To ensure that surfactant does not accumulate in the syringe, tubing, or needle, the entire system is dismantled before refilling with a solution of different concentration, cleaned by placing it in an acetone bath in an ultrasonic cleaner, dried, and flushed with the new solution. The measured values of the initial contact angle are repeatable within $\pm 3^\circ$.

Droplet evaporation is recorded using a high resolution CCD video camera (Pulnix TM-745). Diffused backlighting is used to illuminate the drop, providing high contrast between the edge of the droplet and its background. Video images of the droplet are imported into a computer-based image analysis package (Image Analyst, Automatix Inc.). Evolution of the droplet-surface contact diameter is measured from the video record, using the image of a 1.6 mm diameter ball bearing to provide a calibration scale. The measurement resolution, corresponding to the size of one video pixel, is ± 0.01 mm. Droplet volume is determined from measurements of the contact diameter and droplet height, assuming the droplet to be a segment of a sphere. Liquid-solid contact angle is measured by using the image analysis software to detect the liquid-air interface in a droplet

image, and approximate it by a straight line. As the image is magnified, this line becomes a tangent to the interface through the liquid-solid-air contact point. The contact angle lies between this tangent and the plane of the solid surface. Values obtained using this automated procedure are checked by manually drawing a tangent through the contact point, and measuring the contact angle. The results obtained by these two methods differ by less than uncertainty in measurement, which is $\pm 2°$.

THEORETICAL MODEL

The model of diMarzo et al.[15] is used here to study the evaporation of a gently deposited droplet on a hot steel surface. It is also used to investigate solid surface temperature and heat flux distribution under droplets, where direct measurements are unavailable. Previous experiments[12] and analyses[15] have shown that the heat flux is neither uniform nor constant during the evaporative process. Most of the evaporation is found to take place at the outer edge of the droplet. Some basic assumptions made in formulating the model are:

- Heat conduction is assumed to be the only heat transfer mechanism in the liquid droplet and in the solid. Nucleate or film boiling are not present.
- The solid surface area wetted by the droplet remains constant when the contact angle is greater than the receding angle.
- After the contact angle reaches the receding angle the aspect ratio of the droplet (assumed to be shaped like a spherical cap) remains constant, while the contact diameter decreases with liquid volume.

Model Formulation

The modeling of the coupled solid and liquid thermal behavior is described by the transient conduction equation for both domains with the appropriate boundary conditions:

$$\text{Solid domain:} \quad \frac{\partial T}{\partial t} = \kappa_s \nabla^2 T \tag{1}$$

$$\text{Liquid domain:} \quad \frac{\partial T}{\partial t} = \kappa_l \nabla^2 T \tag{2}$$

By introducing an overall heat transfer coefficient h at the exposed solid surface, the boundary condition at the liquid-vapor interface can be written as[14]:

$$- k_l \nabla T = h\,(T_i - T_a) + 0.624\, k_c \left(\frac{D}{\kappa_a}\right)^{\frac{2}{3}} \frac{\Lambda}{c_a} \frac{x_i - x_a}{1 - x_a} \tag{3}$$

The boundary conditions at the liquid-solid interface and at the exposed solid surface are:

$$\text{at } 0 \le r \le R, z = 0: \qquad T = T_0;\ k_s \frac{\partial T}{\partial z} = k_l \frac{\partial T}{\partial z} \tag{4}$$

$$\text{at } r > R, z = 0: \qquad k_s \frac{\partial T}{\partial z} = h\,(T_{s0} - T_a) + \varepsilon_s\, \sigma\, (T_s^4 - T_a^4) \tag{5}$$

A linear temperature distribution in the solid is required as initial condition. The far-field temperature distribution is assumed unaffected by droplet evaporation. The liquid droplet is assumed to be initially in thermal equilibrium with the ambient air.

Extremely strong local thermal gradients when the drop initially contacts the surface preclude solution of this problem with conventional finite difference schemes. The solution is obtained by using a Boundary Element Method (BEM) for the solid region and a Control Volume Method (CVM) for the liquid region. The BEM is described in detail by Wrobel & Brebbia[21], while the CVM used here is described by Tartarini et al.[22]. Although the droplet and the solid are treated separately by different numerical methods, the temperatures in the droplet and along the solid surface are solved simultaneously at each time step by coupling the CVM and the BEM in the numerical model. The input variables are: *a*) solid surface material; *b*) solid surface initial temperature; *c*) droplet initial volume; *d*) droplet initial shape factor (β_0); and *e*) the value of the receding contact angle (assumed to be 10° in this study, based on experimental observation). All the physical properties of water and most common solid, non-porous materials have already been implemented into the code. Since droplet shape is assumed to be always that of a spherical cap, liquid-solid contact angle θ is a function of the droplet radius (r) and of the droplet apex (a), that is:

$$\theta = 2\ arctg\left(\frac{a}{r}\right) \tag{6}$$

and it can be calculated at each time step. The validity of this assumption was confirmed by experimental contact angle measurements, shown in the next section.

The model has previously been validated by comparing predictions with experimental data provided by Klassen and di Marzo[9]. A comprehensive comparison of the model with the data is obtained in previous works by looking at the overall predicted evaporation time for aluminum (k = 180 W/m°C) and Macor (k = 1.3 W/m°C) and at the experimental results obtained by Klassen and di Marzo[9], and by di Marzo and Evans[14].

RESULTS AND DISCUSSION

Figure 1 shows photographs of the evaporation of droplets of pure water (0 ppm), and 100 ppm and 1000 ppm surfactant in water solutions on a stainless steel surface initially at a temperature of 80°C. Each column shows successive stages in the evaporation of a droplet; the time of each frame, measured from the instant of impact, is marked. A single bubble is seen in each drop, formed by entrapment of air at the liquid-solid interface during droplet deposition. Increasing surfactant concentration reduces contact angle and increases the liquid-solid contact area. Spreading of the droplet results in a significant decrease in droplet evaporation time: the evaporation time of a 1000 ppm surfactant solution droplet is approximately half that of pure water. Evaporation of a 1000 ppm solution droplet leaves a visible residue of surfactant upon evaporation (figure 1), which is cleaned before deposition of another droplet.

To confirm that the numerical simulation accurately models droplet evaporation, code predictions are compared with experimental results over the entire range of surface temperatures used in experiments. Figure 2 shows both experimental measurements and numerical code predictions of volume evolution during evaporation of pure water droplets at three surface

temperatures: 60°C, 80°C and 100°C. Good agreement is seen between measured and predicted values at all surface temperatures.

The model also accurately predicts the increased evaporation rate of droplets whose initial contact angle is reduced by addition of a surfactant. Figure 3 shows a comparison between measurements and code predictions of volume evolution for droplets with 0, 100 and 1000 ppm surfactant added, on a stainless steel surface at 80°C. Reduction in evaporation time because of adding surfactant is summarized in figure 4, which shows droplet evaporation time for $60°C \leq T_S \leq 110°C$. Solid surface temperature above 110°C cause the onset of nucleate boiling, for which the code is no longer applicable. Evaporation time is reduced to approximately 75% and 50% of that of pure water drops by addition of 100 ppm and 1000 ppm surfactant respectively. This reduction in evaporation time is correctly predicted by the numerical code.

Figure 5 shows the measured variation of contact angle during droplet evaporation. A pure water drop has a large initial contact angle (90°±3°). The contact angle decreases as the droplet evaporates, while contact diameter remains unchanged. Corresponding measurements of the diameter wetted by the same drop are shown in figure 6. The contact diameter remains almost constant until the end of the droplet lifetime, as assumed by di Marzo & Evans [14] in modelling droplet evaporation. Adding 100 ppm of surfactant to a water droplet reduces the initial contact angle to 55°±3° (figure 5). The contact angle decreases until it reaches the value of the receding contact angle, which is measured to be 10° and is not changed by addition of surfactant to water. The contact angle then remains constant, while the contact diameter decreases (figure 6). Droplets with 1000 ppm of surfactant have a low initial contact angle (20°±3°). On evaporation the contact angle rapidly reaches the receding value, and is then constant over most of the droplet lifetime. The computer code provides an accurate description of the variation of both contact angle and contact diameter during droplet evaporation.

Decreased droplet evaporation time when contact angle is reduced by adding a surfactant can have two possible causes. Firstly, droplet contact diameter becomes larger, increasing the area for heat transfer from the solid to liquid. Secondly, when the droplet spreads and the liquid layer

becomes thinner heat transfer to the liquid-vapor interface rises, increasing the interface temperature and the saturation vapor pressure at the droplet surface. If this second effect is significant, we expect to see an increase in heat flux from the solid surface to the droplet when initial contact angle is reduced. Figure 7 shows the calculated variation of local heat flux at the center of the surface area wetted by drops evaporating on a surface initially at 80°C, and it confirms that adding 100 ppm or 1000 ppm of surfactant produces a small increase in heat flux. In all three cases (0 ppm, 100 ppm and 1000 ppm) heat flux increases towards the end of droplet lifetime, as droplets evaporate and become thinner. However, increase in surface area wetted by the drop is the more important effect of contact angle reduction, as seen in figure 8 which plots calculated values of the heat flux averaged over the entire wetted area. Addition of surfactant reduces the average heat flux, indicating that increased local heat flux is offset by the larger area wetted by the drop.

The increased effectiveness of droplets in cooling a hot surface when surfactant is added can be demonstrated through comparing temperature profiles in the substrate during droplet evaporation. In figures 9*a-c* the evolution of temperature is shown in a solid surface initially at 80°C, on which droplets with 0 ppm, 100 ppm or 1000 ppm of dissolved surfactant are deposited. Temperature profiles are shown at 10% (figure 9*a*), 50% (figure 9*b*) and 90% (figure 9*c*) respectively of the total evaporation time of each droplet. Temperatures are plotted against a normalized coordinate obtained by dividing the radial distance from the center of the wetted region by the radius of a spherical droplet (R_{sphere} = 1.0 mm in our experiments). Surface temperature is lowest at the center of each droplet, and increases towards its edge. Addition of a surfactant is seen to both significantly enhance cooling at the droplet center, as well as to increase the radius over which surface temperature is lowered by the droplet.

Both experiments and the numerical model have shown that varying initial liquid-solid contact angle can significantly change droplet evaporation time. Figure 10 summarizes the effect of reducing contact angle on evaporation time of droplets on a stainless steel surface initially at 80°C, showing that reducing the initial contact angle from 90° to 20° (the range in our experiments) decreases the evaporation time by approximately 50%. Models of spray evaporation therefore

require accurate information about the initial contact angle to realistically simulate fire extinguishment. These observations also help explain why adding a wetting agent improves the fire extinguishing capabilities of water.

CONCLUSIONS

The cooling of a hot solid surface by evaporation of a liquid droplet has been studied using both experiments and numerical modelling. The effect of varying liquid-solid contact angle on droplet evaporation has been investigated in detail. The model was validated by comparing predictions of droplet evaporation time with experimental measurements, for a range of surface temperatures ($60°C \leq T_S \leq 110°C$) and initial contact angles ($20° \leq \theta_0 \leq 90°$). Addition of a surfactant to a water droplet reduces surface tension and increases its spreading on a solid surface. As the liquid layer becomes thinner, heat transfer from the solid to the liquid-vapor interface is enhanced. Spreading of the droplet also increases the heat transfer area. Both these effects contribute to a faster evaporation rate: decreasing contact angle from 90° to 20° reduced droplet evaporation time by approximately 50%.

ACKNOWLEDGEMENTS

This study was made possible by a grant of the Building and Fire Research Laboratory, National Institute of Standards and Technology. Funding of the computational expenditures was provided by the Italian M.U.R.S.T. and C.N.R. Experiments were funded by a grant from the Canadian N.S.E.R.C.

NOMENCLATURE

a	droplet apex
c	specific heat
D	air-steam mass diffusivity
h	overall heat transfer coefficient
h_c	convective heat transfer coefficient
k	thermal conductivity
r	radial coordinate
R	radius of the wetted area
t	time
T	temperature
x	molar fraction of steam in air
z	axial coordinate

Greek letters

β	shape parameter
ε	emissivity
θ	solid-liquid contact angle
κ	thermal diffusivity
Λ	liquid latent heat of vaporization
σ	Stefan-Boltzmann constant

Subscripts

a	air
i	interfacial
l	liquid
s	solid sphere
0	initial

REFERENCES

1. Toda, S., A study of mist cooling. First report:investigation of mist cooling. *Heat Transfer - Japanese Research* **1**(3), 39-50 (1972).

2. Bonacina, C., Del Giudice, S. & Comini, G., Dropwise Evaporation. *Transactions of the ASME- Journal of Heat Transfer* **101**, 441-446 (1979).

3. Rizza, J. J., A numerical solution to dropwise evaporation. *Transactions of the ASME, Journal of Heat Transfer* **103**, 501-507 (1981)

4. Bolle, L. & Moreau, J. C., Spray cooling of hot surfaces. *Multiphase Science and Technology* **1**, 1-97 (1982).

5. Tio, K. K. & Sadhal, S. S., Dropwise evaporation: thermal analysis of multidrop systems. *International Journal of Heat and Mass Transfer* **35**, 1987-2004, (1992).

6. Simon, F. F. & Hsu, Y. Y., Wetting dynamics of evaporating drops on various surfaces. NASA TM X-67913 (1971).

7. Michiyoshi, I. & Makino, K., Heat transfer characteristics of evaporation of a liquid droplet on heated surfaces. *International Journal of Heat and Mass Transfer* **21**, 605-613 (1978).

8. Zhang, N. & Yang, W. J., Evaporative convection in minute drops on a plate with temperature gradient. *International Journal of Heat and Mass Transfer* **26**, 1479-1488 (1983).

9. Klassen, M. & di Marzo, M., Transient cooling of a hot surface by droplets evaporation. NIST-GCR-90-575 (1990).

10. Xiong, T. Y. & Yuen, M. C., Evaporation of a liquid droplet on a hot plate. *International Journal of Heat and Mass Transfer* **34**, 1881-1894, (1991).

11. Rymkiewicz, J. & Zapalowicz, Z., Analysis of the evaporation process for water droplet on flat heated surface. *International Communications in Heat and Mass Transfer* **20**, 687-697 (1993).

12. Abu-Zaid, M. & Atreya, A., Transient cooling of hot porous and nonporous ceramic solid by droplet evaporation. *Transactions of the ASME-Journal of Heat Transfer* **116**, 694-701 (1994).

13. di Marzo, M. & Evans, D. D., Evaporation of a water droplet deposited on a hot high thermal conductivity surface. *Transactions of the ASME-Journal of Heat Transfer* **111**, 210-213 (1989).

14. di Marzo, M., Tartarini, P., Liao, Y., Evans, D. & Baum, H., Evaporative cooling due to a gently deposited droplet. *International Journal of Heat and Mass Transfer* **36**, 4133-4139 (1993).

15. di Marzo, M., Kidder, C. H. & Tartarini, P., Infrared thermography of dropwise evaporative cooling of a semi-infinite solid subjected to radiant heat input, *Experimental Heat Transfer* **5**, 101-114 (1992).

16 Yang, W. J., Mechanics of droplet evaporation on heated surfaces. *Letters in Heat and Mass Transfer* **5**, 151-166 (1978).

17. Sadhal, S. S. & Plesset, M. S., Effect of solid properties and contact angle in dropwise condensation and evaporation. *Transactions of the ASME-Journal of Heat Transfer* **101**, 48-54 (1979).

18. Tio, K. K. & Sadhal, S.S., Thermal analysis of droplet spray evaporation from a heated solid surface. *Transactions of the ASME-Journal of Heat Transfer* **114**, 220-233 (1992).

19. Herzberg, W. J. & Marian, J. E., The receding contact angle. *Journal of Colloid and Interface Science* **33**, 164-171 (1970).

20. Bryan, J. L., Fire Suppression and Detection Systems, 3rd edition, Macmillan Publishing Company, New York , 331-334 (1993).

21. Wrobel, L.C. & Brebbia, C.A., A Formulation of the Boundary Element Method for Axisymmetric Transient Heat Transfer Conduction. *International Journal of Heat and Mass Transfer* **24**, pp. 843-850 (1981).

22. Tartarini, P., Liao, Y. & diMarzo, M., Transient Cooling of a Hot Surface by Droplets Evaporation. UMCP Mechanical Engineering Report, No. 90-6 (1990).

FIGURE CAPTIONS

Figure 1 The evaporation of droplets of pure water (0 ppm), 100 ppm and 1000 ppm surfactant solutions on a stainless steel surface at 80°C.

Figure 2 Comparison of code predictions (solid lines) with measured (symbols) volume evolution during evaporation of pure water droplets on a stainless steel surface at 60°C, 80°C and 100°C.

Figure 3 Comparison of code predictions (solid lines) with measured (symbols) volume evolution during evaporation of droplets of pure water (0 ppm), 100 ppm and 1000 ppm surfactant solutions on a stainless steel surface at 80°C.

Figure 4 The evaporation time of droplets of pure water (0 ppm), 100 ppm and 1000 ppm surfactant solutions on a stainless steel surface at initial surface temperatures ranging from 60°C to 110°C.

Figure 5 Evolution of contact angle during evaporation of droplets of pure water (0 ppm), 100 ppm and 1000 ppm surfactant solutions on a stainless steel surface at 80°C.

Figure 6 Evolution of liquid-solid contact diameter during evaporation of droplets of pure water (0 ppm), 100 ppm and 1000 ppm surfactant solutions on a stainless steelsurface at 80°C.

Figure 7 Calculated variation of local heat flux at the center of the surface area wetted by droplets evaporating on a stainless steel surface initially at 80 C.

Figure 8 Calculated values of heat flux averaged over the entire wetted area during droplet evaporation on a surface initially at 80 C.

Figure 9 Calculated temperature profiles in a solid surface initially at 80°C, during evaporation of droplets of pure water (0 ppm), 100 ppm and 1000 ppm surfactant solutions at *a*) 10%, *b*) 50%, and *c*) 90% of the total evaporation time.

Figure 10 Effect of reducing contact angle on evaporation time of droplets on a stainless steel surface initially at 80°C.

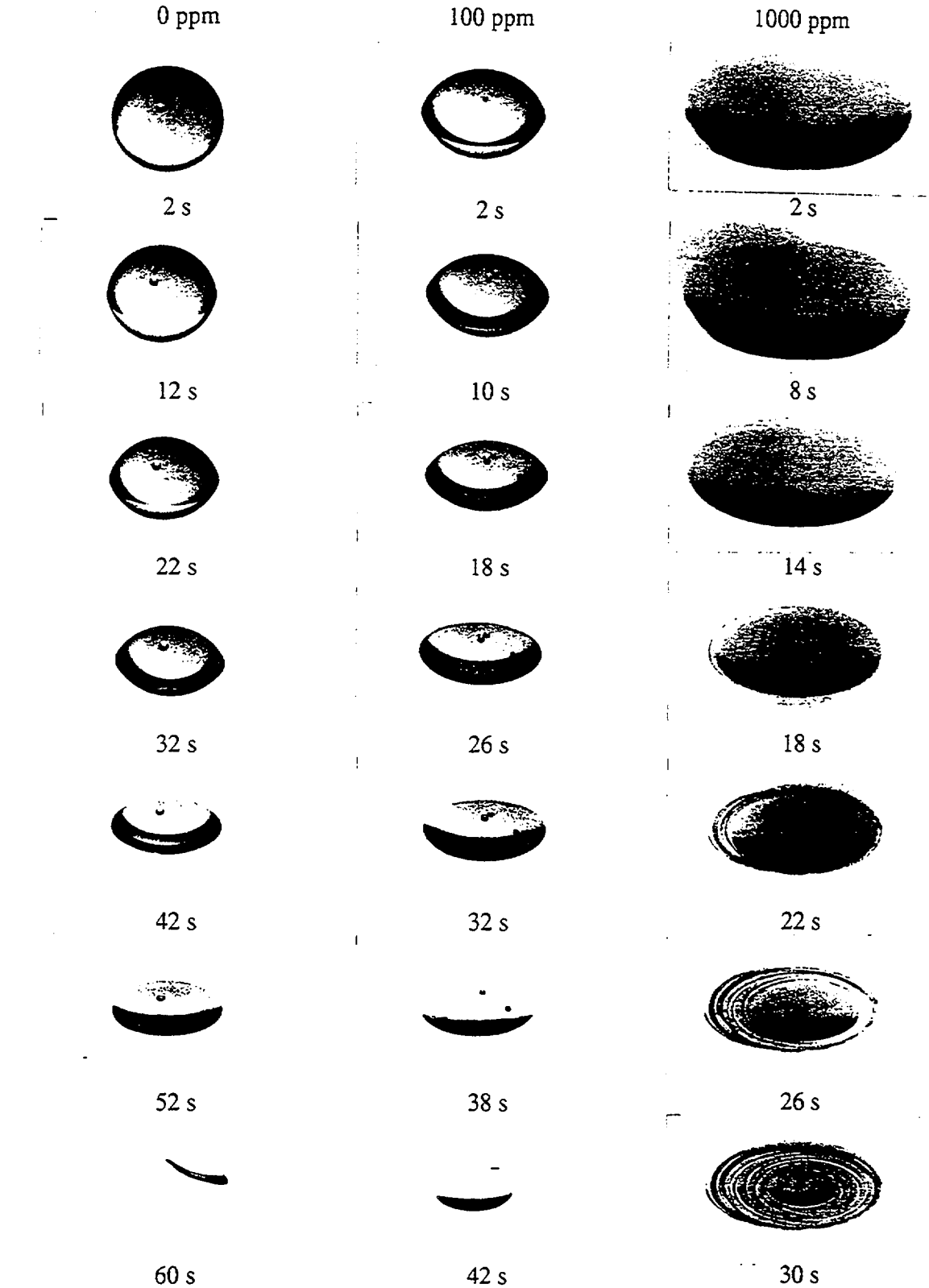

Figure 1 The evaporation of droplets of pure water (0 ppm), 100 ppm and 1000 ppm surfactant solutions on a stainless steel surface at 80°C.

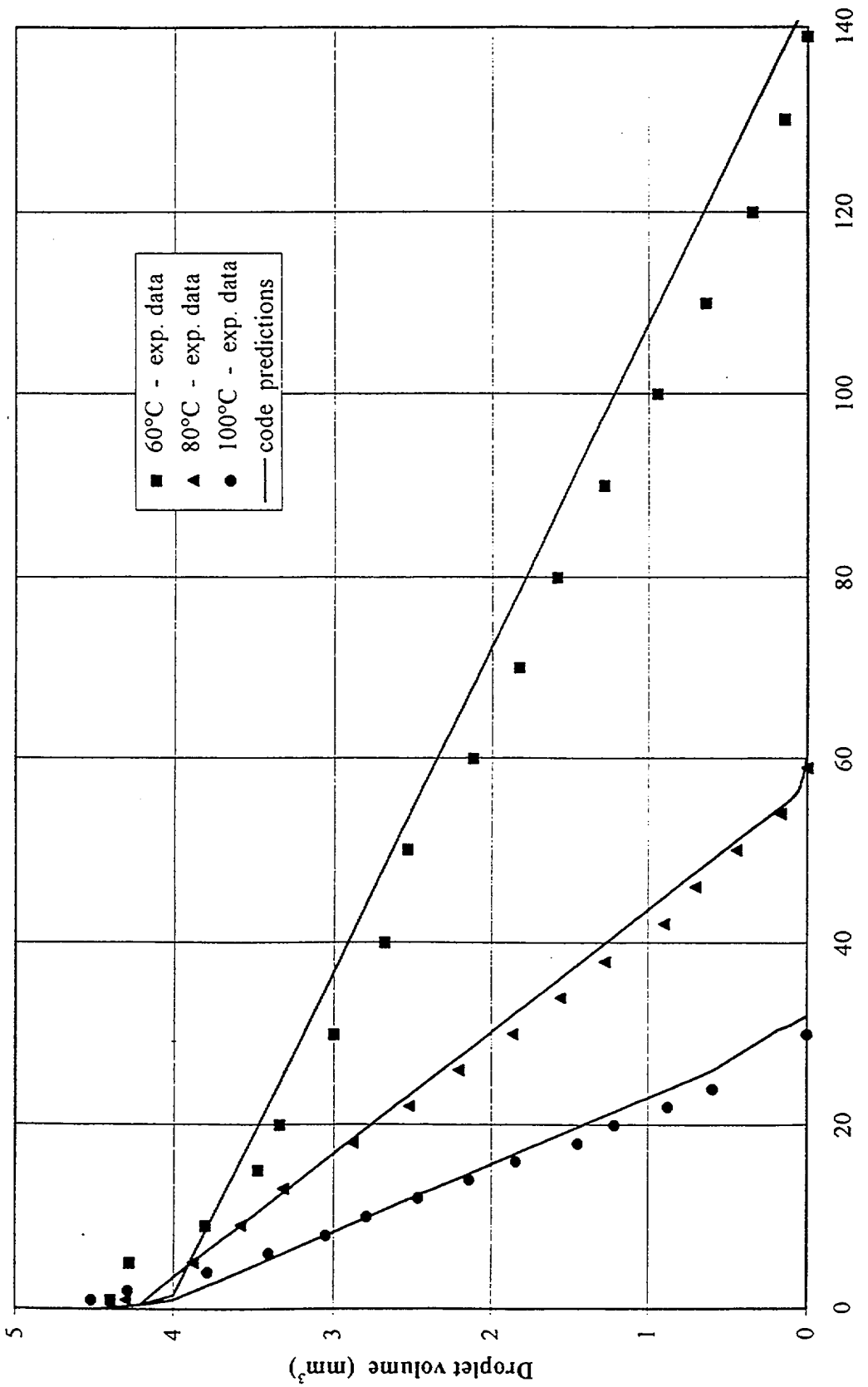

Figure 2 Comparison of code predictions (solid lines) with measured (symbols) volume evolution during evaporation of pure water droplets on a stainless steel surface at 60°C, 80°C and 100°C.

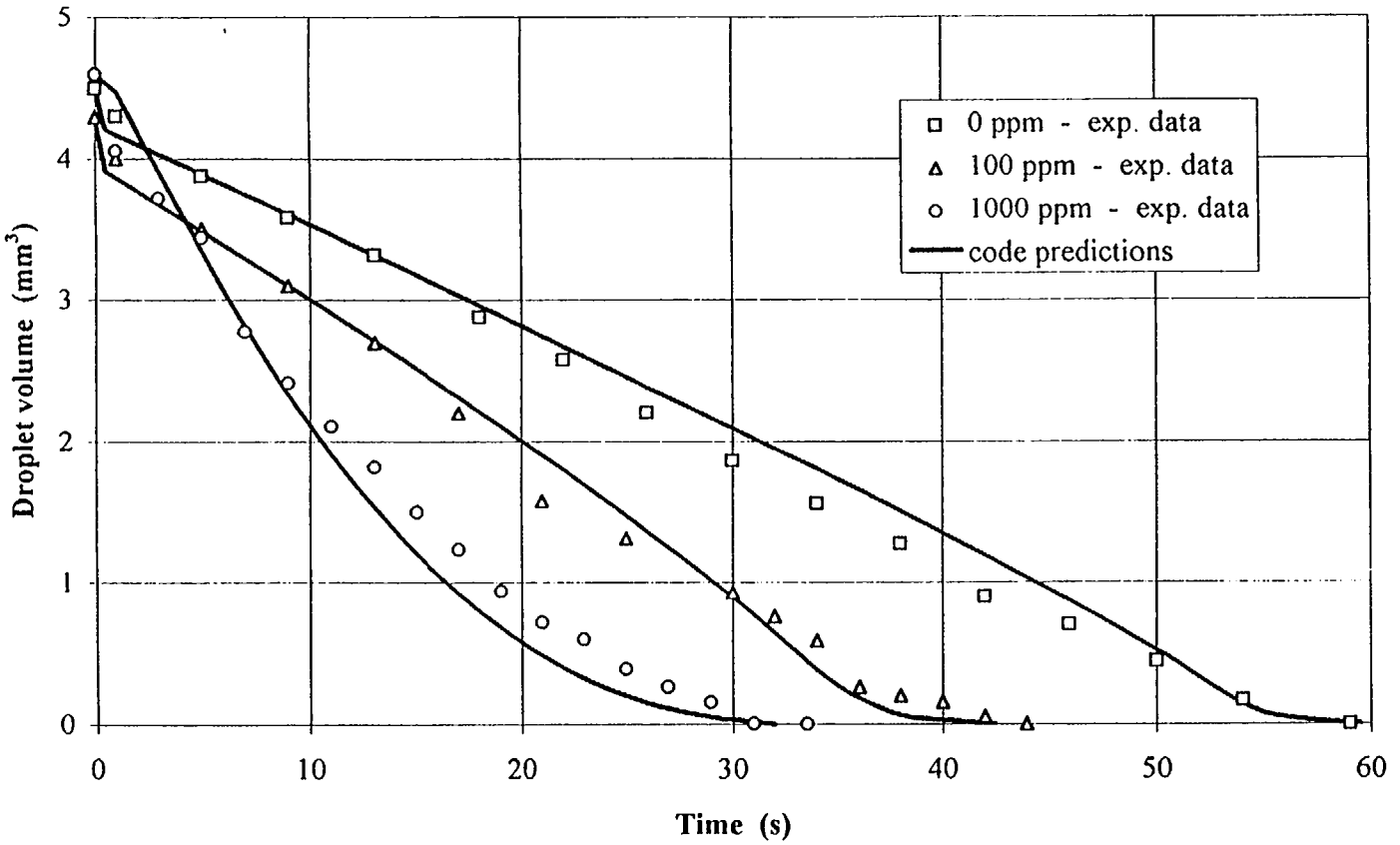

Figure 3 Comparison of code predictions (solid lines) with measured (symbols) volume evolution during evaporation of droplets of pure water (0 ppm), 100 ppm and 1000 ppm surfactant solutions on a stainless steel surface at 80°C.

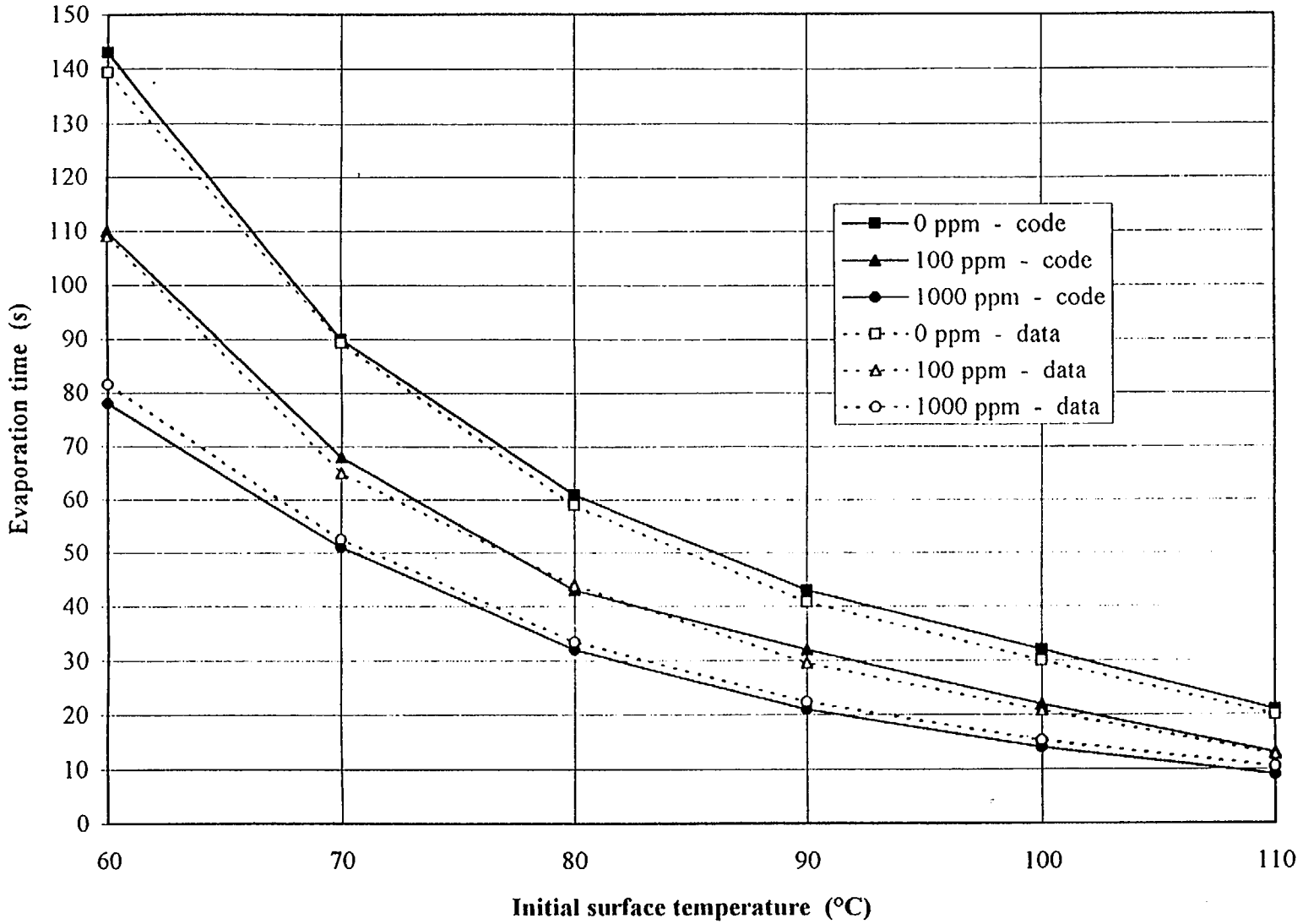

Figure 4 The evaporation time of droplets of pure water (0 ppm), 100 ppm and 1000 ppm surfactant solutions on a stainless steel surface at initial surface temperatures ranging from 60°C to 110°C.

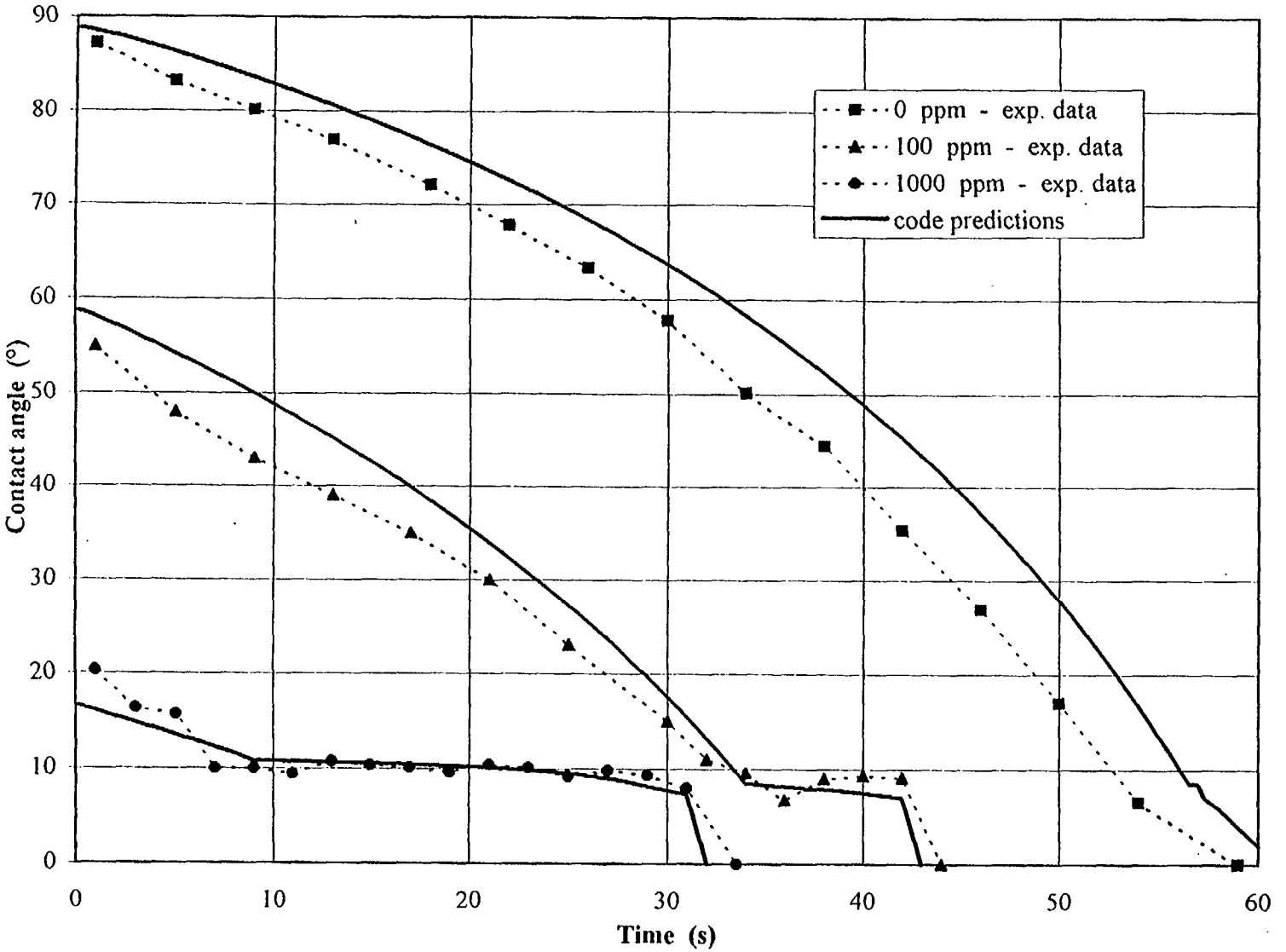

Figure 5 Evolution of contact angle during evaporation of droplets of pure water (0 ppm), 100 ppm and 1000 ppm surfactant solutions on a stainless steel surface at 80°C.

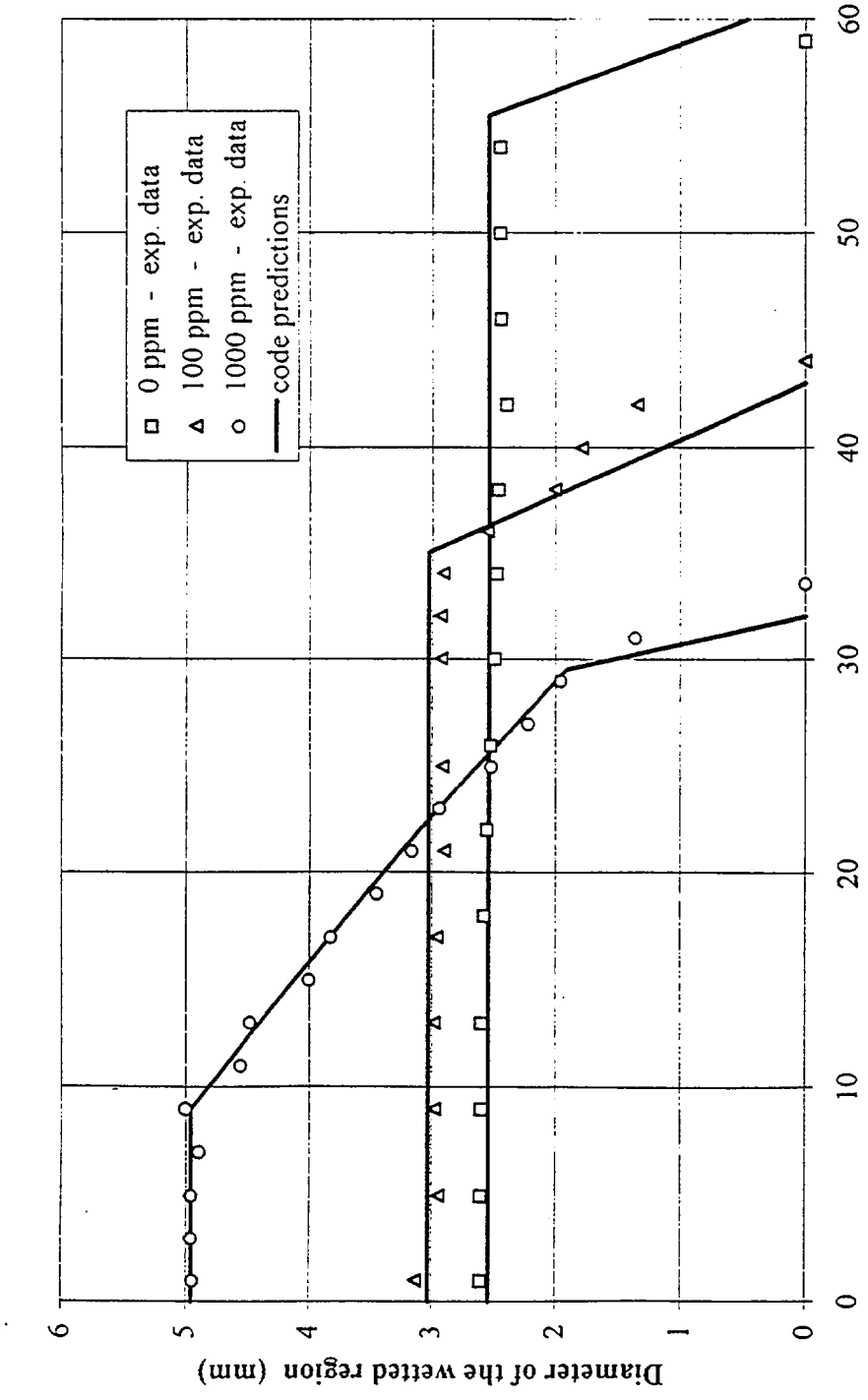

Figure 6 Evolution of liquid-solid contact diameter during evaporation of droplets of pure water (0 ppm), 100 ppm and 1000 ppm surfactant solutions on a stainless steel surface at 80°C.

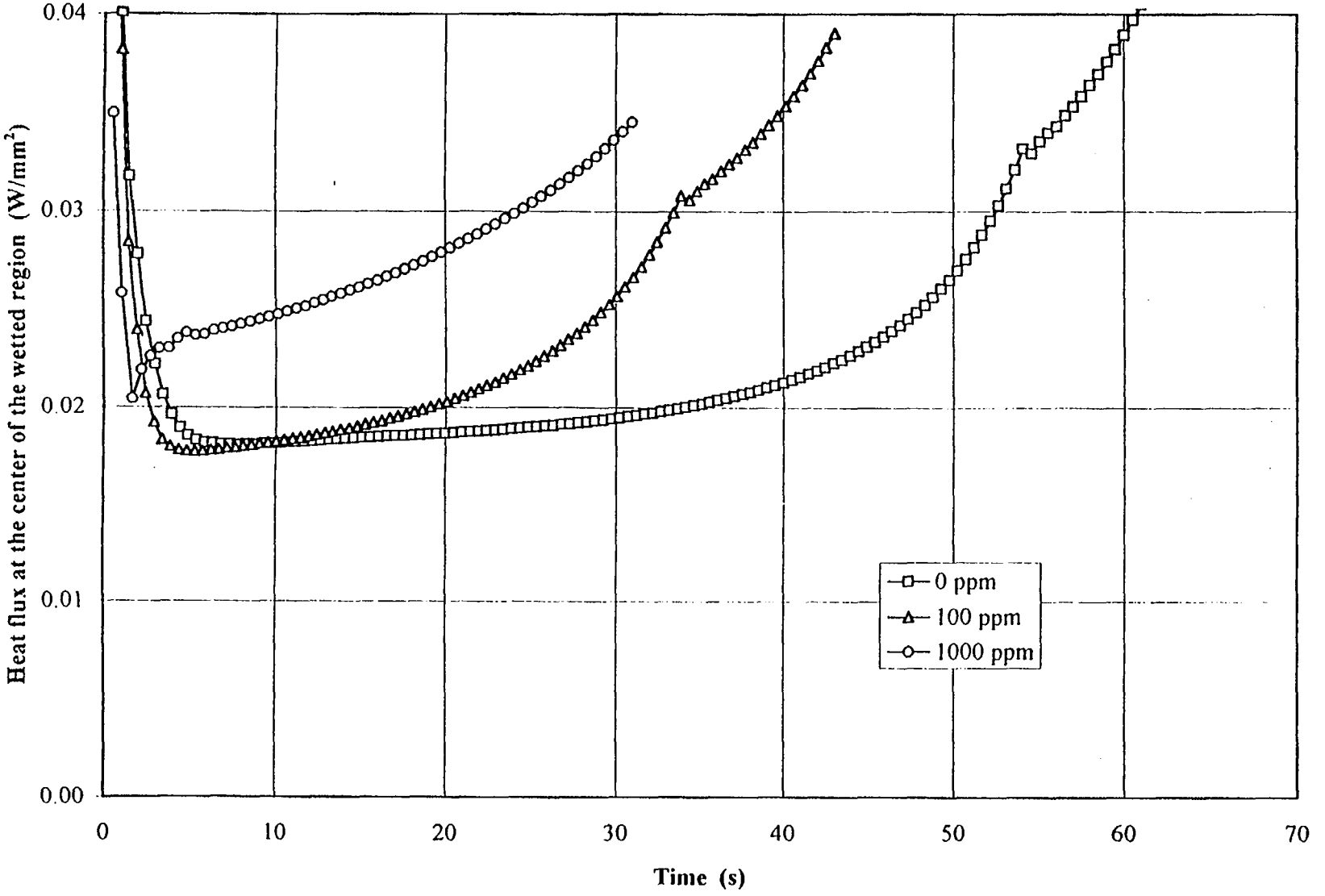

Figure 7 Calculated variation of local heat flux at the center of the surface area wetted by droplets evaporating on a stainless steel surface initially at 80°C.

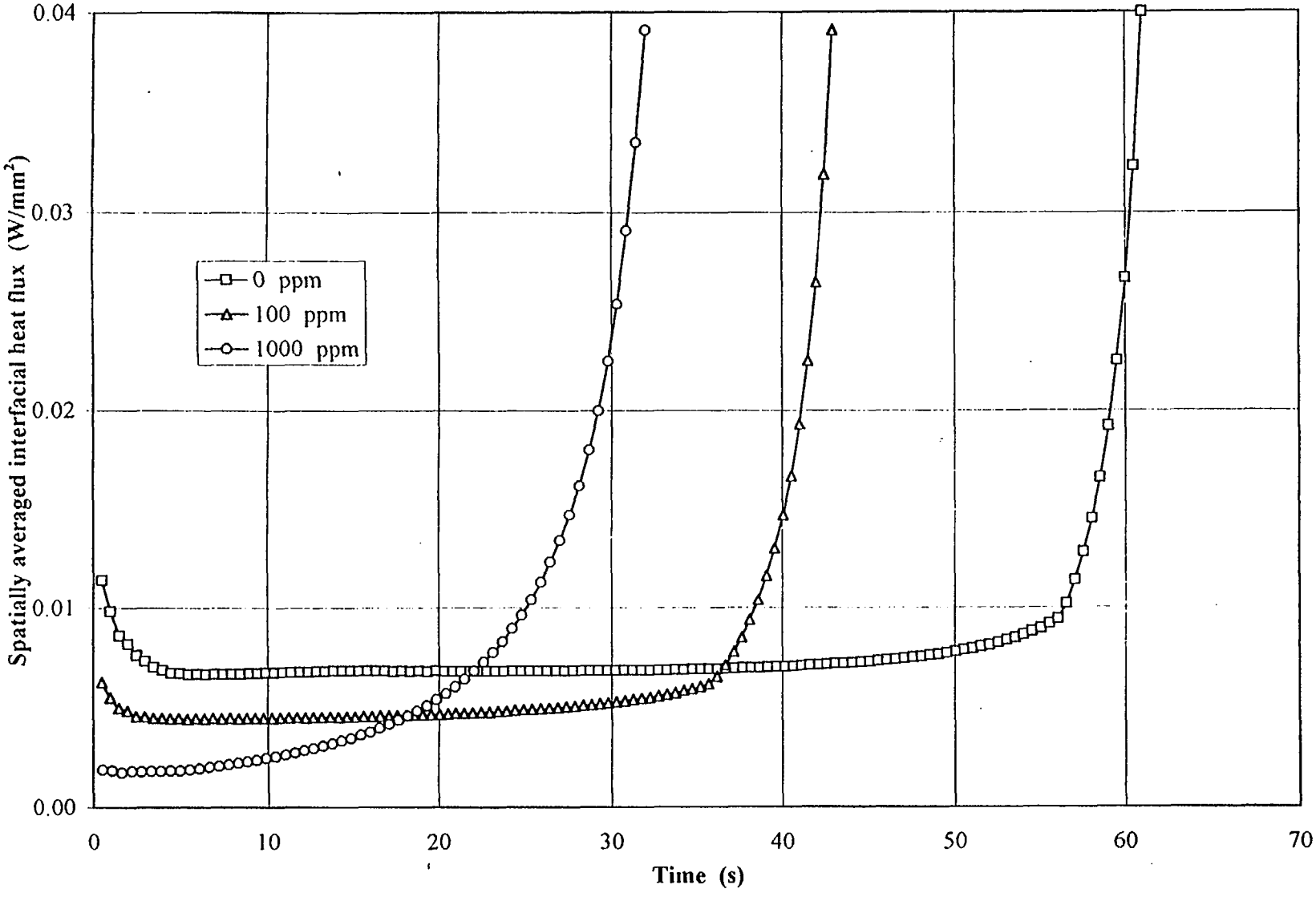

Figure 8 Calculated values of heat flux averaged over the entire wetted area during droplet evaporation on a surface initially at 80°C.

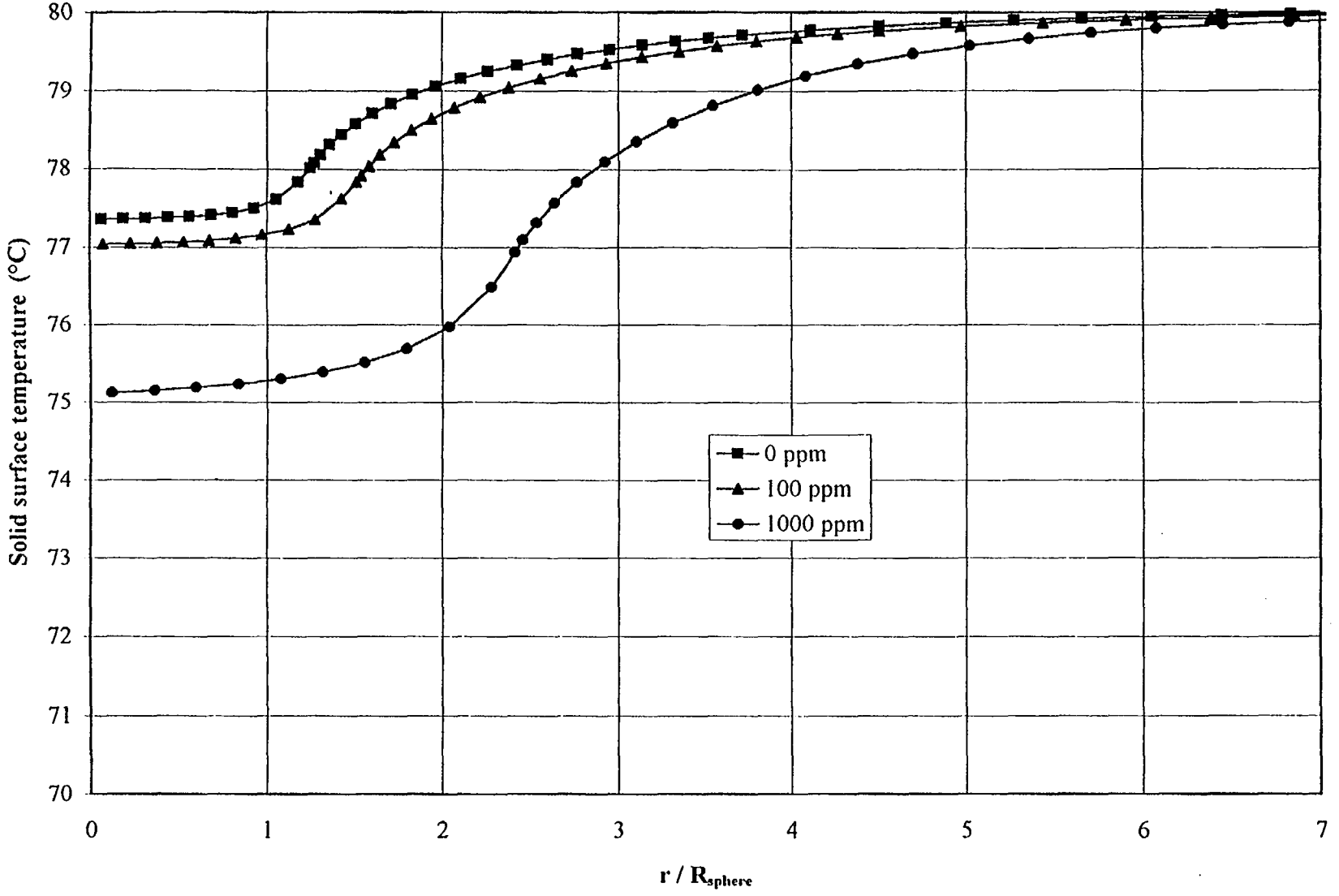

Figure 9 Calculated temperature profiles in a solid surface initially at 80°C, during evaporation of droplets of pure water (0 ppm), 100 ppm and 1000 ppm surfactant solutions at *a*) 10%, *b*).50%, and *c*) 90% of the total evaporation time

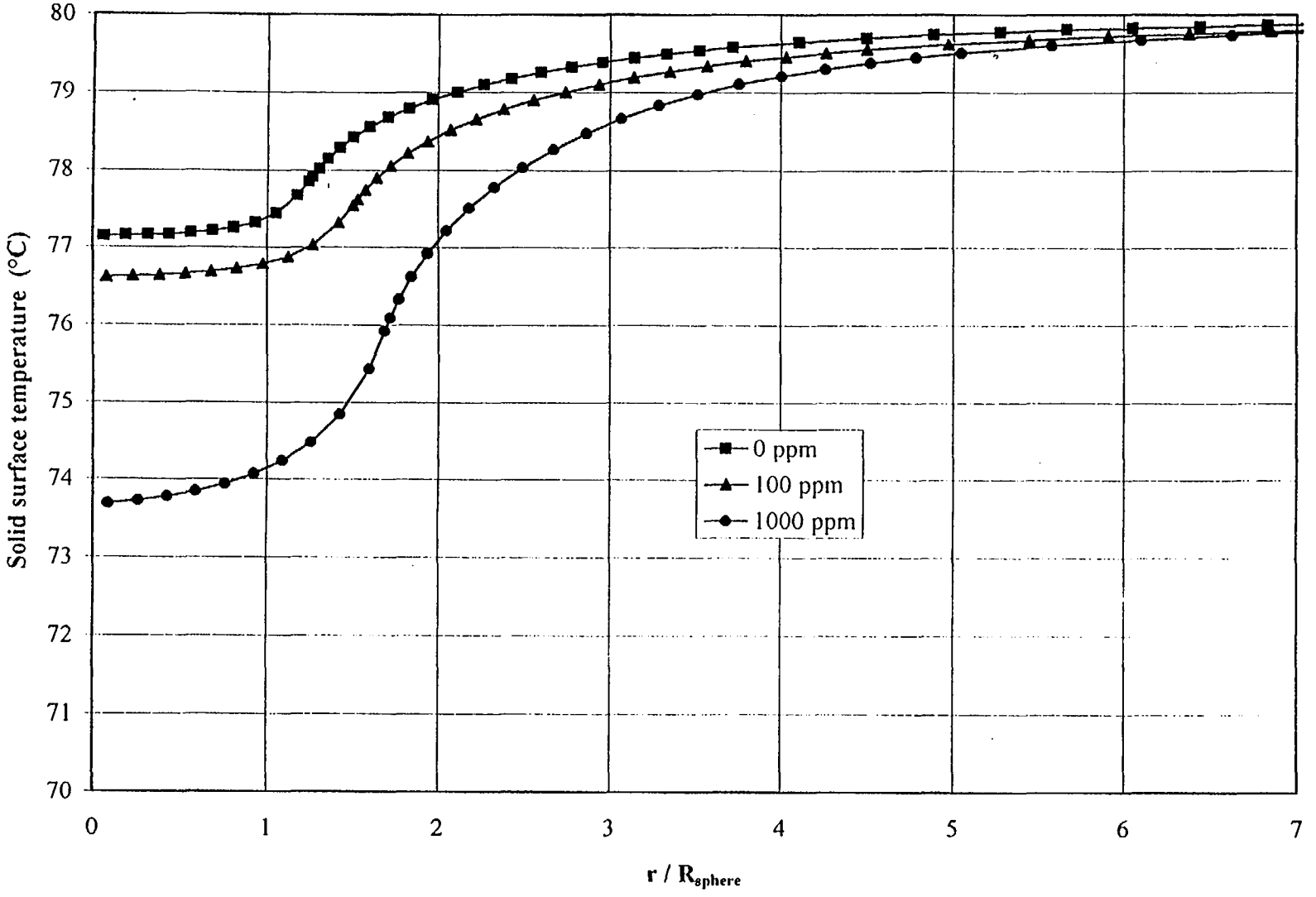
80
79
78
77
76
75
74
73
72
71
70
Solid surface temperature (°C)
0
1
2
3
4
5
6
7
r / R sphere
0 ppm
100 ppm
1000 ppm

Figure 9*b*

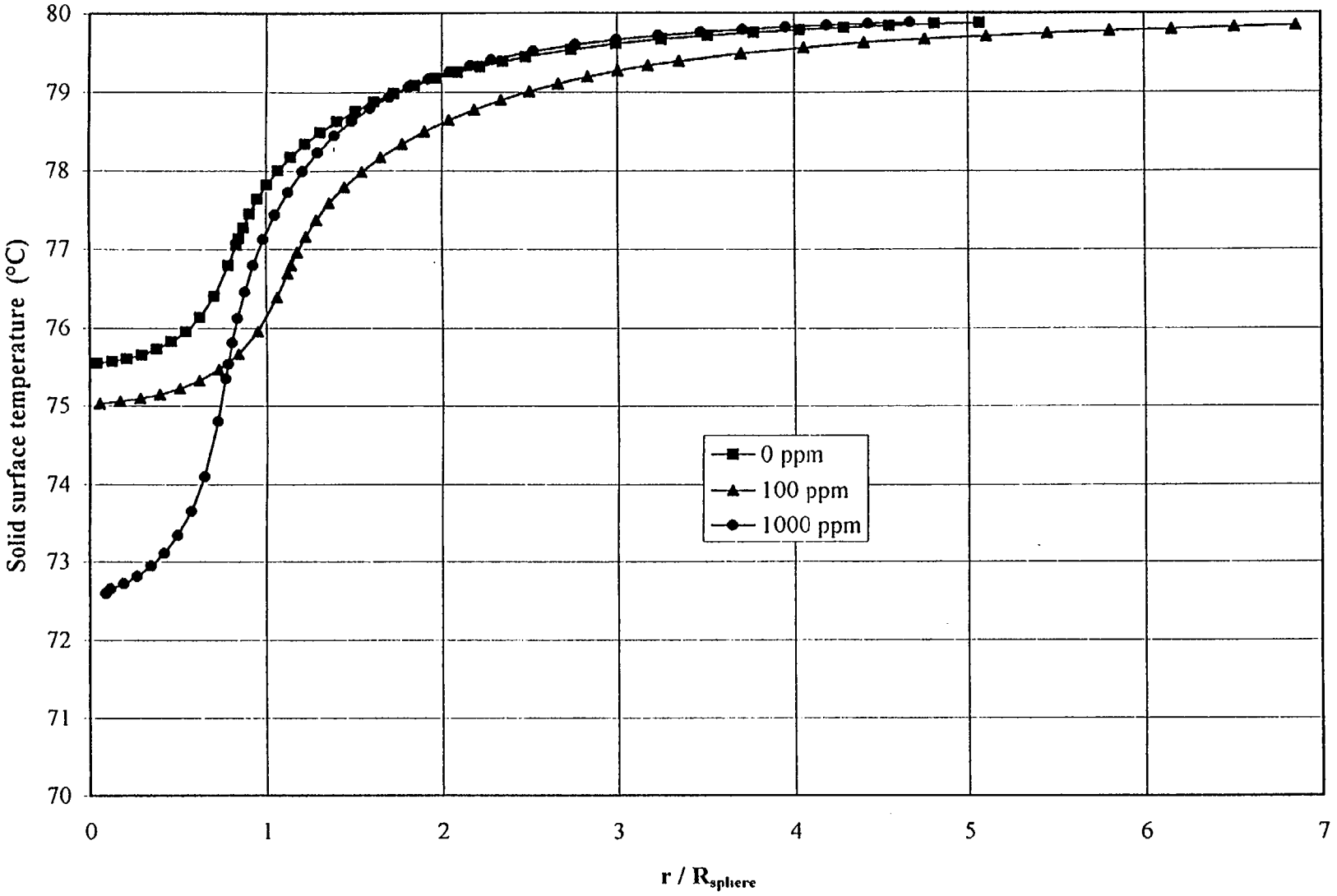
80
79
78
77
76
75
74
73
72
71
70
Solid surface temperature (°C)
0
1
2
3
4
5
6
7
r / R_spliere
0 ppm
100 ppm
1000 ppm

Figure 9c

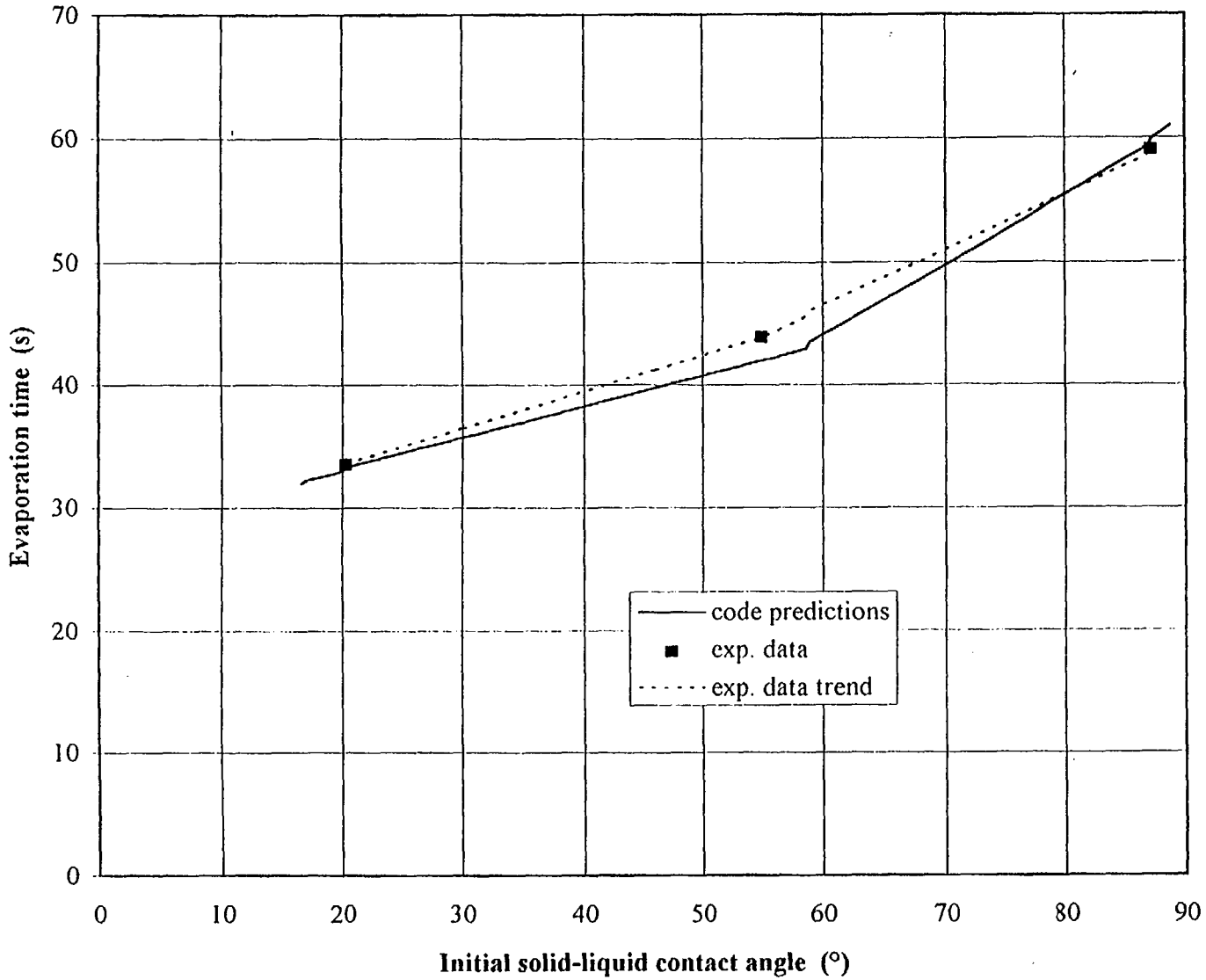

Figure 10 Effect of reducing contact angle on evaporation time of droplets on a stainless steel surface initially at 80°C.

APPENDIX B:

Effect of dissolved gasses in the water

S.C. Tinker & M. diMarzo, Effect of dissolved gasses on spray evaporative cooling with water (1995) unpublished manuscript.

PAPER # 16

Effect of Dissolved Gasses on Spray Evaporative Cooling with Water

S.C. Tinker & M. di Marzo

Mechanical Engineering Department, University of Maryland, College Park, MD 20742

Abstract

An experimental investigation of the effect of non-degassed water used to cool a solid surface is presented. The solid surface is subjected to thermal radiant input from three panels positioned above it. The water is deposited on the surface in the form of a sparse spray with droplets of about 10 μl. Previous experiments with degassed water are compared with these new experiments and the effect of dissolved gasses is quantified in terms of the overall transient thermal behavior of the solid. A lower steady-state average temperature is achieved when gasses are not removed from the water. This result suggests that the configuration of the liquid droplets on the surface is different and that the radiant heat input into the droplet is altered by the gas bubbles present in the deposited droplet. This information provides guidance in practical applications such as sprinkler suppression systems where water damages are a concern.

Keywords: water, spray, cooling, dissolved gasses.

Introduction

Evaporative cooling of hot solid surfaces is a desirable heat transfer process in a number of engineering applications. A sparse spray of water deposited on a solid surface allows for large amounts of heat to be removed due to the high latent heat associated with the evaporation of water. Industrial uses for spray cooling include the quenching of molten metals during casting and the coating of surfaces to form protective finishes. Spray and mist cooling find a variety of uses in the power generation industry, such as the cooling of turbine blades and cooling tower applications. In the area of fire suppression and protection, sparse spray cooling finds numerous uses. These include fire suppression in nuclear power plants, in process chemical storage, and in fuel storage facilities.

Several researchers have focused their attention to the fundamentals of the evaporation of droplets and their cooling effects. Simon and Hsu [1] studied the wetting characteristics of evaporating droplets on various surfaces. They recorded droplet shape histories at room temperature on copper, lucite, and teflon surfaces. Both Toda [2] and Bonacina et al. [3] performed early investigations of spray-surface interactions and provided fundamental insight into the uses of mist cooling. Photographic techniques were employed by Zhang and Yang [4] to determine flow patterns in evaporating droplets on glass and copper plates.

The present work constitutes part of a research effort to quantify and develop models for spray cooling of hot solid surfaces in a fire environment. In 1989, diMarzo and Evans [5] modelled a single droplet evaporating on a high thermal conductivity surface. Subsequently,

a theoretical model using boundary element methods to predict the cooling of a semi-infinite solid due to an evaporating droplet was developed by diMarzo et al. [6]. Both a high and a low thermal-conductivity surface heated from below by conduction were studied. In 1993, Tartarini et al. [7] predicted the transient thermal behavior of a solid caused by the evaporation of a single droplet and proposed a model for the impingement of a sparse spray of droplets. Experimental techniques based on infrared thermography to record the evaporation of a droplet on a radiantly heated semi-infinite solid were developed in 1992 by diMarzo at al. [8]. Dawson and diMarzo [9] extended this experimental work to record the effects of a random distribution of droplets (spray) on the surface. In both cases, the solid exhibited low thermal-conductivity. Computer models of the evaporation of a single droplet for radiative heat input conditions are contributed most recently by White et al. [10] and by Tartarini and diMarzo [11].

The research presented here expands on Dawson's investigation of the cooling of a solid surface by multiple droplets evaporation under radiant heat input. While Dawson used deionized and degassed water in his experiments, the experiments in this work used deionized water which has not been degassed. Therefore, the dissolved gasses are at equilibrium with the air at atmospheric conditions. The purposes of this study are: a) to examine both the temporal and spatial behavior of the surface temperature of a low thermal conductivity, semi-infinite solid subjected to radiant heat input and to a sparse spray of non-degassed, deionized water; and b) to compare these results with the similar ones employing degassed water in order to quantify the effect of dissolved gasses.

Experimental Apparatus

The experimental apparatus is shown in Figure 1. The solid is made of Macor, a glass-like material, and it is square in shape with 15.2 cm sides and 2.54 cm thickness. Table 1 lists the relevant thermophysical properties of Macor. As it can be seen, Macor exhibits a relatively high emissivity and a relatively low thermal conductivity. It also has the ability to withstand high thermal stresses, resulting in a smooth, crack-free surface. The Macor tile is mounted on a chilled plate. The purpose of the chilled plate is to hold the lower surface of the tile at a constant temperature of approximately 30 °C. This is achieved by circulating cold water through the plate. The Macor tile is attached to the chilled plate using silicone heat sink compound.

Three radiant panels are used to heat the solid surface. Two of these panels are positioned above the surface at an angle of 30° and symmetric to the vertical axis through the center of the tile. The third panel surrounds the perimeter of the tile to provide uniform heating to the sides of the Macor tile. An infrared camera, located above, focuses on the solid surface and records its transient thermal behavior. The camera looks through a chilled pipe that is used to absorb stray reflections. A droplet dispenser hangs vertically above the surface and works with a positioning mechanism to provide the droplet distribution on the surface. The motivation for using the radiant heat panels (to provide the heat input to the solid surface) is to simulate a fire environment more realistically. The panels may be assumed to radiate as black bodies. Each panel is conical in shape and capable of reaching temperatures in the range of 800 °C. The temperatures of the panels are controlled by an

Omega CN-7100 digital process controller through a feedback loop from the panels. Power to the panels, which are connected in a delta circuit, is supplied by a 208-volt three-phase power supply.

An Inframetrics Model 525 infrared camera detects radiation wavelengths from 8 to 12 microns and translates thermal variations of an object into a real-time, gray image. These images are made up of dark shades that represent cool regions and light shades that represent hot regions. The camera records the thermal image of the surface onto 8 mm videotape using a Sony high resolution VCR. These tapes are stored for the subsequent data processing. The camera uses a 0.61 meter focal length close up lens which is positioned to view a portion of the surface within the droplet impingement region.

Droplet Size and Distribution

The droplet dispenser consists of a tapered, conical, aluminum body with a bored-out central cavity. The cavity exits through a hole at the bottom of the aluminum body. A size 20 IV needle screws into the hole at the bottom of the cavity. The cavity is continuously fed with water from an open reservoir (positioned to provide the desired static head above the dispenser). A plastic diaphragm and an O-ring seal the cavity at its top. A steel piston rests on top of the diaphragm while a solenoid-spacer mechanism is fitted to the top of the piston. When the solenoid is energized, it pushes down on the spacer, causing the piston to deflect the diaphragm and thus eject a droplet from the needle. An average droplet size of 10 $\pm$ 1 μl is obtained with frequencies as high as one Hertz.

In these spray cooling experiments, attempts are made to distribute the droplets in a random fashion over a circular area of the solid surface. To this end, a positioning mechanism consisting of an aluminum plate with a 25.4 cm hole in the center and three moving solenoid-controlled bumpers which collide with and impart motion to the droplet dispenser. The droplet dispenser, which hangs from four cables, swings within the plate hole as it is impacted by the three bumpers. To keep the motion from decaying or falling into a particular pattern, a motorized cam is used to periodically pluck one of the suspension cables.

Figure 2 shows the droplet distribution recorded during a typical experiment. The distribution affects a larger area than the one which is viewed by the infrared camera. The total area that droplets impinge upon is about 3.3 cm in radius. To determine a function approximating this experimental distribution, the motion of the droplet dispenser needs to be characterized. Its motion is limited by the bumpers. The bumpers move in a synchronous fashion in the horizontal plane, with an innermost position that corresponds to a circle with a radius of 1.8 cm and an outermost position that corresponds to a circle with a radius of 3.3 cm. Confined by the motion of the bumpers, the droplet distributer can only move freely in a 1.8 cm radius. The dispenser is never expected to achieve the maximum radial position of 3.3 cm because the bumpers increasingly impede the dispenser as it travels farther from the center of the distribution area. Therefore, the function describing the droplet distribution (namely the fraction of droplet per unit area d at a given radius r) has the following boundary conditions:

1. at r = 0, d(r) = 0 — which ensures that the distribution is proportional to the surface area
2. at r = 0, d'(r) = 2 — which ensures that the distribution is proportional to the surface area
3. at r = h, d'(r) = 0 — which sets a maximum value for the distribution at the normalized radius h bounding the region of free random motion of the droplet dispenser (i.e. h = 0.56)
4. at r = 1, d = 0 — which insures that the outer maximum radial position is never reached
5. $\int_0^1 d\,dr = 1$ — which is the distribution function normalization statement

With these conditions, the function d, describing the droplet distribution is given as:

$$d = 9.15\,r^4 - 22.64\,r^3 + 11.49\,r^2 + 2.00\,r \qquad (1)$$

To check the validity of this result, the function integral is calculated and plotted in Fig. 3 along with the measurements. Error bars of the actual data are also shown. The error bars are determined based on the assumed outermost possible radial position with respect to the outermost droplet. Figure 3 shows that the calculated distribution is in reasonable agreement with the experimental data.

Experimental Procedure

Experiments are run at initial surface temperatures of approximately 110 °C, 130 °C, 150 °C,

160 °C, and 180 °C. At each initial surface temperature, three mass fluxes of non-degassed, deionized water are tested. Over this set of experiments, the mass flux of water ranges from 0.24 g/m^2s to 1.6 g/m^2s. At the higher mass fluxes, the surface is nearing the flooding conditions. The lowest four initial surface temperatures correspond to evaporative cooling, while the highest temperature corresponds to full nucleate boiling for the Macor surface.

The basic procedure followed for each experimental session is described hereafter. The macor surface is cleaned with ethyl alcohol and a soft cloth, lightly rinsed with distilled water, and allowed to dry. The radiant heaters are turned on and heat the surface for approximately two hours prior to experiment initiation. During this time, the solid surface is able to reach a steady state condition. The temperature of the surface is measured using an Omega thermocouple probe (K-type). The infrared camera, power supply, and video equipment are turned on, two hours prior to experimentation in order to minimize thermal drift. The chilled plate and chilled pipe are circulated with water. The droplet dispenser is turned on and allowed 10 to 15 minutes to stabilize at a given frequency which corresponds to a water mass flux. Once stabilized, 50 droplets are collected in a beaker which is quickly capped to avoid evaporation. The beaker and drops are weighed using a Metler electronic balance and the volume of a single droplet is determined. Droplet volumes generally ranged from 9 μl to 11 μl.

After completing the procedures outlined above an experiment for a particular set of conditions begins. First, the initial surface conditions are recorded, then, the droplets

impinge upon the heated surface for a period of twenty-five minutes. During this period the thermal behavior of the surface is recorded by the infrared camera onto 8 mm videotapes.

Data Processing and Reduction

The data processing and reduction for the experiments follow the same procedure adopted by Dawson [9] in his spray cooling experiments using degassed water. After completing an experimental run at a given initial surface temperature, the data recorded by the infrared camera is processed. The real-time, gray images recorded by the camera provide two types of information: a) the transient average temperature of the surface and b) the spatial distribution on the surface at any time. Both analyses employ a video digitization system to obtain the gray-values from a recorded image. A Matrox MVP-AT frame grabber board is installed in an IBM PC-AT and used to digitize single frames into discrete gray-values (one frame every 30 seconds is sampled). Once digitized, each frame can be analyzed pixel by pixel using Imager-AT software linked with user-written source code. For each frame the infrared intensity scale is calibrated using a temperature versus intensity relationship so that shades of gray may be translated into corresponding temperatures.

To determine the transient average surface temperatures frames are digitized at 30-second intervals of a recorded experimental run. There are 130 shades of gray associated with the infrared intensity levels. Since the temperature range is of 100 °C, the temperature resolution is 0.77 °C/ gray-values. The gray-value of every fifth pixel is used over an image

covering a region of 0.046 m x 0.034 m. The average gray-values are then converted into a single average surface temperature.

Spatial distributions of the surface temperature at a specific time are obtained by considering each pixel in a digitized frame individually. Each pixel can be associated with a Cartesian coordinate using knowledge about the viewed area of a frame. The gray-value for each pixel is converted into a temperature, thus yielding a temperature at a particular location on the surface. Again, every fifth pixel is used. Results are plotted in the form of constant temperature contours. The pixels contained in the total viewed area are 512 by 480 in the horizontal and vertical direction, respectively.

Results and Discussion

Contour plots of the temperature distribution on the Macor surface are shown in Figs. 4(a-c) and 5(a-c) for the indicated initial solid surface temperatures and water mass fluxes. Each sequence of plots shows the surface temperature distribution at three different times: a) early in the transient when the surface temperature is close to its initial value; b) further on in the transient, but before steady state conditions have been reached; and c) at or approaching steady state conditions. Results show very distinct locations where droplets are evaporating on the surface, or have just evaporated from the surface and cause a localized cooling effect. At earlier times, the cooling effect due to evaporating droplets is contained within the local region around the droplet. While at later times, the cooling effect on the surface temperature due to individual droplets tend to merge. Also, more droplets

are found on the surface at later times due to the longer evaporation times associated with the decreasing solid surface temperature. Isothermal contours, at lower temperatures, are found near the perimeter of the plot at later times than those found at early times, indicating that the entire surface is cooling. A fluctuation of about ± 2 °C is associated with these plots, due to electronic noise.

Graphical results of the transient average surface temperature are shown in Figs. 6 and 7. The raw data are shown for both the experiments using non-degassed water degassed water [9], respectively. The general trend apparent in each plot for both the degassed and non-degassed data is the decay of the average surface temperature from its initial value to some steady state value. Dawson suggested a fit to the transient temperature data of the form:

$$T = (T_o - T_s)\, e^{-a\,t} + T_s \qquad (2)$$

which is used to curve-fit all the data representing the transient behavior of the average solid surface temperature. The deviation of the data points from a smooth decay occurs due to the nature of the data acquisition. Since only a portion of the sprayed area is viewed and averaged, at any instant, the number of droplets that can be seen may be different than at other instants thus resulting in oscillations of the average surface temperature.

Examination of these results suggests that the dissolved gasses enhance the heat transfer from the surface by decreasing the incoming radiant input and, therefore, achieving a lower steady state temperature. To quantify this effect, one would attempt to relate the variation in the final steady state temperature to the temperature excursion present in the degassed

water results. Two major effects must be included in the characterization of a given transient: a) ΔT, the solid surface temperature drop; and b) θ, the solid surface initial conditions. These quantities are related to the water mass flux and to the radiant heat input respectively. One could suggest to identify, as independent variable, the ratio of these two quantities while retaining the temperature variation as the dependent variable. Table 2 lists the actual numerical values. This analysis would indicate that the effect of dissolved gasses becomes negligible as the values of the ratio $\Delta T / \theta$ increases. This ratio is large for large temperature drops and for initial solid surface temperatures near the onset of nucleate boiling conditions for degassed water. These are the conditions which are most likely in a fire protection situation. Therefore, the dissolved gasses do not affect significantly the evaporative cooling processes associated with fire safety applications.

Note that for temperatures of the solid surface, where nucleate boiling is observed (i.e. for negative values of θ), these conclusions do not apply. The nature of the vaporization phenomena in nucleate boiling is based on a completely different heat transfer mechanism and an extension of the evaporative results or trends is not justified.

Conclusions

Employing a data acquisition system which uses digital image analysis and infrared thermography, the spatial and temporal behavior of the transient surface temperature of a radiantly heated semi-infinite solid cooled by a sparse spray of non-degassed water is recorded and analyzed. The transient thermal behavior is investigated over a range of

different initial surface temperatures and water mass fluxes. The data acquisition system is able to provide information on both the spatial and temporal behavior of the solid in the form of contour plots and transient average temperature plots, respectively.

Contour plots provide a qualitative description of the surface at any instant in time. Results indicate that localized cooling in the region of droplets occurs during the initial impingement of the sparse spray on the surface. At later times, effects of the droplets tend to merge and the average temperature on the surface decreases. More droplets are also found on the surface at later times due to the longer evaporation times associated with the lower surface temperatures.

Transient surface temperature results are compared against those results obtained from experiments using degassed water. In both cases, the surface exhibits an exponential cooling from its initial temperature to some steady state conditions. For larger values of the ratio $\Delta T / \theta$, a smaller difference in the surface cooling between the non-degassed water and the degassed water is observed. These results also indicate that, for low values of the $\Delta T / \theta$ ratio, the dissolved gasses enhance the cooling process by reducing the incoming radiant input.

Acknowledgements

This research has been sponsored by a grant of the Building and Fire Research Laboratory of the National Institute of Standards and Technology.

Nomenclature

a constant

d droplet distribution function

G droplet mass flux

h maximum normalized radius of free random motion of the droplet distributor

r normalized radius (with respect to its maximum possible value of 3.3 cm)

T average solid surface temperature

T_o initial solid surface temperature

T_s final steady state average solid surface temperature

t time

Greek

ΔT solid surface temperature drop, T_o- T_s

θ difference between the initial solid surface temperature at the onset of nucleate boiling for degassed water (~ 163 °C) and the actual initial solid surface temperature

Superscripts

* identifier of properties for degassed water

' identifier of the first derivative with respect to r

References

1. Simon, F. & Hsu, Y.Y., Wetting dynamics of evaporating drops on various surfaces. *NASA Technical Memo*, NASA TM X-67913 (1971).
2. Toda, S., A study of mist cooling. First report: Investigation of mist cooling. *Heat Transfer, Japanese Research*, Vol. 1 (1972) p. 39-50.
3. Bonacina, C., Del Giudice, S., & Comini, G., Dropwise evaporation. *Journal of Heat Transfer*, Vol. 101 (1979) p. 441-446.
4. Zhang, N. & Yang, W.J., Natural convection in evaporating minute drops. *Journal of Heat Transfer*, Vol. 104 (1982) p. 656-662.
5. diMarzo, M., & Evans, D., Evaporation of a water droplet deposited on a hot high conductivity solid surface. *Journal of Heat Transfer*, Vol. 111 (1989) p. 210-213.
6. diMarzo, M., Tartarini, P., Liao, Y., Evans, D. & Baum, H., Evaporative cooling due to a gently deposited droplet. *International Journal of Heat and Mass Transfer*, Vol. 36 (1993) p. 4133-4139.
7. Tartarini, P., Liao, Y. & diMarzo, M., Numerical simulation of multi-droplet evaporative cooling. *Heat and Technology* Vol. 11 (1993) p. 98-107
8. diMarzo, M., Kidder, C.H. & Tartarini, P., Infrared thermography of dropwise evaporative cooling of a semi-infinite solid subjected to radiant heat input. *Experimental Heat Transfer*, Vol. 5 (1992) p. 101-104.
9. Dawson, H. & diMarzo, M., Multi-droplet evaporative cooling: Experimental results. *AIChE Symposium Series*, Vol. 89 (1993) p. 26-35
10. White, G., Tinker, S. & diMarzo, M., Modelling of dropwise evaporative cooling on a

semi-infinite solid subjected to radiant heat input. *Fire Safety Science-Proceedings of the 4th International Symposium*, ed. T. Kashiwagi, Int. Association of Fire Safety Science (1994) p. 217-228

11. Tartarini, P. & diMarzo, M., Dropwise evaporative cooling in radiative field. *Proceedings of the 10th International Heat Transfer Conference*, ed. G.F. Hewitt, Vol. 6 (1994) p. 277-282.

TABLE ONE

Properties of Macor

Density	2,520	kg/m^3
Thermal Conductivity	1.297	W/m-K
Specific Heat	888.9	J/kg-K
Emissivity	0.84	-

TABLE TWO

Gassed-Degassed Water Comparison

Gassed	Degassed	Result	Comparison
ΔT	θ	$\Delta T / \theta$	$T_s - T_s^*$
61	12	5.1	4
41	12	3.4	5
25(29)[a]	32	0.78(0.90)	8(4)
85	1	85	1
40	1	40	0
77	- 19[b]	-	2

[a] The mass flux for the degassed water is 0.5 g/m^2s while the mass flux for the non-degassed water is 0.57 g/m^2s. The quantities in parentheses are prorated to correct for this mass flux discrepancy.

[b] For degassed water, the initial solid surface temperature at the onset of boiling is 163 °C. A negative value of θ indicates thatnucleate boiling is present. θ of -19 °C corresponds to an initial solid surface temperature of 182 °C.

Captions

Fig. 1. Experimental apparatus

Fig. 2. Typical measured droplet distribution

Fig. 3. Comparison of the integrated distribution function *d* and the cumulative measured droplet distribution

Fig. 4. Surface temperature contour plot for T_o = 151 °C and G = 0.96 g/m²s (a: t = 30 s; b: t = 300 s; c: t = 600 s)

Fig. 5. Surface temperature contour plot for T_o = 162 °C and G = 0.97 g/m²s (a: t = 30 s; b: t = 300 s; c: t = 600 s)

Fig. 6. Transient average surface temperature for T_o = 151 °C and G = 0.96 g/m²s (• : non-degassed, fit: $T = 41\ e^{-0.35\,t} + 110$; ▲ : degassed, fit: $T = 46\ e^{-0.34\,t} + 105$)

Fig. 7. Transient average surface temperature for T_o = 162 °C and G = 0.97 g/m²s (• : non-degassed; ▲ : degassed, fit: $T = 40\ e^{-0.40\,t} + 122$ for both sets of data)

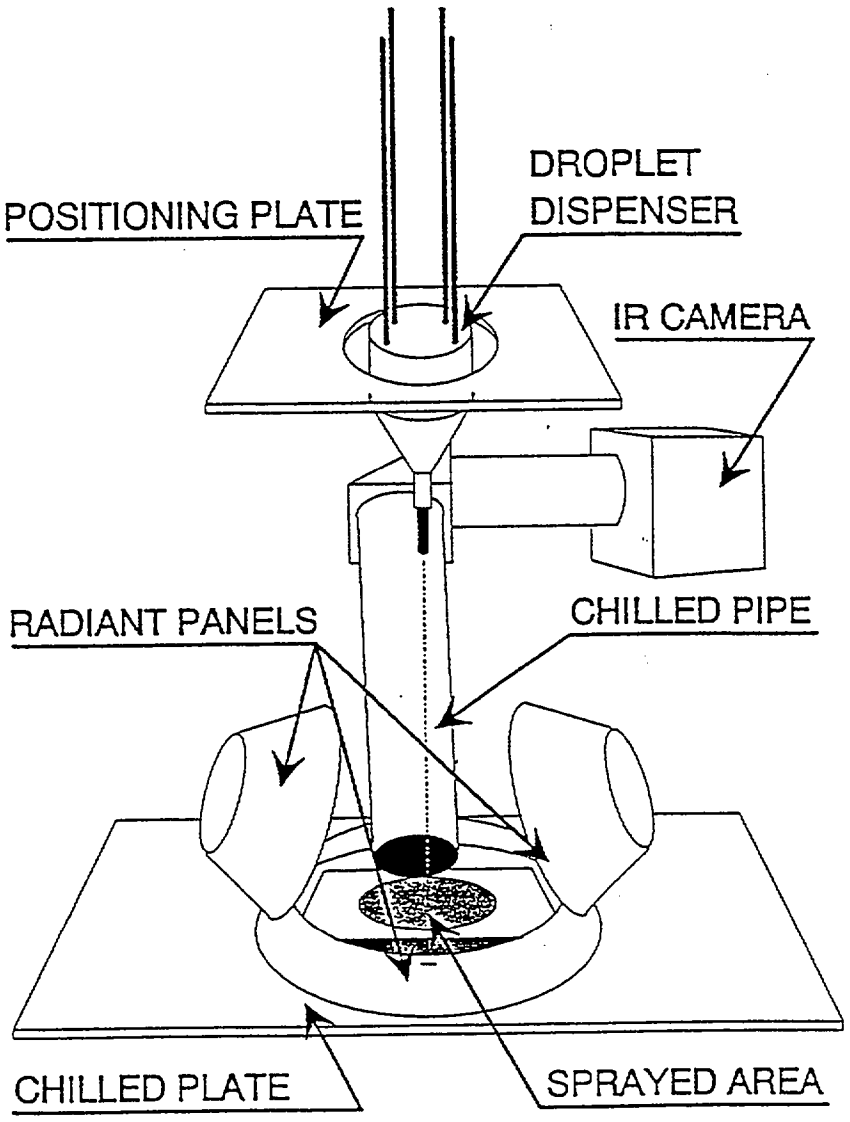
POSITIONING PLATE
DROPLET
DISPENSER
IR CAMERA
RADIANT PANELS
CHILLED PIPE
CHILLED PLATE
SPRAYED AREA

Fig. 1

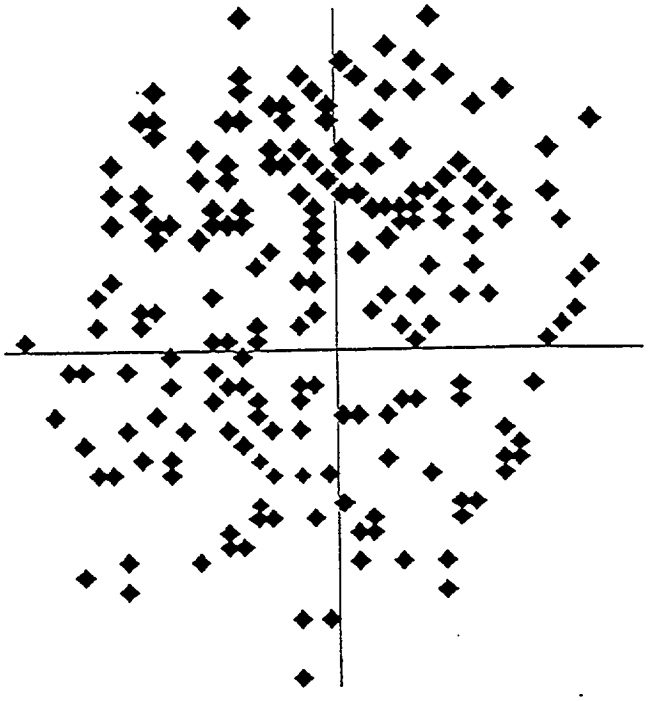

Fig. 2

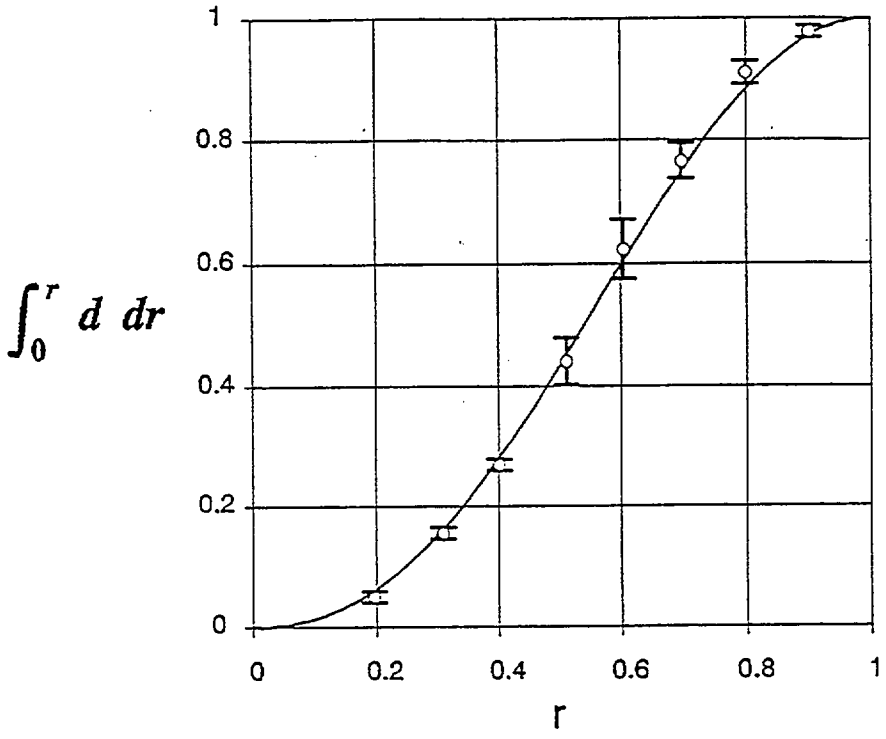

Fig. 3

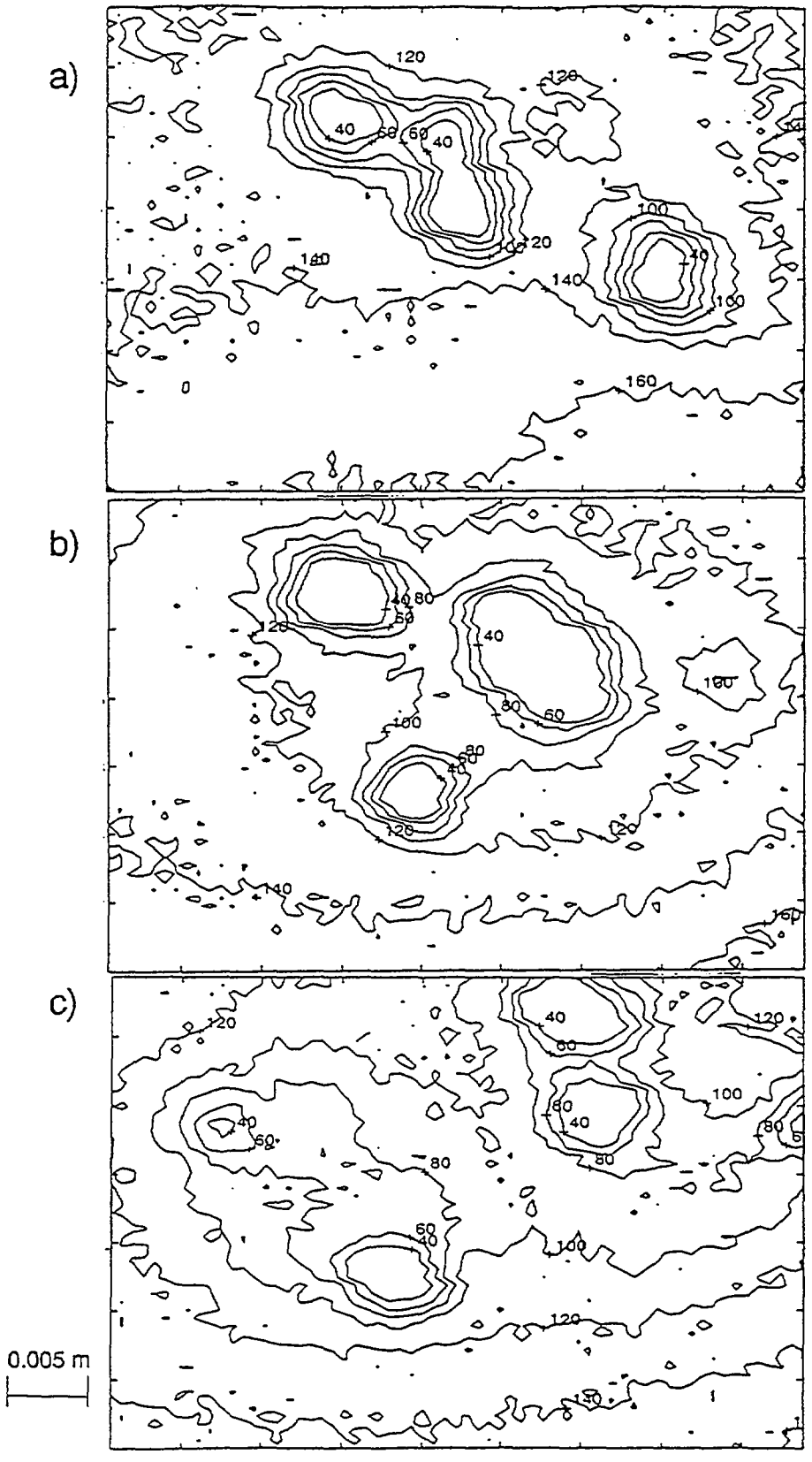

Fig. 4

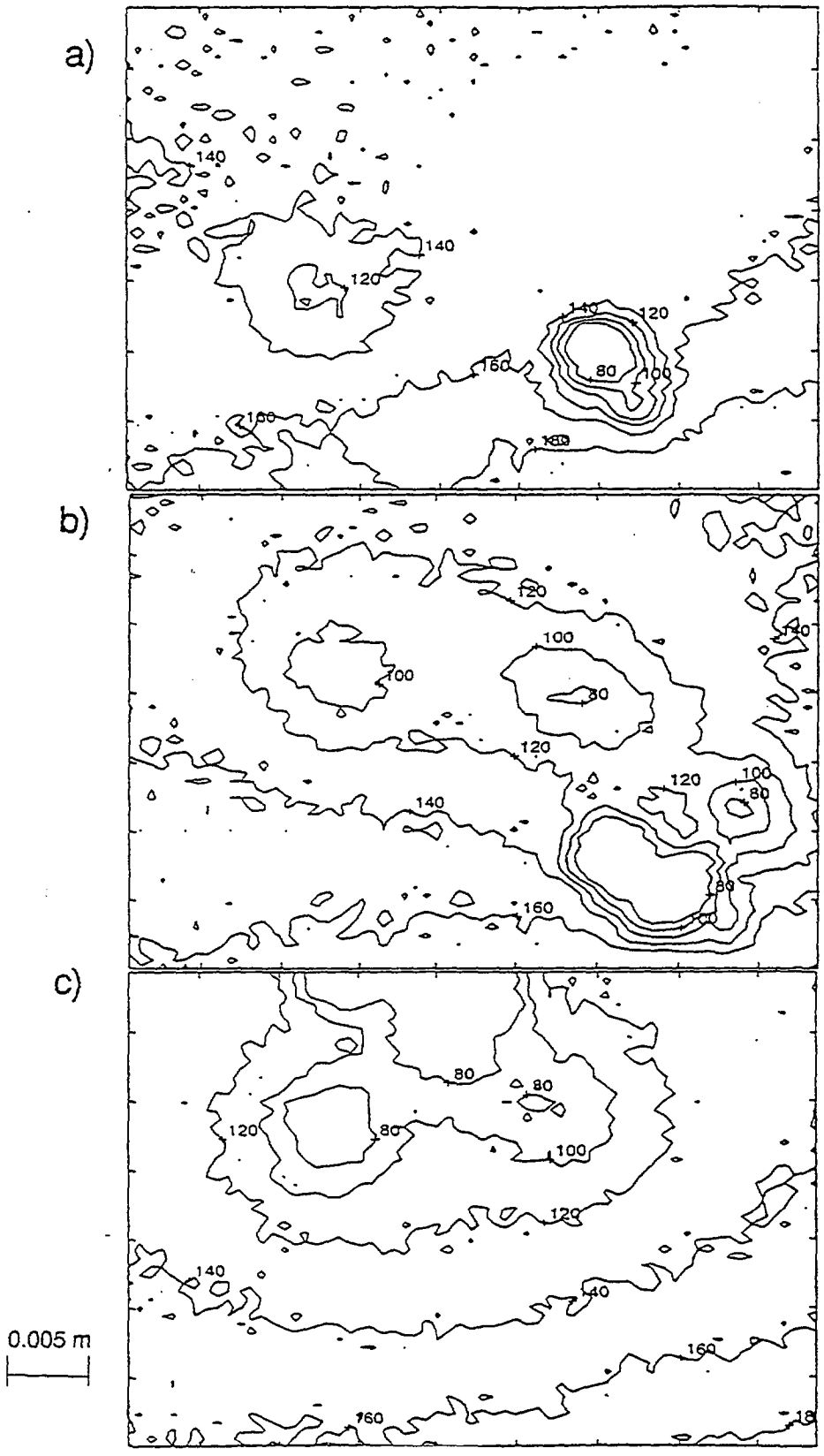

Fig. 5

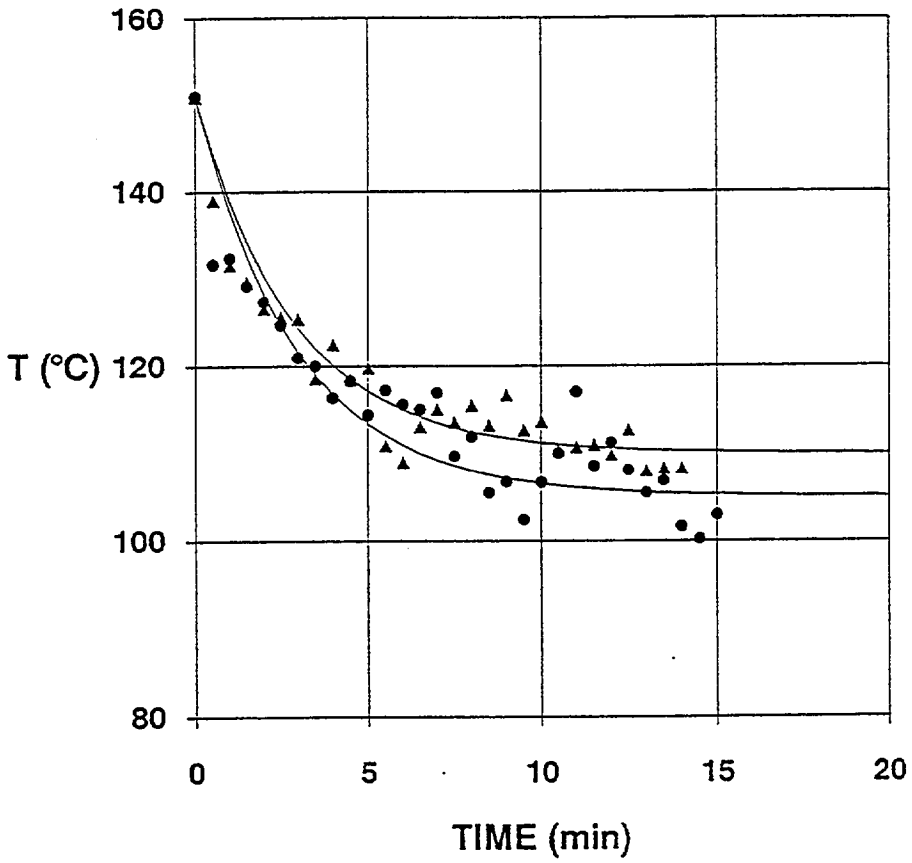

Fig. 6

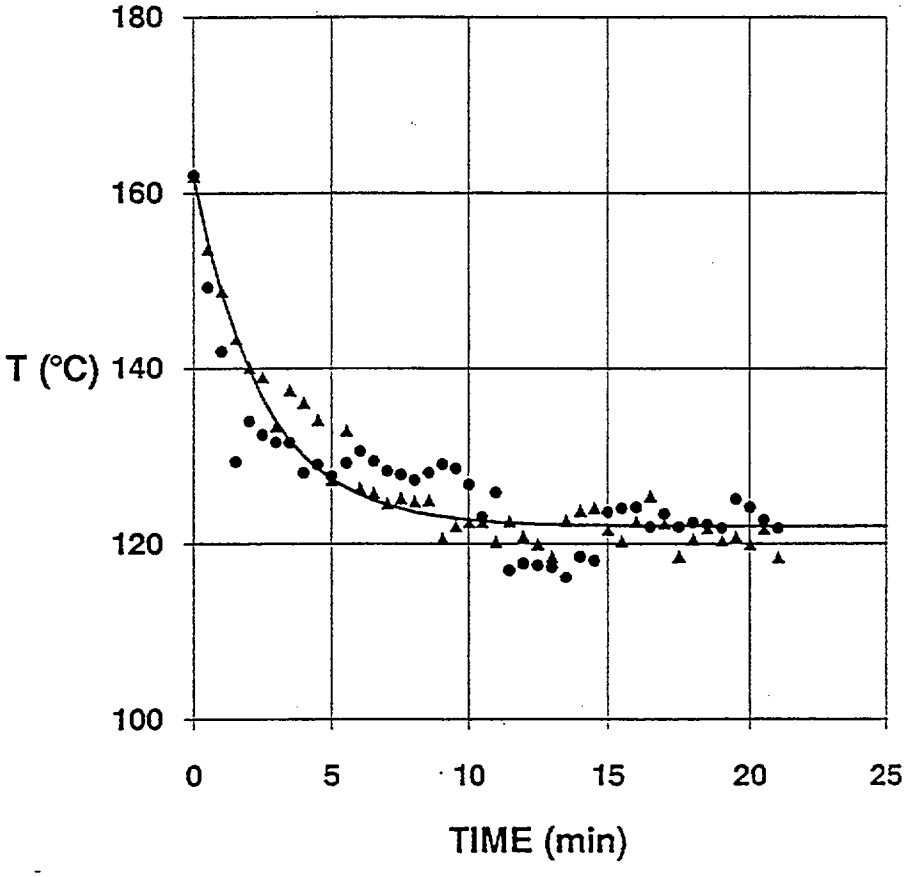

Fig. 7

APPENDIX C:

Criterion for liquid flooding on the solid surface

M. Lederer, M. diMarzo & P. Tartarini, Flooding criterion for evaporative cooling on horizontal semi-infinite solids (1995) unpublished manuscript.

PAPER # 17

FLOODING CRITERION FOR EVAPORATIVE COOLING ON HORIZONTAL SEMI INFINITE SOLIDS

M. Lederer, M. di Marzo
Mechanical Engineering Department
University of Maryland
College Park, MD 20742

P. Tartarini
Istituto di Fisica Tecnica
Universita' di Bologna
40136 Bologna, Italy

ABSTRACT

The evaporative cooling of a sparse spray impacting on a hot solid is investigated to determine the limiting condition associated with the liquid flooding of the solid surface. The flooding condition is identified when the evaporation rate is insufficient to remove the amount of water being deposited on the surface. The flooding criteria is derived as a function of the initial single droplet volume prior to deposition, the Evaporation-Recovery Cycle (ERC) and the area of influence, which describes the region of the solid surface associated with a single droplet cooling effect. These last two quantities, the ERC and the area of influence, are evaluated by integrating previously obtained theoretical and experimental information with selected experimental data obtained in this study. The flooding criteria, while semi-empirical in its derivation, can be generalized to all non-porous solids under a variety of conditions. The spray is sparse and the water droplets are considered of uniform size. Extension to a spray with non-uniform droplet distribution is not considered here.

NOMENCLATURE

A	area influenced by the evaporative cooling of a single droplet, m^2
c_S	specific heat of the solid, J/kg K
erf	error function
F_R	recovery factor: = τ_{ERC}/τ
J_0,J_1	Bessels functions
JA	Jakob number: = $c_S (T_0 - T)/\Lambda$
k_S	thermal conductivity of the solid, W/m K
r	radial coordinate, m
R	radius of the solid-liquid interface, m
T	solid surface temperature, K
T_0	initial solid surface temperature, K
U_{max}	water spray volumetric flux at the onset of flooding, m/s
V	droplet volume at deposition, m^3

Greek

α_S	thermal diffusivity of the solid, m^2/s
β	shape parameter: = $(3\ V/4\ \pi)^{1/3}/R$
δ	non-dimensional thermal penetration length: = $(\alpha_S\ \tau)^{1/2}/R$
η	non-dimensional radial coordinate: = r/R
η_i	non-dimensional radius of influence: = 0.6 $\eta_{\text{closed-form solution}}$ with $\phi = 10^{-3}$

θ non-dimensional solid surface temperature: Equation 1

λ dummy variable of integration

Λ latent heat of vaporization, J/kg

ρ_L density of the water, kg/m^3

ρ_S density of the solid, kg/m^3

τ single droplet evaporation time, s

τ_{ERC} single droplet Evaporation-Recovery Cycle (ERC), s

ϕ parameter defining the radius of influence: Equation 4

INTRODUCTION

The cooling effect of water sprays on solid surfaces has been the subject of numerous investigations. Toda (1972) and Bonacina et al. (1979) provided some early insight in the phenomena. Rizza (1981) and Tio & Sadhal (1992) modeled the spray cooling phenomena. Grissom & Wierum (1981) defined the range of conditions for evaporative cooling. Several investigators focussed their attention on the behavior of single droplets both experimentally and theoretically. Pedersen (1970), Makino & Michiyoshi (1987), Zhang & Wang (1982) and Chandra & Avedisian (1991) made great strides in the understanding of the phenomena while Seki et al. (1972), diMarzo & Evans (1989), diMarzo et al. (1993), Tartarini & diMarzo (1994) and White et al. (1994) provided models for single droplet evaporation for a broad range of conditions.

This work focusses on the issue outlined by Grissom & Wierum (1981): the maximum water flux that can be evaporated on a hot surface defines the limit between evaporative cooling and flooding of the solid surface. The criterion for the evaluation of the maximum water flux presented here is grounded in the single droplet models previously derived. Therefore, a brief background is provide to summarize these earlier findings.

BACKGROUND

Extensive experimental and theoretical investigations resulted in the formulation of a coupled model of the interaction of a water droplet deposited on a solid surface. The reader should consult diMarzo et al. (1993) and White et al. (1994) for the details. The coupled model is based on the simultaneous solution of the liquid and solid domains with mixed numerical techniques which included a boundary element method for the treatment of the solid domain. The water droplet is subjected to an energy and mass balance boundary condition at its exposed surface. The heat input can be by conduction from below the solid or by radiation from above the solid surface. In this second case, the droplet evaporation is caused by direct radiant heat input as well as by conduction at the liquid-solid interface. Note that the coupled model is limited to evaporative conditions. This means that the vapor is generated at the water droplet exposed surface and nucleate boiling at the solid surface is suppressed.

The solution obtain with the coupled model provides an accurate representation of the physical phenomena and has been validated against numerous data sets. However, it is not

in a simple form amenable to the derivation of a flooding criterion. A closed-form solution for a similar problem is used as a fitting routine which well represents the model results. Note that this solution is only a fitting routine since the details of the coupled model results are not captured in full. The closed-form solution is obtained by Carslow & Jaeger (1959) for the case of a constant heat flux applied over a circular region of a semi infinite solid surface. The temperature distribution over the solid surface is given, in non-dimensional form, as:

$$\theta = JA \left(\frac{\rho_S}{\rho_L} \right) \delta^2 \beta^3$$
$$= \frac{4}{3} \int_0^\infty J_0(\lambda \eta) J_1(\lambda) \, erf(\lambda \delta) \frac{d\lambda}{\lambda} \qquad (1,2)$$

In this expression, the parameter δ represents a non-dimensional thermal penetration depth normalized with respect to the radius of the solid-liquid interface. The parameter β, introduced by Bonacina (1979), characterizes the shape of a droplet deposited on a solid. This parameter, which is referred to as the shape parameter, is the ratio of the radius of the solid-liquid interface over the radius of an equivalent-volume-droplet in spherical configuration.

FLOODING CRITERION

The flooding criterion is based on a single droplet cooling effect considerations. The maximum heat flux, that can be removed without causing flooding, is achieved when a droplet impacts the same site with a frequency that enables the surface temperature to cycle indefinitely. This implies that the initial solid surface temperature is recovered after the

complete evaporation of a given droplet prior to the deposition of the subsequent one. The area of the surface involved in this periodical heat transfer process is defined as the area of influence or the area influenced by the evaporative process. The flooding criterion can be expressed in terms of the maximum volumetric water flux, U_{max}. The heat associated with the vaporization of a droplet of volume, V, is applied uniformly to the area influenced by the droplet, A, over the total droplet Evaporation-Recovery Cycle (ERC), τ_{ERC}. Therefore, the flooding criterion can be written as:

$$U_{max} = \frac{V}{A\,\tau_{ERC}} \tag{3}$$

In order to derive the flooding criterion, one must evaluate the area of influence, A, and the evaporation-recovery cycle, τ_{ERC}. This is accomplished in the following.

Evaporation-Recovery Cycle

The ERC is determined experimentally by depositing a sequence of droplets, on the same point of the solid surface, while heating the solid by conduction from below. For a given heat flux, one can determine the maximum frequency of deposition which corresponds to the onset of flooding. These experiments are also corroborated by computations performed with the coupled model (White et al. 1994; diMarzo et al. 1993) and by experimental observations of the infrared thermography of the surface (Klassen et al. 1992; diMarzo et al. 1992). From all these sources it has been determined that the recovery time, for a broad range of conditions,

lasts 30 percent of the evaporation time. Figure 1 provides a typical comparison of the ERC evaluated by multiplying the evaporation time, τ, by the recovery factor, F_R, which is set to 1.3. These results indicates that this approach provides a reasonable estimate for τ_{ERC} to be used in Equation 3.

Area of Influence

The determination of the area influenced by the single droplet evaporative transient is a more complex endeavor. The first step is to introduce the concept of radius of influence as the radial position beyond which the heat flux in the radial direction is less than a given percent ϕ of the reference heat flux associated with the droplet vaporization. This reference heat flux is the heat of vaporization of a droplet of volume V applied to the solid-liquid interface of radius R over the evaporation time τ. This definition of radius of influence can be written as:

$$-k_S \frac{\partial T}{\partial r} = \phi \frac{\rho_L V \Lambda}{\pi R^2 \tau} \tag{4}$$

In terms of the same non-dimensional variable used in Equations 1 and 2, Equation 4 becomes (see diMarzo et al. 1993):

$$\int_0^\infty J_1(\lambda \eta)\, J_1(\lambda)\, erf(\lambda \delta)\, d\lambda = \phi \tag{5}$$

This result defines a functional relationship between the non-dimensional radial position η and the parameter ϕ for given values of the non-dimensional penetration depth δ.

In order to evaluate the radius of influence (i.e. the area of influence), two steps are needed: a) the relationship between the closed-form and the coupled model results must be found; and b) the value of ϕ must be estimated.

Figure 2 provides the comparison between the above expression (Equation 5) and the coupled model results, for a broad range of conditions and for ϕ ranging over several orders of magnitude. As it can be seen, it is reasonable to modify the results by considering sixty percent of the value of η obtained with the closed-form solution. Note that materials with low thermal diffusivity solids (i.e. glass, quartz, etc.) exhibit low values of η (up to 4 in the figure). In this case, a smaller multiplier could be used (i.e. 50%) since the points are above the 45° line. For high thermal diffusivity materials (i.e. steel, aluminum), large values of η are observed. In this case the opposite trend is observed and a larger multiplier (i.e. 70%) could be used since the point are below the 45° lines. In summary, the selection proposed here is a reasonable compromise for all possible solids within the 15% accuracy, identified in the figure by the dashed lines.

The next step is the evaluation of the parameter ϕ. This step is carried out experimentally by setting two parallel streams of droplets at the near flooding conditions. The first stream impacts a fixed point while the other stream impacts locations which are made progressively closer to the fixed location. As the distance between these two sites is decreased, the onset of flooding is observed. By determining the minimum distance, for which the two streams of

droplets are independent of each other, one obtains the radius of influence. Note that this experimental determination of the radius of influence is not ideal since a one-dimensional measurement (i.e. along a single radius) is substituted for a two-dimensional phenomenon. In reality, a single droplet is surrounded by other randomly distributed evaporating droplets. This observation is most important and limits the significance of the data to the determination of the order of magnitude for the parameter ϕ and not to its specific numerical value.

In this spirit, Figure 3 illustrates data obtained on Macor (a glass-like material). Note the behavior in the low range near the origin where significant discrepancies in the trend between the closed-form solution and the data indicate that the two-dimensional effects are indeed important. Due to this realization, data at higher values of δ (i.e. for high thermal conductivity materials) are not obtained because of the uncertainty associated with the two-dimensional effect. For this study the value of $\phi = 10^{-3}$ is selected. This selection can be regarded as the fitting of a single semi-empirical parameter for the flooding criterion formulation. It is due to this occurrence that no claim of a fully theoretical approach is made in this study.

Figure 4 provides the values of the radius of influence for a variety of conditions using Equation 5 with ϕ set equal to 10^{-3} and with η_i equal to sixty percent of the value of η obtained from the equation. To further simplify the evaluation of the radius of influence, these results can be represented with an exponential fit given as:

$$\eta_i = 11\ (1 - e^{-\delta/6}) \tag{6}$$

This expression, which is applicable to most solid materials (e.g. glass, quartz, steel, aluminum), is used to evaluate the area of influence in Equation 3. Recall that the radius of the solid-liquid interfacial region can be expressed as a function of the shape parameter β to yield the following result:

$$A = \pi\ (\beta\ \eta_i)^2 \left(\frac{3\ V}{4\ \pi}\right)^{2/3} \tag{7}$$

This formulation can now be substituted in Equation 3.

Criterion Evaluation

The final form of the criterion, with the substitution of Equation 7 and into Equation 3 and with the introduction of the recovery factor $F_R = 1.3$, yields:

This criterion is general in that the closed-form solution is fitted to the coupled model which has been validated for a broad range of material thermal properties. Further, the criterion is readily extended to the case of radiant heat input from above since it has been shown (White et al. 1994) that the closed-form solution provides a good representation of the droplet evaporative transient also for that case. Finally, note that, in order to determine U_{max}, it is

necessary to know the following:

1. the shape parameter β
2. the droplet volume V
3. the evaporation time τ
4. the solid thermal diffusivity α_s

These quantities are known (i.e. α_s and V) or can be evaluated with a simple single droplet experiment (i.e. β and τ). It is important to realize that this flooding criterion is derived for a spray with single-sized-droplet distribution. The extension to the case of a spray with a drop size distribution is not considered here.

Figure 5 compares the flooding criterion with the data available from experiments reported by Dawson & diMarzo (1993). These experiments are for spray cooling of a surface heated by radiation from above. As it can be seen, the criterion provides an excellent representation of the experimental conditions. The uncertainties associated with the criterion are due to the semi-empirical determination of the parameter ϕ. Consider also that the experimental determination of the onset of flooding conditions is not clearly defined since it requires the establishment of a quasi-steady-state. This condition is not easily met, during spray cooling with a sparse spray, because local conditions vary greatly depending on the specific droplet deposition pattern. Therefore, the average surface temperature of a portion of the solid will

vary significantly about its average. These considerations of the inherent fluctuating behavior of the surface temperature support the order-of-magnitude approach for the selection of the parameter ϕ. In the figure, the onset of nucleate boiling is shown at 163 °C. This is the case for water droplets deposited on Macor.

CONCLUSIONS

A criterion for the determination of the onset of flooding condition of a hot surface subjected to a water sparse spray is presented. The criterion is formulated on the basis of a single droplet vaporization process via the introduction of two parameters: the ERC and the area of influence. These two parameters are evaluated from experimental and theoretical considerations for single droplets.

The final form of the criterion is based on the determination of the parameter ϕ which represents the ratio of the limiting radial heat flux in the direction of an evaporating droplet and the reference heat flux associated with the whole droplet vaporization process. A simple experiment is used to inform the selection of the parameter ϕ which is set at 0.1 percent of the reference value (i.e. $\phi = 10^{-3}$). With this selection, a closed-form solution is used to fit the data of a previously developed coupled model for the single droplet vaporization. The overall results are well represented by an exponential curve fit which enables the derivation of the flooding criterion in its final form.

The criterion is based on four parameters which are readily available or that can be determined from single droplet vaporization experiments. Experimental data on sparse spray confirm that the criterion is able to bound the region where evaporative cooling can be achieved without flooding the solid surface.

ACKNOWLEDGMENTS

This study has been supported by the Building and Fire Laboratory of the National Institute of Standards and Technology.

REFERENCES

Bonacina, C., Del Giudice, S. & Comini, G., 1979, "Dropwise Evaporation," Journal of Heat Transfer, Vol. 101, pp. 441-446.

Carslow, H.S. & Jaeger, J.C., 1959, Conduction of Heat in Solids, Clarendon Press, Oxford.

Chandra, S. & Avedisian, C.T., 1991, "On the Collision of a Droplet With a Solid Surface," Proc. Of the Royal Society, Vol. 432, pp. 13-41.

Dawson, H.F. & diMarzo, M., 1993, "Multi-Droplet Evaporative Cooling: Experimental Results," AIChE Symposium Series, Vol. 89, pp. 26-35.

diMarzo, M. & Evans, D., 1989, "Evaporation of a Water Droplet Deposited on a Hot High Thermal Conductivity Solid," Journal of Heat Transfer, Vol. 111, pp. 210-213.

diMarzo, M., Kidder, C.H. & Tartarini, P., 1992, "Infrared Thermography of Dropwise Evaporative Cooling of a Semi Infinite Solid Subjected to Radiant Heat Input," Experimental

Heat Transfer, Vol. 5, pp. 101-114.

diMarzo, M., Tartarini, P., Yiao, L., Evans, D., & Baum, H., 1993, "Evaporative Cooling Due to a Gently Deposited Droplet," Int. J. Heat and Mass Transfer, Vol. 36, pp. 4133-4139.

Grissom, W.M. & Wierum, F.A., 1981, "Liquid Spray Cooling on a Heated Surface," Int. J. Heat and Mass Transfer, Vol. 24, pp. 261-271.

Klassen, M., diMarzo, M. & Sirkis, J., 1992, "Infrared Thermography of Dropwise Evaporative Cooling," Experimental Thermal and Fluid Science, Vol. 5, pp. 136-141.

Makino, K. & Michiyoshi, I., 1984, "The Behavior of a Water Droplet on Heated Surfaces," Int. J. Heat and Mass Transfer, Vol. 27, pp. 781-791.

Pedersen, C.O., 1970, "An Experimental Study of the Behavior and Heat Transfer Characteristics of Water Droplets Impinging Upon a Heated Surface," Int. J. Heat and Mass Transfer, Vol. 13, pp. 369-381.

Rizza, J.J., 1981, "A numerical Solution to Dropwise Evaporation," Journal of Heat Transfer, Vol. 103, pp. 501-507.

Seki, M., Kawamura, H. & Sanokawa, K., 1978, "Transient Temperature Profile of a Hot Wall Due to an Impinging Water Droplet," Journal of Heat Transfer, Vol. 100, pp. 167-169.

Tartarini, P. & diMarzo, M., 1994, "Dropwise Evaporative Cooling in Radiative Fields," Heat Transfer 1994, Vol. 6, pp. 277-282.

Tio, K.K. & Sadhal, S.S., 1992, "Thermal Analysis of Droplet Spray Evaporation from a Heated Solid Surface," Journal of Heat Transfer, Vol. 114, pp. 220-233.

Toda, S., 1972, "A Study of Mist Cooling. First Report: Investigation of Mist Cooling," Heat

Transfer, Japanese Research, Vol. 1, No. 3, pp. 35-50.

White, G., Tinker, S. & diMarzo, M., 1994, Modeling of Dropwise Evaporative Cooling on a Semi-Infinite Solid Subjected to Radiant Heat Input," Fire Safety Science, IAFSS, pp. 217-228.

Zhang, N. & Wang, W.J., 1982, "Natural Convection in Evaporating Minute Droplets," Journal of Heat Transfer, Vol. 104, pp. 656-662.

CAPTIONS

Figure 1 - The evaporation-recovery cycle: comparison of τ with τ_{ERC} when $F_R = 1.3$

Figure 2 - The closed-from solution as a fit of the coupled model: comparison of η from the coupled model with sixty percent of η obtained from the closed-form solution

Figure 3 - Determination of the parameter ϕ: comparison of the data with the trends obtained with the closed-form solution

Figure 4 - Adequacy of the exponential fit for the representation of the radius of influence: comparison of the results of the closed-form solution with the fit.

Figure 5 - Criterion evaluation: comparison of the criterion with the data from sparse water sprays (Dawson & diMarzo 1993)

FIGURE 1

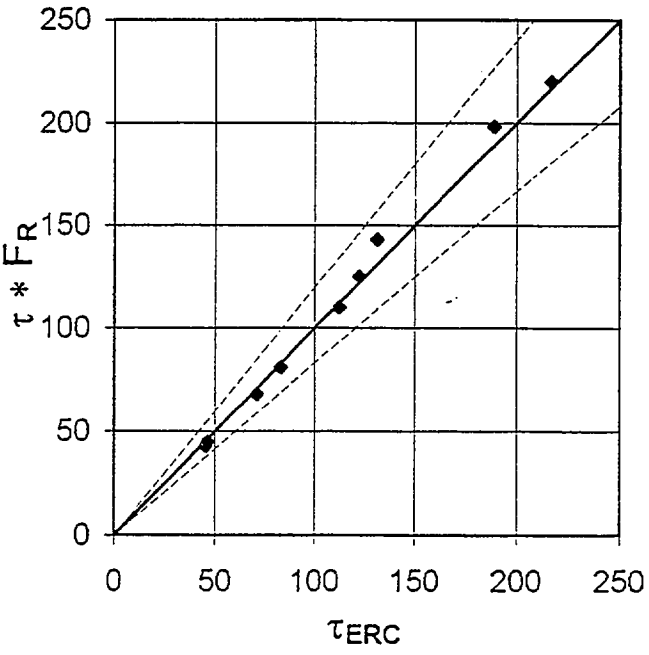

FIGURE 2

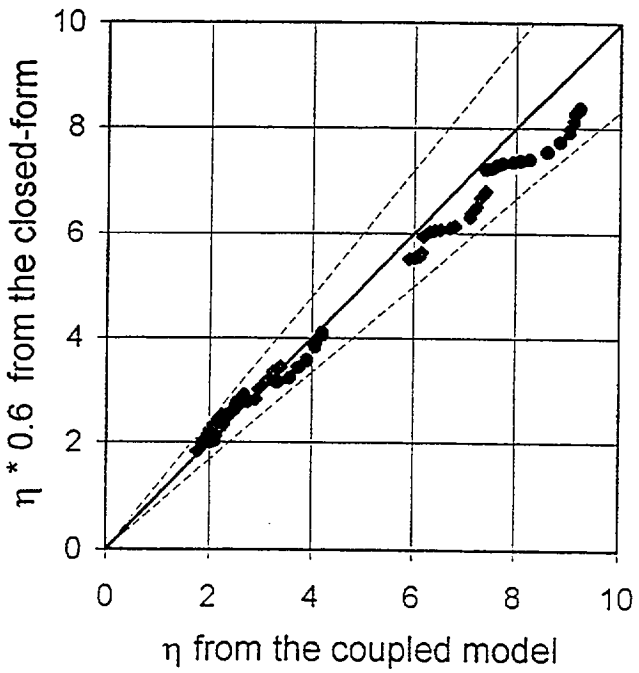
10
8
6
4
2
0
η * 0.6 from the closed-form
0
2
4
6
8
10
η from the coupled model

FIGURE 3

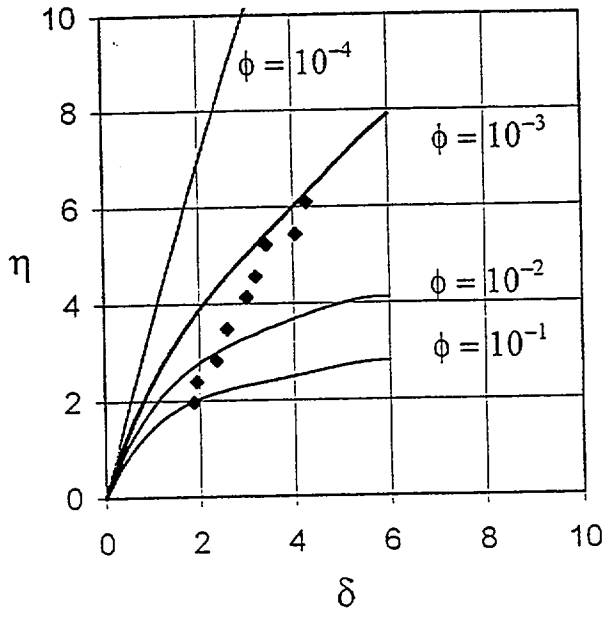

FIGURE 4

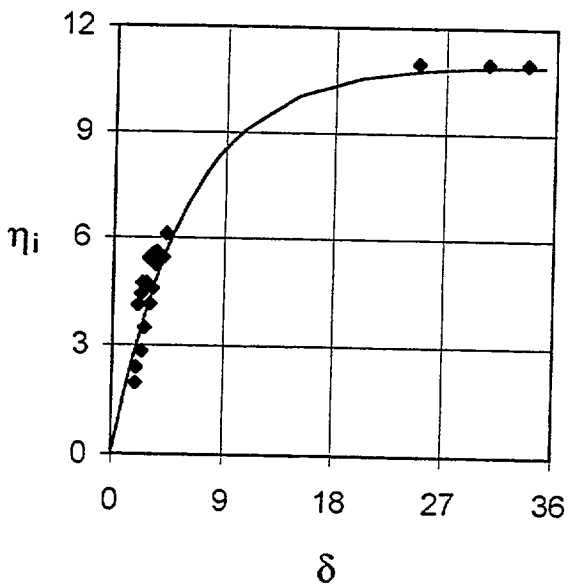

FIGURE 5

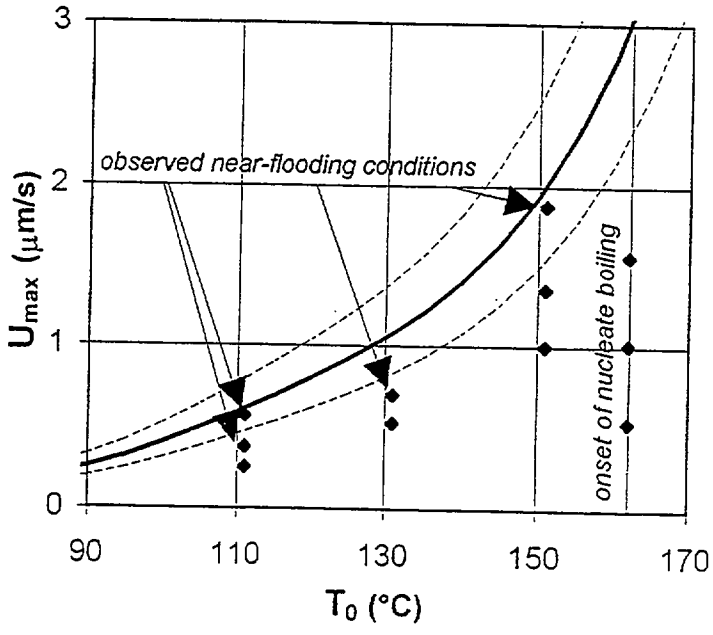
3
2
1
0
U_{max} (μm/s)
observed near-flooding conditions
onset of nucleate boiling
90
110
130
150
170
T_0 (°C)

NIST-114
(REV. 6-93)
ADMAN 4.09

U.S. DEPARTMENT OF COMMERCE
NATIONAL INSTITUTE OF STANDARDS AND TECHNOLOGY

MANUSCRIPT REVIEW AND APPROVAL

(ERB USE ONLY)
ERB CONTROL NUMBER | DIVISION
PUBLICATION REPORT NUMBER: NIST-GCR-96-687 | CATEGORY CODE
PUBLICATION DATE: June 1996 | NUMBER PRINTED PAGES

INSTRUCTIONS: ATTACH ORIGINAL OF THIS FORM TO ONE (1) COPY OF MANUSCRIPT AND SEND TO THE SECRETARY, APPROPRIATE EDITORIAL REVIEW BOARD

TITLE AND SUBTITLE (CITE IN FULL)

Sparse Water Sprays in Fire Protection

CONTRACT OR GRANT NUMBER: 60NANB5D0136

TYPE OF REPORT AND/OR PERIOD COVERED: December 1995

AUTHOR(S) (LAST NAME, FIRST INITIAL, SECOND INITIAL)
di Marzo, M.
Department of Mechanical Engineering
University of Maryland, College Park, MD 20742

PERFORMING ORGANIZATION (CHECK (X) ONE BOX)
[ ] NIST/GAITHERSBURG
[ ] NIST/BOULDER
[ ] JILA/BOULDER

LABORATORY AND DIVISION NAMES (FIRST NIST AUTHOR ONLY)

SPONSORING ORGANIZATION NAME AND COMPLETE ADDRESS (STREET, CITY, STATE, ZIP)
U.S. Department of Commerce
National Institute of Standards and Technology
Gaithersburg, MD 20899

PROPOSED FOR NIST PUBLICATION

[ ] JOURNAL OF RESEARCH (NIST JRES)	[ ] MONOGRAPH (NIST MN)	[ ] LETTER CIRCULAR
[ ] J. PHYS. & CHEM. REF. DATA (JPCRD)	[ ] NATL. STD. REF. DATA SERIES (NIST NSRDS)	[ ] BUILDING SCIENCE SERIES
[ ] HANDBOOK (NIST HB)	[ ] FEDERAL INF. PROCESS. STDS. (NIST FIPS)	[ ] PRODUCT STANDARDS
[ ] SPECIAL PUBLICATION (NIST SP)	[ ] LIST OF PUBLICATIONS (NIST LP)	[X] OTHER NIST-GCR
[ ] TECHNICAL NOTE (NIST TN)	[ ] NIST INTERAGENCY/INTERNAL REPORT (NISTIR)	

PROPOSED FOR NON-NIST PUBLICATION (CITE FULLY) [ ] U.S. [ ] FOREIGN

PUBLISHING MEDIUM
[ ] PAPER [ ] CD-ROM
[ ] DISKETTE (SPECIFY) _____
[ ] OTHER (SPECIFY)

SUPPLEMENTARY NOTES

ABSTRACT (A 2000-CHARACTER OR LESS FACTUAL SUMMARY OF MOST SIGNIFICANT INFORMATION. IF DOCUMENT INCLUDES A SIGNIFICANT BIBLIOGRAPHY OR LITERATURE SURVEY, CITE IT HERE. SPELL OUT ACRONYMS ON FIRST REFERENCE.) (CONTINUE ON SEPARATE PAGE, IF NECESSARY.)

A comprehensive review of the findings that punctuated ten years of research on dropwise evaporative cooling is presented. The first studies consider a single droplet evaporating on a high thermal conductivity solid surface. The solid-liquid coupling is addressed when considering the case of a low thermal conductivity solid. A powerful, non-intrusive, infrared thermographic technique is instrumental in describing the thermal behavior of the solid surface. The applications relevant to fire suppression suggest the input of radiant heat from above the surface instead of heat conducted through the solid. One the single droplet behavior is fully documented experimentally and accurately modelled, the study of sparse water sprays is undertaken. A superposition model is formulated which well represents the experimental data.

KEY WORDS (MAXIMUM OF 9; 28 CHARACTERS AND SPACES EACH; SEPARATE WITH SEMICOLONS; ALPHABETIC ORDER; CAPITALIZE ONLY PROPER NAMES)
drop size measurements; evaporation cooling; fire research; fire suppression; solid surfaces; thermal condustivity; water sprays

AVAILABILITY
[X] UNLIMITED [ ] FOR OFFICIAL DISTRIBUTION - DO NOT RELEASE TO NTIS
[ ] ORDER FROM SUPERINTENDENT OF DOCUMENTS, U.S. GPO, WASHINGTON, DC 20402
[X] ORDER FROM NTIS, SPRINGFIELD, VA 22161

NOTE TO AUTHOR(S): IF YOU DO NOT WISH THIS MANUSCRIPT ANNOUNCED BEFORE PUBLICATION, PLEASE CHECK HERE. [ ]

WORDPERFECT